2020

The neurotoxic effects of Manganese and the novel protective role of Drp1 in the autophagy pathway

Sportelli, Carolina

Copyright Statement

UNIVERSITY OF
PLYMOUTH

The neurotoxic effects of Manganese and the novel protective role of Drp1 in the autophagy pathway

by

CAROLINA SPORTELLI

A thesis submitted to the University of Plymouth
in partial fulfilment of the degree of

DOCTOR OF PHILOSOPHY

Peninsula Medical School

October 2019

Acknowledgements

This thesis could not have been completed without the support of colleagues, friends and family. I would like to take this opportunity to thank you all for contributing to this big part of my life.

First and foremost I would like to thank my Director of Studies, Prof Kim Tieu, who has been a great mentor for me. I would like to express my most sincere appreciation for encouraging my research throughout the years and for helping me mature as a scientist.

To my supervisors, Dr Shouqing Luo and Prof Robert Fern, for the continued support and guidance throughout the project, thank you for your time and constructive comments in my progress meetings throughout my study, especially whilst working as a long-distant student from Miami.

To Dr Oleg Anichtchik and Dr Shouqing Luo for assisting with troubleshooting and supplying cells and reagents, thank you for going out of your way to help me on many occasions.

I wish to extend my gratitude to all the friendly and cheerful people of the lab at Plymouth University and Florida International University, thanks for making my time in the lab more pleasant and for the help and support you have always offered me.

A special thanks goes to Rebecca, you have been a great colleague in the lab, but also a friend in real life. Thank you for your support with the seahorse assay and for taking your time to perform surgery on my LC3 mice. Working with you has been such a good learning experience.

To Jenny, who has been by my side since day one, you have helped me deal with so many different issues that I will never be able to thank you enough. I am so glad we embarked this journey together. I couldn't have asked for a better PhD friend. Your friendship has enriched my life.

Above all, I would like to express my heart-felt gratitude to my beloved partner Martino, without whom this would have never been possible. You have been a colleague, friend and life partner. You have stimulated, encouraged, helped me grow and challenge myself every day, thank you my love for always being there, for believing in me and for coping with all my anxieties and weirdness. Thank you for reading this work throughout and for giving me feedback and comments. Thank you for the scientific conversations in the pub and at home, you helped me so much, I would have been lost without you. You have shared and suffered this journey with me, from Plymouth to Miami and back to London. Cheesecake night was the best thing that ever happened to me. You inspire me every day and make me happy. Thank you. I love you deeply.

Alla mia famiglia, grazie per avermi incoraggiata, supportata e aiutata durante tutto il mio percorso. Siete nel mio cuore sempre, siete la parte più bella di me e l'amore che provo per voi va oltre ogni possibile immaginazione.

Ai miei genitori, dai quali mi è stata instillata la convinzione che nella vita posso raggiungere qualsiasi meta. Grazie per esserci stati sempre. "Quante volte vi ho pensato nei momenti più importanti, quando sola in laboratorio affrontavo i miei giganti … quante volte ho detto basta ma chi me lo fa fare, però poi pensando a voi non riuscivo mai a mollare". A voi che siete 'la mia voce più importante' dedico questo lavoro, per tutto ciò che avete SEMPRE fatto per noi figli. Senza il vostro appoggio non sarei qui oggi. Grazie Mamma. Grazie Papà.

Author's Declaration

At no time during the registration for the degree of Doctor of Philosophy has the author been registered for any other University award without prior agreement of the Doctoral College Quality Sub-Committee.

Work submitted for this research degree at the University of Plymouth has not formed part of any other degree either at the University of Plymouth or at another establishment.

Relevant scientific seminars and conferences were regularly attended at which work was often presented. 1 paper has been published in a peer-reviewed journal.

Publications (or public presentation of creative research outputs):

Helley, M. P., Pinnell, J., **Sportelli, C**. & Tieu, K. 2017. *Mitochondria: A Common Target for Genetic Mutations and Environmental Toxicants in Parkinson's Disease.* Frontiers in genetics, 8, 177.

Conferences:

Presentation (Poster):

C. Sportelli, R. Z. Fan, M. P. Helley, T. Guilarte and K. Tieu (2019). *Autophagy: An Early Pathogenic Target of Manganese but a Therapeutic Target of Drp1 Inhibition*. Society of Toxicology (SOT) 58th Annual Meeting, Baltimore, US.

Attended:

- XXI World Congress on Parkinson's Disease and Related Disorders, Milan, Italy (2015).
- Mitochondrial Biogenesis and Dynamics in Health, Disease and Aging Conference, West Palm Beach, US (2017).

Word count of main body of thesis: 48,838 words

Signed 

Date 12/09/2020

Abstract

The neurotoxic effects of Manganese and the novel protective role of Drp1 in the autophagy pathway

Carolina Sportelli

The precise pathological mechanism of Manganese (Mn) is not yet known however prior evidence suggests a prominent role of mitochondrial dysfunction. Relevant to Parkinson's disease, Mn is known to bind to α-synuclein and increase its aggregation. Autophagy is also implicated in neurodegeneration however little is known about the effects of Mn on this pathway. The aim of this thesis was to investigate the effects of Mn on autophagy, α-synuclein aggregation and mitochondrial function in multiple paradigms. The effects of inhibiting the mitochondrial fission protein Drp1 were also assessed in these cellular contexts following Mn exposure.

Acute exposure to sub-lethal Mn concentrations, *in vitro* and *in vivo,* caused an inhibition of autophagy flux in the absence of mitochondrial dysfunction. Despite this, Drp1 inhibition improved Mn-induced autophagy impairment and reduced cell death. In a cellular model of α-synuclein overexpression, in addition to the effect on autophagy, Mn also potentiated α-synuclein aggregation; rescued by Drp1 inhibition. This was observed at a later timepoint, suggesting that α-synuclein aggregation could be a consequence of impaired autophagy.

The effects of chronic Mn accumulation on neurodegenerative pathology were assessed in six month old transgenic *SLC39A14* knockout mice. Accumulated levels of the autophagy markers, LC3 and p62, were identified in both DAergic and GABAergic neurons, indicative of impaired autophagy. These neurons exhibited normal mitochondrial morphology, corroborating results from previous chapters. No alterations in striatal TH density or microglial

activation within the *substantia nigra* were observed at this timepoint, however increased astrocyte activation was identified.

This study is the first to examine the effects of Mn exposure on mitochondrial function, autophagy flux and α-synuclein aggregation concurrently. Results demonstrate that the autophagy pathway is primarily affected, followed by α-synuclein aggregation whereas mitochondrial function remains unaffected. Despite this, the inhibition of Drp1 ameliorated the effects of Mn on these pathways. The discovery that the pathogenic and protective mechanisms of Mn and Drp1 inhibition, respectively, intersect at the autophagic pathway is novel and suggestive of a therapeutic target.

Table of Contents

List of Figures

List of Tables

Abbreviations and Acronyms

Abbreviations	Definition
ABC	ATP-binding cassette
ABC solution	Avidin–biotin complex
AD	Alzheimer's disease
AMPK	5' adenosine monophosphate-activated protein kinase
AP	Anterior-posterior
Asn	Asparagine
Asp	Aspartate
ASPA	Animals for Scientific Procedures Act
ATG	Autophagy-related (proteins)
ATP	Adenosine triphosphate
ATP13A2	ATPase 13A2
AUC	Area under the curve
BSA	Bovine serum albumin
BCA	Bicinchoninic acid assay
BBB	Blood-brain barrier
C. elegans	*Caenorhabditis elegans*
CAG	CMV early enhancer/chicken beta actin
Calcein AM	Calcein (fluorexon) acetoxymethyl
CD4/8	Cluster of differentiation 4/8
cDNA	Complementary DNA
CHCHD2	Coiled-Coil-Helix-Coiled-Coil-Helix Domain Containing 2
CMA	Chaperone-mediated autophagy
CMT2A	Charcot–Marie–Tooth disease type 2A
CMV	Cytomegalovirus
CNS	Central nervous system
CO_2	Carbon dioxide
CQ	Chloroquine
COX	Cytochrome c oxidase

COX-2	Cyclo-oxygenase-2
CSF	Cerebrospinal fluid
DA	Dopamine
DAB	3,3’-diaminobenzidine-tetrahydrochloride
DAergic	Dopaminergic
DAPI	4′,6-diamidino-2-phenylindole
DAT	Dopamine transporter
DMEM	Dulbecco’s modified eagle medium
DMSO	Dimethyl sulfoxide
DMT1	Divalent metal transporter 1
DNA	Deoxyribonucleic acid
dNTPs	Deoxynucleotide triphosphates
DOPAC	3,4-dihydroxyphenylacetic acid
Drp1/Dlp1	Dynamin-related protein 1/ Dynamin-1-like protein
DV	Dorso-ventral
eGFP	Enhanced green fluorescent protein
ER	Endoplasmic reticulum
ETC	Electron transport chain
EM	Electron microscopy
EDTA	Ethylenediaminetetraacetic acid
EPG5	Ectopic P granules protein 5
FBS	Fetal bovine serum
FCCP	Carbonyl cyanide-4-phenylhydrazone
Fis1	Mitochondrial fission 1 protein
FIP200	FAK family-interacting protein of 200 kDa
g	Gravity
GBA	Glucocerebrosidase
GCase	β-Glucocerebrosidase
GCTA	Genome-wide complex trait analysis
GABA	Gamma aminobutyric acid
GAD65/67	Glutamate decarboxylase 65/67

GAPDH	Glyceraldehyde 3-phosphate dehydrogenase
GD	Gaucher disease
GAPs	GTPase-activating proteins
GDP	Guanosine diphosphate
GEFs	Guanine nucleotide exchange factors
GFAP	Glial fibrillary acidic protein
Glu	Glutamate
GP	Globus pallidus
GTP	Guanosine-5'-triphosphate
GWAS	Genome-wide association studies
HA	Human influenza hemagglutinin
HEPES	4-(2-hydroxyethyl)-1-piperazineethanesulfonic acid
HLA-DR	Human leukocyte antigen D-related
HOPS	Homotypic fusion and protein sorting
HPLC	High performance liquid chromatography
Hsc70	Heat shock cognate protein of 70 kDa
HVA	Homovanillic acid
Iba1	Ionized calcium binding adaptor molecule 1
IC_{50}	Half maximal inhibitory concentration
ICC	Immunocytochemistry
ICS	Institut Clinique de la Souris
ICUC	Institutional Animal Care and Use Committee
IF	Immunofluorescence
IFNγ	Interferone gamma
IgG/Y	Immunoglobulin G/Y
IL	Interleukin
IMM	Inner mitochondrial membrane
IMS	Intermembrane space
iNOS	Inducible nitric oxide synthase
KOMP	Knockout mouse project
LBs	Lewy bodies

LAMP 1/2A	Lysosome-associated membrane protein type 1/2A
LC3	Microtubule-associated protein 1A/1B-light chain 3
LIR	LC3-interacting region
LPS	Lipopolysaccharide
LRRK2	Leucine-rich repeat kinase 2
MAM	Mitochondria-associated endoplasmic reticulum membrane
Maneb	Manganese ethylenebisdithiocarbamate
Mdivi-1	Mitochondrial division inhibitor-1
Mfn 1/2	Mitofusin 1/2
Mid49/51	Mitochondrial dynamics protein 49/51
Mff	Mitochondrial fission factor
ML	Medio-lateral
Mn	Manganese
$MnCl_2$	Manganese (II) chloride
Mn-SOD	Mn-superoxide dismutase
MPP^+	1-methyl-4-phenylpyridinium
MPTP	1-methyl-4-phenyl-1,2,3,6-tetrahydropyridine
MRI	Magnetic resonance imaging
mtDNA	Mitochondrial DNA
MTOC	Microtubule organizing centre
mTOR	Mammalian target of rapamycin
NAC	Non amyloid β-component
NADH	Nicotinamide adenine dinucleotide – hydrogen (reduced)
NADPH oxidase	Nicotinamide adenine dinucleotide phosphate oxidase
NF-Kβ	Nuclear factor kappa-light-chain-enhancer of activated B cells
NGS	Normal goat serum
NMDA	N-methyl-D-aspartate
NO	Nitric oxide
NOS	Nitric oxide synthase
OATP	Organic anion transporter polypeptide
OCR	Oxygen consumption rate

OCT	Optimal cutting temperature
OCT-3	Optical density
OD	Organic cation transporter-3
OMM	Outer mitochondrial membrane
OPA1	Optic atrophy 1
OXPHOS	Oxidative phosphorylation
PBS	Phosphate buffered saline
PCR	Polymerase chain reaction
PD	Parkinson’s disease
PE	Phosphatidylethanolamine
PFA	Paraformaldehyde
PFFs	Preformed fibrils
PGC1-α	Peroxisome proliferator-activated receptor gamma coactivator 1-alpha
PINK1	Phosphatase and tensin homolog-induced putative kinase 1
PIs	Phosphoinositides
PI3P	Phosphatidylinositol 3,4,5-triphosphate
pK_a	Acid association constant
PonA	PonastroneA
PQ	Paraquat
pSer	Phosphorylated serine
PTMs	Post-translational modifications
PtdIns	Phosphatidylinositol
PVDF	Polyvinylidene difluoride
qPCR	Quantitative real-time polymerase chain reaction
rAAV	Recombinant adeno-associated virus
Rab	Ras-related
RFP	Red fluorescent protein
RIPA buffer	Radioimmunoprecipitation assay buffer
ROI	Region of interest
ROS	Reactive oxygen species
rpm	Revolutions per minute

RPMI	Roswell Park Memorial Institute
Rubicon	Run domain Beclin-1 interacting and cysteine-rich containing protein
SDS	Sodium dodecyl sulfate
SEM	Standard error of mean
siRNA	Small interfering ribonucleic acid
SLC22A3	Solute carrier family 22 member 3
SLC30A10	Solute carrier family 30 member 10
SLC39A14	Solute carrier family 39 member 14
SLC39A8	Solute carrier family 39 member 8
SNARE	Soluble N-ethylmaleimide-sensitive factor attachment protein receptors
SNpc	*Substantia nigra pars compacta*
SPCA1	Secretory pathway Ca2+-ATPase isoform 1
SRC	Spare respiratory capacity
STX17	Syntaxin 17
SYT11	Synaptotagmin 11
TBC1D15	TBC1 domain family member 15
TBE buffer	Tris-borate-edta buffer
TBS	Tris buffered saline
TEM	Transmission electron microscopy
Tfam	Mitochondrial transcription factor A
TFEB	Transcription factor EB
TGF-β	Transforming growth factor beta
TfR	Transferrin receptor
TH	Tyrosine hydroxylase
Thy-1	Thymocyte differentiation antigen 1
TLRs	Toll-like receptors
TMEM175	Transmembrane protein 175
TMRM	Tetramethylrhodamine
TNF-α	Tumour necrosis factor-alpha
TOM20/22/40	Translocase of the outer membrane 20/22/40
TrkB	Tropomyosin receptor kinase B

TSPO	Translocator protein
ULK	Unc-51-like kinase
UPS	Ubiquitin-proteasome system
UVRAG	Ultraviolet radiation resistance-associated gene protein
VEGF	Vascular endothelial growth factor
VMAT2	Vesicular monoamine transporter 2
Vps 15/34	Vacuolar protein sorting 15/34
VTA	Ventral tegmental area
WT	Wild-type
3-MA	3-Methyladenine
6-OHDA	6-hydroxydopamine
$\Delta\psi m$	Mitochondrial membrane potential

Chapter 1
Introduction

1.1 Introduction to Parkinson's disease

1.1.1 History and epidemiology

Known as the second most prevalent neurodegenerative disorder after Alzheimer's disease (AD), Parkinson's disease (PD) is an age-related disorder that impacts about 6.2 million people worldwide, a figure that is estimated to rise and strike roughly 14.2 million individuals by 2040 (Dorsey and Bloem, 2018). PD was first described by James Parkinson, in 1817, as a neurological syndrome termed 'shaking palsy' (Parkinson, 2002). PD pathology is mainly characterised by a selective degeneration of dopaminergic (DAergic) neurons in the *substantia nigra pars compacta* (SNpc) and the presence of fibrillar aggregates referred to as Lewy bodies (LBs), which manifest in clinical phenotypes such as resting tremor, bradykinesia, rigidity, and postural instability (Schapira, 2009). Although the aetiology of PD is not fully understood, several risk factors and genetic mutations have been discovered and suggested to play a crucial role in the development and progression of the disease.

The incidence of PD increases with age and is estimated to affect roughly 1% of the population over 60 at any time during their life (Tysnes and Storstein, 2017). PD is 1.5 times more prevalent in men than in women (Taylor et al., 2007). This difference could be related to more frequent occupational exposures in men and neuroprotection from oestrogens in women and X-linked genetic factors (Gatto et al., 2014, Cerri et al., 2019).

1.1.2 Clinical features

The cardinal motor features of PD start to develop once the DAergic cells (more than 50% in comparison to a young adult) in the nigrostriatal system are lost (Reeve et al., 2014, Chung et al., 2001). The disease is usually diagnosed according to the presence of motor symptoms first described by Hughes et al. (1992).

Non-motor symptoms are also a common feature of PD and they may appear in the early pre-symptomatic stage as well as throughout the disease course, negatively influencing the patient's health-related quality of life.

Age is the greatest risk factor for developing PD. Evidence shows that incidence rates increase strongly at the age of 60, peak at 85-89 years and then decline after 90 years of age (Driver et al., 2009).

1.1.3 Pathological features

The pathological hallmarks of PD are the loss of the nigrostriatal DAergic neurons and the presence of eosinophilic protein deposits, named Lewy bodies (LBs) (**Figure 1.1**), located in the SNpc of the remaining DAergic neurons (Przedborski, 2017). They usually are observed within the cell soma, but also reside in neurites or free in the extracellular space (Gibb et al., 1991). Although the pathophysiologic significance of these inclusion bodies still remains largely unknown, the main biochemical components of LBs are α-synuclein (Spillantini et al., 1997, Spillantini et al., 1998), .ubiquitin (Kuzuhara et al., 1988) and more recently lipids, mitochondria and other organelles (Shahmoradian et al., 2019).

The cell bodies of the nigrostriatal neurons that reside in the SNpc project their axons to the striatum (comprised of the caudate nucleus and the putamen) and those in the ventral tegmental area (VTA) project to the cortical and limbic areas (Bjorklund and Dunnett, 2007, Hegarty et al., 2013). The ultimate functional output of the striatum involves the coordination of movement. Loss of DAergic neurons, rich in neuromelanin (Marsden, 1983), results in the gross depigmentation of the SNpc, along with the depletion of dopamine (DA) in the putamen (Bernheimer et al., 1973) (**Figure 1.1**). The mesolimbic DAergic neurons, the cell bodies of which are located in the VTA, are much less affected in PD (Uhl et al., 1985) and this leads to a significantly less depletion of DA in the caudate (Price et al., 1978). PD is commonly thought

to be characterised solely by DAergic neuron loss, however the neurodegeneration extends well beyond DAergic neurons. Other catecholaminergic cell groups are targeted and they include the locus coeruleus, some cells of the sympathoadrenal system and the serotoninergic neurons of the raphe nuclei. Loss of cholinergic neurons of the nucleus basalis of Meynert is also observed, and this may be responsible, at least in part, for dementia (Whitehouse et al., 1983, Hornykiewicz and Kish, 1987).

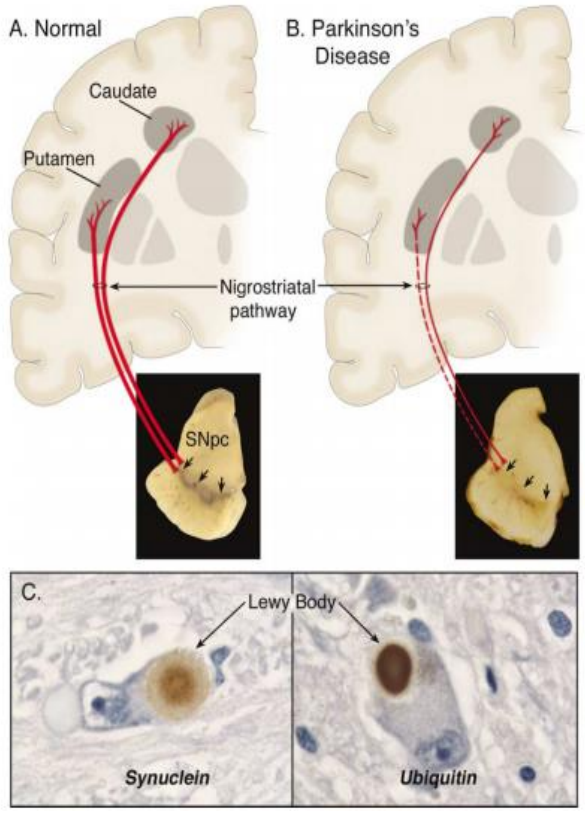

Figure 1.1 Neuropathology of PD. (A) Schematic representation of the nigrostriatal pathway (in red) consisting of projections from DAergic neurons in the SNpc to the striatum (i.e., caudate nucleus and putamen). **(B)** Schematic representation of the degenerated nigrostriatal pathway (in red). The loss of DAergic input to the putamen (dashed red line) is more severe compared to that projected to the caudate (red solid line). **(C)** Immunostaining with an antibody against α-synuclein reveals a Lewy body (brown reaction product in cell indicated by black arrow) with an intensely immunoreactive central zone surrounded by a faintly immunoreactive peripheral zone (left image). Conversely, immunostaining with an antibody against ubiquitin yields more diffuse immunoreactivity within the Lewy body (right image). Adapted from Dauer and Przedborski (2003).

1.1.4 Aetiology of Parkinson's disease

The relative contributions of genetic versus environmental factors, regarding the development and progression of PD, have been hotly debated. Genetic studies have been the predominant driving force in PD research over the last few decades, although currently only less than 10% of PD cases can be directly linked to monogenic mutations (Klein and Westenberger, 2012). The remaining cases have been attributed to environmental exposures and gene-environment interactions, making PD a multifactorial disorder with a complex aetiology. Despite many years of focused research, the causes of PD remain to be elucidated. Understanding the causes of this disease is pivotal as that knowledge could lead to directed research that will develop new and potential therapies.

1.1.5 Genetic mutations in Parkinson's disease

Since the discovery of the first missense substitution in *SNCA*, the gene encoding α-synuclein (Polymeropoulos et al., 1997), the understanding of the genetic contribution to PD has progressed rapidly. Genome-wide association studies (GWAS) and Genome-wide complex trait analysis (GCTA, which estimates phenotypic variance explained by all genome-wide single-nucleotide polymorphisms for complex traits) have led to important genetic discoveries associated with an increased risk of developing PD. Currently, over 20 known genes are linked to different forms of PD (*PARK* loci) and the underlying gene mutation has been identified in 11 of them (Hernandez et al., 2016, Blauwendraat et al., 2020). Several associated risk-conferring loci, that do not have the *PARK* designation, have also been identified to have modest influence on lifetime risk of developing PD (Simón-Sánchez et al., 2009, Satake et al., 2009, Nalls et al., 2014, Nalls et al., 2019). Recently, the most comprehensive understanding of the genetic architecture of PD was carried out in a GWAS. The authors revealed 90

independent risk-associated variants, providing a biological context for these risk factors, and demonstrated that a considerable genetic component of PD still remains unidentified (Nalls et al., 2019, Blauwendraat et al., 2020). The major monogenic mutations and associated risk genes in PD are summarised in **Table 1.1**.

A comprehensive description of genetic factors involved in PD pathogenesis is beyond the scope of this introduction and the following section will focus on *SNCA*, *PINK1* and *Parkin*; for a detailed review of PD genetics see Helley et al., (2017).

Table 1.1 Major monogenic mutations and associated risk genes in PD. Adapted from Helley et al. (2017).

Gene	PARK Locus	Gene Locus	Inheritance	Mutations	Prevalence
SNCA	*PARK 1/4*	*4q21-22*	AD	A53T, A30P, E46K, G51D, H50Q, duplications, triplications	Rare, A53T is most frequent but only found in seven families worldwide
LRRK2	*PARK 8*	*12q12*	AD	>100 missense and non-sense mutations high risk variants, >15 of which are pathogenic	Up to 40% of familial and up to 10% of sporadic cases
VPS35	*PARK 17*	*16q11.2*	AD	D620N	1% of familial and 0.2% of sporadic cases
CHCHD2	*PARK 22*	*7q11.2*	AD	10 mutations	Not available
GBA	*N/A*	*1q21*	AD	>300 mutations, L444P and N370S are most common	Varies in different PD populations but up to 31% in Ashkenazi Jewish PD patients
Parkin	*PARK 2*	*1p35-36*	AR	~147 exonic mutations	77% familial EOPD and 10–20% EOPD in general
PINK1	*PARK 6*	*6q25.2-27*	AR	>60 mutations	>9% EOPD
DJ-1	*PARK 7*	*1p36*	AR	>10 mutations	1–2% EOPD
ATP13A2	*PARK 9*	*1p36*	AR	>10 mutations	Rare (found in 11 families)
FBXO7	*PARK 15*	*22q12-13*	AR	R378G, R498X, T22M, L34R	Rare
PLA2G6	*PARK 14*	*22q13.1*	AR	R741Q, R747W and more	Rare

EOPD, Early-onset PD (Age at onset <50 years old); LOPD, Late-onset PD (Age at onset ≥ 50 years old); AD, Autosomal dominant; AR, Autosomal recessive; GW, Genome-Wide.

1.1.5.1 *SNCA*

The *SNCA* unequivocally associated with familial parkinsonism, is key to the pathophysiology of both familial and sporadic PD. It is well known for encoding α-synuclein and although mutations in this gene are overall rare, the *SNCA* locus can be described as the most powerful variant factor for PD development (Lill et al., 2012, Nalls et al., 2019). The first point mutation, A53T, was discovered more than 20 years ago on chromosome 4q22.1 (Polymeropoulos et al., 1997). Since then, additional pathogenic missense mutations (A30P, E46K, G51D, and H50Q), as well as gene duplications and triplications, have been identified in familial PD (Kruger et al., 1998, Singleton et al., 2003, Zarranz et al., 2004, Appel-Cresswell et al., 2013, Lesage et al., 2013). Of note, a-synuclein overexpression and mutations are disease causing, however additional not-fully penetrant polymorphisms/variants, associated with a risk of developing PD, have also been discovered (Nalls et al., 2019). Shortly after the first genetic finding (Polymeropoulos et al., 1997), a-synuclein was described as a key factor of sporadic PD as the main component of LBs (Spillantini et al., 1997). Since then, research has largely centred around the role of a-synuclein-associated mechanisms to further understand PD pathogenesis.

a-synuclein is a small protein (140 amino acids) highly expressed in the brain, mainly in presynaptic axon terminals and is comprised of three domains: residues 1–60 as N-terminal region, residues 61–95 as central region and residues 96–140 as C-terminus region. The central region, identified as the hydrophobic non amyloid β-component (NAC) domain, is critical for fibril formation (El-Agnaf et al., 1998). The C-terminal acidic tail domain is the major site for post translational modifications (PTMs), protein truncation (Li et al., 2005) and interaction with modulators of a-synuclein aggregation including metal cations (Binolfi et al., 2006). The overall a-synuclein protein is formed of seven imperfect 11 residues repeats with a conserved KTKEGV sequence: four resides in the amphipathic N-terminal region and three in the NAC core (George et al., 1995).

α-synuclein is a multifunctional protein involved in a range of cellular functions and has been reported to interact with and affect a variety of proteins, in particular at the presynaptic terminal (**Figure 1.2**). There is evidence on the ability of α-synuclein to bind to the SNARE-protein synaptobrevin-2 and chaperone SNARE-complex assembly and subsequently promote neurotransmitter release (Burre et al., 2010, Burre et al., 2012), regulate membrane interaction of the G-protein Rab3 (Chen et al., 2013), bind and modulate synapsin III (Zaltieri et al., 2015), bind to VMAT2 (Guo et al., 2008), stimulate and modulate dopamine and serotonin transporters (Wersinger et al., 2006, Swant et al., 2011, Butler et al., 2015) and regulate tyrosine hydroxylase (Perez et al., 2002, Baptista et al., 2003, Yu et al., 2004). In addition to interacting with various proteins at the presynaptic level, α-synuclein has also been reported to interact with mitochondria (Nakamura et al., 2008, Li et al., 2007, Di Maio et al., 2016), the endoplasmic reticulum (Cooper et al., 2006, Thayanidhi et al., 2010) and nuclei (Kontopoulos et al., 2006). α-synuclein has also been shown to modulate lipid synthesis (Ruipérez et al., 2010) and prevent oxidation of unsaturated lipids in vesicles by acting as an antioxidant (Hashimoto et al., 2002, Zhu et al., 2006).

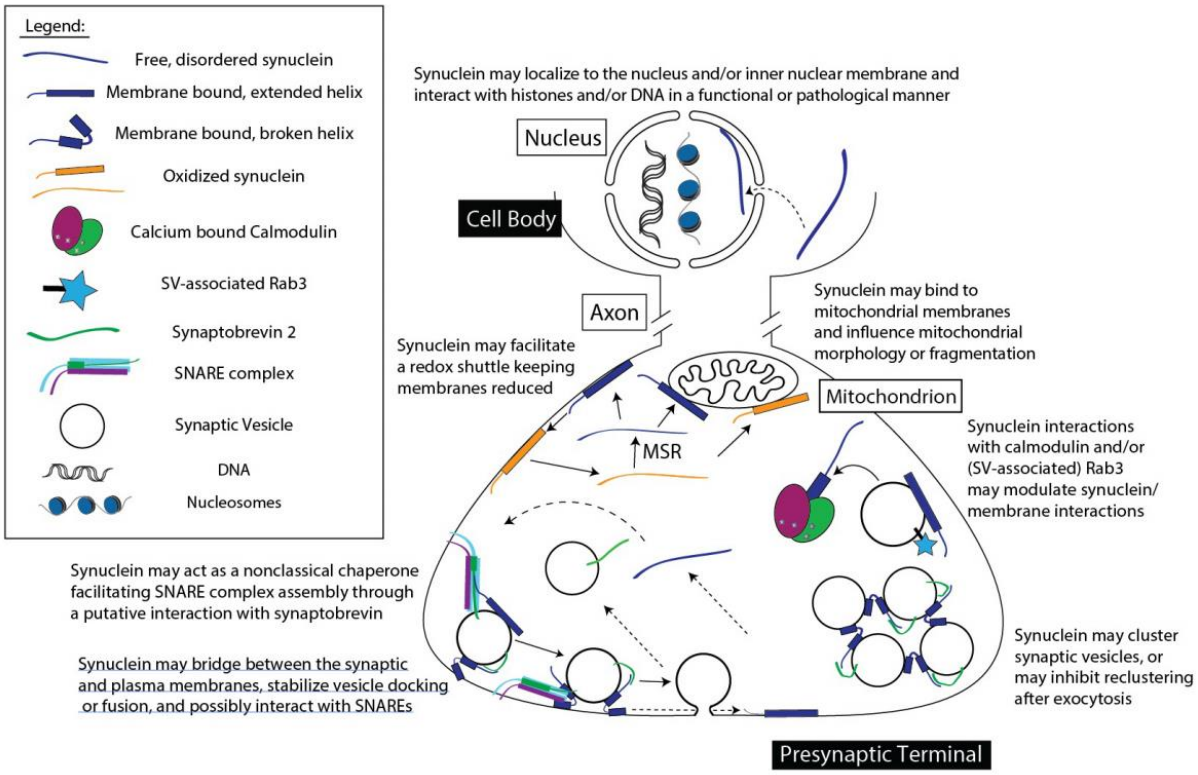

Figure 1.2 Cellular membranes, targets and pathways potentially involved in the normal, physiological functions of α-synuclein. α-synuclein is a highly soluble, cytoplasmic protein, that binds to a variety of cellular membranes of different properties and compositions. These interactions are considered critical for at least some normal functions of α-synuclein and may well play critical roles in both the aggregation of the protein and its mechanisms of toxicity. In physiological conditions, α-synuclein adopts an unfolded conformation, however it can also form a multimeric structure when bound to synaptic vesicles (Davidson et al., 1998, Weinreb et al., 1996, Ahn et al., 2002, Burre et al., 2010, Fauvet et al., 2012, Theillet et al., 2016). This suggests that the dynamic regulation of α-synuclein function depends on the local cellular environment. Others have suggested that native α-synuclein is a tetramer that co-exists, in a dynamic equilibrium, with the unfolded monomer. Any perturbation of this dynamic equilibrium promotes the incrementation of the monomer form, which is associated with aggregation and pathology (Bartels et al., 2011, Wang et al., 2011b, Dettmer et al., 2015). Image from Snead and Eliezer (2014).

α-synuclein is known to interact with mitochondria via its N-terminal domain (Nakamura et al., 2008, Rostovtseva et al., 2015, Di Maio et al., 2016). However, it has also been argued that α-synuclein does not localise to mitochondria but to the mitochondria-associated endoplasmic reticulum membrane (MAM), where it regulates mitochondrial morphology. This function can be impaired by pathogenic mutations in α-synuclein (Guardia-Laguarta et al., 2014). Although

the interaction between mitochondria and α-synuclein is still poorly understood, α-synuclein preferentially binds to highly negative charged membranes, facilitated by the presence of cardiolipin. Cardiolipin is a scaffold protein for the components of the electron transport chain (ETC) and its interaction with α-synuclein is sought to potentially stabilise ETC proteins (Chicco and Sparagna, 2007, Guardia-Laguarta et al., 2015).

α-synuclein possesses an interesting characteristic that both overexpression of wild-type (WT) and mutant forms of the protein can cause pathology. This is mainly due to α-synuclein tendency to aggregate, gradually evolving from small soluble oligomers to larger insoluble fibrils, ultimately generating LBs. It is still unclear what α-synuclein conformations have disease-modifying effects on DAergic neurons and whether LBs represent compensatory storage forms of the toxic aggregates or whether LBs themselves lead to neuronal cell death (Olanow et al., 2004, Wakabayashi et al., 2007).

Although the genetic variants of α-synuclein represent only a small percentage of PD cases, these findings have strengthened the argument for the central role of this protein in PD pathogenesis. In addition, since α-synuclein is the major component of LBs, present in the majority of PD patients, it is likely that α-synuclein plays a pivotal role in the multiple cellular mechanisms involved in PD pathophysiology; these will be discussed in the following relevant sections.

1.1.5.2 *PINK1* and *Parkin*

Loss of function mutations in *PINK1* and *Parkin* represent the most common cause of autosomal recessive early-onset familial PD, with or without the presence of LB pathology (Kitada et al., 1998, Sasaki et al., 2004, Valente et al., 2004, Samaranch et al., 2010). Firstly described in 1997 in 13 Japanese families (Matsumine et al., 1997), *Parkin* mutations are

considered to be the most prevalent autosomal recessive PD mutations accounting for 77% of familial cases (with an age of onset < 30 years) and 10–20% of early-onset PD in general (Klein and Lohmann-Hedrich, 2007, Kilarski et al., 2012, Klein and Westenberger, 2012). *Parkin* is comprised of 12 exons that encode the 465 amino acid protein, Parkin (Kitada et al., 1998). Parkin is an E3 ubiquitin ligase with an amino-terminal ubiquitin-like (Ubl) domain and a carboxyl-terminal ubiquitin ligase domain (Shimura et al., 2000, Hristova et al., 2009). In 2001, the second gene causing early PD onset was identified in an Italian family (Valente et al., 2001), *PINK1*, responsible for 9% of cases (Klein and Westenberger, 2012). The 8 exon *PINK1* gene encodes the 581 amino acid protein phosphatase and tensin homolog (PTEN)-induced kinase1 (PINK1) (Valente et al., 2004). The protein consists of a C-terminal kinase domain and a mitochondrial targeting sequence in the N terminus, consistent with its mitochondrial localisation in cells (Valente et al., 2004, Zhou et al., 2008).

PINK1 and Parkin are mainly involved in a signalling pathway that activates mitochondrial quality control pathways in response to mitochondrial damage and are tightly associated with mitochondrial dysfunction in PD. Under basal conditions, PINK1 binds to the outer mitochondrial membrane (OMM) and is then transferred to the inner mitochondrial membrane (IMM) via the translocase of the outer mitochondrial (TOM) complex and the and translocase of the inner membrane 23 (TIM23). Here, full length PINK1 is cleaved by IMM-bound proteases and degraded by the proteasome, leading to low levels of PINK1 in healthy mitochondria (Meissner et al., 2011, Yamano and Youle, 2013). Upon mitochondrial damage and loss of membrane potential, PINK1 import to the IMM is impaired, causing it to accumulate at the OMM (Jin et al., 2010, Lazarou et al., 2012, Okatsu et al., 2013). This accumulation leads to PINK1 homodimerisation and subsequent autophosphorylation, which induces kinase activation and phosphorylation of both ubiquitin and the Ubl domain of Parkin at residue Ser65. This phosphorylation stimulates Parkin activity and its recruitment from the

cytosol to the mitochondria (Kondapalli et al., 2012, Shiba-Fukushima et al., 2012). The concerted action between PINK1 and Parkin causes the polyubiquitination of multiple OMM substrates and subsequent targeting to the autophagic machinery for lysosomal degradation.

In addition, PINK1 and Parkin are involved in the regulation of mitochondrial dynamics, through mechanisms involving the turnover of fission and fusion associated proteins (Deng et al., 2008, Poole et al., 2008, Gegg et al., 2010, Buhlman et al., 2014, Pryde et al., 2016), and in mitochondrial biogenesis by an indirect interaction with Peroxisome proliferator-activated receptor gamma coactivator 1-α (PGC1-α) (Shin et al., 2011, Stevens et al., 2015, Lee et al., 2017).

1.2 Toxicants and environmental factors in Parkinson's disease

The discovery of genetic mutations and their functional characterisation in cellular and animal models have yielded crucial understanding of the pathogenesis of PD. However, prior to the discovery of the first genetic mutation linked to PD, research was mainly focused on environmental factors and their implication in the progression of the disease. This dominant environmental theory started with the discovery of 1-methyl-4-phenyl-1,2,3,6-tetrahydropyridine (MPTP), a contaminant of a synthetic opiate, which caused irreversible parkinsonism (Langston et al., 1983). This discovery led to a number of epidemiological studies and meta-analyses, which identified various environmental factors, including pesticides and heavy metals, that increased the risk of developing PD (Tanner et al., 2011, Wang et al., 2011a, Caudle et al., 2012, Kamel, 2013). Pesticides and heavy metals are perhaps the most widely studied environmental toxicants involved in PD pathogenesis, and the ability of some to persist in the environment long after their application increases the possibility of human exposure to these contaminants.

1.2.1 Pesticides

The link between occupational exposure of two pesticides, rotenone and paraquat, and PD was first reported in individuals who made use of either pesticide and developed the disease 2-2.5 times more often than nonusers (Tanner et al., 2011). Results from this case–control study confirmed the association of PD with the use of pesticides classified as complex I inhibitors or oxidative stressors. This study provided a link between basic research and human populations and yielded new insights into the pathogenesis of PD. Since then, tremendous progress has been made into understanding, in more depth, the mechanisms of action of these

pesticides and their effects in relation to PD. More in depth description of the association between pesticides and PD can be found in section 7.1.1 and 7.1.2.

1.2.2 Heavy metals

Several studies have reported changes in metal levels in the brain of deceased PD patients compared to non-PD controls of similar age, and suggested that high exposure to metals could be associated with an increased risk of developing PD (Rybicki et al., 1993, Forte et al., 2005, Willis et al., 2010, Ogunrin et al., 2013). Several epidemiological studies have reported a substantial association between PD and long-term exposure to heavy metals (Tanner et al., 1987, Winkel et al., 1995, Gorell et al., 1997, Gorell et al., 1999, Miller et al., 2003). In particular, in the occupational setting, the exposure to specific heavy metals, including manganese (Mn), were found to double the risk of developing PD (Coon et al., 2006, Racette et al., 2017). Despite their requirements in many physiological activities, excessive metal levels can produce detrimental effects to mitochondrial function by generating oxidative stress (Martinez-Finley et al., 2013, Kumudini et al., 2014, Park et al., 2015a). Furthermore, metal overexpression can cause DNA damage, protein misfolding, ER stress, autophagy dysregulation, activation of apoptosis and interaction with proteins involved in the development of neurodegeneration, such as α-synuclein and β-amyloid, and alter their structures (Malecki, 2001, Cervantes-Cervantes et al., 2005, Ha et al., 2007, Gunter et al., 2010, Salvador et al., 2010, Seo et al., 2013, Stephenson et al., 2013, Zhang et al., 2013, Angeli et al., 2014, Chen et al., 2016).

Of the heavy metals implicated in PD, Mn is one of the major elements that has been associated with parkinsonism.

1.3 Manganese neurotoxicity and Parkinson's disease

1.3.1 Manganese properties and uses

Manganese (Mn) is an essential trace metal required for normal development and function (Sadler, 1982, Horning et al., 2015). The primary route of human Mn intake is through the diet and it has been established that the daily uptake of Mn should be 2.3 mg for men and 1.8 mg for women (Greger, 1998). This daily requirement is reflected in the role of Mn as a cofactor for a variety of metalloproteins, including Mn-superoxide dismutase (MnSOD), arginase and pyruvate carboxylase. Mn is also essential for the function of a variety of enzymes, including glutamine synthetase and hydrolases (Wedler et al., 1982, Borgstahl et al., 1992, Kanyo et al., 1996, Reddi et al., 2009). Mn has 11 oxidation states, with Mn^{2+} and Mn^{3+} being the most common in biological systems, and its metabolism is associated with iron due to their similar redox behaviour (Claus Henn et al., 2011, Kim et al., 2013, Kwakye et al., 2015). Mn redox state influences its kinetics and toxicity (Reaney et al., 2002, Reaney et al., 2006). Mn valence states can vary within the body and *in vitro* results suggest that Mn^{3+} species are more cytotoxic than Mn^{2+} (Chen et al., 2001).

1.3.2 Manganese transport

As Mn is key to various cellular events but becomes toxic at high levels, the intracellular Mn concentration needs to be kept under strict control (Peres et al., 2016b). Mn enters the human body through ingestion, inhalation, dermal permeation, or administered via intravenous injection (Chen et al., 2018b). The principal route of Mn intake is via food consumption. In adults, only 3-5% of ingested Mn is absorbed through the intestinal epithelium, distributed to various tissues and then excreted via bile (Davidsson et al., 1989a) (**Figure 1.3**).

Mn can enter the brain via three routes: the blood-brain barrier (BBB), the blood-cerebrospinal fluid (CSF) barrier and the olfactory tract. BBB and the blood CSF barrier represent the main interfaces that regulate brain Mn homeostasis. The BBB consists of capillary endothelial cells and acts as a separator between blood and brain interstitial fluid (Abbott and Friedman, 2012). The blood-CSF barrier separates blood from the CSF and consists of epithelial cells of the choroid plexus (Strazielle and Ghersi-Egea, 2000). Mn can cross both barriers, utilising several different transport mechanisms (Crossgrove et al., 2003, Yokel, 2009, Bornhorst et al., 2012), however an *in vitro* study assessing Mn transfer to the brain, whilst monitoring its effect on the barrier properties, uncovered a stronger Mn sensitivity to the blood-CSF barrier compared with BBB (Bornhorst et al., 2012), suggesting it might represent the main route for Mn to reach the brain.

The olfactory route is an alternative pathway for Mn transport to the brain. The majority of clinical reported cases caused by Mn intoxication derive from occupational exposure. In particular, the adult population with the highest risk for Mn intoxication is represented by industrial workers, including miners (Rodier, 1955), smelters (Cook et al., 1974) and welders (Bowler et al., 2011), who inhale a significant amount of Mn-containing fume and dust. Mn is then absorbed in the lungs and enters the blood circulation. This led studies to investigate the nose and olfactory system as a possible route of direct entry to the CNS and recognised the olfactory pathway as a key contributor to Mn accumulation in the brain (Henriksson and Tjalve, 2000, Dorman et al., 2006a, Elder et al., 2006). In particular Elder et al. (2006) showed that Mn can be transported along the olfactory nerve directly into the olfactory bulb and further into the CNS, bypassing the protective blood brain barrier (BBB). Following 12 days of intranasal Mn exposure, Mn concentrations increased in the olfactory bulb, striatum, frontal cortex and cerebellum and caused neuroinflammatory changes, indicating that the olfactory neuronal

pathway represents an efficient way for transporting inhaled Mn into the CNS (Elder et al., 2006).

Intravenous administration of agents containing high levels of Mn represent an additional route of Mn exposure. In contrast to others, this exposure route bypasses the regulation at the gastrointestinal tract resulting in 100% absorption of the metal (Aschner and Aschner, 2005), which is quickly distributed to different tissues.

Mn transport has been mainly studied in mammalian systems and studies have largely focused on cellular influx mechanisms. Depending on its oxidative state, Mn can be imported in the central nervous system (CNS) via multiple membrane importers (Davidsson et al., 1989b). Mn^{2+} is the main form of Mn that exists in the blood and is normally complexed with different molecules, including α2-macroglobulin, albumin and citrate (Harris and Chen, 1994, Crossgrove et al., 2003, Nischwitz et al., 2008); Mn^{2+} is then secreted in the bile, and some can be oxidised to Mn^{3+} by ceruloplasmin (Jursa and Smith, 2009). The plasma carrier protein for Mn^{3+} is transferrin, which is synthesised in the liver and secreted in the plasma (Gunter et al., 2013). Mn^{3+} enters the brain via TfR-mediated mechanisms, whereas Mn^{2+} uptake occurs mainly as free ion species or by carrier-mediated processes (Aschner and Gannon, 1994, Crossgrove et al., 2003, Yokel, 2009). Mn can access neurons and glia via the divalent metal transporter 1 (DMT1), transferrin receptor (TfR), calcium (Ca) channels, zinc transporters (ZIP8 and ZIP14), members of the organic anion transporter polypeptide (OATP) or ATP-binding cassette (ABC) superfamilies (when bound to citrate) and diffusion (Crossgrove et al., 2003, Crossgrove and Yokel, 2004, Huang et al., 2004, Crossgrove and Yokel, 2005, Gunter et al., 2013). It is important to note that these transporters, in addition to Mn, also transport other metals, such as iron (Fe), copper (Cu), zinc (Zn), and calcium (Ca). Studies performed in yeast and *C. elegans* have reported a homeostatic regulation of influx transporters to regulate

Mn cellular levels depending on Mn deficiency and/or toxicity (Au et al., 2009, Jensen et al., 2009).

Efflux transporters represent an essential process that regulates Mn cellular levels. To date, not many transporters have been found to mediate Mn efflux. Four separate transporters/pumps have been found to be involved in Mn efflux: the solute carriers, ferroportin and SLC30A10, the secretory pathway Ca^{2+}-ATPase 1 (SPCA1) and ATPase 13A2 (ATP13A2) (Yin et al., 2010, Leitch et al., 2011, Mukhopadhyay and Linstedt, 2011, Madejczyk and Ballatori, 2012, Leyva-Illades et al., 2014). Although results have demonstrated that both ferroportin and SPCA1 are implicated in Mn efflux and detoxification in cell culture (Yin et al., 2010, Leitch et al., 2011, Mukhopadhyay and Linstedt, 2011, Madejczyk and Ballatori, 2012), their roles in mediating Mn detoxification at the whole organism level still remain to be investigated. On the contrary, SLC30A10 appears to have a crucial role in maintaining cellular Mn levels and protecting against Mn-induced toxicity (Leyva-Illades et al., 2014). ATP13A2 (*PARK9*) is a multifunctional protein highly expressed in the brain, especially in the SNpc, and mutations in ATP13A2 have been discovered in early onset parkinsonism (Di Fonzo et al., 2007), thus suggesting a link with PD. Its substrate specificity and physiological function are not fully understood, however studies suggest ATP13A2 is involved in lysosomal degradation of proteins, Mn homeostasis, and most recently Zn transport (Ramirez et al., 2006, Gitler et al., 2009, Ramonet et al., 2011, Chesi et al., 2012). Various studies revealed an interaction between ATP13A2 and Mn. Loss of function of ATP13A2 enhanced Mn toxicity, promotes α-synuclein accumulation and cause mitochondrial dysfunction. Expression of ATP13A2 was shown to exert a protective role against Mn- and α-synuclein-induced toxicity. In addition, ATP13A2 was upregulated in response to Mn treatment (Gitler et al., 2009, Tan et al., 2011, Kong et al., 2014). These results suggest that ATP13A2 can transport Mn from the cytosol to the lumen of lysosomes, and thus, act as a Mn efflux transporter. Ultimately, they reveal a connection

between PD genetics (α-synuclein and *PARK9*) and an environmental risk factor (*PARK9* and Mn).

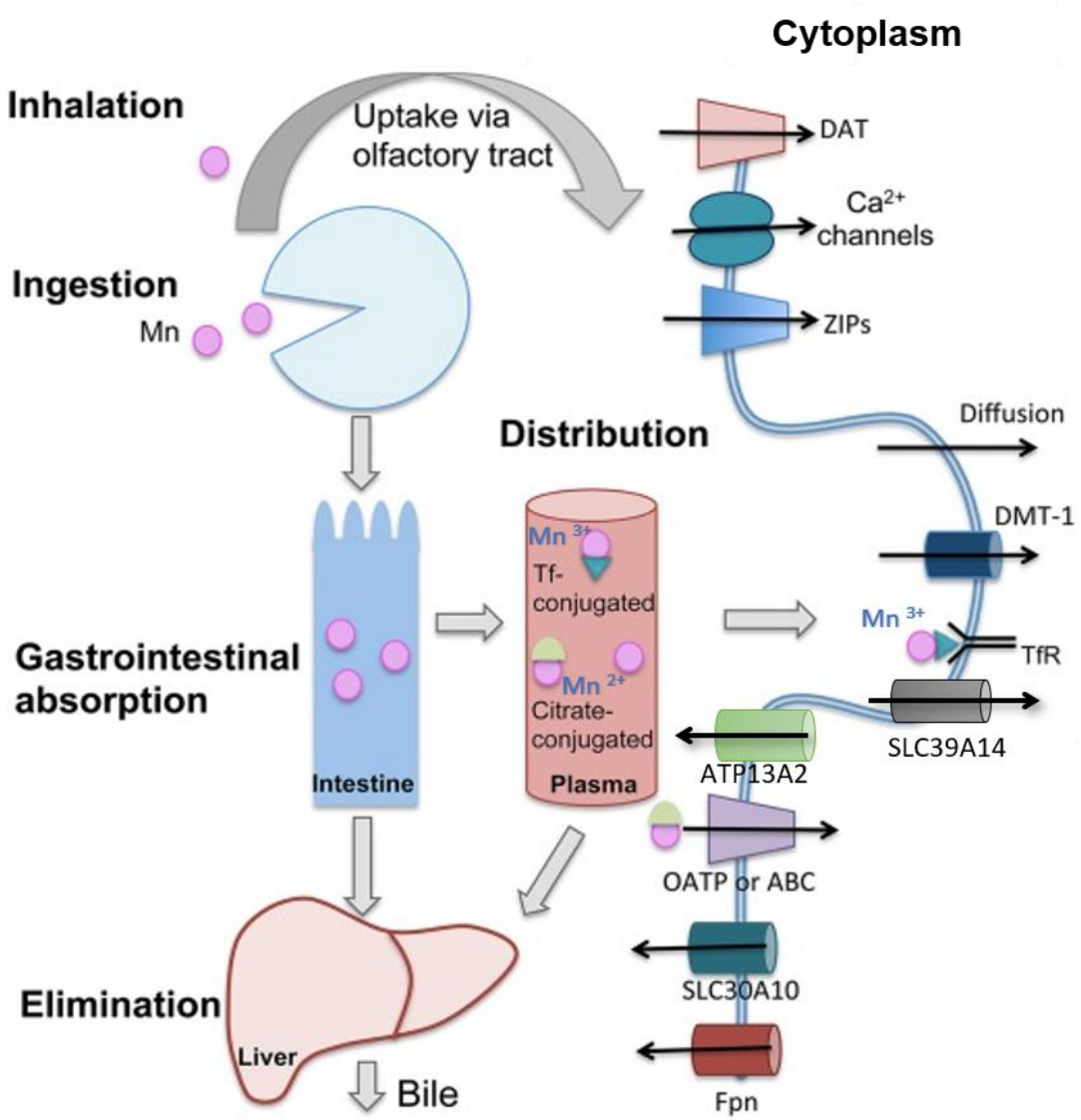

Figure 1.3 Overview of Mn metabolism and mechanisms of transport. Only 3–5% of ingested Mn is absorbed through the intestinal epithelium and the majority is excreted via bile. The image shows that in plasma, Mn is either conjugated with transferrin (Tf) or citrate and can then be distributed to various tissues. Mn can cross the BBB and access neurons and glia. Several proteins are implicated in Mn transport across the plasma membrane. When conjugated with Tf and recognized by the transferrin receptor (TfR), Mn is endocytosed and can enter the cytoplasm through DMT-1. When conjugated to citrate Mn may be carried by members of the organic anion transporter polypeptide (Oatp) or ATP- binding cassette (ABC) superfamilies. Mn can also cross the plasma membrane via diffusion or through the dopamine transporter (DAT). Given their similarities (valence), Mn can cross Ca^{2+} channels in mitochondria. SLC30A10 and ferroportin and ATP13A2 are three of the known Mn efflux transporters known to export Mn in the extracellular space. SLC39A14 represents the newly discovered Mn^{2+} influx transporter. Adapted from Peres et al., (2016a).

1.3.3 Manganese toxicity

Despite its essentiality, excessive and prolonged exposure to Mn can lead to its accumulation in the basal ganglia, triggering a disease referred to as Manganism. This is characterised by motor impairments, behavioural changes and cognitive alterations (Couper, 1837). A population-based case-control study assessed the occupational exposures to several heavy metals including Mn and suggested that chronic occupational exposure to Mn (>1 mg/m^3) is a risk factor for PD (Gorell et al., 1999). Hypermagnesemia can also occur in individuals with chronic liver failure (Hauser et al., 1994, Krieger et al., 1995) or patients receiving total parenteral nutrition (Fitzgerald et al., 1999, Bertinet et al., 2000). Further, studies have shown an association in patients undergoing hemodialysis and elevated serum Mn levels, accompanied with changes in the basal ganglia (da Silva et al., 2007). Interestingly, studies revealed that both humans and rats with chronic Fe deficiency could accumulate Mn at high levels in the basal ganglia (Herrero Hernandez et al., 2002, Kim et al., 2005, Fitsanakis et al., 2008, Fitsanakis et al., 2011). These results indicate that changes in Fe dietary, whether increased or decreased, could contribute to Mn deposition in the brain and this could be due to the competition of Fe and Mn for shared metal transporters. Furthermore, individuals that consume well water containing high levels of the metal (Kawamura et al., 1941, Wasserman et al., 2006) or soy-based infant formulas (Krachler and Rossipal, 2000) are at higher risk for Mn intoxication. In addition to environmental exposure, genetic mutations have also been implicated in Mn neurotoxicity (discussed in section 1.3.4).

Various studies have reported that Mn accumulates mainly in the liver, brain and bone (Rahil-Khazen et al., 2002, Krebs et al., 2014, Liu et al., 2014), however the brain is the most susceptible organ to Mn intoxication as most of the patients with Mn poisoning show symptoms of neurological dysfunction. Neurons are more vulnerable to Mn intoxication possibly due to their long lifespan and high energy demand. In particular, the ability of Mn to induce reactive

oxygen species (ROS) and alter ATP production (Martinez-Finley et al., 2013), may render neurons more suspectable the metal. Given its paramagnetic property, brain Mn can be detected using T1-weighted magnetic resonance imaging. Brain MRI results from welders and smelters exposed to Mn have shown that it primarily accumulates in the striatum, *globus pallidus* (GP) and SN (Yamada et al., 1986, Jiang et al., 2007, Dydak et al., 2011).

Clinical effects of Mn toxicity also include psychiatric disturbances and cognitive deficits as evidenced by a study performed in welders (Josephs et al., 2005). Several studies in non-human primates were carried out to assess the behavioural, neuroimaging and neuropathological consequences of chronic Mn exposure. They reported that animals developed subtle deficits in spatial working memory, reduced spontaneous activity and manual dexterity, in addition to an increase in compulsive-like behaviours (Schneider et al., 2006, Schneider et al., 2009, Schneider et al., 2015).

In addition to neuronal loss and behavioural changes caused by Mn exposure, numerous studies have described pathologic changes in the GP, a region that is rich in γ-aminobutyric acid (GABA) projections (Macdonald and Olsen, 1994). GABA is known as the most abundant inhibitory neurotransmitter in the adult brain, located in medium spiny neurons of the striatum, where it mediates DAergic activity (Ade et al., 2008). Yamada et al. (1986) reported a loss of GABAergic cells, reduction of myelinated fibres and moderate astrocytic proliferation following chronic Mn poisoning. Studies performed in Mn-treated non-human primates, further confirmed that GABAergic neurons were affected in the GP (Eriksson et al., 1987). Interestingly the effects of Mn toxicity on GABAergic neurotransmission are controversial. Some studies associate exposure to Mn with significantly elevated striatal GABA levels (Gwiazda et al., 2002, Garcia et al., 2006, Reaney et al., 2006, Anderson et al., 2008, Fordahl et al., 2010), while others report reduced GABA levels (Erikson et al., 2002, Takeda et al., 2002, Struve et al., 2007, Stanwood et al., 2009). Despite the inconsistency of

studies examining the effects of Mn on the GABA system, it is clear that the GABAergic system is affected by Mn exposure. More studies are needed to establish whether GABAergic cells are directly impaired by Mn accumulation or whether GABA variations are the result of any other changes in basal ganglia circuitry.

Another crucial neurotransmitter in the brain that plays a key role in movement coordination and cognition is dopamine (DA), synthesised in DAergic terminals by the tyrosine hydroxylase (TH) enzyme. The majority of the studies assessing Mn-induced neuro-chemical and pathological changes have focused on the DAergic system due to its association with movement control. Although yet to be fully understood, there is increasing evidence of Mn accumulation in DA-rich brain regions, causing a reduction in DA levels in the striatum (Seth and Chandra, 1984, Tran et al., 2002). As DAT has been hypothesised to mediate Mn transport, Erikson et al. (2005) assessed changes in Mn accumulation in dopamine transporter knockout (DAT-KO) mice compared to WT. Their results clearly displayed reduced Mn in the striatum of exposed DAT-KO mice compared to WT, suggesting DAT involvement in facilitating striatal Mn accumulation. Other studies have shown that subcutaneous injection in mice or intravenous injection of Mn in non-human primates caused a decrease in striatal DA release (Olanow et al., 1996, Guilarte et al., 2006a, Khalid et al., 2011). Additionally, following acute intraperitoneal Mn injections, disruption in multiple neurotransmitter systems, including 3,4-dihydroxyphenylacetic acid (DOPAC) and homovanillic acid (HVA), were observed in the rat brain. These deficits could be responsible, in part, for the described locomotor deficits (O'Neal et al., 2014).

Evidence suggesting Mn can cause neuronal loss in the SNpc and induce neurodegeneration, derive from rodents either injected with Mn directly into the SNpc or the striatum (Diaz-Veliz et al., 2004, Zhao et al., 2009, Fernandes et al., 2010, Mo et al., 2016), intraperitoneally (Stanwood et al., 2009, Robison et al., 2015), via inhalation (Ordonez-Librado et al., 2010) or

by oral gavage (Langley et al., 2018). Several studies have investigated the correlation between Mn neurotoxicity on the expression of DA receptors (D_1 and D_2) and DAT, however results are controversial. Oral administration of $MnCl_2$ in neonate rats caused a reduction in D_1 receptors and DAT levels in the nucleus accumbens and the dorsal striatum and an increase in D_2 receptor expression in the prefrontal cortex (Kern et al., 2010). Nam and Kim (2008), showed that intraperitoneal injections of $MnCl_2$ caused a dose-dependent increase of striatal D_2 receptor expression at both mRNA and protein levels. However Seth and Chandra (1984) reported a significant reduction in striatal D_2 receptor levels in developing rats following Mn poisoning. These differences could be caused by various factors, such as duration of exposure, routes of administration, age of the experimental animals and Mn redox state (Bouabid et al., 2016).

1.3.4 Genetic disorders of manganese metabolism

Multiple metal transporters have been implicated in causing excess Mn accumulation and neurological disorders (Horning et al., 2015). The DMT-1, TFR and FPN1, mainly considered Fe transporters are also involved in Mn metabolic pathways, as evidenced by changes in Mn transport in mice harbouring deficits in Fe metabolism (Kim et al., 2013, Seo and Wessling-Resnick, 2015). Recently, transporters known for carrying Zn have also been implicated in Mn metabolism. The SLC30 (ZnT, zinc transporter) and SLC39 (ZIP, Zinc-Iron Permease) transporters maintain cellular Zn homeostasis in the body by operating in opposing directions (Huang and Tepaamorndech, 2013). ZnT proteins have dual roles and can function as cation diffusion proteins and reduce intracellular Zn concentrations either by transporting (efflux) the metal to the extracellular space or by sequestrating it into intracellular compartments (Huang and Tepaamorndech, 2013, Kambe et al., 2014). In contrast, ZIP proteins increase cytoplasmic

Zn concentrations when depleted, through influx at the plasma membrane or from endosomes, mitochondrial and lysosomes (Lichten and Cousins, 2009, Jeong and Eide, 2013).

Recent studies have shown that alterations in function/localization of ZnT10 (SLC30A10) cause parkinsonism and dystonia with hypermagnesemia (Quadri et al., 2012, Tuschl et al., 2012). Affected patients were born to consanguineous parents and harboured homozygous *SLC30A10* mutations (missense or frameshift mutations). SLC30A10 was found to be widely expressed in the basal ganglia and serum Mn appeared to be increased by10-fold compared to normal levels. These patients had no history of exposure to high Mn levels, indicating that loss-of-function mutations in *SLC30A10* are associated with Mn retention (Quadri et al., 2012, Tuschl et al., 2012). To further investigate the function of the SLC30A10 protein and understand why mutations in this gene caused parkinsonism, Leyva-Illades et al. (2014) performed a combination of mechanistic and functional studies *in vitro* using HeLa cells and primary midbrain neurons and *in vivo* using *C. elegans*. Their results demonstrated that SLC30A10 is a cell surface-localized Mn efflux transporter that protects against Mn-induced toxicity by reducing its intracellular levels (Leyva-Illades et al., 2014). SLC30A10 mutations block the transporter ability to execute its efflux activity, promoting Mn accumulation. Using imaging tools, Carmona et al. (2019) confirmed the role of SLC30A10 in HeLa cells expressing either SLC30A10 WT or the disease-causing 105–107 mutant (SLC30A10-Δ105-107). They further identified the Golgi apparatus as the main compartment of Mn accumulation in SLC30A10 mutants, inferring possible interactions with the vesicular trafficking complex as disease causative (Carmona et al., 2019). Collectively, these results describe the cellular function of SLC30A10 and mechanisms by which mutations in this protein affect Mn homeostasis and contribute to the progression of a familial parkinsonian syndrome.

The liver has a key role in maintaining Mn homeostasis in the body as it represents the major route for its elimination, by secreting excess Mn into the bile (Papavasiliou et al., 1966, Roth,

2006). Patients with mutations in the hepatic metal ion transporter SLC39A8 have been linked, contrarily to SLC30A10, to reduced blood Mn levels (Boycott et al., 2015). Mn deficiency causes reduced activity of Mn-dependent enzymes including the β-1,4-galactosyltransferase and MnSOD. This leads to a congenital glycosylation disorder, as well as mitochondrial deficiency (Park et al., 2015b, Riley et al., 2017). Lin et al. (2017) showed that both *SLC39A8* global- and liver specific-knockout mice developed markedly decreased Mn levels in multiple organs. In addition, SLC39A8 was shown to localise to apical canalicular membrane of hepatocytes and promote Mn absorption from the bile to the hepatocytes, thereby reducing biliary Mn excretion (Lin et al., 2017). While the efflux transporter SLC30A10 and the influx transporter SLC39A14 (discussed later) work together to reduce Mn overload, SLC39A8 has an opposing role in promoting Mn uptake into the organism.

SLC39A14 was first discovered for its role in Zn uptake in the liver in response to acute inflammation. Studies performed by Liuzzi et al. (2005) showed that, amongst all the ZnT and ZIP transporter genes, ZIP14 (SLC39A14) was the most upregulated under inflammatory conditions (turpentine and LPS). Additionally, proinflammatory cytokines, such as IL-1β, stimulated the production of nitric oxide, which increased SLC39A14 transcriptional activity and enhanced Zn transport (Lichten et al., 2009). Despite the attention given to ZIP14 in relation to Zn transport, *in vitro* evidence suggested that this specific transporter also transports Mn (Fujishiro et al., 2014).

Recently, mutations in *SLC39A14* have indeed been shown to disrupt Mn homeostasis, resulting in its accumulation, particularly in the GP and the striatum and cause childhood-onset parkinsonism–dystonia (Tuschl et al., 2016). In addition, SLC39A14 was shown to function primarily as a Mn transporter, as homozygous SLC39A14 mutations impair Mn uptake, without affecting other metals. These results were corroborated in a zebrafish model carrying CRISPR-induced mutations in the SLC39A14 orthologue (Tuschl et al., 2016). MRI scans

from patients with both *SLC39A14* and *SLC30A10* mutations appear similar with both exhibiting cerebral Mn deposition, neuronal loss and spongiosis in the GP as well as myelin and axonal loss throughout various white matter regions (Lechpammer et al., 2014, Tuschl et al., 2016). Individuals with *SLC39A14* deficiency or mutations, however, do not develop polycythaemia or liver disease and their Fe levels appear to be normal (Tuschl et al., 2016). Under physiological conditions, Tuschl et al. (2016) suggest that Mn is absorbed in the duodenum and then transported into the liver via the SLC39A14 transporter and excreted into the bile via SLC30A10. On the contrary, SLC39A14 deficiency impairs hepatic Mn uptake and biliary excretion, causing Mn accumulation in the blood and brain. To test this hypothesis, Xin et al. (2017) generated and characterised global and hepatocyte-specific *SLC39A14*-knockout mice. Global *SLC39A14*-knockout mice (*SLC39A14*$^{-/-}$) displayed high Mn concentrations in the brain and other extrahepatic tissues, accompanied by motor deficits that were ameliorated by treatment with the metal chelator $Na_2CaEDTA$. In contrast, hepatocyte-specific *SLC39A14*-knockout mice did not develop Mn accumulation in the brain or other extrahepatic tissues and did not present motor deficits, except for significantly reduced hepatic Mn levels. These results suggest that selective hepatocytic loss of SLC39A14 expression is not sufficient to induce Mn accumulation. In addition, these mice exhibited normal Mn, Zn and Cu levels in all the studied tissues, except for the liver in which Mn levels were significantly reduced (Xin et al., 2017). Interestingly, hepatocyte-specific *SLC39A14*-knockout mice fed with a high Mn diet displayed increased Mn levels in the brain, but not in the liver, suggesting the brain of these mice is highly susceptible to Mn toxicity possibly caused by the inability to sequester Mn in the liver. Jenkitkasemwong et al. (2018) not only confirmed that SLC39A14 deficiency alters Mn homeostasis causing it to accumulate in the brain, but additionally showed that *SLC39A14*$^{-/-}$ mice also display impaired Mn excretion. Following Mn administration via tail vein injection, mice were housed individually in metabolic cages and feces/urine were

collected. The diminished excretion of Mn by *SLC39A14*$^{-/-}$ mice, six hours after Mn injection, appeared to be caused by impaired uptake of plasma Mn by the liver and pancreas compared to WT mice and therefore reduc Mn elimination in the bile (Jenkitkasemwong et al., 2018). Similarly to patients with loss-of-function mutations in *SLC39A14*, *SLC39A14*$^{-/-}$ mice display motor deficits, that cannot be corrected by a low-Mn diet.

Overall, identification of new inherited Mn transporter defects caused by mutations in three solute carrier proteins, SLC30A10, SLC39A14, and SLC39A8 has furthered our understanding on Mn homeostasis and Mn-related disease changes.

1.3.5 Differences between Manganism and Parkinson's disease

Regardless of the source, Mn overexposure can cause an irreversible, progressive condition that resembles PD. As stated previously, PD is known to be a motor disorder that results from selective loss of DAergic neurons in the SNpc. In contrast, Manganism is known to target GABAergic neurons in the GP and, relatively, spare the nigrostriatal DAergic system (Crossgrove and Zheng, 2004, Olanow et al., 1996) (**Figure 1.4**). Symptoms produced by Mn overexposure are characterised by dystonic movement of the extremities with tremor and a distinctive gait referred to as 'cock-walk' in which patients walk on their toes, leaning forward (Barbeau, 1984). Despite the noticeable presence of bradykinesia and rigidity, tremor is not as evident in Mn-overexposed patients (Lucchini et al., 2009). Further, levodopa, the most commonly used and effective drug in PD is ineffective in alleviating Mn-induced motor symptoms (Koller et al., 2004, Cersosimo and Koller, 2006). Guilarte et al. (2006a) also reported that monkeys repeatedly exposed to Mn developed a deficit in DA release, with no changes in striatal DA concentrations or in DAT levels, suggesting a dysfunction rather than a degeneration of the DAergic system. Despite differences between these two disorders, Mn

could still be involved in PD pathogenesis by interacting with the genetic makeup of an individual and enhancing its susceptibility to develop or accelerate the progression of the disease. Epidemiological studies have investigated the relationship between PD and blood and/or urine levels of heavy metals and discovered an accumulation of Mn levels in PD patients (Fukushima et al., 2010, Fukushima et al., 2013). In addition, rodents exposed to Mn for four weeks displayed a significant accumulation of Mn in DAergic neurons as compared to controls (Robison et al., 2012, Robison et al., 2015).

Similar to PD, however, Manganism is a progressive neurodegenerative disorder, with only partial recovery of certain symptoms following elimination of the source for an extended period of time (Bowler et al., 2011).

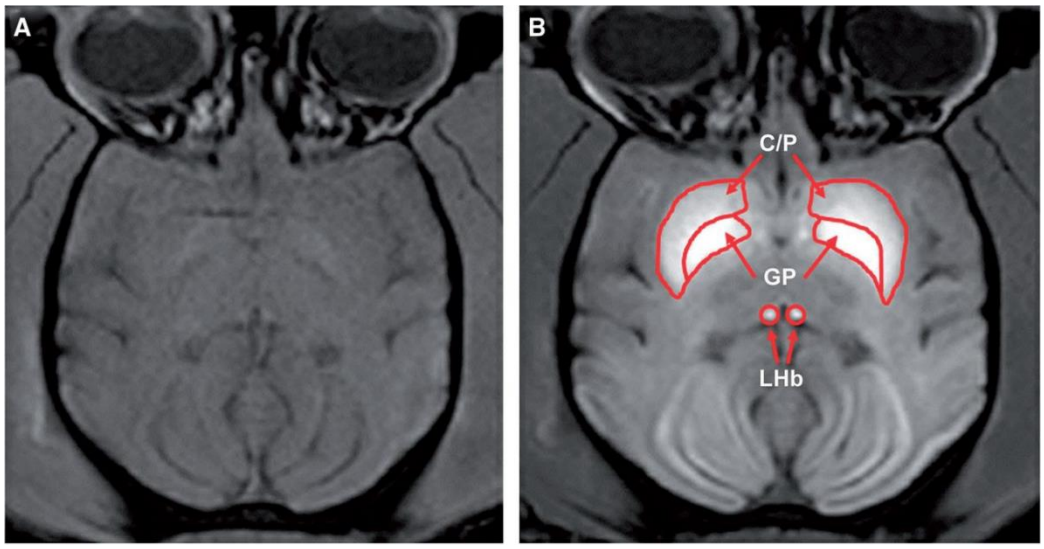

Figure 1.4 T1-weighted MRI images of the same monkey brain at the level of the globus pallidus before (A) and after (B) 17 months of Mn administration. Mn administration produces bilateral hyperintensive signal throughout the brain compared to baseline images. Abbreviation: C/P, caudate/putamen; GP, globus pallidus; LHb, lateral habenula. From Guilarte and Gonzales (2015).

1.4 Mechanisms of pathophysiology in Parkinson's disease

The aetiology of PD is complex and multi-factorial, however multiple studies have provided important insight into mechanisms of neuronal dysfunction and degeneration. These non-mutually exclusive mechanisms include mitochondrial dysfunction, accumulation of toxic misfolded proteins and impaired proteostasis and neuroinflammation.

1.4.1 Mitochondrial dysfunction

Mitochondria are well-defined cytoplasmic structures that have been long considered as vital organelles, primarily for their key role in ATP synthesis. They are also crucial for various other cellular processes including programmed cell death, innate immunity, autophagy, redox signalling, calcium homeostasis and stem cells reprogramming (Kamer and Mootha, 2015, Rambold and Pearce, 2018, Nikoletopoulou et al., 2013). By electron microscopy (EM) the mitochondrial ultrastructure is visible as a double membrane system, where the OMM faces the cytosol, and the IMM protrudes into the mitochondrial matrix, which contains mitochondrial DNA (mtDNA). The intermembrane space (IMS) is the compartment between the IMM and OMM. Over the last 30 years the concept of mitochondria as static and isolated structures has changed drastically. Indeed, mitochondria are extremely dynamic organelles that undergo constant morphological changes through fission/fusion processes (**Figure 1.5**). The balance between these two opposite processes is essential for regulating mitochondrial number, size and position within the cytoplasm and is referred to as 'mitochondrial dynamics' (Liesa et al., 2009). Neurons are highly active cells with a complex shape that require energy at distal location in relation to their soma and are thus highly dependent on mitochondrial function.

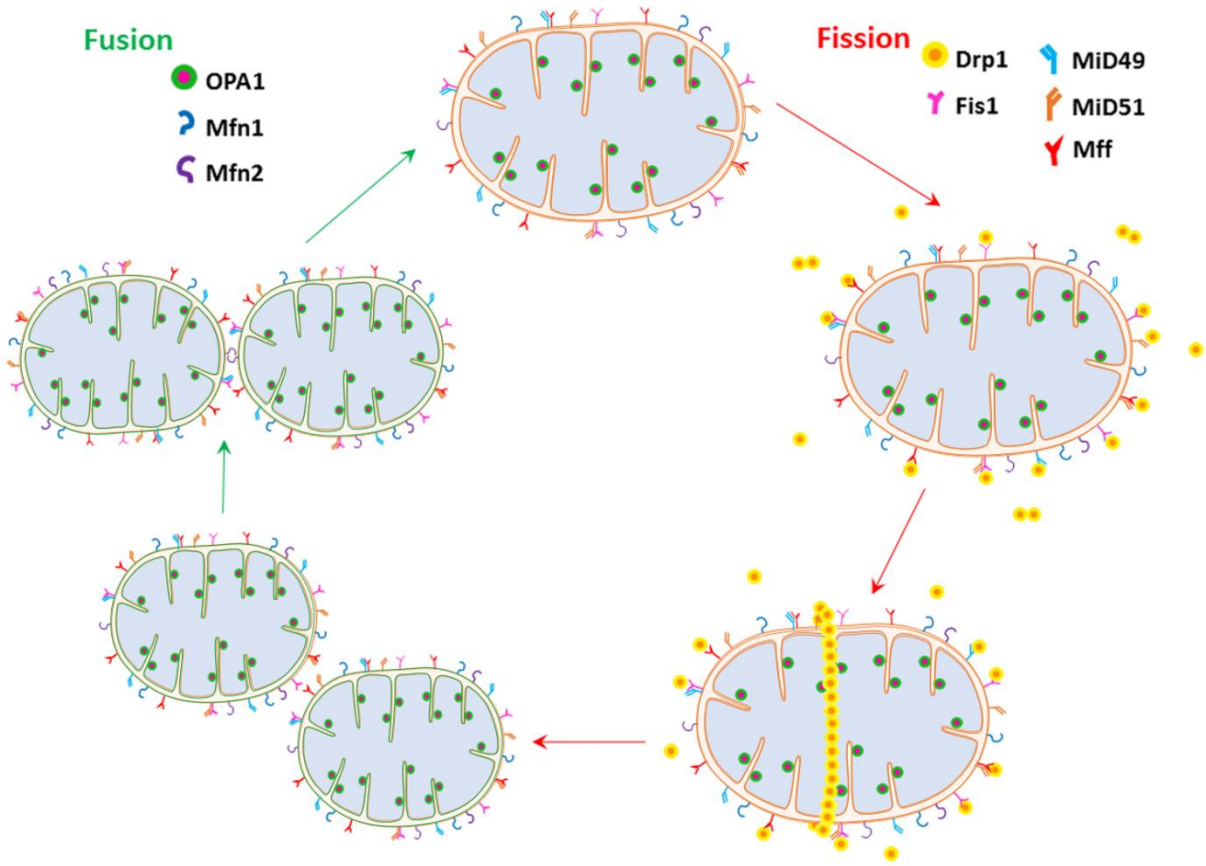

Figure 1.5 Schematic representation of mitochondrial fission and fusion processes. Mitochondrial dynamics represent a continuous process whereby pre-existing mitochondria alter their morphologic profile thus adapting to the specific demands of the cell. Following biogenesis, mitochondria may be broken into smaller, more mobile organelles through fission and fused to form larger, more respiratory active structures through fusion. During fission Drp1 translocates from the cytosol to the mitochondrial outer membrane, oligomerises and subsequently produces small and motile mitochondria. MFF and Fis1, along with MiD49 and MiD51, represent outer mitochondrial-anchored fission proteins required for Drp1 stabilization. Fusion is mediated by three mammalian proteins: Mfn1 and Mfn2 for outer membrane fusion, and OPA1 for inner membrane fusion. Adapted from Pinnell and Tieu (2017).

In mammals, mitofusins (Mfn1 and Mfn2) and optic atrophy 1 (OPA1) represent the major regulators of mitochondrial fusion. During fusion the coordination of the OMM and the IMM are required to generate larger mitochondria. This event promotes an exchange of substrates and mtDNA between healthy and dysfunctional mitochondria (also known as functional complementation), along with an increase of ATP supply (Chen and Chan, 2010, Youle and

van der Bliek, 2012). Genetic deletion of mitofusin proteins culminate in the progressive abrogation of fusion and causes mitochondrial dysfunction in both culture and tissues (Chen et al., 2003, Chen et al., 2005, Chen et al., 2010). Mfn2, in particular, has been implicated in physiological processes such as transport, ER tethering and calcium uptake (de Brito and Scorrano, 2008, Misko et al., 2010, Filadi et al., 2015). Neurons lacking Mfn2 have been associated with increased ER stress, decreased anterograde transport of mitochondria along microtubules, lower axonal and synaptic densities of mitochondria, and organelle accumulation in the soma (Baloh et al., 2007, Chen et al., 2007a, Pham et al., 2012). Among different cell types, neurons are particularly sensitive to Mfn2 defects as they require functional mitochondria located at dendrites and synaptic termini, to support proper ATP production and Ca^{2+} buffering (Celsi et al., 2009). Mfn2 mutations have been linked to a neurological disorder, characterised by degeneration of long peripheral nerves, known as Charcot–Marie–Tooth disease type 2A (CMT2A) (Zuchner et al., 2004). This disorder is a subtype of a heterogeneous group of congenital neuromuscular diseases that target motor and sensory neurons, known as CMT disease (Cartoni and Martinou, 2009).

On the other hand, fission requires the cytosolic dynamin related protein 1 (Drp1), a GTPase protein that uses energy released from GTP hydrolysis to promote division. The fission mechanism is still not fully understood, however, once recruited to the OMM by Mid49 and Mid51 (essential for the stabilisation of Drp1), by the mitochondrial fission factor (Mff) and fission-1 (Fis1), Drp1 assembles into a dimeric ring like structure and constricts the mitochondria until fission takes place (Ingerman et al., 2005). The resulting mitochondria are smaller and more motile and can therefore be transported to distal parts of the cell. Further, fission segregates mitochondria with healthy and damaged mtDNA, marks them for mitophagy and facilitates mitochondrial quality control (Scott and Youle, 2010, Youle and van der Bliek, 2012, Archer, 2013). Mutations in Drp1 and Mff have been implicated with severe neurologic

phenotypes in humans (Waterham et al., 2007, Vanstone et al., 2015, Koch et al., 2016, Nasca et al., 2018). For example, Koch et al. (2016) established that Mff loss of function is associated with early-onset Leigh-like basal ganglia disease. Waterham et al. (2007) reported microcephaly, abnormal brain development, optic atrophy and hypoplasia in a new born with defects in both mitochondrial and peroxisomes' fission, as well as a heterozygous, dominant-negative mutation in Drp1 (coding-sequence mutation in the middle domain of Drp1). In addition, Drp1-null mice die by embryonic day 11.5 from developmental defects of the cerebellum (Wakabayashi et al., 2009). This lethality is not caused by the loss or reduction of ATP levels, but is due to swollen mitochondria in Purkinje cells and impaired apoptosis (Wakabayashi et al., 2009). Further, post-natal deletion of Drp1 in Purkinje cells have been shown to cause mitochondrial tubules to elongate due to excess fusion and form large mitochondria, oxidative stress, respiratory dysfunction, accumulation of ubiquitinated proteins and consequently neurodegeneration (Kageyama et al., 2012). Mitochondrial defects were, however, restored with antioxidants treatment (Kageyama et al., 2012). These results not only show that Drp1 is required for embryonic and brain development in mice, but also demonstrate how Drp1 may suppress oxidative damage and promotes neuronal survival. Therefore, a balance of mitochondrial dynamics is not only necessary for mitochondrial morphology but also for cell function and survival.

The first evidences that implicated mitochondrial dysfunction in the development of PD derived from studies performed in the late 80's. Results showed that the activity of the mitochondrial complex I, in the SN of PD patients, was significantly decreased (Bindoff et al., 1989, Schapira et al., 1989). Mutations in the mtDNA have also been related to PD. Mitochondrial oxidative phosphorylation requires both mitochondrial and nuclear DNA-encoded proteins. mtDNA encodes 13 proteins that are all subunits of respiratory chain complexes, 22 tRNAs, and 2 rRNAs. Studies performed in DAergic neurons of the SNpc

revealed that these had high levels of mtDNA deletions. MtDNA mutations were somatic and associated with respiratory chain deficiency (Bender et al., 2006). In particular, the highest rates of mtDNA deletions (>60%) were observed in neurons with deficient cytochrome c oxidase (COX) activity (Kraytsberg et al., 2006). These results suggest that mtDNA deletions may be directly responsible for impairing cellular respiration. It is important to note that mtDNA mutations were specific to DAergic neurons and this could potentially increase their susceptibility to oxidative stress, which could then contribute to their selective loss in PD (Bender et al., 2006, Kraytsberg et al., 2006). This suggestion is supported by studies performed in MitoPark mice, which present a deletion of the mitochondrial transcription factor A (*Tfam*) gene, master regulator of mtDNA transcription, in DAergic neurons (Ekstrand et al., 2007). Ekstrand et al. (2007) discovered that DAergic neurons of the SNpc had reduced mtDNA expression and respiratory chain impairments. Mitochondrial impairment led to a deterioration of motor function along with intraneural inclusions and loss of DAergic neurons. Impairment in the release of DA was also found in six-eight weeks old MitoPark mice suggesting that nigrostriatal dysfunction could proceed any behavioural deficits in this genetic PD model (Good et al., 2011). No strong evidence clearly shows that mtDNA mutations are a major primary cause of PD, however mtDNA mutations could accumulate with time as a consequence of cellular stress and mitochondrial replication errors. Once the mtDNA mutations are too severe, the resulting respiratory deficiency could contribute to neuronal degeneration and cell death. Of note, complex I is particularly vulnerable to mtDNA modifications, since seven of its subunits are encoded by mtDNA (Janssen et al., 2006).

Mitochondrial dysfunction associated with PD pathogenesis can also result from impaired mitochondrial trafficking. Mitochondria move along axons relying on motor proteins and microtubules via retrograde (towards the cell body) and anterograde (towards the terminus) transport. Retrograde transport is controlled by dynein motors while anterograde movements

are driven by kinesin motors (Devine and Kittler, 2018). MPP^+ was reported to affect mitochondrial motility and alter mitochondrial directionality, by reducing anterograde transport and increasing retrograde, thus impeding delivery of mitochondria to synapses (Kim-Han et al., 2011). Additionally, Sterky et al. (2011) showed that DA neurons of MitoPark mice exhibited an impaired anterograde axonal transport of mitochondria along with respiratory chain deficiency and mitochondrial fragmentation. Of particular interest for PD pathogenesis is the axonal trafficking of α-synuclein and mitochondria. α-synuclein oligomers were shown to impair anterograde axonal transport of mitochondria by causing subcellular changes in adaptor motor proteins and energy deficits (Prots et al., 2018).

Various epidemiological studies have also demonstrated that pesticides and other toxins involved in PD pathogenesis can directly target mitochondria and induce neurodegeneration. The first direct evidence that linked mitochondrial dysfunction and PD came from the discovery of MPTP, a neurotoxin that caused chronic parkinsonism in drug-abused patients (Langston et al., 1983). MPP^+ the known metabolite of MPTP, is known for its ability to inhibit mainly complex I but also complex III and IV (Nicklas et al., 1985, Desai et al., 1996), decrease ATP production, generate ROS (Fabre et al., 1999), reduce mitochondrial gene expression (Piao et al., 2012), alter mitochondrial proteins such as chaperones, metabolic enzymes, oxidative phosphorylation-related proteins, inner and outer mitochondrial proteins (Burte et al., 2011), induce changes in proteins involved in DA signalling, ubiquitin system, calcium signalling, oxidative stress response and apoptosis (Zhang et al., 2010). In addition, chronic and systematic exposure to rotenone was reported to inhibit complex I activity (Betarbet et al., 2000). Paraquat causes extensive mitochondrial oxidative damage by accumulating in the mitochondrial matrix and generating free radicals (Cocheme and Murphy, 2008). Maneb was also shown to inhibit mitochondrial complex III (Zhang et al., 2003a).

Heavy metals are crucial for enzyme function and protein folding, but in excess they can lead to neurotoxic oxidative processes. As mitochondria are highly susceptible to oxidative stress caused by radicals produced during ATP synthesis, mitochondrial bio-metal homeostasis must be well regulated to safely control the redox potential of metal enzyme cofactors (Grubman et al., 2014). Cu, Zn, Fe and Mn are all localised to various compartments of the mitochondria and a range of cofactors, chaperones and ion pumps regulate their levels and function (Pierrel et al., 2007). Relevant to this work, mitochondria are known to be one of the major sites of Mn-induced cellular dysfunction (Cotzias and Greenough, 1958). In fact, Mn can be rapidly transported into the mitochondrial matrix as Mn^{2+} via the calcium (Ca^{2+}) uniporter channel. Slow export, however, occurs via the Na^{+}-independent Ca^{2+} -channel. An overexposure of Mn, therefore, causes an increased accumulation of Mn within the mitochondria and subsequent inhibition of Na^{+}-dependent and -independent Ca^{2+} -efflux; this results in elevated Ca^{2+} levels within the mitochondrial matrix (Gavin et al., 1990), which can promote ROS formation and inhibit the ETC (Kowaltowski et al., 1995, Kruman and Mattson, 1999). Generally, the superoxide radical ($O_2^{-\bullet}$) is the first ROS species that is formed. This can be converted into hydrogen peroxide (H_2O_2) by superoxide dismutase (MnSOD catalyses the reaction in the brain mitochondria). In the presence of Mn or other metals, H_2O_2 can be converted through the Fenton reaction, into the very reactive hydroxyl radical ($OH^{\bullet}$) (Goldstein et al., 1993). The ROS generated by increased mitochondrial Mn has been demonstrated to initiate a cascade of events including the opening of the permeability pore, loss of membrane potential, reduction in ATP synthesis and mitochondrial swelling, that will eventually lead to cellular apoptosis (Gavin et al., 1990, Gavin et al., 1992, Kowaltowski et al., 1998, Gavin et al., 1999, Barhoumi et al., 2004, Gunter et al., 2012, Martinez-Finley et al., 2013).

In addition, studies have shown that Mn can be actively sequestered and accumulate in the mitochondria, resulting in increased formation of ROS and subsequent inhibition of OXPHOS

(Gavin et al., 1990, Gavin et al., 1992, Kruman and Mattson, 1999). Zhang et al. (2003b) reported that chronic injection of $MnCl_2$ in both male and female rats for six weeks, directly inhibited complex I-IV of brain mitochondria. Mn toxicity was further associated with mitochondrial dysfunction and DNA fragmentation in rat primary neuron cultures (Malecki, 2001). Astrocytic mitochondria have also been shown to be a direct target of Mn-induced toxicity, as reported by studies examining mitochondrial calcium responses in primary cortical astrocytes stimulated with ATP (Tjalkens et al., 2006). In addition, Mn reduces mitochondrial membrane potential and increases ROS in cultured astroglial cells (Barhoumi et al., 2004).

The above studies described the effects of Mn on oxidative phosphorylation, however not much is known about the effects of Mn toxicity on mitochondrial dynamics. Alaimo et al. (2013) used human Gli36 cells to investigate possible mitochondrial dynamics changes in Mn-exposed human astrocytes. Results indicated that, in addition to triggering the mitochondrial apoptotic pathway Mn causes a deregulation in mitochondria-shaping proteins (Opa-1, Mfn-2 and Drp-1) expression levels (Alaimo et al., 2013). In a subsequent study, Alaimo et al. (2014) demonstrated that, in addition to $\Delta\psi m$ dissipation, high concentrations of Mn (750 µM $MnCl_2$) generate an imbalance in fusion/fission equilibrium resulting in an increased mitochondrial fragmentation. The authors showed a reduced presence of Opa1 on mitochondria and an increased translocation of Drp1 to the mitochondria following Mn exposure, indicative of increased mitochondrial fission. These defects were restored by inhibiting Drp1 both genetically and pharmacologically (Alaimo et al., 2014). Sarkar et al. (2018) further examined the interrelationship between mitochondrial dysfunction and astrocytic inflammation in Mn neurotoxicity. Their results clearly indicated that Mn induces neuroinflammation in astrocytes through mitochondrial bioenergetics impairment. Treatment with mito-apocynin (a mitochondrial targeted antioxidant) attenuated these mitochondrial deficits (Sarkar et al.,

2018). Collectively these studies imply that restoring mitochondrial health in various cell types could be neuroprotective against Mn-induced neurotoxicity.

The role of mitochondrial dysfunction in PD has been further strengthened following the discovery and study of genes implicated in familial PD. Strong evidence in both human and animal PD models show disruptions in mitochondrial dynamics and transport, bioenergetics defects, complex I inhibition and increased ROS (Moon and Paek, 2015, Park et al., 2018).

Many PD-associated *PARK* genes have been linked to mitochondrial dysfunction. In particular, the association between a-synuclein, PINK1, Parkin pathologies and mitochondrial dysfunction may play a crucial role in PD. Various studies have investigated the interplay between mitochondria and α-synuclein physiologically and in pathological conditions. α-synuclein is now known to be a key physiological modulator of mitochondrial homeostasis by interacting with directly with MAM and regulating ATP synthase to improve the efficiency of ATP production (Nakamura et al., 2008, Guardia-Laguarta et al., 2014, Ludtmann et al., 2016). This interaction allows a-synuclein, when overexpressed or mutated, to cause structural changes in mitochondria, oxidative stress and/or bioenergetic defects (Hsu et al., 2000, Martin et al., 2006, Stichel et al., 2007, Devi et al., 2008, Parihar et al., 2008, Liu et al., 2009a, Chinta et al., 2010, Loeb et al., 2010, Nakamura et al., 2011). Accumulation of WT α-synuclein was shown to reduce complex I activity and promote ROS generation in DAergic neurons of PD patients (Devi et al., 2008). Recent studies have established that mice overexpressing human WT α-synuclein under the Thy1 promoter exhibit mitochondrial dysfunction (between four and eight months of age) in DAergic neurons, long before the onset of striatal DA loss, which occurs at 14 months (Subramaniam et al., 2014). Further, A53T human α-synuclein overexpressing transgenic mice displayed early-onset mitochondria abnormalities, which preceded DAergic degeneration (Chen et al., 2015a). Di Maio et al. (2016) discovered that certain post-translationally modified forms of α-synuclein (soluble oligomers, DA-

modification, and S129E) can bind specifically to TOM20 preventing its interaction with the co-receptor, TOM22 and impair mitochondrial protein import. Interestingly, in both α-synuclein overexpressing WT mice and post-mortem human tissue from PD brains, mitochondrial dysfunction was associated with TOM40 reduction, a specific component of the mitochondrial transport machinery. TOM40 deficits led to increased mitochondrial DNA deletions, oxidative DNA damage, decreased ATP production and altered levels of complex I proteins (Bender et al., 2013). Bender et al. (2013) also showed that overexpression of TOM40 rescued energy deficits and oxidative damage in these mice.

Dynamic processes such as mitochondrial fusion/fission and axonal transport are also affected by α-synuclein. Severe mitochondrial fragmentation and reduced motility both *in vitro* and *in vivo* have been previously shown in overexpressing WT and mutated forms of α-synuclein (Kamp et al., 2010, Nakamura et al., 2011, Gui et al., 2012, Chen et al., 2015a, Bido et al., 2017). In a zebrafish model of α-synuclein toxicity, sensory neurons displayed fragmented mitochondria, which could occasionally cause mitochondrial swelling within the axon (O'Donnell et al., 2014). A recent study investigated the detrimental effect of A53T mutation on primary neurons and found that mitochondrial motility was selectively impaired, as was mitochondrial membrane potential and respiratory capacity (Li et al., 2014a). α-synuclein has also been shown to bind to the promoter region of PGC1α, under oxidative stress conditions and inhibit the expression of downstream genes, therefore impacting and reducing mitochondrial biogenesis (Siddiqui et al., 2012). Impairment of complex I function and increased production of reactive oxygen species ROS have been observed in α-synuclein overexpressing or A53T mutated cells (Devi et al., 2008, Loeb et al., 2010, Reeve et al., 2015). In addition, experiments in recombinant WT and mutant α-synuclein rats were shown to affect mitochondrial membrane potential and ATP production (Banerjee et al., 2010). In summary, α-synuclein can impair mitochondrial function at multiple levels: by impairing the electron

transport chain (ETC), causing an imbalance in mitochondrial dynamics and reducing mitochondrial biogenesis.

Abnormalities in mitochondrial function and morphology have additionally been reported in multiple *in vitro* and *in vivo* models of PINK1 and Parkin. In particular, PINK1 deficient and PD-associated mutant models feature reduced mitochondrial membrane potential, ATP levels, decreased respiratory capacity, increased mitochondrial Ca levels and permeability transition pore opening, increased oxidative stress, protein aggregation and reduced proteosomal activity (Gautier et al., 2008, Piccoli et al., 2008, Gandhi et al., 2009, Gegg et al., 2009, Liu et al., 2009b, Morais et al., 2009, Dagda et al., 2009, Cui et al., 2010, Heeman et al., 2011, Gautier et al., 2012, Morais et al., 2014). Additionally, *PINK1*-deficient mice display complex I deficits (Gautier et al., 2008, Morais et al., 2014) and reduced calcium buffering capacity (Akundi et al., 2011) in isolated brain mitochondria. Aged *Parkin* knock-out brains further exhibit deficits in the expression of multiple mitochondrial proteins, causing reduced respiratory capacity and increased oxidative damage (Palacino et al., 2004, Periquet et al., 2005, Stichel et al., 2007).

It is evident that mitochondria are a common pathogenic target for both genes and environmental toxicants linked to PD. Given the extensive and key role of mitochondria, ranging from the classic "powerhouses" of the cell, to maintaining calcium homeostasis, controlling synaptic activity, initiating apoptosis and the spread of α-synuclein (discussed in 1.4.2), it is not surprising that impaired mitochondrial function would negatively impact neuronal function and viability and contribute to PD pathology.

1.4.1.1 Drp1

In vitro and *in vivo* studies have shown that DAergic neurotoxins MPP+, 6-OHDA and rotenone could induce Drp1 hyperactivity and mitochondrial fragmentation leading to DAergic cell death in neuronal cultures (Barsoum et al., 2006a, Meuer et al., 2007, Gomez-Lazaro et al., 2008). Inhibition of Drp1 or overexpression of Mfn1 could prevent this neurotoxin-induced mitochondrial fission and neuronal cell death. Several groups have and highlighted the importance of Drp1 function and its potential as a therapeutic target in neurodegenerative disorders. In particular, inhibition of the mitochondrial fission factor Drp1, both genetically and using small molecules, was reported to protect cells from neurodegeneration in different models of PD (Dagda et al., 2009, Lutz et al., 2009, Cui et al., 2010). Mitochondrial division inhibitor 1 (mdivi-1) is a small-molecule inhibitor of Drp1, first characterised by Cassidy-Stone et al (2008). By directly binding to Drp1, mdivi-1 blocks its assembly into oligomeric ring structures and its GTPase activity, therefore interfering with its physiological function (Cassidy-Stone et al., 2008). Mdivi-1 has been used in multiple disease studies, and data suggest efficacy in several models of neurodegeneration. Xie et al. (2013) showed that mdivi-1 could exert neuroprotective effects against hippocampal neuron damage induced by seizures. Abnormal mitochondrial function and morphology induced by mutant $PINK1^{L347P}$ in N27 cells was prevented by exposing cells to 10 μM mdivi-1 (Cui et al., 2010). Recently, Bido et al. (2017) showed that mdivi-1 could reduce neurodegeneration, α-synuclein aggregation and mitochondrial fragmentation in a A53T-α-synuclein rat model of PD. In addition to mdivi-1, Qi et al. (2013) used a model of PD in neuronal cultures and demonstrated that the peptide P110 (selective Drp1 inhibitor) conferred neuroprotection against mitochondrial fragmentation and ROS production. Inhibition of mitochondrial fission also improved mitochondrial membrane potential and mitochondrial integrity by reducing apoptosis and restoring LC3-II puncta to control levels (Qi et al., 2013). Results indicating that P110 could provide

neuroprotective effects was further strengthened by Filichia et al. (2016) who reported that P110 could restore DAergic neuronal loss, DAergic nerve terminal damage and behavioural deficits caused by MPTP.

Drp1 function has also been targeted using genetic approaches, such as viral vectors that harbour dominant negative Drp1 mutations. These mutations are non-functional and impair Drp1 oligomer formation, preventing excessive fission. Stereotactic injection of recombinant adeno-associated viral (rAAV) to deliver Drp1 dominant negative K38A to the SN has been shown to attenuate neurotoxicity and restore pre-existing striatal DA release deficits in *PINK1*$^{-/-}$ and MPTP pre-treated mice (Rappold et al., 2014). The A395D dominant negative Drp1 mutation, first discovered in a neonate with microcephaly (Waterham et al., 2007) promoted mitochondrial elongation in HeLa cells as a consequence of decreased fission (Chang et al., 2010). A recent study compared the cellular impact of a novel Drp1 mutation, R403C, to the previously described A395D variant (Fahrner et al., 2016). The group reported that the R403C mutation, acting as a dominant-negative of Drp1, reduced Drp1 recruitment to the mitochondria and oligomerization, impairing mitochondrial fission activity. In addition, R403C mutation appeared less severe and more tolerated at the phenotypic and cellular level compare to the previously reported A395D mutation (Chang et al., 2010, Fahrner et al., 2016). Fan et al. (2019) also reported that blocking Drp1, using multiple approaches (gene silencing overexpression of K38A and mdivi-1), improved mitochondrial function and autophagic flux in experimental models of α-synuclein.

Overall, this evidence suggests that Drp1 inhibition could represent a potential treatment for PD.

1.4.2 α-synuclein aggregation and spread

Protein aggregation is a common theme underlying neurodegenerative diseases. Research in PD has largely focused on protein misfolding and aggregation given the association of α-synuclein gene mutations with familial forms of the disease and the discovery of the protein as the main component of LBs. Despite the controversy regarding the native conformation of α-synuclein and which conformation is more susceptible to aggregation, it is now clear that transition to an aggregated β-sheet conformation is necessary for insoluble inclusions or LBs (Miraglia et al., 2018). The aggregation process has been suggested to be a nucleation reaction that is sought to develop in a sequential way. Here, soluble species undergo a process that generates oligomeric species, which can then form protofilaments and eventually mature fibrils (**Figure 1.6**).

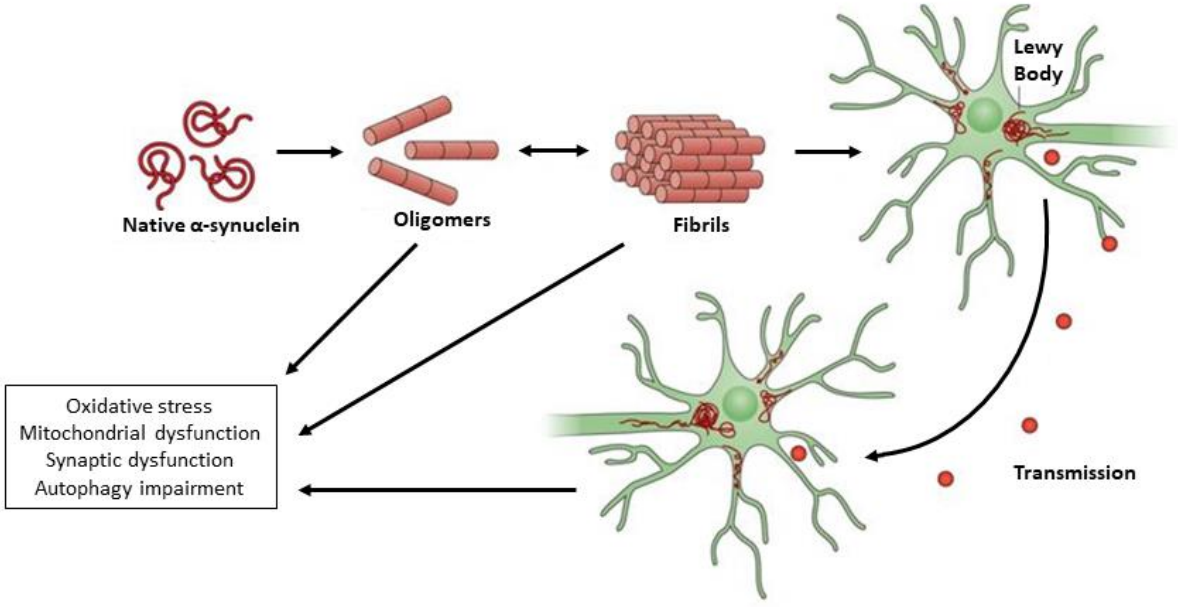

Figure 1.6 Hypothetical model of α-synuclein toxicity and spread of pathology in PD. Schematic illustration of the stepwise process whereby normal, highly soluble a-synuclein misfolds and is converted into pathological oligomers and higher-order aggregates that fibrillise and deposit into LBs in affected neurons of the PD brain. α-synuclein can also be transmitted inter-cellularly. Several of the proposed toxic consequences of the accumulation and spread of α-synuclein are illustrated in the right part of the figure. Adapted from Kingwell (2017).

In vitro evidence suggests a precise time course, with an initial lag phase, in which α-synuclein monomers are converted into insoluble β-sheet rich structures (nucleation), a growth phase and a plateau state (reached when the monomer concentration is depleted) that terminates with the accumulation of protofibrils and amyloid fibrils (Lashuel et al., 2002, Vilar et al., 2008, Cremades et al., 2012, Tuttle et al., 2016). *In vitro* results have also demonstrated that α-synuclein fibrils may have either a ribbon or a fibril structure (Bousset et al., 2013, Guo et al., 2013). In addition to fibrils, stable toxic oligomers of α-synuclein have also been described to accumulate during this process (Cremades et al., 2012, Chen et al., 2015b). Oligomers are defined as low-molecular weight aggregates, soluble or insoluble, that do not have a fibrillary organisation. Similar to α-synuclein fibrils, various forms of oligomers have been described *in vitro*, differing in size and morphology (Lashuel et al., 2002). α-synuclein fibrils are believed to grow by adding monomers onto existing aggregates rather than oligomers (Buell et al., 2014). Both oligomers and fibrils have toxic effects with different mechanisms of pathology.

The pathogenic aggregation of α-synuclein is a critical event in PD pathogenesis and it can be caused by both endogenous and exogenous factors, including metals and pesticides, genetic mutations, PTMs and protein-protein interactions (Deleersnijder et al., 2013). The hypothesis that α-synuclein fibrillation could worsen PD pathology and promote its disease progression derives from the discovery of two α-synuclein mutants (A53T and E46K), linked to early-onset PD, which exhibited an increased fibrillation propensity *in vitro* (Conway et al., 1998, Narhi et al., 1999, Greenbaum et al., 2005). In addition, a novel pathogenic mutation of α-synuclein (H50Q) has also been shown to accelerate α-synuclein aggregation (Appel-Cresswell et al., 2013, Proukakis et al., 2013, Ghosh et al., 2013). On the contrary, other α-synuclein mutations (G51D, and A53E) associated with familial forms of PD have been proven to decrease α-synuclein fibrillation (Ghosh et al., 2014, Fares et al., 2014). Less agreement exists concerning the effects of the PD-associated A30P mutation, as this variant has been reported to either slow

(Lemkau et al., 2012) or accelerate α-synuclein aggregation (Narhi et al., 1999, Li et al., 2001, Lashuel et al., 2002, Li et al., 2002), or have no effect (Conway et al., 2000) compared to the WT protein. Overall, these studies suggest that α-synuclein fibrillation rate is not directly correlated to disease pathogenesis and that monitoring the effects of α-synuclein mutations on the oligomerisation rate could possibly resolve this complexity. Evaluation of α-synuclein oligomerisation kinetics may represent a promising approach since pre fibrillar α-synuclein oligomers have been suggested to be the most toxic entity responsible for DAergic loss in PD (Winner et al., 2011).

Studies performed on human *α*-synuclein transgenic mice revealed that the accumulation of oligomers mainly occurred at synaptic sites causing synaptic and neuronal degeneration (Rockenstein et al., 2014). Consistent with these results, oligomers have been found to reduce neuronal excitability (Kaufmann et al., 2016) and affect synaptic function by altering lipid raft composition and increasing N-methyl-D-aspartate (NMDA) receptor activation at postsynaptic membranes (Diogenes et al., 2012, Emanuele et al., 2016). These alterations can impact mitochondrial function (Sarafian et al., 2013), cytoskeletal architecture (Chen et al., 2007b, Prots et al., 2013), protein clearance pathways (Cuervo et al., 2004, Xilouri et al., 2009, Emmanouilidou et al., 2010) and enhance oxidative stress (Junn and Mouradian, 2002).

In addition, α-synuclein is subject to extensive PTMs including phosphorylation, which is the most widely studied. PTMs have been shown to impact α-synuclein aggregation and oligomerisation in different ways. Using specific antibodies, Fujiwara et al. (2002) discovered that a major constituent of LBs in PD brain tissue was α-synuclein phosphorylated at residue S129. Moreover, the soluble fraction (non-fibrillar) of tissue from PD patients, containing α-synuclein, was also found to be phosphorylated at S129 (Anderson et al., 2006). The exact effects of phosphorylation at S129 on α-synuclein have not been fully understood, however several studies have demonstrated that phosphorylation accelerated α-

synuclein aggregation and toxicity in different cell models (Smith et al., 2005, Sugeno et al., 2008). In addition, phosphorylation accelerated DAergic neuronal loss in transgenic mice overexpressing α-synuclein compared to those expressing WT or phosphorylation-deficient (S129A) forms (Chen and Feany, 2005, Wakamatsu et al., 2007, Rieker et al., 2011). These discoveries suggest that phosphorylation could alter α-synuclein tendency to aggregate or form oligomeric species and may therefore affect PD progression or initiation.

Increasing evidence is indicating that α-synuclein may self-propagate and spread progressively between interconnected brain regions via cell-to-cell transmission mechanisms including non-classical exocytosis, exosome release and nanotubes that directly connect the cytoplasm of two cells (Guo and Lee, 2014) (**Figure 1.6**). Additionally, α-synuclein aggregates have been identified in enteric neurons of patients with early-stage PD (Hilton et al., 2014). These results have strengthened the hypothesis that an unknown pathogen (virus or bacterium) in the gut could be responsible for PD pathology initiation (Braak et al., 2003b). This theory, known as the Braak's hypothesis, suggests that PD may originate from the gastro-intestinal tract, where an as-of-yet unidentified triggering event initiates a pathological cascade, involving α-synuclein, which slowly migrates to the brain, starting from the olfactory bulb and the gut (Braak et al., 2003a, Hawkes et al., 2007). Soon after Braak's hypothesis, two groups independently reported that PD patients, transplanted with embryonic mesencephalic neurons into the striatum, developed LBs 11-16 years after grafting, suggesting that the disease could have propagated from the host to graft cells because these cells were relatively young (Kordower et al., 2008, Li et al., 2008). Following these findings, the terms "prion" and "prion-like" started to be widely used to define the potential pathogenic mechanism of the α-synuclein protein. *In vitro* studies demonstrated that introduction of α-synuclein preformed fibrils (PFFs) could act as a seed and recruit endogenous α-synuclein into pathologic, insoluble inclusions that resembled LBs (Luk et al., 2009, Hansen et al., 2011, Volpicelli-Daley et al., 2011). The

formation of these α-synuclein aggregates in recipient cells led to synaptic dysfunction, which culminated in neuronal loss. Once demonstrated that α-synuclein could be transmitted between cells, the potential pathogenic effect of α-synuclein transmission was explored *in vivo*. Both synthetic and murine disease-associated forms of α-synuclein greatly accelerated the formation and propagation of pathological inclusions and triggered an early onset of characteristic motor clinical signs compared with that of uninoculated mice (Luk et al., 2012a, Luk et al., 2012b). More recently, Recasens et al. (2014) validated the ability of α-synuclein species, derived from LBs extracts, inoculated in both mice and monkeys, to initiate a PD-like pathological process. This included intracellular and presynaptic accumulations of pathological α-synuclein in different brain regions.

Mitochondria have been repeatedly implicated in the proposed propagation of α-synuclein. For example, Baumuratov et al. (2016) discovered structural mitochondrial abnormalities in enteric neurons of post-mortem tissues from PD patients. Further, Braidy et al. (2014) showed that α-synuclein could accumulate in primary human foetal enteric neurons from the gastrointestinal tract and spread between foetal enteric neurons. In addition, accumulation of α-synuclein led to impaired mitochondrial complex I activity, reduced mitochondrial function which culminated in cell death. Another study demonstrated that rotenone exposure in mice, triggered α-synuclein release from enteric neurons (Pan-Montojo et al., 2012). α-synuclein was then taken up by presynaptic sympathetic neurites, which retrogradely transported the protein to the soma, where it accumulated (Pan-Montojo et al., 2012). Additionally, rat ventral midbrain neurons exposed to exogenous PFFs displayed impaired mitochondria and selective DA neurodegeneration; combined exposure to PFFs and rotenone resulted in an additive toxicity (Tapias et al., 2017). These results suggest that pesticides can initiate the progression of PD pathology.

Impaired lysosomal degradation has also been shown to promote α-synuclein release from cells, in multiple models (Lee et al., 2013, Braidy et al., 2014, Jiang et al., 2017). For example, Lee et al. (2013) showed that autophagy inhibition, both pharmacologically and genetically, caused increased exocytosis of α-synuclein, which promoted α-synuclein deposition and cell death in neighbouring neurons. Interestingly, a study showed that cells with endo-lysosomal membrane permeabilization were more vulnerable to the seeding effects of α-synuclein aggregates (Jiang et al., 2017). This study suggests that lysosomal impairment might play an important role in PD progression as it accelerates the seeding progression of α-synuclein. Collectively, these studies and others, demonstrate that α-synuclein spreads from one neuron to another and that mitochondria and autophagy are central to the resultant pathology.

1.4.3 Autophagy dysfunction

Oxidative stress, mitochondrial dysfunction and α-synuclein aggregation represent some of the main pathological features that contribute to PD pathology, however all these factors are linked to proteostasis mechanisms such as the ubiquitin-proteasome system (UPS) and selective autophagy. Autophagy, is required in normal and stress conditions and is a highly conserved metabolic process, responsible for degrading most long-lived proteins, unwanted aggregate-prone proteins and dysfunctional organelles from accumulating to toxic levels (Button et al., 2015). Cytosolic proteins are degraded through three distinct autophagy mechanisms, according to the different pathways by which the cargo is delivered to the lysosomes or vacuoles: chaperone-mediated autophagy (CMA), microautophagy, and macroautophagy.

The first line of defence in degrading soluble misfolded proteins is the UPS, a selective proteolytic system in which recognised substrates are tagged with ubiquitin for processive degradation by the proteasome (Nandi et al., 2006). The UPS is responsible for degrading 80-90% of short-lived, abnormal, denatured, or damaged proteins (Rock et al., 1994). Specific

misfolded proteins can be degraded by the CMA, a process based on the recognition of a specific KFERQ motif, found in roughly 30% of cytoplasmic proteins, including α-synuclein (Dice, 1990, Vogiatzi et al., 2008). This amino acid sequence can be recognised by the cytosolic chaperone heat shock cognate protein of 70 kDa (hsc70), which targets the substrates and translocates to the lysosomal membrane where it interacts with the lysosome-associated membrane protein type 2a (LAMP2A) (Chiang et al., 1989, Cuervo and Dice, 1996). Substrates are then translocated to the lumen and degraded into amino acids by lysosomal hydrolases. Some misfolded proteins that escape the surveillance of the UPS and CMA or tend to form aggregates are directed to macroautophagy. The focus of this chapter will be on macroautophagy (here referred to as "autophagy"), which is believed to be crucial for the timely removal of aggregated forms of pathogenic proteins in neurodegenerative diseases and is the most extensively studied (Mizushima et al., 2011). During autophagy the cytoplasmic cargo (comprised of many cellular constituents) is engulfed by double membranous structures named autophagosomes and delivered to lysosomes for degradation; complete autophagic degradation is termed 'autophagy flux' (**Figure 1.7**).

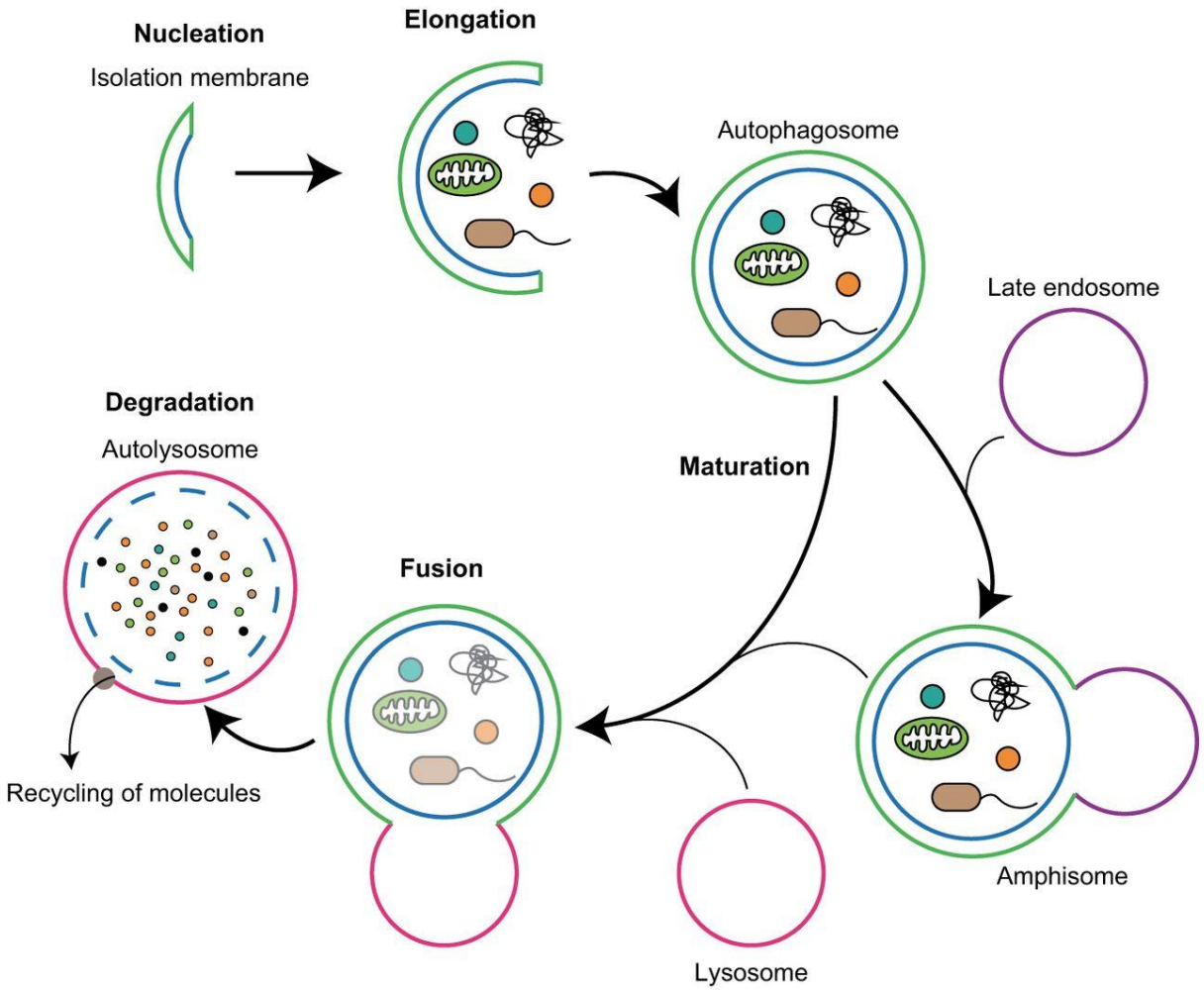

Figure 1.7 Overview of the autophagy pathway. Schematic representation depicting the process of macroautophagy (referred to as autophagy). When autophagy is induced, cytoplasmic materials are sequestered by a double-membraned structure, called autophagosome. These autophagosomes fuse with late endosomes (termed amphisomes) or lysosomes to become autolysosomes, in which the sequestered cargos are degraded and recycled for the maintenance of cellular homeostasis. Autophagy can be divided into five steps: formation of the isolation membrane (nucleation), elongation of the isolation membrane (elongation), completion and transport of the autophagosome (maturation), docking and fusion between autophagosome and lysosome (fusion), lysosomal degradation of the autophagic cargo (degradation). Figure from Nakamura and Yoshimori (2017).

Autophagy begins with the formation of an isolation membrane (also called a phagophore) and it involves the UNC-51–like kinase (ULK) complex, (including ULK1, Atg13, FIP200, and Atg101) and the class III phosphatidylinositol (PtdIns) 3-kinase or PI3K-III complex (including Beclin 1, Atg14L, Vps15, Vps34, and Ambra1). The presence of an activatory stimulus, such as deprivation of nutrients or growth factors or the presence of a dysfunctional

organelle, is able to activate the AMP-activated protein kinase (AMPK) pathway and/or inhibit the mammalian target of rapamycin (mTOR). As a consequence, the ULK1 complex is activated by phosphorylation and then translocates to the ER. Activated ULK1 phosphorylates Beclin-1 on Ser14, promoting the activity of the ATG14L-containing VPS34 complexes (Russell et al., 2013). VPS34 then produces phosphatidylinositol 3,4,5-triphosphate (PI3P) (Matsunaga et al., 2010) at the site of phagophore nucleation and recruits proteins involved in the phagophore elongation. Multiple autophagy (ATG) proteins are required, for the elongation process that involves two steps. The first stage represents the development of the ATG-5-ATG12-ATG16L complex to allow vesicle membrane formation, whilst the second involves the cleavage of LC3 by ATG4B to form LC3-I. This is followed by conjugation to phosphatidylethanolamine (PE), mediated by ATG7 and ATG3, to form LC3-II. The latter protein is necessary for the recruitment of membrane components allowing vesicle elongation as well as the recognition of autophagic cargoes and fusion of autophagosomes with lysosomes. As the phagophore expands and fuses, the ATG5-ATG12-ATG16L complex dissociates from the outer membrane while LC3-II remains integrated with the completed autophagosome. LC3-II acts as docking site of adaptor proteins and cargo receptors. The substrates that need to be degraded are recognised and bound by receptor proteins, such as p62, allowing them to be engulfed upon vesicle fusion. The resulting autophagosomes are subsequently transported along microtubules to the microtubule organizing centre (MTOC), where the lysosomes are clustered. Here they will fuse with lysosomes to form autolysosomes. Due to the acidic environment within lysosomes and the presence of multiple proteases, the autophagy substrates will be degraded, and the resultant products are recycled by the cell (Klionsky and Schulman, 2014).

Cellular mechanisms related to autophagy initiation and autophagosome maturation have been relatively well characterised, whilst the process involving fusion of autophagosomes with

lysosomes is still largely unknown. The current knowledge of the proteins implicated in the fusion of autophagosome to lysosomes is based on the general understanding of intracellular membrane trafficking, particularly three sets of protein families: Ras-related protein in brain (Rab) GTPases, membrane-tethering complexes and soluble N-ethylmaleimide-sensitive factor attachment protein receptors (SNAREs) (Nakamura and Yoshimori, 2017) More in depth description of the roles of Rabs, SNAREs and tethering factors can be found in section 7.1.3.

Interestingly, Phosphoinositides (PIs) are involved in intracellular membrane trafficking. Recent studies have uncovered roles for PIs during the late stage of autophagy, including the transport of autophagosomes and the autophagosome-lysosome fusion (Nakamura and Yoshimori, 2017).

The transcription factor EB (TFEB) is also known to be involved in regulating the expression of lysosomal genes. Once TFEB translocates to the nucleus, it upregulates autophagy and lysosomal genes enabling the activation of its target genes, autophagosome formation and autophagosome-lysosome fusion (Settembre et al., 2011, Martini-Stoica et al., 2016). Studies have also demonstrated that overexpression of TFEB improved degradation of complex molecules, such as the pathogenic protein huntingtin and glycosaminoglycans (Sardiello et al., 2009, Tsunemi et al., 2012).

For cells to be healthy and viable, a homeostatic balance between synthesis and degradation of cellular organelles is necessary, a process highly dependent upon an intact autophagy pathway. Although it has been shown that the number of autophagosomes present in neurons is low compared to other cell types, defective lysosomal clearance can still lead to accumulation of autophagosomes with toxic consequences (Boland et al., 2008). It has been shown that mice that have defective autophagy cannot survive and that knockouts of multiple *ATG* genes cause neurodegeneration along with aggregate formation (Kuma et al., 2004, Hara et al., 2006,

Komatsu et al., 2006). Deficiency in *ATG7* or in the PD-associated protein ATP13A2 induces PD neurodegeneration (Komatsu et al., 2006, Ahmed et al., 2012, Dehay et al., 2012b, Friedman et al., 2012, Usenovic et al., 2012, Bento et al., 2016, Sato et al., 2018). Interestingly, studies indicate that constitutive neuronal autophagy may represent a crucial regulatory pathway for axonal homeostasis. The loss of basal autophagy either by deletion of *ATG* genes or lysosomal protease inhibition in neurons, led to disruption of axonal transport of specific cargoes, causing them to accumulate and cause axonal swelling (Hara et al., 2006, Komatsu et al., 2006, Yue, 2007, Lee et al., 2011). Autophagy affects many pathways and increasing evidence have linked reduced clearance of proteins to neurodegeneration. In regard to α-synuclein, initial studies have proposed that the UPS represented the main proteolytic system responsible for α-synuclein degradation (Bennett et al., 1999), however more recent studies suggest that the lysosome may be the main route for its clearance (Webb et al., 2003, Cuervo et al., 2004, Lee et al., 2004).

Several are the studies that have described α-synuclein involvement in autophagy dysfunction. Initial studies reported apoptosis and autophagic degeneration in the SN of PD patients (Anglade et al., 1997). Additionally, Yu et al (2009) revealed accumulated levels of LC3-II and Beclin proteins in brains of patients with Dementia with LBs and in the SN of mice overexpressing A53T mutant α-synuclein, compared to controls. Further, aged mutant mice displayed higher autophagy biomarker levels compared to younger animals, indicative of a less efficient autophagy pathway. RNA interference against Beclin or ATG5, or chemical inhibition by 3MA were used to block autophagy. This blockade promoted α-synuclein aggregation *in vitro*, confirming the interplay between autophagy and α-synuclein clearance (Yu et al., 2009). PC12 cells expressing A53T mutant human α-synuclein displayed an increased amount of autophagic–vesicular structures along with a disruption of lysosomal hydrolysis and proteasomal function (Stefanis et al., 2001). Tanik et al. (2013) showed that following

internalisation of PFFs in α-synuclein-expressing HEK293 cells or cultured primary neurons, α-synuclein inclusions were resistant to degradation despite their interaction with autophagy-lysosomal pathway and UPS components. Interestingly, despite the reduction of α- synuclein expression, α-synuclein aggregates persisted, suggesting that once seeding occurs, these inclusions are refractory to clearance from cells. Following these results, the same group used ultrastructural analyses and live imaging to demonstrate that α-synuclein accumulations impaired axonal transport of signalling and degradative organelles by affecting the transport of Rab7 and TrkB receptor–containing endosomes (receptors known to undergo predominantly retrograde axonal transport in endosomes). They also reported abnormalities in autophagosome acidification, and autophagosome/lysosome fusion as evidenced by a reduced colocalization of LC3 with LAMP1 (Volpicelli-Daley et al., 2014). Overall, evidence from *in vivo* and *in vitro* models associate α-synuclein with autophagy impairment. Indeed, increase of α-synuclein aggregation and/or impairment in autophagy pathways promote higher α-synuclein levels and/or the inhibition of their degradation, creating a loop cycle of neurotoxicity.

Another mechanism implicated in α-synuclein turnover is the CMA, a form of autophagy that is often up-regulated in response to cellular stress (Cuervo and Dice, 2000a, Cuervo and Dice, 2000b). Cuervo et al. (2004) showed that unlike WT α-synuclein, which could be degraded by the CMA, mutant A30P and A53T could bind to LAMP-2A (with a high affinity) and act as uptake blockers, inhibiting their own degradation and preventing the binding of other substrates. Xilouri et al. (2009) showed that A53T mutant α-synuclein could cause CMA impairment, as observed in adenoviral transfected PC12 and SH-SY5Y cells and that this dysfunction promoted global lysosomal dysfunction. Interestingly, Martinez-Vicente et al. (2008) assessed the effects of α-synuclein PTMs on the CMA pathway. Their results showed that oxidation and nitration impaired α-synuclein degradation without affecting the clearance of other substrates. Phosphorylation and exposure to DA, on the other hand, completely

prevented protein removal through CMA pathway. In addition, post mortem brain samples from PD patients exhibited a decreased expression of both hsc70 and LAMP-2A in the SNpc and amygdala as compared to healthy controls (Alvarez-Erviti et al., 2010). Further, loss of LAMP-2A was correlated with an accumulation of α-synuclein and consequential nigral cell death (Xilouri et al., 2016). Most of these studies suggest that α-synuclein mutants or PTMs can impede substrate delivery into lysosomes by blocking LAMP-2A, thereby disrupting CMA. Recently, however, Mazzulli et al. (2016) reported that α-synuclein accumulation could reduce the enzymatic activity of multiple lysosomal hydrolases, causing lysosomal dysfunction that was not dependent on CMA. α-synuclein accumulation altered the ER-Golgi localisation of Rab1a, a key mediator of vesicular transport. Rab1a overexpression restored protein trafficking and lysosomal function, along with Golgi structure, and reduced pathological α-synuclein in patient neurons (Mazzulli et al., 2016).

Evidence supporting a role for dysfunctional autophagy as a causative factor in PD also derive from studies on mitophagy. Autosomal recessive forms of juvenile PD have been associated with mutations in genes encoding PINK1 (Valente et al., 2004) and the E3 ubiquitin ligase Parkin (Kitada et al., 1998). Studies have demonstrated that PINK1 and Parkin operate in the same pathway to promote autophagic clearance of mitochondria or mitophagy. PINK1 is stabilised on the outer membrane of impaired mitochondria, where it recruits and activates Parkin and ultimately leads to the sequestration of dysfunctional mitochondria into autophagosomes (Narendra et al., 2008, Matsuda et al., 2010). Since PINK1 and Parkin were shown to be implicated in coordinating the selective clearance of damaged mitochondria via the autophagy/lysosome pathway, this also provided a link between the two major cellular dysfunctions implicated in PD pathogenesis: mitochondrial and cellular degradation impairments (Springer and Kahle, 2011). Importantly, PD-associated mutations in either genes inhibited mitophagy at different steps and through distinct mechanisms, highlighting the

etiological importance of this pathway (Geisler et al., 2010a, Geisler et al., 2010b, Lee et al., 2010, Fiesel et al., 2015).

Mitochondrial dysfunction induced by LRRK2 also provides a strong link to the impaired autophagy. Several groups have demonstrated, both *in vitro* and *in vivo*, that LRRK2 mutation can cause an accumulation in autophagic and lysosomal structures (MacLeod et al., 2006, Plowey et al., 2008, Gómez-Suaga et al., 2012). PD patient-derived induced pluripotent stem cells (iPSCs) expressing LRRK2-G2019S also exhibited a block in autophagy flux (Sánchez-Danés et al., 2012). Interestingly, by inhibiting Drp1, using the Drp1 peptide inhibitor P110, autophagy function was improved and the detrimental changes in cell morphology caused by the G2019S mutation were reduced in both PD patient fibroblasts and DAergic neurons derived from iPSCs (Su and Qi, 2013).

Further insights into lysosomal dysfunction in PD come from studies investigating the lysosomal enzyme β-glucocerebrosidase (GBA). The prevalence of GBA mutations varies in different PD populations but these mutations have been reported in more than 30% of PD patients with Ashkenazi Jewish ancestry (Sidransky and Lopez, 2012). This gene encodes glucocerebrosidase (GCase), a lysosomal hydrolase that converts the sphingolipid glucosylceramide to glucose and ceramide in the lysosomal membrane. Homozygous *GBA* mutations cause Gaucher disease (Tsuji et al., 1987), a lysosomal storage disorder in which the substrate glucosylceramide accumulates, impairing the autophagy pathway. Further, inhibition of GBA was shown to enhance intercellular transmission of α-synuclein species, therefore contributing to the spread of PD pathology (Bae et al., 2014). In brain regions of PD patients with increased α-synuclein expression, GBA activity was significantly reduced (Mazzulli et al., 2011, Gegg et al., 2012, Murphy et al., 2014). This further impaired α-synuclein clearance mediated by autophagy.

Perhaps the most direct evidence linking lysosomal dysfunction to PD is the demonstration that loss-of-function mutations in the *ATP13A2* gene, cause a juvenile and early-onset form of parkinsonism (Ramirez et al., 2006). Despite its multifunctionality, ATP13A2 has been linked to endosome-lysosome dynamics (Dehay et al., 2012b, Usenovic et al., 2012), and mutations or genetic depletion of this gene caused decreased lysosomal acidification, impaired proteolytic processing of lysosomal proteases, reduced degradation of lysosomal substrates (e.g., *SNCA*) and diminished clearance and subsequent accumulation of autophagosomes. These alterations could lead to cell death and might contribute to the formation of LBs (Dehay et al., 2012a). Recent studies have shown that ATP13A2 depletion negatively regulates another PD-associated gene, synaptotagmin 11 (*SYT11*) at both transcriptional and post-translational levels. Decreased SYT11 causes lysosomal dysfunction and impairs degradation of autophagosomes. Overexpression of SYT11 in ATP13A2 knockdown cells was able to rescue the autophagy blockade observed in these cells, indicating that ATP13A2-induced blockage of autophagy (under ATP13A2-depleting conditions) is triggered by decreased expression of SYT11. These results demonstrated that both ATP13A2 and SYT11 are crucial for the survival of cells under pathological conditions (Bento et al., 2016).

The effects of parkinsonian toxins including MPTP, rotenone, PQ and 6-OHDA have also been assessed in relation to the autophagy pathway, where evidence suggests these neurotoxic agents promote the accumulation of autophagic vacuoles, indicative of autophagy induction (Chen et al., 2007c, Gonzalez-Polo et al., 2007, Zhu et al., 2007, Dagda et al., 2008, Yu et al., 2009), as a likely response to mitochondrial impairment and generation of oxidative stress. On the contrary, Burton et al. (2012) showed that low concentrations of rotenone not only induced the accumulation of autophagic vacuoles, as evidenced by the increase in LC3-II levels, but also caused both p62 and α-synuclein levels to rise and this is indicative of an impairment in lysosomal degradation. These results were assessed and confirmed in a rotenone-treated rat

model (Wu et al., 2015). Recently, autophagic flux was determined by western blot (WB) analysis in PC12 cells exposed to PQ, which displayed increase levels of both LC3-II and p62 proteins compared to control cells (Zhou et al., 2017).

The role of dysfunctional autophagy in neurodegenerative disorders has been studied in depth in the last decade, however, little is known about the effects of Mn on autophagy and how these effects can promote PD pathogenesis. SH-SY5Y cells, expressing mRFP-GFP tandem fluorescence-tagged LC3, displayed an induction of autophagy in response to 6 h exposure of 500 μM $MnCl_2$. This was evidenced by an increased amount of red LC3 puncta when compared to untreated cells (Tai et al., 2016). Furthermore, C6 astrocytoma cells, treated with 750 μM $MnCl_2$ for up to 24 h, exhibited increased LC3-II and Beclin 1 levels and autophagic vesicles labelled with monodansylcadaverine (marker for autophagic vacuoles) or LC3, compared to control cells (Gorojod et al., 2015). In a time course study carried out by Ma et al. (2017), in SH-SY5Y cells, it was discovered that autophagy was activated in cells exposed to 400 μM $MnCl_2$ for 0–12 h; whilst the autophagy-lysosome pathway was impaired following 24 h treatment. Zhou et al. (2018) conducted a study to assess the effect of Mn exposure on autophagy, and whether and how modulation of the autophagy pathway could affect Mn toxicity in PC12 cells. Their results revealed that exposure to 300 μM $MnCl_2$ for 12 h caused an increased expression of autophagic marker LC3-II protein, as well as accumulation of p62, indicative of autophagy dysfunction. In addition to this, other studies have reported autophagy impairment caused by Mn (Wang et al., 2017, Chen et al., 2018a). Interestingly, pre-incubation of cells with chloroquine (CQ) inhibited autophagy flux and exacerbated Mn-induced cytotoxicity, whilst rapamycin treatment promoted autophagy activation and significantly reduced cell death caused by Mn treatment (Zhou et al., 2018). The effects of Mn on autophagy function *in vivo* are controversial and not fully understood; these are discussed in section 4.1.

1.4.4 Neuroinflammation

Chronic neuroinflammation is another hallmark of PD pathophysiology. Although inflammation may not typically represent an initiating factor in neurodegenerative disorders, emerging evidence implicates microglia and astrocytes in the disease progression.

Microglia are the principal innate immune cells in the brain involved in inflammatory responses and have fundamental roles in CNS homeostasis. The first evidence implicating microglia in PD pathology derives from post-mortem analysis of PD brain samples that exhibited human leukocyte antigen D-related- (HLA-DR) positive reactive microglia (McGeer et al., 1988). In addition, biochemical analysis revealed high levels of pro-inflammatory mediators including tumour necrosis factor-α (TNF-α), interleukins (IL-2, IL-4, IL-6, IL-1), and interferon γ (IFNγ), in the serum of PD patients (Mogi et al., 1996, Brodacki et al., 2008). Post-mortem studies also uncovered upregulated levels of cytokines in the CSF and nigrostriatal regions of PD patients compared to age-matched healthy controls (Mogi et al., 1994, Blum-Degen et al., 1995, Mogi et al., 1995, Mount et al., 2007). Activation of microglia can be triggered by bacterial and viral molecules, disease-related proteins (amyloid β and α-synuclein) and soluble toxic mediators released by dying neurons (von Bernhardi et al., 2015).

Despite the appearance of microglia being evenly distributed within the nervous parenchyma, more in-depth studies have revealed that neither the morphology nor the distribution are equal in all brain locations, providing evidence that microglial cells are sensitive to the surrounding microenvironment (Lawson et al., 1990). According to their shape, microglial cells can be classified into three broadly distinct subtypes: compact, longitudinally branched and radially branched (Lawson et al., 1990). In addition, these morphologies are closely related to their functional state (Davis et al., 1994). Under physiological conditions, microglia appear ramified. During neuroinflammation or after injury, ramified microglia can transform into an “activated

state", characterised by swollen ramified cells with a larger cell body and shorter, thick processes. Alternatively, microglia can adopt a "reactive state", characterised by small, spherical cells, that can also exhibit rod-shape or amoeboid-like morphologies (Davis et al., 1994). Additionally, microglia can be classified according to two distinct phenotypes: the 'pro-inflammatory' and the 'anti-inflammatory' phenotype. Depending on the activated phenotype, microglia can produce either cytotoxic or neuroprotective effects. The classical 'pro-inflammatory' microglial phenotype is characterised by the production of pro-inflammatory cytokines, such as TNF-α, IL-1β, IL-6, IL-12, and other cytotoxic molecules including superoxide, nitric oxide (NO) and ROS. They are involved in the amplification of pro-inflammatory responses during injuries and infections. Whereas 'anti-inflammatory or 'pro-resolution' microglia can produce neuroprotective effects through a variety of cytokines with anti-inflammatory properties, such as IL-4, IL-13, IL-10, and TGF-β (Tang and Le, 2016).

Besides microglia, astrocytes have also been implicated in the neuropathology of PD (Venkateshappa et al., 2012). Under physiological conditions, astrocytes are implicated in the development and plasticity of the CNS, providing energy to neurons and maintaining brain homeostasis (Rothstein et al., 1996, Anderson and Swanson, 2000, Olsen et al., 2006, Stobart and Anderson, 2013). Studies performed in post-mortem brain tissue of PD patients, displayed an increase in astroglial cells (Damier et al., 1993), along with an incremented number of dystrophic astrocytes compared to healthy neurons (Braak et al., 2007). Furthermore, there is evidence that suggests an upregulation of calcium-binding protein S100b, highly expressed in astrocytes (Donato, 2001), in the SNpc of post-mortem PD patients (Bianchi et al., 2007). By exposing microglia to increasing concentrations of S100b, Bianchi et al. (2007) showed an upregulation of the inducible nitric oxide synthase (iNOS) which, in turn, stimulated the expression of the pro-inflammatory enzyme cyclo-oxygenase-2 (COX-2) in microglia. These results suggest that S100b could act as a cytokine involved in the inflammatory response in the

course of brain insults. It has been shown that astrocytes response to *in vitro* stimulation is relatively slower than microglial activation. Microglia are the primary responders to LPS treatment, and they respond to inflammation by releasing mediators such as TNF-α and IL-1β that activate astrocytes (Saijo et al., 2009).

Along with activated microglia and astrocytes, the infiltration of the adaptive immune system has also been shown to promote PD pathophysiology. The BBB is a key mediator between the peripheral circulation and the CNS. It regulates ion balance, facilitates nutrient transport and restricts the passage of pathogens and harmful substances (Desai et al., 2007). A deterioration and dysregulation of the BBB has been proposed to represent a relevant factor contributing to PD progression (Kortekaas et al., 2005, Pisani et al., 2012). There is evidence of severe morphological changes of endothelial cells in the SNpc of PD brains (Faucheux et al., 1999, Kortekaas et al., 2005, Guan et al., 2013) and a strong correlation between disruption of BBB and loss of DAergic neurons in mice injected with vascular endothelial growth factor (VEGF) (a potent inducer of BBB damages) (Rite et al., 2007, Yasuda et al., 2007). Interestingly, VEGF expression levels were found dramatically increased in both PD patients and the MPTP-induced mice (Yasuda et al., 2007). Further studies revealed the presence of both $CD4^+$ and $CD8^+$ T lymphocytes in close proximity of blood vessels and degenerating neurons in post-mortem PD brains (Brochard et al., 2009).

Overall, results from both animal and clinical studies have supported the evidence of an involvement of inflammation in the progression of PD, however a better understanding of the relationship between the CNS and immune system and the molecular mechanisms that underlie their crosstalk is needed to fully understand the pathological processes of PD.

1.5 Gene-environment interactions in Parkinson's disease

Within the last few decades, the genetics associated with PD has dominated the research field although, currently, only a small fraction of PD cases can be directly linked to monogenic mutations. The remaining cases are attributed to other risk associated genes and environmental exposures making PD a multifactorial disorder with a complex aetiology. Given the fact that independently genetic and environmental factors cannot account for all sporadic PD cases, the view of gene-environment factors (combination of environmental exposures and individual genetic susceptibility) has increasingly been appreciated and is now thought to play a central role in the development and progression of PD.

A major topic of debate is the role of heterozygous *Parkin* and *PINK1* mutations that contribute to the development of parkinsonism in several patients (Klein et al., 2007), by increasing the susceptibility of an individual to environmental toxicants. Equally interesting is a study that implicated common single Mendelian mutation of *LRKK2* in sporadic PD (Gilks et al., 2005). In addition, a large-scale meta-analysis study discovered additional familial PD genes among the risk loci identified for idiopathic PD (Nalls et al., 2014). Whilst evidence from multiple epidemiological studies have identified specific gene-environment interactions relevant to PD (Cannon and Greenamyre, 2013), a significant amount of data derives from genetically modified experimental models that assessed the sensitivity of neurons to toxicants.

There is evidence implicating rotenone in increasing the likelihood of PD onset/progression when associated with several PD related genes. Casarejos et al. (2006) assessed the effects of rotenone on both midbrain neuronal cultures from *Parkin*-knockout and WT mice. Results showed an increased sensitivity to the neurotoxin in *Parkin*-knockout culture, with increased apoptosis and cell loss compared to the WT cultures. As Parkin is known for its role in the mitophagy pathway, it is possible that the effects of *Parkin* defective cells exposed to rotenone

may be related to the reduced clearance of damaged mitochondria. In addition, increased neuronal vulnerability to rotenone and *VPS35* mutations have also been described (Tsika et al., 2014, Liu et al., 2017), indicating that PD susceptibility, due to combinatory effects of rotenone and genetic modifications, is not limited to a single gene. Furthermore, rotenone was shown to induce α-synuclein aggregation in PC12 cells (Yuan et al., 2015) and enhance α-synuclein phosphorylation at Ser129 (Wang et al., 2016a, Arawaka et al., 2017).

The association of PQ with multiple PD related genes has further implicated pesticides in exacerbating the risk of developing PD. Mitochondrial membrane potential, morphology and ATP synthesis were assessed in *PINK1*-silenced SH-SY5Y cells treated with PQ. Results revealed that PQ not only caused a reduction in cell viability, but also reduced ATP levels and promoted oxidative stress (Gegg et al., 2009). In addition, 2 mM PQ caused an increased sensitivity to oxidative stress in adult flies that carried Coiled-Coil-Helix-Coiled-Coil-Helix Domain Containing 2 (CHCHD2) mutations (Meng et al., 2017). Manning-Bog et al. (2002a) reported interactions between α-synuclein and PQ *in vivo*. Following PQ serial injections, α-synuclein levels were significantly up-regulated in neurons exposed to the herbicide. Further, thioflavin S staining revealed that α-synuclein-PQ interactions promoted protein aggregation (Manning-Bog et al., 2002a). An additional study showed that oral exposure to PQ triggered the earlier expression of phosphorylated α-synuclein (pSer129) in the enteric nervous system of A53T mutant human α-synuclein transgenic mice (Naudet et al., 2017). The effects of PQ (with or without maneb) have also been investigated in A53T transgenic α-synuclein mice. Exposure to PQ and maneb reportedly resulted in widespread α-synuclein pathology and mitochondrial degeneration, not present in littermate controls (Norris et al., 2007).

Throughout the literature there is increasing evidence on interactions between Mn exposure and PD-related genes. Mn and α-synuclein interactions were assessed in biophysical studies using Nuclear Magnetic Resonance. Results showed that although Mn can bind to α-synuclein *via* three residues in the C-terminal domain: Asp-121, Asn-122 and Glu-123, Mn displayed poor affinity for α-synuclein (1 mM range) compared to other metals (Binolfi et al., 2006). As for the deleterious effects on cell survival, Mn treatment induced α-synuclein overexpression in cultured cells (Cai et al., 2010, Li et al., 2010) and accelerated its fibrillization rate *in vitro* (Uversky et al., 2001). SK-N-MC neuroblastoma cells stably expressing DAT, upon transfection with human α-synuclein, showed increased sensitivity to Mn treatment (Pifl et al., 2004). As Mn and α-synuclein impair mitochondrial function and other cellular processes, their combined effect may have a synergistic effect on cell viability. In addition, Dučić et al. (2015) further evaluated this interplay in Mn-treated rat primary midbrain neurons overexpressing α-synuclein, using X-ray fluorescence imaging. Their results indicated that α-synuclein overexpression enhanced intracellular Mn levels, leaving other metals levels unaltered. This study proposes an indirect mechanism by which α-synuclein could regulate Mn accumulation. A recent study examined α-synuclein immunoreactivity in the frontal cortex of Mn-exposed *Cynomolgus macaques.* Their results clearly showed increased α-synuclein-positive cells in the gray matter of these non-human primates and some of these neurons also exhibited loss of Nissl staining with spherical α-synuclein-positive aggregates (Verina et al., 2013). Another study assessed the effects of Mn on transgenic C57BL/6J mice expressing human WT α-synuclein or A53T/A30P doubly mutated human α-synuclein mice (under TH promoter) and non-transgenic littermates. Mice were exposed to $MnCl_2$-enriched (1%) or control food, starting at the age of four months. Their results revealed a decreased DA turnover in the striatum of transgenic mice expressing human WT α-synuclein, but not in mice expressing A53T and A30P mutations, nor in non-transgenic littermates (Peneder et al., 2011).

Mn has been reported by several groups to enhance α-synuclein aggregation and induce neurotoxicity when combined with α-synuclein, however some laboratories have also showed that WT α-synuclein can be protective against Mn-induced neurotoxicity in *C. elegans* (Bornhorst et al., 2014) and rat DAergic neuronal cells (Harischandra et al., 2015). The latter study demonstrated that α-synuclein could protect cells only in the early stages of Mn exposure, suggesting that, at later time points, Mn accumulation would eventually induce protein aggregation and neurotoxicity (Harischandra et al., 2015).

Most of the current evidence on ATP13A2 function derives from studies which focused on its interaction with α-synuclein (Lopes da Fonseca and Outeiro, 2014). Given its physiological role in lysosomal function it is not surprising that ATP13A2 mutations can induce lysosomal dysfunction and accumulation of aggregated α-synuclein (Gitler et al., 2009, Usenovic and Krainc, 2012, Lopes da Fonseca et al., 2016). On the contrary, ATP13A2 was shown to be protective in Mn mediated α-synuclein toxicity, in both yeast and SH-SY5Y cells (Gitler et al., 2009). However, mutations in the ATP13A2 gene were unable to rescue Mn-induced toxicity in mammalian cell culture (Tan et al., 2011). Further, two ATP13A2 polymorphisms were shown to enhance the neurotoxic effects of Mn in humans (Rentschler et al., 2012).

To further investigate the effects of Mn and PD-linked genes, Sriram et al. (2010) assessed the association of *PARK* genes and mitochondrial function in causing DAergic abnormality. Results showed that Mn accumulation caused mitochondrial impairment and loss of TH protein. Interestingly, they discovered an altered expression of Parkin and DJ-1 proteins in DAergic neurons (Sriram et al., 2010). In addition, Parkin has been reported to alter Mn transport (Roth et al., 2010). DMT1 represents one of the transporters involved in Mn uptake and is comprised of four isoforms (Garrick et al., 2006). There is supporting evidence that implicate PINK1 and Parkin in the ubiquitination and subsequent proteasomal degradation of

one of these isoforms (Roth et al., 2010). Therefore, PINK1 and Parkin mutations could facilitate Mn transport, leading to its accumulation in the basal ganglia and facilitating its toxicity. Further association between Mn and DJ-1 was assessed by Lee et al. (2012) who demonstrated that Mn could reduce both protein and RNA levels of DJ-1 and impair mitochondrial function. The effects produced by Mn resemble those induced by mutant forms of DJ-1. The fact that both factors can individually promote oxidative stress, increase the opening of the mitochondrial permeability transition pore, disrupt membrane potential and impair ATP production, suggest possible exacerbating effects of both Mn and DJ-1 on mitochondrial function. Moreover, Mn can also affect both the kinase and ATP activity of *LRRK2* G2019S mutant (Lovitt et al., 2010). While Mn suppresses the kinase activity of WT LRRK2, the G2019S mutation abolishes this inhibition and remains highly active. Covy and Giasson (2011) suggested that LRRK2 could act as a sensor for cytoplasmic Mn levels, whilst the G2019S mutation could abrogate this function. This hypothesis will need *in vivo* validation, however it is possible that the relative low levels of LRRK2 in DAergic neurons (Galter et al., 2006, West et al., 2014) render these cells more vulnerable to the effects associated with the G2019S mutation. Additionally, when LRRK2 was silenced using shRNA, Mn promoted oxidative stress and mitochondrial dysfunction (Roth and Eichhorn, 2013). A recent study assessed the effects of LRRK2 on Mn-triggered neuroinflammation and its possible mechanism. It was discovered that Mn exposure could not only promote damage in DAergic neurons and promote microglia inflammation in the SN of treated mice and in microglial cultures, but also that LRRK2 was highly upregulated. Interestingly, inhibition of LRRK2 reduced the expression of inflammatory cytokines and reduced autophagy impairment caused by Mn (Chen et al., 2018a).

Overall, these findings bring additional support to the theory that neurotoxic agents such as rotenone, PQ or Mn, when combined with PD-related genes can be potential triggers for PD

pathology (**Figure 1.8**). Therefore, genetically complex diseases, such as PD, are likely the result of an intricate interplay between an individual's genetic make-up and environmental or lifestyle influences that an individual is exposed to.

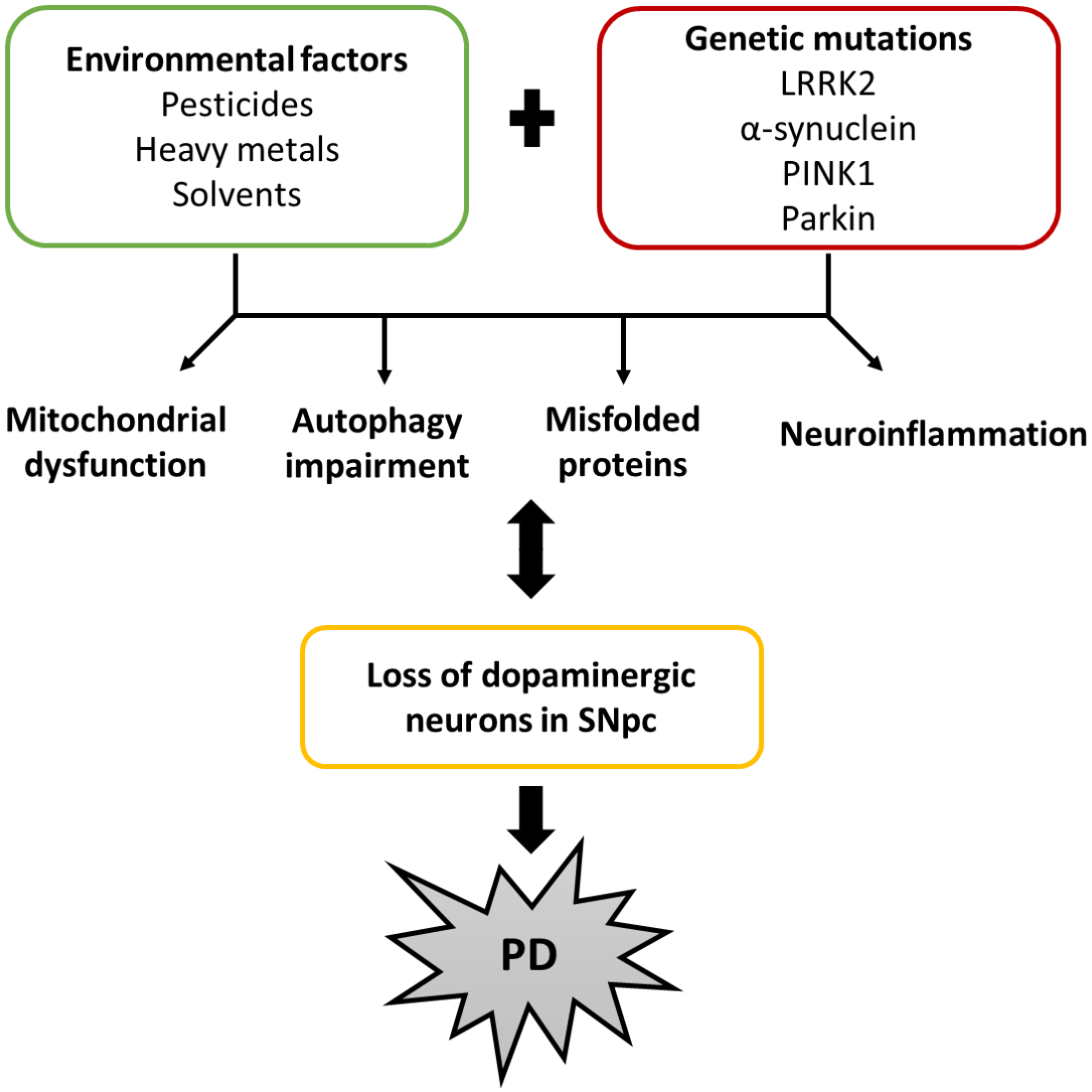

Figure 1.8 Gene-environment interactions in PD. The majority of PD cases are most likely influenced by both genetic predisposition and environmental exposures. The number and diversity of gene-environment interactions that could bear pathogenic relevance to PD is very large, but the current figure displays only those interactions discussed in the text.

1.6 Hypothesis and aims

PD is defined as a multifactorial disease, which is not only ascribed to genetic factors (representing less than 10% of cases) and normal ageing, but also to a range of environmental influences. Mn represents one such example and although the precise mechanism of Mn-inducing parkinsonism is not yet known, prior studies have implicated multiple PD-associated mechanisms, namely mitochondrial and autophagy dysfunction in models of Mn toxicity (Gavin et al., 1992, Gavin et al., 1999, Milatovic et al., 2007, Zhang et al., 2013). Mn has also been shown to interact with a-synuclein and promote its aggregation (Uversky et al., 2001, Bates et al., 2015). It is not fully understood however, how these pathways interact to produce a neurodegenerative phenotype. Increasing evidence show that there is a critical interplay between mitochondria and autophagy. A reduced autophagic activity and impaired mitochondrial function have been described in many neurodegenerative diseases, including PD, as many of the PARK genes implicated in familial PD, have functions related to autophagy and mitochondrial function. Mitochondrial dysfunction could inhibit the autophagy pathway, perhaps by reducing ATP availability and increasing ROS. Equally, impaired autophagy could cause mitochondrial dysfunction by reducing the clearance of damaged or dysfunctional organelles. The complex relationship between these two cellular pathways still remains to be determined, in particular the question regarding whether mitochondrial impairment precedes dysfunctional autophagy or *vice versa* following Mn exposure. The inhibition of the mitochondrial fission protein Drp1 represents a therapeutic strategy that has been demonstrated to be beneficial in multiple models of neurodegeneration (Cui et al., 2010, Qi et al., 2013, Rappold et al., 2014, Kandimalla et al., 2016, Manczak et al., 2016, Bido et al., 2017, Fan et al., 2019). Previous data from our group demonstrated that mice injected with recombinant adeno-associated virus (rAAV2) encoding the Drp1 dominant negative form (Drp1-K38A) displayed a significant reduction in neuronal loss, synaptic dysfunction and α-synuclein

aggregates in brain regions affected in PD (Rappold et al., 2014, Bido et al., 2017). I postulate that, in addition to its well-established role in mitochondrial fission, Drp1 has also a direct effect on autophagy. Blocking Drp1 will confer protection against α-synuclein and Mn-induced protein aggregation and neurotoxicity. To test this hypothesis, I propose to accomplish the following aims:

1) Investigate the effects of Mn exposure on autophagy flux, mitochondrial function and α-synuclein aggregation in multiple cell lines. Evaluate the neuroprotective effects of Drp1 inhibition on Mn-induced toxicity.

2) Determine the effects of acute subcutaneous Mn exposure on autophagy flux and mitochondrial morphology in TH- and GAD67-positive neurons from multiple mouse strains. Explore the effect of manipulating Drp1 in TH-positive neurons to restore Mn-induced changes.

3) Assess changes in the autophagy pathway and mitochondrial morphology in *SLC39A14* knockout (*SLC39A14*$^{-/-}$) mice with markedly elevated Mn levels in the brain and other organs.

Chapter 2
Materials and Methods

2.1 Cell culture

HeLa cells, stably expressing mRFP-GFP-LC3 (kindly provided by Dr. Shouqing Luo, ptfLC3 plasmid, Addgene #21074), were grown in Dulbecco's Modified Eagle's Medium (DMEM, Gibco) supplemented with 10% Fetal Bovine Serum (FBS, Gibco), 100 U/mL penicillin/ 100 µg/mL streptomycin and 100 µg/mL G418 (Gibco) at 37 °C in 5% CO_2. BE(2)-M17 (human neuroblastoma cells, kindly provided by Dr Oleg Anichtchik) were grown in DMEM, supplemented with 10% FBS and 100 U/mL penicillin/streptomycin at 37 °C in 5% CO_2. Inducible rat dopaminergic neuronal N27 cells (original WT cells provided by Dr. Anumantha Kanthasamy) expressing human WT α-synuclein were generated by our laboratory using the ecdysone inducible system (provides a tight regulation of the transgene expression) as previously described (Cui et al., 2010). N27 cells were grown in Roswell Park Memorial Institute (RPMI, Gibco) 1640 medium, supplemented with 10% FBS, 500 µg/mL G418 and 200 µg/mL Hygromycin (Gibco) at 37 °C in 5% CO_2. The inducible overexpression of human WT α-synuclein was induced by the introduction of 20 µM PonA (an ecdysone homolog compound) for 24 or 48 h. All cell lines were grown to 70-80% confluency and then seeded/transfected in either 6, 24 or 96-well plates. The following day, cells were exposed to compounds at the indicated concentrations (**Table 2.1**).

All cell lines used in the current study were available in the lab. The HeLa reporter cell line (stably expressing mRFP-GFP-LC3) was chosen because these cells were genetically engineered for direct monitoring of autophagy flux. mRFP-GFP-LC3 vesicle analysis allows us to monitor autophagosome synthesis and autophagosome-lysosome fusion by labelling autophagosomes (green and red) and autolysosomes (red), since the low lysosomal pH quenches the GFP signal. Human M17 neuroblastoma cells were used as a model for human DAergic neuron-like cells because they express dopamine synthesis enzymes (Baptista et al., 2003). N27 cells were used because these are rat DAergic neuronal cells that our lab has

genetically modified to express inducible human WT α-synuclein (Fan et al., 2019). As missense mutations in SNCA are rare and responsible for a small fraction of PD cases, a WT human α-synuclein overexpressing cell line was chosen to study sporadic PD and its potential relationship with Mn toxicity.

2.2 Cell viability assay

Cells were seeded at various densities dependent on the cell line, in 96-well plates. M17 cells were plated at 1.2×10^4 cells/well (for 24 h treatments) and 1×10^4 cells/well (for 48 h treatments) respectively. N27 were plated at 1×10^4 cells/well (for 24 h treatments) and 8×10^3 cells/well (for 48 h treatments) respectively. HeLa cells were respectively plated at a density of 6×10^3 cells/well (for 24 h treatments) or 4×10^3 cells/well (for 48 h treatments) in 96-well plates. Cells were treated with different concentrations of Mn for 24 or 48 h (M17 cells were seeded on poly-D-lysine precoated wells).

Cell viability was assessed using the Calcein AM assay (Thermo Fisher) in accordance with the manufacture's protocol. Briefly, cells were washed three times with 0.1 M PBS, then incubated in 100 µL Calcein AM (2 µM in 0.1 M PBS) at room temperature for 1 h, protected from light. Six replicate wells were included for each condition. Four wells of assay media were included as blanks. The fluorescent signal from the Calcein AM dye was measured using a plate reader (Synergy H1, Biotek). The parameters measured were 495 nm and 520 nm for excitation/emission wavelengths, respectfully. For analysis, an average blank value was subtracted from all wells and then normalised to control values. Healthy cells will retain the Calcein AM dye and fluoresce whereas dead cells will not. Therefore, a decrease in fluorescent signal is representative of cell death.

Table 2.1 Chemical Compounds used in cell culture experiments.

Chemical	Supplier	Catalogue #	Diluent	Working concentration
$MnCl_2$	Fisher	M87-100	Water or Media	62.5, 125, 25, 500, 1000, 2000 µM
CQ	Sigma	C6628	Sterile PBS	10 µM
PonA	Enzo	ALX-370-014	Ethanol	20 µM
Mdivi-1	Bionet	Customer made	DMSO	10 µM
PQ	Sigma	856177	Sterile PBS	50, 100, 200, 400, 800, 1600 µM

2.3 Reverse transfection

The following 'reverse transfection' procedure was used to increase transfection efficiency. Cells were transfected with DNA plasmid (LC3-cherry 0.3 µg/well, mCherry-hLC3B-pcDNA3.1 plasmid) and/or either 10 nM siRNA (siGenome smartpool DNM1L, Dharmacon, against both human or rat Drp1) or with a scrambled control siRNA using Lipofectamine™ 3000 according to the manufacturer's instructions (**Table 2.2**). Briefly, the Lipofectamine™ 3000 Reagent was diluted with Opti-MEM™ Medium and mixed by pipetting. Then, a master mix of DNA and/or siRNA was prepared by diluting DNA and/or siRNA, to concentrations described above, in OptiMEM™ Medium. When transfecting cells with a DNA plasmid, P3000™ Reagent was also added and mixed by pipetting. When transfecting cells with siRNA the P3000 reagent was not added. Then, the tube containing DNA/siRNA master mix was combined with the diluted Lipofectamine™ 3000 Reagent (1:1

ratio). The new mixture, mixed by pipetting, was then incubated for 10–15 min at room temperature. During this time cells were detached by incubated with 0.05% Trypsin-EDTA, quenched with media, spun down (2.5 x g for 3 min) to collect the cell pellet, resuspended with OptiMEM™ Medium and counted using a hematocytometer. Subsequently, M17 ($1x10^5$ cells/well), N27 ($8x10^4$ cells/well) and HeLa ($1.5x10^5$) cells were added to the preformed DNA/siRNA-lipid complex solution and plated in appropriate wells (M17 and N27 cells were always transfected in 24-well plates, while HeLa cells were transfected in 6-well plates). For immunofluorescence experiments, cells were plated directly on poly-D-lysine coated glass coverslips. After 8-10 h, Opti-MEM was replaced with complete growth media. 24 h post-transfection cells were treated with compounds at the indicated concentrations and incubated for another 24 or 48 h.

Table 2.2 Lipofectamine™ 3000 Reagent Protocol conditions. Each volume is indicated for one well.

Component	96-well	24-well	6-well
P3000™ Reagent per well	0.2 µL	1 µL	5 µL
Lipofectamine™ 3000 Reagent per well	0.15 µL	0.75 µL	3.75 µL
Opti-MEM™ Medium per well	10 µL	50 µL	250 µL

2.4 Immunocytochemistry (ICC)

Cells, grown on poly-D-lysine-coated coverslips (0.1 mg/mL poly-D-lysine), were treated and then fixed by incubating with 4% paraformaldehyde (PFA) in cell culture media for 20 min at 37 °C. The following steps were performed with gentle agitation on a platform shaker.

Following washing with 0.1 M PBS, non-specific binding sites were blocked by incubating coverslips in 0.1 M PBS 4% normal goat serum (NGS), 0.1% TritonX-100 for 1 h at room temperature. Coverslips were then incubated in primary antibody solution, made in 0.1 M PBS, 2% NGS, 0.1% TritonX-100, overnight at 4 °C. **Table 2.3** contains information on the primary antibodies used in this study. For co-localisation experiments, primary antibodies were pooled together before being applied. Coverslips were then washed with 0.1 M PBS and incubated in secondary antibody solution, made in 0.1 M PBS, 2% NGS, for 1 h at room temperature protected from light. **Table 2.4** contains information on the secondary antibodies used. For co-localisation experiments, secondary antibodies were pooled together before being applied. Coverslips were again washed in 0.1 M PBS before being inverted and mounted onto glass microscope slides using ProLong gold antifade mounting reagent. Slides were air dried overnight, protected from light, before being sealed with nail polish and stored at 4 °C until ready for imaging. For experiments with HeLa cells that did not require antibody staining, coverslips were fixed and washed as described above before being directly mounted on microscope slides. Images were captured using an Olympus Fluoview FV10i confocal microscope. All images were taken using a 60X objective with variable optic zoom (2X and 3X zoom).

Specificity of primary and secondary antibody was not tested in this thesis. All the antibodies used in this thesis have been previously validated and published either by our lab (Cui et al., 2010, Rappold et al., 2014, Fan et al., 2019) or other groups. For example, to validate the specificity of the Drp1 antibodies, our lab used cells from Drp1-knockdown, knockout or overexpressing samples. For all the experiments, optimisation of suitable concentrations to use were performed but not shown in this thesis.

Table 2.3 Primary antibodies used for ICC.

Target	Specificity	Host	Supplier	Catalogue #	Dilution
α-Synuclein	Human, Rat	Rabbit Polyclonal	Millipore	AB5038	1:2,000
α-Synuclein	Human, Rat, Mouse	Mouse Monoclonal	BD Biosciences	610787	1:500
p62/SQSTM1	Human, Rat, Mouse, Hamster	Rabbit Polyclonal	MBL Intl.	PM045	1:500
TOM20	Human, Rat, Mouse, Avian	Rabbit Polyclonal	Santa Cruz	FL-145	1:500
DRP-1	Human, Rat, Mouse, Dog	Mouse Monoclonal	BD Biosciences	611113	1:500

Table 2.4 Secondary antibodies used for ICC/IF/DAB.

Target	Conjugate	Host	Supplier	Catalogue #	Dilution
Rabbit IgG	AlexaFluor-488	Goat	Invitrogen	A-11034	1:1,000
Rabbit IgG	AlexaFluor-568	Goat	Invitrogen	A-11011	1:1,000
Mouse IgG	AlexaFluor-350	Goat	Invitrogen	A-21049	1:1,000
Mouse IgG	AlexaFluor-488	Goat	Invitrogen	A-11029	1:1,000
Mouse IgG	AlexaFluor-568	Goat	Invitrogen	A-11004	1:1,000
Chicken IgY	AlexaFluor-568	Goat	Invitrogen	A-11041	1:1,000
Chicken IgY	AlexaFluor-647	Goat	Abcam	ab150175	1:1,000
Biotinylated Rabbit IgG	Biotinylated	Goat	Vector Laboratories	BA-1000	1:200
Biotinylated Mouse IgG	Biotinylated	Goat	Vector Laboratories	BA-9200	1:200

2.5 Detection of proteinase K insoluble α-synuclein species

Inducible N27 cells were transfected with rat Drp1 siRNA and plated ($8x10^4$ cells/well) onto poly-D-lysine coated glass coverslips and treated with 20 µM PonA or vehicle (100% ethanol), with or without the addition of 125 µM Mn for 24 or 48 h; 10 µM CQ was included as a positive control. Cells were processed for ICC as described above however, prior to blocking, coverslips were either treated with 0.34 U/mL proteinase K (Sigma) or vehicle (0.1 M PBS) for 15-20 min at room temperature, protected from light with shaking. Cells were subsequently stained for α-synuclein using the AB5038 α-synuclein antibody (**Table 2.3**), which is particularly effective at identifying higher order structures of the protein. Following imaging the number of insoluble aggregates was quantified using ImageJ. The image was first converted to 8-bit greyscale, background was removed by choosing the appropriate threshold value, and particles were analysed. DAPI staining was used to identify the number of cells in each image. The number of puncta per cell was determined by counting at least 30 cells per condition, for triplicate experiments, followed by One Way Anova with Tukey's post-hoc analysis.

2.6 Autophagy flux assessment using the tandem mRFP-GFP-LC3 fluorescent probe

HeLa (1.5×10^5 cells/well) cells were transfected with human Drp-1 siRNA and/or treated with compounds as described previously in a 6-well plate. 24 h post treatment, cells were fixed and ICC was performed, if necessary, as previously described. Following imaging, ImageJ was used to score the amount of green and red vesicles and DAPI staining was used to identify the number of cells in each image. Following conversion to 8-bit greyscale, background was removed by choosing the appropriate threshold value, and particles were analysed. Control cells were used to set the appropriate threshold value for each experiment. Green vesicles

represent autophagosomes and red vesicles symbolise both autophagosomes and autolysosomes (as the low pH inside the lysosome quenches the fluorescent signal of GFP). The number of autolysosomes was calculated by subtracting the number of green puncta from that of the red puncta as described by Button et al. (2014). The average number of puncta per cell in GFP or RFP-positive cells was determined by counting at least 30 cells per treatment group per experiment, for triplicate experiments (for a total of approximately 90 cells per treatment group). The average number of GFP and RFP puncta was first calculated for each experiment by dividing the total number of puncta for each treatment group by the total number of cells within that group. This was then averaged between each experimental repeat. No cell marker was used to identify cell borders, the total number of puncta within an image was divided by the number of cells within that image. This reduced biased as all cells were included in the count. This analysis method was utilised by Fan et al. (2019). This same method was used to analyse CAG-RFP-EGFP-LC3 transgenic mice. For these experiments 20 marker-positive (either TH or GAD67) neurons per animal were counted. One Way Anova with Tukey's post-hoc analysis was performed for statistical analysis.

2.7 Quantification of p62 and LC3 puncta

M17 (1.5×10^5 cells/well) and N27 (8×10^4 cells/well) cells were transfected with LC3-cherry and/or Drp1 siRNA (human or rat accordingly) in 24-well plates and then treated with compounds as described previously. 24 h post treatment, cells were fixed and ICC was performed as previously described. Following imaging, ImageJ was used to score the number of LC3 and p62 puncta. Following conversion to 8-bit greyscale, a convolve filter (normalize Kernel) and 3 x 3 median filter to reduce noise ("despeckle") were applied. A threshold was then determined, and particles were analysed. The number of puncta per cell was determined

by counting at least 20 cells per condition, for triplicate experiments. This method was also used to analyse LC3 and p62 puncta in mouse brain sections. For these experiments 20 marker-positive (either TH of GAD67) neurons per animal were counted. One Way Anova with Tukey's post-hoc analysis was performed for statistical analysis.

2.8 Mitochondrial morphology assessment *in vitro*

M17 ($8x10^4$ cells/well) and N27 ($6x10^4$ cells/well) cells were grown on poly-D-lysine-coated glass coverslips in 24-well plates. 24 h post treatment cells were fixed and ICC performed as previously described. Measurements of mitochondrial size were quantified using ImageJ. After opening the image as an 8-bit grayscale, a convolve filter (normalize Kernel) and 3 x 3 median filter to reduce noise ("despeckle") were applied to the image. Quantitative measurement of mitochondrial perimeter was calculated as previously described by Cui et al. (2010). The appropriate threshold value was then applied, and particles were analysed. More than 2000 mitochondria from 50 cells per experiment were measured in 3 independent experiments. The length and average number of mitochondria per cell was categorised and graphed into eight groups (bins) according to their sizes (0.5, 1, 2, 4, 6, 8, 10 and more). Unpaired two-tailed Student's *t* test was performed to assess statistical difference between control and Mn-treated cells.

2.9 Gel electrophoresis and western blotting

M17 ($3x10^5$ cells/well), N27 ($3x10^5$ cells/well) and mRFP-GFP-LC3 HeLa ($2.5x10^5$ cells/well) cells were grown in 6-well plates, transfected and treated for 24 h. Cells were then washed with 0.1 M PBS and detached using 0.05% Trypsin-EDTA for 30 sec, quenched with media and cell pellets were collected by pipetting. Cell suspensions were centrifuged at 1 x g for 5 min and

the supernatant disposed. Pellets were washed with 0.1 M PBS, centrifuged at 1.5 x g for 5 min and the supernatant disposed. Pellets were either used immediately or stored at -20 °C until required. For experiments assessing LC3 and p62 levels the BCA method was not used as the cell pellet (from each 6-well plate) was directly lysed in sample loading buffer and immediately used for experimentation. Cell pellets were resuspended in 20 µL 0.1 M PBS, then lysed by adding equal volume of 2x Laemmli sample buffer (Bio-Rad) and mixed by pipetting. For all remaining experiments, 30 µg of protein were diluted 1:1 in 2X Laemmli sample buffer and loaded to each well following BCA determination (see section 2.10). Proteins were denatured by boiling at 95 °C for 5-10 min. 30-40 µL or 30 µg of each sample were loaded per well alongside 5 µL of a pre-stained Protein ladder (Chameleon Duo) on 10% or 12% polyacrylamide gels. Tanks were filled with running buffer (0.1% SDS, 20 mM Tris-HCl and 192 mM glycine) and gel electrophoresis was performed at 120 V for 90 min using the Bio-Rad Mini PROTEAN Handcast system. Next, proteins were transferred to 0.2 µm pore PVDF membrane (immobilon P^{sq}, briefly activated by submersion in methanol) using the Bio-Rad Mini Trans-Blot Cell with a wet transfer method. Briefly, a Mini gel holder cassette was placed in a tray containing transfer buffer (20 mM Tris-HCl, 192 mM Glycine, 10% methanol) and the transfer sandwich was created as follows: a foam blotting pad was added to the black side of the cassette followed by a blotting filter pad, the electrophoresis gel, activated membrane, blotting filter pad and finally a foam blotting pad. A roller was used to remove air bubbles from the sandwich and the gel holder cassette was closed and secured in place. The transfer assembly was then inserted into the Trans-Blot Cell within the transfer tank taking care to align the black sides of each component to ensure the correct migration of proteins. The tank was filled with transfer buffer and the transfer was run at 100 V for 90 min on ice. Membranes were then briefly submerged in 100% methanol, rinsed with ultra-pure water and then washed with TBS (50 mM Tris-HCl, pH 7.6; 150 mM NaCl) for 2 min prior blocking. Membranes were blocked

with Odyssey Blocking Buffer (LI-COR) or TBS + 0.1% Tween + 5% Skim milk for 1 hour at room temperature. Membranes were washed 3 times for 5 min with TBS + 0.1% Tween and then probed with primary antibodies (**Table 2.5**) diluted in Odyssey Blocking Buffer or TBS + 0.1% Tween at 4 ˚C overnight, whilst shaking. Membranes were washed 3 times for 5 min with TBS + 0.1% Tween and then incubated with appropriate species matched secondary antibodies (**Table 2.6**) diluted in Odyssey Blocking Buffer or TBS + 0.1% Tween. Prior to imaging, membranes were washed again with TBS + 0.1% Tween and finally with TBS to remove residual Tween 20. Membranes were then visualized and analysed using the Li-Cor Odyssey CLx system.

Table 2.5 Primary antibodies used for WB.

Target	Specificity	Host	Supplier	Catalogue #	Dilution
LC3	Wide range	Rabbit polyclonal	Novus Biologicals	NB100-2220	1:500
p62	Human, Rat, Mouse, Hamster	Rabbit polyclonal	MBL	PM045	1:1000
DRP-1	Human, Rat, Mouse, Dog	Mouse Monoclonal	BD Biosciences	611113	1:500
TOM20	Human, Rat, Mouse, Avian	Rabbit Polyclonal	Santa Cruz	FL-145	1:500
B-actin	Wide range	Mouse monoclonal	Sigma	A5441	1:20,000
GFAP	Human, Pig, Rat	Mouse Monoclonal	Sigma	G3893	1:500
TH	Human, Rat, Mouse	Rabbit polyclonal	Millipore	657012	1:500

Table 2.6 Secondary antibodies used for WB.

Target	Conjugate	Host	Supplier	Catalogue #	Dilution
Rabbit IgG	AlexaFluor-680	Goat	Li-Cor	926-68071	1:10,000
Mouse IgG	AlexaFluor-800	Goat	Li-Cor	926-32210	1:10,000/ 1:30,000
Rabbit IgG	AlexaFluor-800	Goat	Li-Cor	926-32211	1:10,000
Mouse IgG	AlexaFluor-680	Goat	Li-Cor	926-68070	1:10,000/ 1:30,000

2.10 Determining protein concentration (BCA colorimetric method)

Protein estimation was performed using a Pierce BCA Protein Assay Kit (Thermo Fisher) according to manufacturer's instructions. All Bovine Serum Albumin (BSA) standards and protein samples were ran in duplicate. BSA standards were created by serially diluting 2 mg/mL stock in a 96-well plate at a ratio of 1:1 with RIPA buffer (2000 ng/µL, 1000 ng/µL, 500 ng/µL, 250 ng/µL, 125 ng/µL, 62.5 ng/µL, 32.5 ng/µL, 0 ng/µL). Samples were then diluted 1:20 with RIPA buffer and then loaded into the plate. The AB reagent was then prepared by mixing Reagent A to Reagent B in a 50:1 ratio. 200 µL of AB reagent was then pipetted to each well (both standards and samples), including 2 blank control wells. The plate was then incubated at 37 °C for 30 min and the sample absorbance was read at 562 nm to determine the optical density (OD). The blank-corrected OD of the samples and standards were averaged and plotted in a xy scatter graph (average OD_{562} (y value) versus protein concentration (x value)). Protein concentrations for unknown samples were then calculated using the equation x=(y-c)/m where m is the gradient of the standard curve and c is the intercept of the y axis. 30 µg of protein were mixed with 2x Laemmli sample buffer (Bio-Rad) and incubated at 95 °C for 5-10

min. Samples and ladder were then loaded on 10% or 12% polyacrylamide gels and WB was performed as previously described (see section 2.9).

2.11 Seahorse assay (Seahorse XF Cell Mito Stress Test)

M17 (1.5×10^4) and N27 (1.5×10^4) cells were plated in XF^{e}96 cell culture microplates (M17 cells were grown on poly-D-lysine precoated wells). Cells were then treated for 24 or 48 h as previously described.

On the day prior to performing the assay, a sensor cartridge was hydrated by adding 200 µL of Seahorse XF Calibrant to each well and incubated at 37 °C overnight in a non-CO_2 incubator.

The following day, XF Base Media (DMEM, low glucose, pyruvate, Gibco), was prepared by adding 0.83 g to 100 mL of sterile cell culture grade H_2O. The media was stirred until fully dissolved, HEPES was added to a final concentration of 4 mM. pH was adjusted to 7.4 with 0.1 N NaOH and the media was maintained at 37 °C until ready to use. When ready, the assay media was filtered with a syringe. Cells were then washed twice and a final volume of 175 µL of assay media was added to each well. The culture plate was placed in a non-CO_2 incubator for 45-90 min prior the assay, to remove all of the CO_2 from the media. The sensor cartridge has four ports for chemical compound loading. For the seahorse experiments performed in this thesis, oligomycin, FCCP and rotenone/antimycin A were loaded into port A-C, respectively. Port D was not used. Prior optimisation experiments were performed within the laboratory to determine optimal concentrations of each compound for the specific cell lines used. The following optimal concentrations were determined: Oligomycin (1.26 µM), FCCP (0.5 µM), rotenone/antimycin A (1 µM each). In order to deliver the correct amount of each compound to the wells, a stock concentration was loaded into the appropriate ports of the sensor cartridge: Oligomycin (10 µM), FCCP (4.5 µM), rotenone/antimycin A (10 µM each). The hydrated

sensor cartridge was then loaded into the machine for calibration (15-30 min). Once calibration was completed, the calibration plate was replaced with the cell culture microplate and the experiment began. Upon completion of an XF assay, cells were fixed in 4% PFA for 20 min at 37 °C, washed 3 times with 0.1 M PBS and incubated with DAPI (5 µg/mL) for 20 min at room temperature, protected from light. After a final series of washing steps, DAPI signal was measured using a plate reader (Synergy H1, Biotek). The parameters measured were respectfully 358 nm and 461 nm for excitation/emission wavelengths.

For analysis and interpretation of data, the Wave software was used. It automatically calculates and reports the assay parameters of the Seahorse XF Cell Mito Stress Test as absolute Oxygen Consumption Rate (OCR) in pmol O_2/min (**Table 2.7**). The seahorse assay and analysis of data was performed by my colleague Dr Rebecca Z Fan.

Table 2.7 Seahorse XF Cell Mito Stress Test Parameter Equations.

Parameter value	Equation
Non-mitochondrial oxygen consumption	Minimum rate measurement after Rotenone/antimycin A injection
Basal Respiration	(Last rate measurement before first injection) – (Non-Mitochondrial Respiration Rate)
Maximal Respiration	(Maximum rate measurement after FCCP injection) – (Non-Mitochondrial Respiration)
H+ (Proton) Leak	(Minimum rate measurement after Oligomycin injection) – (Non-Mitochondrial Respiration Rate)
ATP Production	(Last rate measurement before Oligomycin injection) – (Minimum rate measurement after Oligomycin injection)
Spare Respiratory Capacity	(Maximal Respiration) – (Basal Respiration)
Spare Respiratory Capacity as a %	(Maximal Respiration) / (Basal Respiration) × 100
Coupling Efficiency as a %	ATP Production Rate) / (Basal Respiration Rate) × 100

2.12 TMRM measurement of membrane potential in flow cytometry

M17 and N27 cells were plated ($1x10^5$ cells/well) into 24-well plates (duplicates for each group) and treated with the appropriate compounds for 24 h. Cells were then washed with 0.1 M PBS and 0.05% Trypsin-EDTA was added to each well (just enough to cover the whole surface of the well) for 30 s. Trypsin was quenched by directly adding 500 µL of flow fluid (0.1 M PBS + 1% FBS) to each well. Cells were then transferred to 1.5 mL Eppendorf tubes and centrifuged at 1000 x g for 3 min. The supernatant was removed and the cell pellet was re-suspended with 750 µL of HBSS (Gibco) solution (containing 50 nM TMRM for treatment groups and 50 nM TMRM + 20 µM FCCP as positive control). Cells were incubated at 37 °C for 20 min, centrifuged at 1 x g for 5 min and pellets re-suspended in 400 – 500 µL of flow fluid, depending on pellet size (For M17 cells, 100 nM TMRM and 40 µM of FCCP were used followed by a 15 min incubation at 37 °C). Cells were then analysed by flow cytometry (BD Melody FACS machine). Non-cellular debris and dead cells were gated out and 10,000 events from live cells were collected for each analysis. TMRM fluorescence was used to set the threshold and results are expressed as percentage of all cells with threshold value above the one set by FCCP. The assay and analysis of the data was performed by my colleague Dr Rebecca Z Fan.

2.13 Animals and treatment

Animal care and procedures were approved and conducted in accordance with Home Office Animals for Scientific Procedures Act (ASPA) 1986 guidelines and Institutional Animal Care and Use Committee (IACUC) regulations. All animals were group housed and maintained on a 12 h light/dark cycle, with access to food (PicoLab Irradiated 5V75 diet) and water *ad libitum*. Three different mice strains were used for experiments. The Drp1 heterozygous global

knockout (Drp1$^{+/-}$) mice and control, WT Drp1$^{+/+}$ mice were acquired from Institut Clinique de la Souris (ICS), Mouse Clinical Institute, France. Heterozygous mice were crossed with C57BL/6 mice to establish and maintain the colony. **Figure 2.1** describes the generation of the mouse line as well as the position of the primers used for genotyping for each possible allele. No changes during development were visible in these mice compared to littermate controls apart from mild coat changes in aged mice, which, however, were not used in this study.

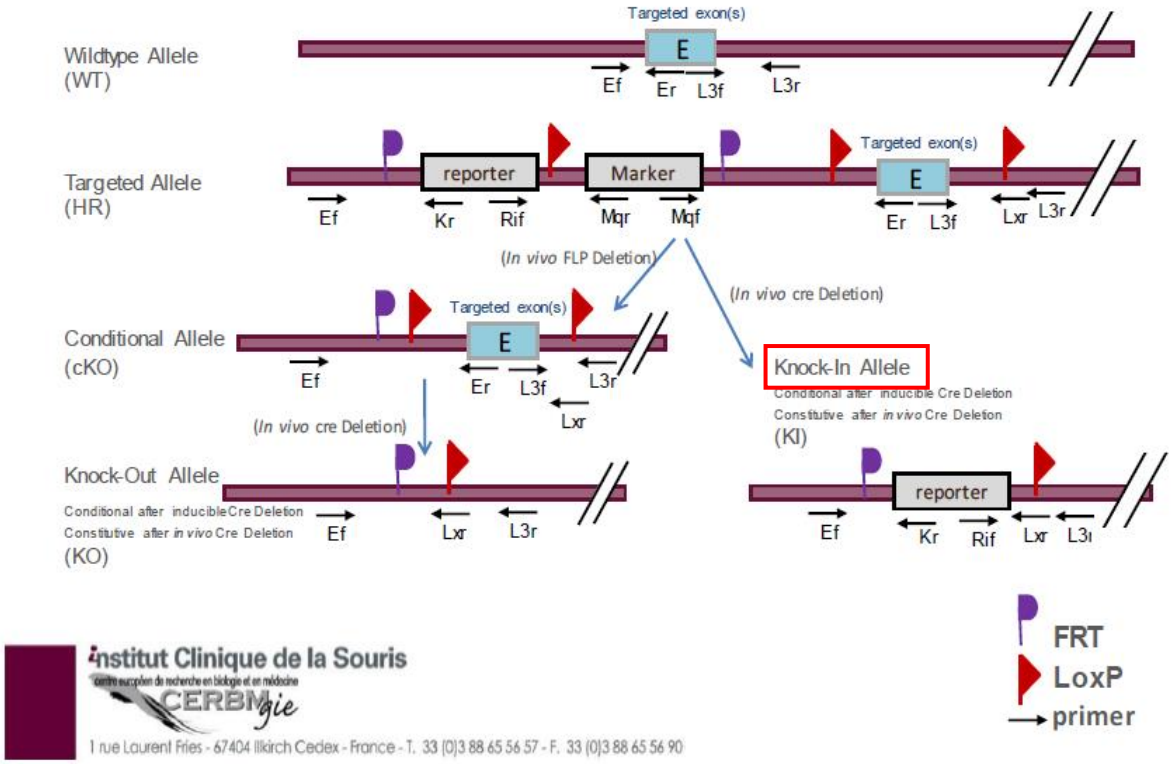

Figure 2.1 Generation of the Drp1 mouse line and position of the primers used for genotyping. This figure depicts the creation of the Drp1 heterozygous global knockout (Drp1$^{+/-}$) mice using the KOMP repository system of transgenic creation. Both conditional and global knockout mice can be created from a common ancestor by flipase or cre deletion, respectively. For this study, global heterozygous Drp1 knockout mice (highlighted in red) were purchased directly from ICS. The lettering underneath the genetic diagram represents a flexible primer system for genotyping these mice. In this study, the Ef, Er and Kr primers were used.

The C57BL/6-Tg (CAG-RFP/EGFP/Map1lc3b) 1Hill/J (CAG-RFP-EGFP-LC3 transgenic mice), were acquired from the Jackson Laboratory (# 027139). These mice have been designed with a human cytomegalovirus (CMV) immediate early promoter enhancer that drives the expression of a red fluorescent protein (RFP), an enhanced green fluorescent protein (EGFP), and a microtubule-associated protein 1 light chain 3 alpha (Map1lc3a) or LC3 gene. Mice were received as heterozygotes and crossed with C57BL/6 mice to establish and maintain the colony. Heterozygous mice showed no developmental defects or phenotypic abnormalities compared to littermate controls.

Both WT (*SLC39A14*$^{+/+}$) and KO (*SLC39A14*$^{-/-}$) mice were kindly provided by Dr Thomas R Guilarte. ZIP14 (SLC39A14) is a zinc transporter that has been shown to also transport Mn. Heterozygous mice were crossed to yield homozygous, heterozygous and WT at a Mendelian ratio of 1:2:1. Mice were bred and genotyped by the Guilarte research group. The mice received were all approximately 6 month old (mixture of males and females).

All mice used in the current study are summarised in **Table 2.8**.

Table 2.8 Animals used for experiments.

Experiment	Mouse strain	Animals used
Effects of Mn on autophagy and mitochondrial morphology	*Drp1*$^{+/-}$ and littermate control *Drp1*$^{+/+}$ mice	24
Effects of Mn on autophagy flux	*CAG-RFP-EGFP-LC3* transgenic mice	12
Blocking Drp1 as a protective strategy against Mn-induced changes in autophagy	CAG-RFP-EGFP-LC3 transgenic mice	8
Assessment of changes in autophagy and mitochondrial morphology	*SLC39A14*$^{-/-}$ homozygous mice	11
Total 55		

2.14 Genotyping

All mice were genotyped using DNA prepared from ear biopsies of two–three week old mice. Genomic DNA was extracted by a rapid alkaline procedure: a skin biopsy was placed in 75 µL alkaline solution (25 mM NaOH, 0.2 mM EDTA) and heated to 96 °C for 45 min. After cooling, 75 µL of cold neutralization solution (40 mM Tris-HCl pH 7.6) was added. The residual tissue was pulsed down by brief centrifugation (30 s at 15,000 x g) and 1 µL of DNA was added to the PCR reaction (1.5 mM $MgCl_2$, 0.2 mM dNTP mix, 0.4 µM Primers, 0.02 U/µL Taq polymerase in PCR buffer (20 mM Tris-HCl pH 8.4, 50 mM KCl)) (Invitrogen) of 25 µL total volume. The PCR was then performed using a thermal cycler (Veriti, Applied Biosystems) according to PCR cycle instruction listed in **Table 2.9**.

Following PCR, DNA was separated by gel electrophoresis on a 1% agarose gel. Agarose was dissolved in TBE buffer (89 mM Tris base, 89 mM Boric acid, 2 mM EDTA pH 8.3) and microwaved until completely dissolved. The agarose was then allowed to cool slightly and 3.75 µL Gel Red (Biotium) was added to the mix. The molten agarose was immediately poured into the gel mould with the comb already in place and left to set for 20-30 min. Once set, the gel was transferred to a tank ensuring that all the wells were fully immersed in TBE buffer. 1 µL ladder (Gene Ruler Mix Ladder, ThermoScientific) with 1 µL loading dye (6x DNA Loading Dye, Thermoscientific) and 4 µL H_2O was loaded into the first well. For each sample, 2 µL loading dye was mixed with 10 µL PCR product and then loaded into the appropriate wells. The gel was run at 120V/200mA for 90-120 min. Once completed, the gel was visualised under UV light (ChemiDoc XRS system, Biorad).

2.15 Manganese administration *in vivo*

For treatments, mice were subcutaneously injected over the shoulders, into the loose skin over the neck (26-gauge needles) with 50 mg/kg $MnCl_2$ or vehicle (ddH_2O) once every 3 days (0, 3, 6) and sacrificed 24 h after each injection, unless stated otherwise as previously described (Dodd et al., 2005). Mice were checked and weighed every day. No changes in body weight or behaviour were noticed and no mortality was associated with the treatment. All mice (mixture of males and females) injected with Mn were approximately three month old.

Table 2.9 PCR conditions used for each animal strain.

Mouse strain	**Primer sequence**	**PCR cycle**
CAG-RFP-EGFP-LC3 transgenic mice	Control Forward (10 µM) (5’ CTAGGCCACAGAATTGAAAGATCT 3’) Control Reverse (10 µM) (5’ GTAGGTGGAAATTCTAGCATCATCC 3’) Mutant Forward (10 µM) (5’ CATGGACGAGCTGTACAAGT 3’) Mutant Reverse (10 µM) (5’ CACCGTGATCAGGTACAAGGA 3’)	95 °C, 3 min 94 °C, 30 s 58 °C, 30 s 72 °C, 1 min (35 cycles) 72 °C, 5 min
Drp1 heterozygous knockout (*Drp1*$^{+/-}$) mice	Primer Ef (10 µM) (5’ GATTGGGCAGGAGCAAGATTCTC 3’) Primer Er (10 µM) (5’ GTGAGCTGACTGATGTAGGTGCTG 3’) Primer Kr (10 µM) (5’ GGGCAAGAACATAAAGTGACCCTCC 3’)	95 °C, 4 min 94 °C, 30 s 61 °C, 30 s 72 °C, 1 min (35 cycles) 72 °C, 7 min
The *SLC39A14*$^{-/-}$ homozygous mice	Control Forward (10 µM) (5’TCATGGACCGCTATGGAAAG 3’) Control Reverse (10 µM) (5’ GTGTCCAGCGGTATCAACAGAGAG 3’) Mutant Forward (10 µM) 5’ TGCCTGGCACATAGAATGC 3’ Mutant Reverse (10 µM) 5’ GCAGCGCATCGCCTTCTATC 3’	95 °C, 5 min 95 °C, 30 s 53 °C, 30 s 72 °C, 1 min (35 cycles) 72 °C, 10 min

2.16 Stereotactic surgery

In order to assess the effects of blocking mitochondrial fission in Mn-treated mice, rAAV2/9 vectors encoding human Drp1-K38A (GTPase deficient dominant negative form of Drp1) were stereotactically delivered unilaterally to the SNpc using a set of pre-defined coordinates (AP: -3.1, ML: ± 1.3, DV: -4.2, relative to the Bregma) (Rappold et al., 2014). Viral vector production generation was performed by Université de Bordeaux (Dr Erwan Bezard's Lab) as previously described (Bido et al., 2017). Briefly, mRFP-GFP-LC3 mice (six week old) were anaesthetised using gaseous delivery of isoflurane (5%), until a loss of the pedal reflex was observed, and transferred to a stereotactic frame. Anaesthesia was maintained throughout the surgery with 1-3% isoflurane, titrated to effect, and body temperature was maintained at 37 °C using a heated platform and rectal temperature probe. An incision was made along the midline from between the eyes to just before the middle of the ears to expose the bregma landmark (junction of sagittal and coronal suture lines) on the skull. The desired injection sites were identified and a small hole was drilled in the skull. The injection set up consisted of a frame-mounted micromanipulator, holding an UltraMicro pump (WPI Instruments) with a Hamilton syringe and a 33-gauge needle (Hamilton). The needle was lowered into the parenchyma at a rate of 0.8 mm/min, and then held in place for 2 min before injection. 1 µL of rAAV2/9 containing Drp1-K38A (1×10^9 U/µL) was delivered to the right hemisphere whereas a sham surgery using 1 µL of sterile H_2O was performed on the left hemisphere as a control. As LC3 mice already express GFP, AAV-GFP could not be used as a control and thus the sham surgery on the left hemisphere was performed. All injections were performed at a rate of 0.2 µL/min. After injection, the needle was left in place for 2 min, then withdrawn at a rate of 0.4 mm/min. The wound was closed using a discontinuous suturing technique using absorbable Vicryl sutures and mice were left to recover at 37 °C before being returned to their original cage. Stereotactic

surgery was performed by my colleague Dr Rebecca Z Fan. Mice were monitored daily for the first two weeks post-surgery and once weekly thereafter.

Six weeks post-surgery, mice were subcutaneously injected with 50 mg/kg $MnCl_2$ once every 3 days (0, 3, 6) and all mice were sacrificed on day 7. Quantification of autolysosomes and autophagosomes in DAergic neurons within the SNpc was assessed using immunofluorescent staining and analysis as described in sections 2.6 and 2.19 respectively.

2.17 Protein isolation from brain samples

Prior to brain dissection, empty 1.5 mL Eppendorf tubes were labelled and weighed for each sample to be collected. Following gross brain dissection, discrete brain regions were dissected, cut into small pieces and placed in tubes on ice. Tubes were weighed again and the net wet weight of the tissue was calculated. A ratio of 1:10 of RIPA buffer (25 mM Tris-HCl pH 7.6, 150 mM NaCl, 5mM EDTA, 1% Triton X-1000, 0.1% sodium dodecyl sulfate (SDS), 1% sodium deoxycholate, ddH_2O) supplemented with 1% protease inhibitor cocktail (Sigma) was added to each brain sample, on ice. Samples were then homogenised with a plastic homogeniser twisting completely 10-12 times. The whole sample was then transferred to a 26-gauge needle and passed through 5-6 times. Samples were then centrifuged at 12,000 rpm for 25 min at 4 °C. Supernatant was collected and stored in the -80 °C freezer until ready for use. Following protein concentration determination (section 2.10), 30 μg of protein were mixed with 2x Laemmli sample buffer (Bio-Rad) and incubated at 95 °C for 5-10 min. Samples and ladder were then loaded on 10% or 12% polyacrylamide gels and WB was performed (see section 2.9).

2.18 Tissue preparation for IF and IHC

Animals were euthanised by intra-peritoneal injection of a lethal dose of sodium pentobarbital (for an average size mouse this is 0.06 cc). A subxiphoid incision was made with a pair of microdissection scissors to expose the heart. A haemostat was then applied to the abdominal aorta and vein. Using a pair of microdissection scissors an incision was made in the right atrium and then the perfusion needle was inserted into the left ventricle near the apex (from interior to superior). Perfusion, with a peristaltic pump calibrated to 10 mL/min, was performed with 3 min of 0.9 % saline followed by 8 min of 4% PFA in 0.1 M phosphate buffer. Whole brains were immediately dissected and post-fixed in the same fixative overnight at 4 °C before sequential overnight incubations in 15% and 30% sucrose in 0.1 M phosphate buffer. Brains were then snap frozen in methyl-butane at -55 °C and stored at -80 °C until sectioned. After mounting in OCT medium, brains were cryo-sectioned at 30 µm (Leica CM3050 S cryostat) and sections containing SN and striatum regions were collected for staining. All staining techniques were performed on free floating sections with gentle agitation throughout.

2.19 Immunofluorescent (IF) staining

For immunofluorescent staining, tissue sections were washed in 0.1 M TBS before non-specific binding sites were blocked in 0.1 M TBS 4% NGS, 0.1% TritonX-100 for 1 h at room temperature. Primary antibodies (**Table 2.10**), diluted in 0.1 M TBS 2% NGS, 0.1% TritonX-100, were then added and incubated overnight at 4 °C. Following washing, sections were incubated with secondary antibodies, diluted in 0.1 M TBS, 2% NGS, for 1 h at room temperature protected from light (**Table 2.4**). Sections were again washed and then incubated with DAPI (2 µg/mL) for 10 min at room temperature, protected from light. After a final series of washing steps, sections were mounted and coverslipped using ProLong gold antifade

mounting media. Slides were air-dried overnight, protected from light, sealed with nail polish and stored at 4 °C until being imaged. Images were captured using an Olympus Fluoview FV10i confocal microscope. All images were taken, blinded, using a 60X objective with variable optic zoom (3X zoom).

Table 2.10 Primary antibodies used for IF/DAB.

Target	Specificity	Host	Supplier	Catalogue #	Dilution
p62/SQSTM1	Human, Rat, Mouse, Hamster	Rabbit Polyclonal	MBL Intl.	PM045	1:250
p62/SQSTM1	Wide range	Rabbit Polyclonal	Novus Biologicals	NBP1-48320	1:500
LC3	Wide range	Rabbit Polyclonal	Novus Biologicals	NB100-2220	1:250
TOM20	Human, Rat, Mouse, Avian	Rabbit Polyclonal	Santa Cruz	FL-145	1:500
DRP-1	Human, Rat, Mouse, Dog	Mouse Monoclonal	BD Biosciences	611113	1:500
HA	Wide range	Mouse Monoclonal	Roche	12CA5	1:200
TH	Mouse, Rat, Human	Rabbit Polyclonal	Millipore	657012	1:1,000/ 1:2000 (DAB)
TH	Mouse, Rat, Human	Chicken Polyclonal	Abcam	76442	1:1000
GFAP	Human, Pig, Rat	Mouse Monoclonal	Sigma	G3893	1:500/ 1:500 (DAB)

Iba1	Mouse, Rat, Human	Rabbit Polyclonal	Wako	019-19741	1:500 (DAB)
GAD67	Human, Rat, Mouse	Mouse Monoclonal	Millipore	MAB5406	1:500

2.20 Immunohistochemistry (DAB)

All DAB immunostaining was performed using the Vector Laboratories VECTASTAIN ABC Kit (PK-4001) according to manufacturer's instructions. Following perfusion and sectioning, tissue sections were washed in 0.1 M TBS prior to 10 min incubation in 10% methanol/3% H_2O_2. Tissues were again washed with 0.1 M TBS before non-specific binding sites were blocked in 0.1 M TBS, 5% NGS for 1 h. Sections were then incubated overnight at 4 °C in primary antibody (**Table 2.10**) in 0.1 M TBS, 2% NGS. The following day, sections were washed with 0.1 M TBS and then incubated in biotinylated secondary antibodies (**Table 2.4**) for 1 h in 0.1 M TBS, 2% NGS. Sections were again washed with 0.1 M TBS and then incubated in Avidin–Biotin Complex (ABC) solution for 1 h at room temperature. The ABC solution was made at least 30 min before use by adding 2 drops of Solution A to 10 mL 0.1 M TBS, mixing and then adding 2 drops of Solution B with further mixing. Following washes with 0.1 M TBS, the peroxidase was developed by incubating the sections with 20 mg (2 tablets) 3,3'-diaminobenzidine-tetrahydrochloride (DAB) (Sigma D-5905), 200 mg/ml NH_4Cl, 3 mg/mL glucose oxidase, 250 mg/ml D-glucose in 50 mL 0.1 M Tris-HCl pH 7.6, filtered before use, for 10-15 min at room temperature, protected from light. Sections were washed with 0.1 M TBS and then mounted on SuperFrost slides and air-dried overnight. The following day, slides were dehydrated (5 min in distilled water, 10 min in 70% Ethanol, 10 min in 95 % Ethanol, 2x 10 min in 100% Ethanol, 2x 10 min in Xylene). Finally, sections were coverslipped with Permount mounting medium while still wet and left to dry in a fume hood. Images were

captured using an Olympus BX43 brightfield microscope. All images were taken using 20X and 100X objectives.

Of note, for DAB staining, H_2O_2 was not added but rather I used the generation system with glucose oxidase as enzyme that catalyses the reaction to generate H_2O_2 at a slower and more controlled rate.

2.21 qPCR

Total RNA was isolated from mouse brain samples by phase separation using Trizol Reagent (Invitrogen). Total wet weight of brain tissue was calculated and 1 mL of Trizol Reagent was added. Tissue was homogenised with 10-15 strokes of a plastic homogeniser and incubated on ice for 5 min. 200 µL of chloroform was added and samples were mixed by inversion, incubated for 3 min at room temperature and phase separated by centrifugation for 15 min at 12,000 x g at 4 °C. The mixture separates into a lower red phenol-chloroform phase, an interphase and a colourless upper RNA-containing phase. This upper phase was collected and 500 µL of isopropanol added to precipitate the RNA. This mixture was mixed by pipetting, incubated at room temperature for 10 min then centrifuged for 10 min at 12,000 x g at 4 °C. The supernatant was discarded and the RNA pellet was washed with 1 mL of 75% ethanol, vortexed and centrifuged for 5 min at 7,500 x g at 4 °C. The supernatant was discarded and RNA pellet air dried for 10 min before being resuspended in 50 µL RNase-free water and heated at 55 °C for 10 min to aid solubilisation. RNA was quantified using a NanoDrop One (Thermo) and reverse transcription performed using SuperScript VILO cDNA synthesis kit (25 °C for 10 min, 42 °C for 60 min, 85 °C for 5 min). cDNA was stored at -20 °C until used. 10 ng of cDNA was loaded into each well of a 96-well plate and qPCR was performed on a QuantStudio 12K flex (Thermo) using TaqMan Fast Advanced Master Mix (Thermo) and TaqMan assays for Drp1 (FAM-

MGB, Mm01342903_m1) and GAPDH (FAM-MGB, Mm99999915_g1) as an endogenous control gene. The reaction conditions were as follows: 50 °C for 2 min, 95 °C for 2 min and 40 cycles of 95 °C for 3 s and 60 °C for 30 s. Relative quantification was performed in Microsoft Excel using the $2^{-\Delta\Delta CT}$ method. Statistical analysis was then performed using an Unpaired two-tailed Student's *t* test analysis. Each reaction was run in triplicate, for three independent experiments, and analysed by my colleague Dr. Martin Helley.

2.22 Mitochondrial morphology assessment *in vivo*

Following imaging, mitochondrial length was quantified using ImageJ, using a method previously described (Chen et al., 2015a). First a region of interest (ROI) was drawn around the TH or GAD67 positive neurons. Each image was converted to an 8-bit grayscale image. A threshold filter was applied, followed by the application of a 3 x 3 median filter ("Despeckle"). Using the skeleton plugin, the mitochondrial network of each cell was skeletonized to one-pixel-wide lines (skeletons). The length of all skeletons was measured using the analyse particles tool (settings were adjusted as required) and the area reported represented the total length of skeletons. To calculate the average length of mitochondria per neuron, the total length of skeletons was divided by the total number of skeletons (referred in ImageJ as 'count'). Unpaired two-tailed Student's *t* test was used to reveal the statistic difference of the average mitochondria length between vehicle and Mn-exposed groups.

2.23 Striatal optical density measurement

Striatal optical density (OD) of TH fibres was determined via ImageJ analysis. Following DAB immunostaining, all sections were scanned (Epson Perfection V800 Photo Scanner) and saved as 8-bit grayscale images. The ImageJ software was then set to record uncalibrated OD

(Analyse > Calibrate > select ‘uncalibrated OD’ from the dropdown menu) for each individual image. The program was set to provide relevant measurements (Analyse > Set measures > uncheck all boxes > check mean gray value and integrated density). The striatum and a small region of cortex for each striatal section were then outlined (with the freehand tool) and measured (by clicking CTRL + M on the keyboard) to record the data. For each measurement the software will provide the following data:

- Mean gray value: Average gray value within the section. This represents the sum of the gray values of all the pixels in the section, divided by the number pixels.
- Integrated density: the product of area and mean gray value.
- Raw Integrated density: sum of values of the pixels in the image.

The data was measured for all sections on the slide/for one animal. For the current analysis both mean gray area and integrated density were used. The specific OD of TH-staining was then obtained by subtracting the cortex OD from the striatal OD, to adjust for background staining in each section.

2.24 Sholl analysis of microglial morphology

Sholl analysis was used to assess microglial morphology, following Iba1 immunostaining (DAB). At least 20 microglia within the SNpc were imaged per animal. Following imaging, using the 100X objective, on the bright field microscope, the image was opened in ImageJ and converted to 8-bit grayscale. A threshold filter was applied to a level that was representative of the original. The binary command was then applied and the freehand selection tool was used to draw around each cell of interest, excluding the outside area around the cell (Edit > Clear outside). Using the straight-line tool, a line was drawn from the cell soma to the most distal

branch of each microglia. Neurons were then analysed by choosing the Sholl analysis parameter with a 5-radius increment setting (**Figure 2.2**).

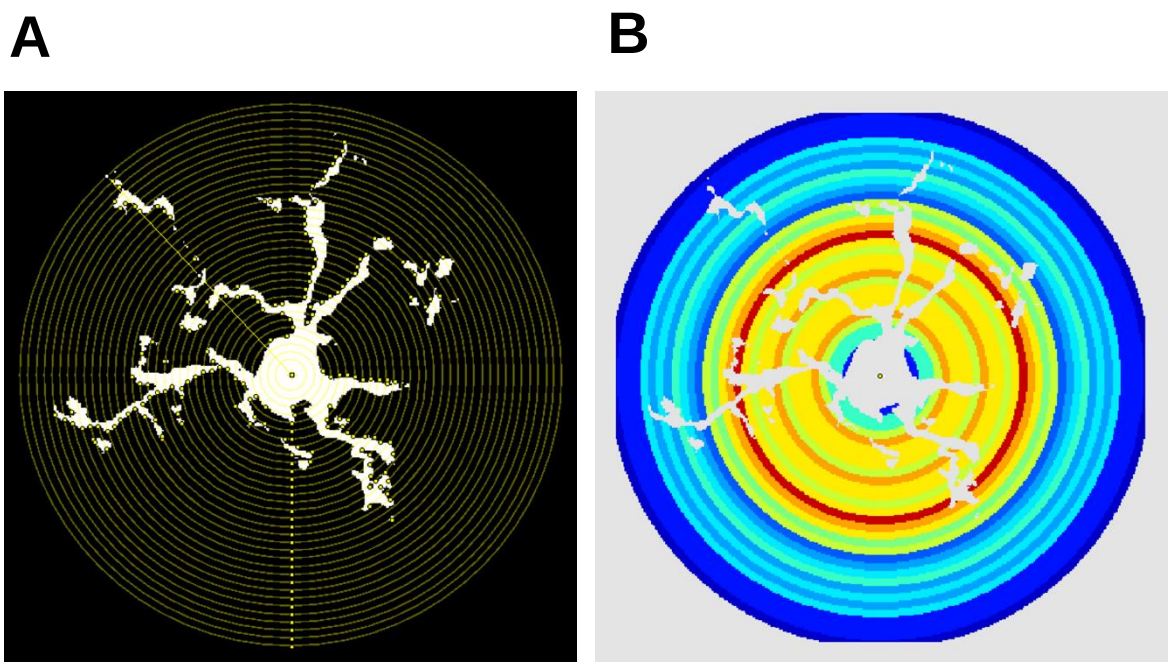

Figure 2.2 Representative visualisation of Sholl analysis performed on Iba1-stained microglia using ImageJ. (A) Image showing the distribution of radii from the cell soma. Points at which microglia processes intersect these radii are denoted by yellow dots. (B) Coloured heat-map of branch density. The red colour is representative of an increased number of intersects at the indicated radius, whilst blue colours show reduced intersections. The number of intersects is then plotted against the distance of each radius from the soma on a line graph.

The number of intersections at each radial increment was averaged for each mouse; the empty cells were filled with 0 (important for averaging). After unblinding, the animals were grouped and averaged according to their treatment. The graph represents the average number of intersections per cell. The area under the curve (AUC) was also calculated for each replicate and plotted with a graph. Statistical analysis was then performed on the AUC data using Unpaired two-tailed Student's *t* test analysis. The Sholl analysis was performed by my colleague Dr. Martin Helley.

2.25 Immunohistochemistry of glial cell markers in the SNpc

The quantification of % area of positive staining was used for the assessment of astrocyte and microglia activation, following GFAP and Iba1 DAB staining, respectively. The SNpc was captured across at least 4 sections per animal using the 20X objective. Using ImageJ, images were first converted into 8-bit grayscale images, then a threshold filter was applied (on a black background). Area fraction was then obtained using the 'Analyse particles' tool (the value is represented in %). Following unblinding, results were averaged depending on treatment group.

2.26 Statistical analysis

All values are expressed as mean ± standard error mean (SEM). Differences between means were analysed using a One-way analysis of variance followed by Tukey *post-hoc* test or unpaired two-tailed Student's *t* test, as appropriate. All analyses were performed using Sigma Stat v4.0. Differences were considered statistically significant when $P < 0.05$. All graphs were generated using GraphPad Prism software.

Chapter 3

Cellular mechanisms of Manganese toxicity: a primary role for autophagy

3.1 Introduction

The precise pathological mechanism of Mn toxicity is still not fully understood, however evidence indicates that mitochondria actively sequester Mn and this accumulation can promote mitochondrial damage (Gavin et al., 1992), by modulating oxidative phosphorylation (Malecki, 2001, Zhang et al., 2004) and/or mitochondrial dynamics (Alaimo et al., 2013, Alaimo et al., 2014). Mn can additionally trigger α-synuclein misfolding and accumulation at certain concentrations (Peres et al., 2016a). The dysregulation of proteostasis pathways, including autophagy, are considered to be central in the progression of neurodegenerative disorders including PD. There is, however, limited evidence to suggest that Mn can alter the autophagy pathway, as most results are controversial (Gorojod et al., 2015, Tai et al., 2016, Ma et al., 2017, Chen et al., 2018a, Zhou et al., 2018).

Whilst it has been shown that Mn exposure can promote mitochondrial dysfunction, there is no evidence on whether any other cellular processes are altered at that same concentration and time point. Mn is accumulated to a greater extent in lysosomes than in mitochondria (Suzuki et al., 1983, Okamoto et al., 1997, Gorojod et al., 2017), which, as mentioned above, have been classically considered as the main target of Mn toxicity. This raises the question of whether mitochondria are the primary target of Mn and provides evidence to suggest autophagy as an additional affected pathway. Addressing this issue may have a significant impact on understanding the neurotoxic mechanisms of Mn. To this end, I decided to explore this *in vitro* using multiple cell lines. Inhibition of Drp1 has been shown to be protective in several models of neurodegeneration (Rappold et al., 2014, Bido et al., 2017, Fan et al., 2019). I, therefore, postulate that Drp1 inhibition will confer protection against Mn-induced neurotoxicity. To test these hypotheses, I proposed to assess changes in autophagy, α-synuclein aggregation, mitochondrial morphology and function concurrently in cells exposed to $MnCl_2$. In addition, I inhibited Drp1 genetically and pharmacologically to restore these Mn-induced changes.

3.2 Results

3.2.1 Effects of Mn on cell viability

At relatively high concentrations (350 -750 µM), Mn has been reported to induce mitochondrial dysfunction, increase mitochondrial fission and promote autophagy impairment (Alaimo et al., 2013, Alaimo et al., 2014, Gorojod et al., 2015). Given the complex relationship between mitochondria and autophagy and the unanswered question whether mitochondrial dysfunction precedes autophagy impairment or *vice versa*, it is imperative to comprehend whether these impairments are the cause or consequence of cytotoxicity. To this end, time course and dose-response cytotoxicity studies were performed by exposing HeLa, M17 and N27 cells to increasing concentrations (62.5 – 2000 µM) of $MnCl_2$. Cell viability was measured after 24 and 48 h of $MnCl_2$ treatment, using Calcein AM, and the Lethal Dose-50 (LD_{50}), a concentration at which 50% of cells are killed, was calculated. Mn caused a decrease in cell viability in a time-dependent manner in all cell lines (**Figure 3.1**). Whilst the higher concentrations (500 – 2000 µM) of $MnCl_2$ were toxic to all cell types (over 60% cell death), HeLa cells were less sensitive to Mn-induced toxicity when compared to M17 and N27 neuronal cells at both 24 and 48 h.

A

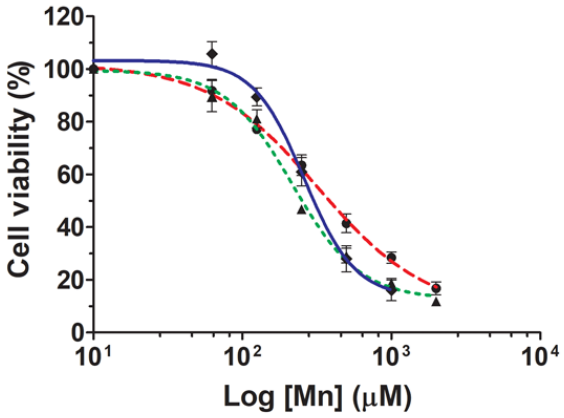

B

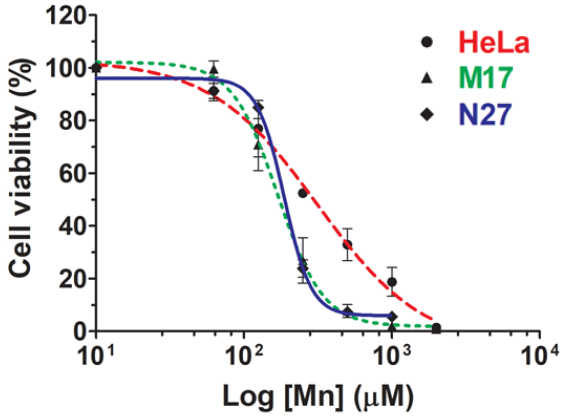

C

Cell lines	LD_{50} ± SEM (μM)	
	24h	48h
HeLa	323.7 ± 8.7	314.5 ± 15.84
M17	217.6 ± 4.8 ***	168.8 ± 5.6 ***
N27	260.6 ± 7.5 **,#	186.9 ± 2.5 ***

Figure 3.1 Mn reduces cell viability in a dose-dependent fashion. HeLa, M17 and N27 cells were cultured in 96-well plates and exposed to varying concentrations of $MnCl_2$ (62.5 – 2000 μM) for (**A**) 24 and (**B**) 48 h. Values are relative to 100% for the vehicle-treated group and they are represented as mean ± SEM (n=3 independent experiments, with 6 wells per group, per experiment). (**C**) Summary table of LD_{50} values generated using GraphPad Prism. One Way Anova with Tukey's post-hoc analysis ** $P < 0.01$, *** $P < 0.001$ compared to HeLa cells, # $P < 0.05$ compared to M17 cells.

3.2.2 Effects of Mn on the autophagy pathway

Defects in the autophagy pathway and the resulting accumulation of protein aggregates represent one of the common pathobiological features of PD pathology (Antony et al., 2013). As the effects of Mn on this process are not fully understood, it was crucial to investigate the effects of Mn on autophagy. To do so, the HeLa mRFP-GFP-LC3 stably expressing cells were used. These cells were designed to rapidly assess changes in autophagy flux based on different pH stability of GFP and mRFP fluorescent proteins (**Figure 3.2**). They express the mRFP-GFP-LC3 fusion protein in which the autophagosome marker protein LC3 (microtubule-associated protein 1 light chain 3) is fused to two fluorescent reporter proteins: monomeric RFP (acid-stable) and GFP (acid-sensitive). Autophagosomes appear yellow (green and red signal) whilst autolysosomes are red, since the acidic lysosomal pH quenches the GFP signal more rapidly than the mRFP (Kimura et al., 2007). The number of fluorescent puncta structures per cell was used to assess autophagic flux as described in section 2.6.

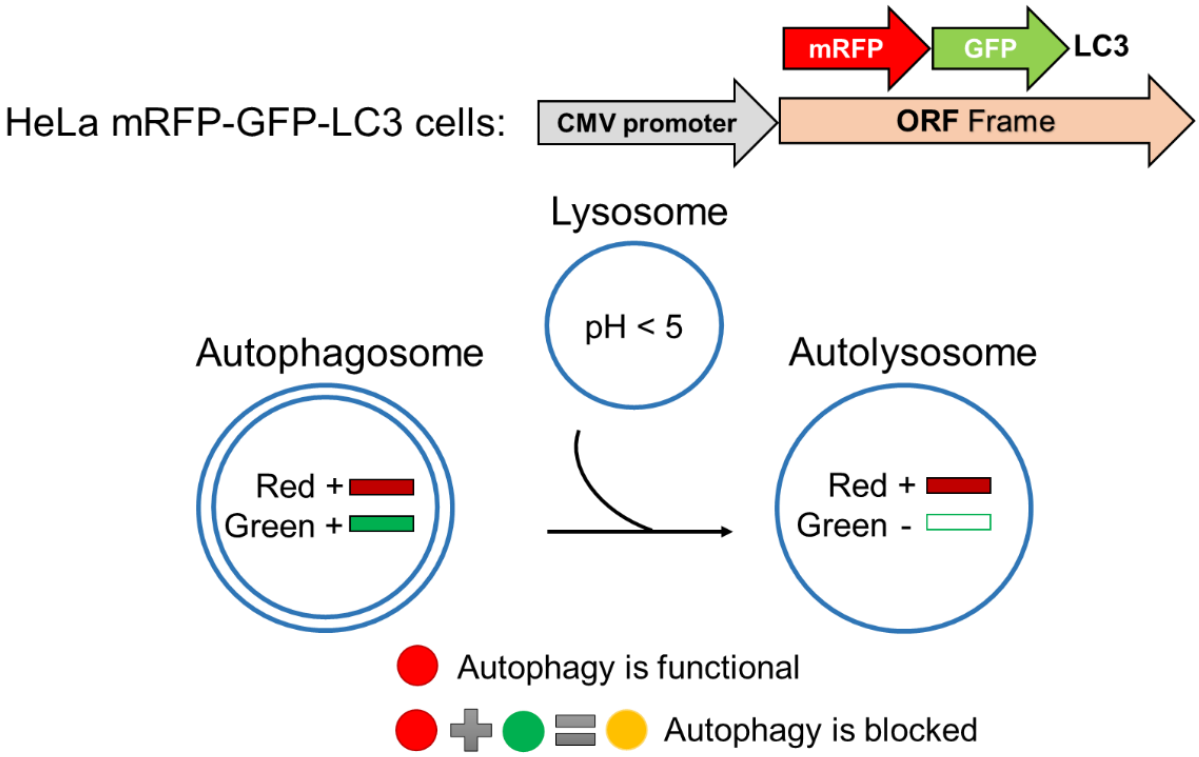

Figure 3.2 Monitoring autophagic flux in HeLa mRFP-GFP-LC3 expressing cells. During the early stage of autophagosomes biogenesis, puncta will accumulate and display both green and red fluorescent signals ($GFP^{+}RFP^{+}$). During the late stage of the autophagic process (autolysosomes formation), the green signals are quenched in the acidic autolysosomes, while the red signals are retained ($GFP^{-}RFP^{+}$). If autophagy flux is blocked the green signal will not be quenched by the lysosomes and both the green and the red signal (yellow) will be expressed.

HeLa mRFP-GFP-LC3 cells were exposed to different concentrations of $MnCl_2$ (62.5 – 500 µM) for 24 h. Following Mn treatment, the number of autophagosomes increased, in a dose dependent fashion, whilst autolysosomes markedly decreased compared to control cells (**Figure 3.3**). These results are indicative of a blockade in autophagy flux. As all Mn concentrations caused a statistically significant blockade in the autophagy flux, and considering the cell viability data, the lowest concentration of $MnCl_2$ (62.5 µM, which caused 8.13 % cell death), was chosen as the preferred concentration for future experiments using HeLa cells.

To further validate these results in a more relevant model to PD, ICC was performed in M17 human DAergic-like neuroblastoma cells following $MnCl_2$ treatment. M17 cells were transiently transfected with LC3-cherry plasmid and then treated with increasing concentrations of $MnCl_2$ (62.5 – 500 µM) for 24 h. Chloroquine (CQ), a well-known lysosomotropic compound (de Duve et al., 1974), was used a positive control for autophagy inhibition. Staining with p62 was performed and the number of LC3- and p62-positive puncta were quantified. In control cells, the staining pattern of LC3 and p62 was largely diffuse, with a small number of visible puncta. Following Mn treatment, the diffuse staining pattern of LC3 and p62 visibly changed to a more punctate pattern, which is representative of a recruitment, and subsequent accumulation, of LC3 and p62 to the autophagosome. Following quantification, results clearly demonstrate accumulation of LC3 and p62 positive puncta, in a dose-dependent manner, in Mn-exposed cells (**Figure 3.4**).

Again, as a result of statistical analysis, 125 µM $MnCl_2$ (which caused 18.9 % cell death) was the lowest concentration of Mn treatment that induced a significant detectable blockade in autophagy by increasing both LC3 (39.58 ± 2.99) and p62 (28.31 ± 2.07) levels in comparison to control (LC3,19.47 ± 1.90; p62 9.06 ± 0.24) levels and was therefore chosen as the preferred concentration for subsequent experiments.

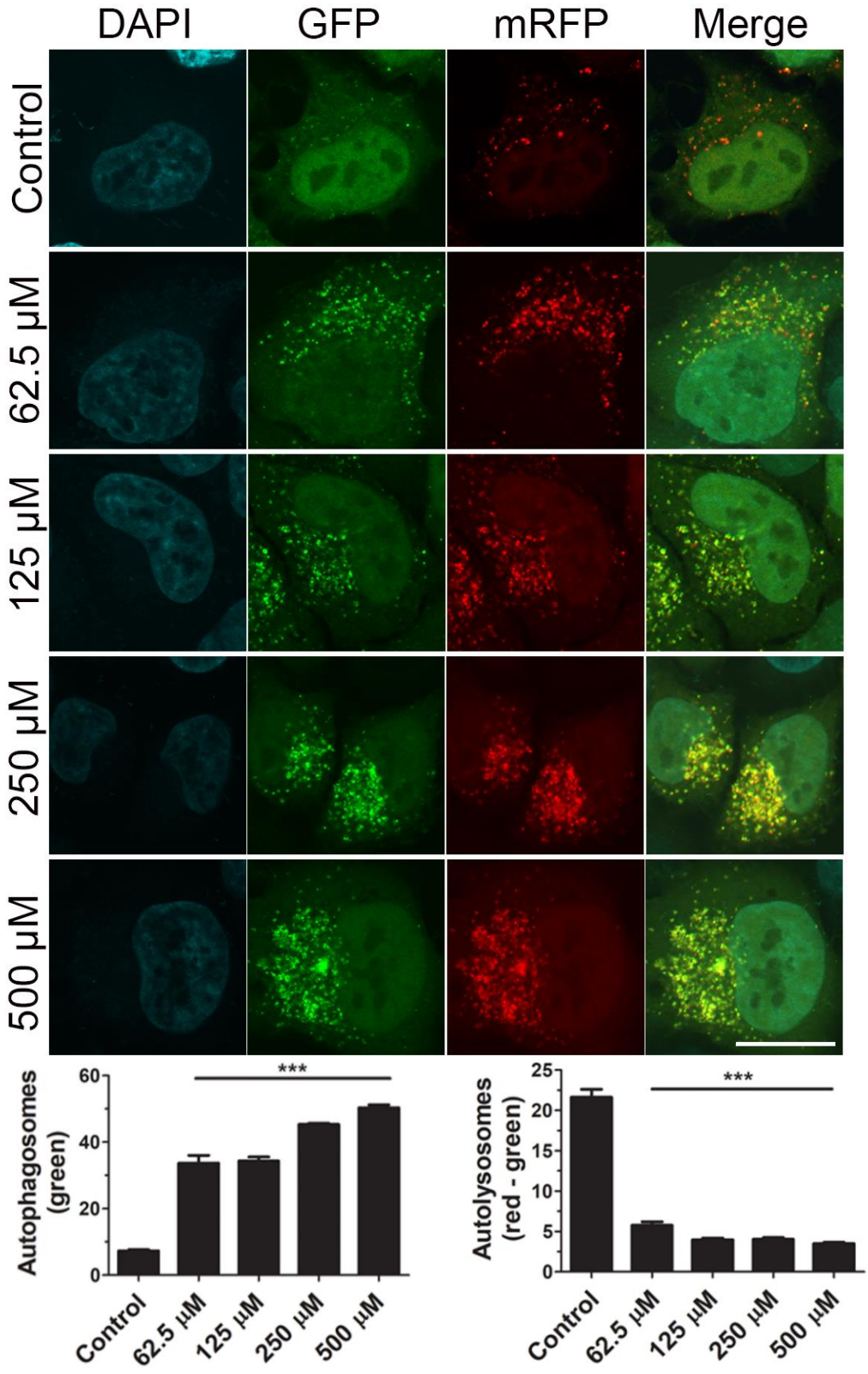

Figure 3.3 Mn inhibits autophagy flux in HeLa cells. mRFP-GFP-LC3 stably expressing HeLa cells were treated with $MnCl_2$ at different concentrations (62.5 – 500 µM) for 24 h. The number of autophagosomes (green vesicles) and autolysosomes (red vesicles minus green vesicles) per cell were quantified in at least 30 cells per condition, for triplicate experiments. Data are shown as mean ± SEM (n=3 independent experiments). One Way Anova with Tukey's post-hoc analysis ***: $P < 0.001$ compared to control cells. Scale bar 20 µm.

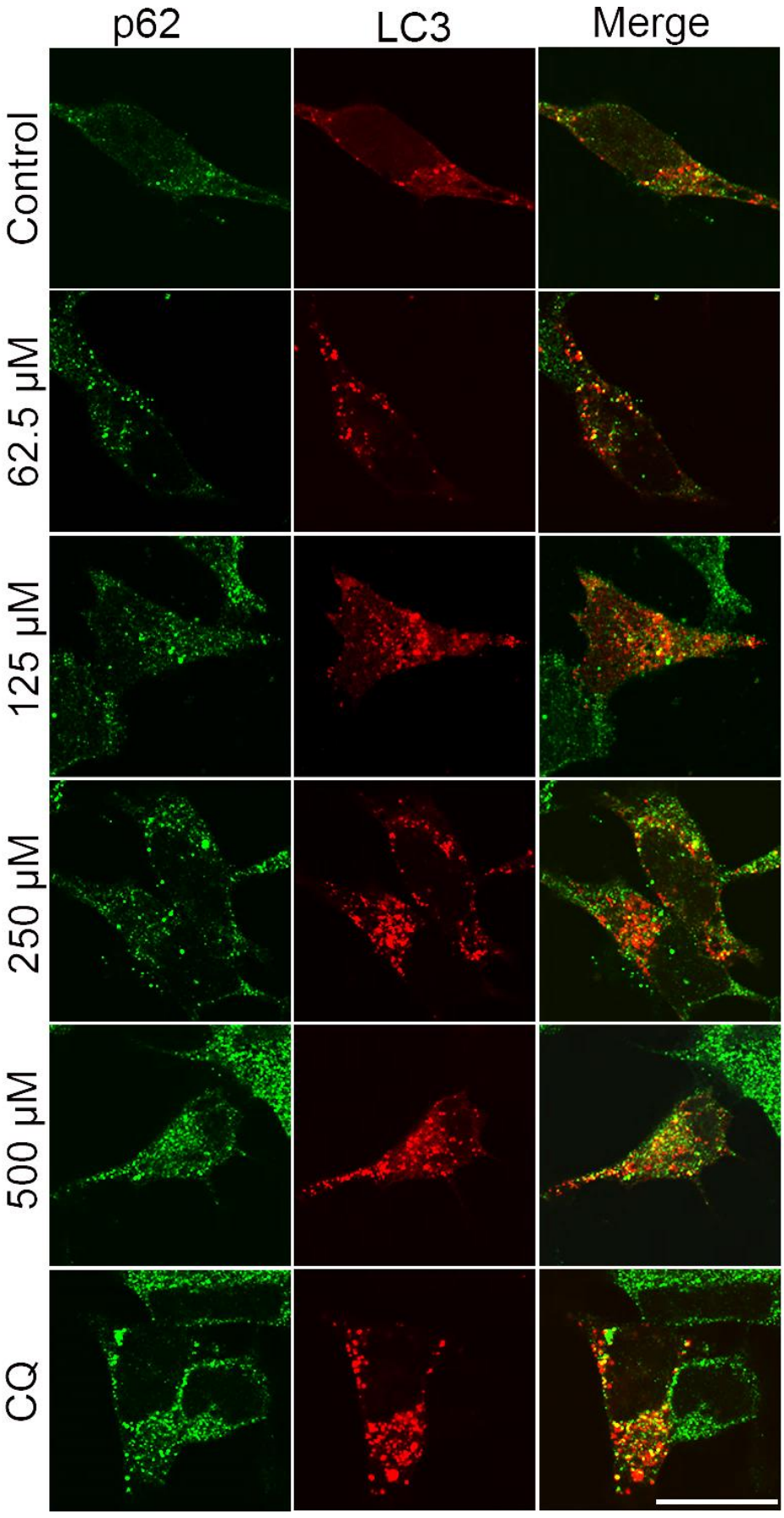

Figure continues on next page

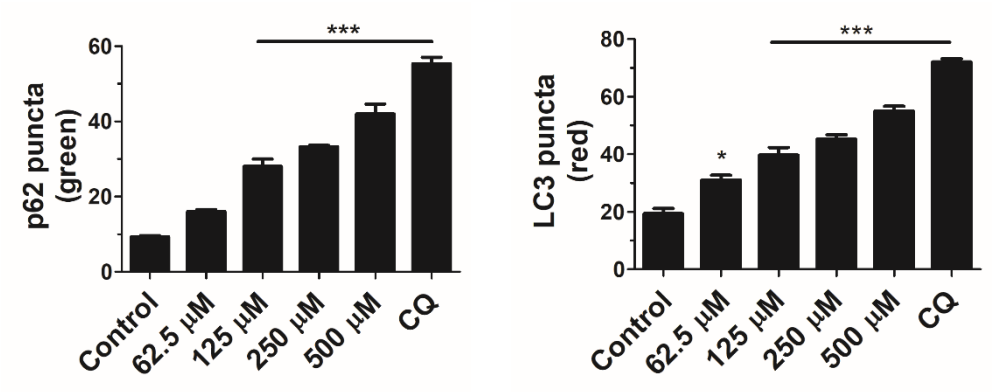

Figure 3.4 Mn treatment blocks autophagy in neuroblastoma cells. M17 cells were transfected with LC3-cherry plasmid (0.3 μg). 24 h post-transfection cells were treated with $MnCl_2$ (62.5 – 500 μM) or CQ (10 μM) for another 24 h. Images show LC3 fluorescence (red) and p62 staining (green). The number of LC3 and p62 puncta per cell was quantified in at least 20 LC3-cherry-positive cells per condition, for triplicate experiments. Data are shown as mean ± SEM (n=3 independent experiments). One Way Anova with Tukey's post-hoc analysis *: $P < 0.05$; ***: $P < 0.001$ compared to control. Scale bar 20 μm.

3.2.3 Effects of Drp1 inhibition on Mn-induced changes

Pharmacologically or genetically targeting the function of Drp1 has previously been shown to be protective in several models of PD (Cui et al., 2010, Rappold et al., 2014). Furthermore, results from our laboratory demonstrated that inhibition of Drp1 could restore the impaired autophagy flux of cells exposed to α-synuclein (Fan et al., 2019). Therefore, I investigated whether the deficit in the autophagy pathway, caused by Mn exposure, could be rectified by blocking mitochondrial fission (via gene silencing and small molecule). HeLa and M17 cells were transiently transfected with the appropriate Drp1 small interfering RNA (siRNA, human) and siRNA scramble, to assess the efficiency of Drp1 knock-down after 48 h (**Figure 3.5**). The efficiency of knocking down Drp1 was verified using WB and results clearly showed reduced Drp1 levels of over 70% in both cell lines compared to control and scramble cells. Scramble siRNA did not affect Drp1 protein expression compared to control cells.

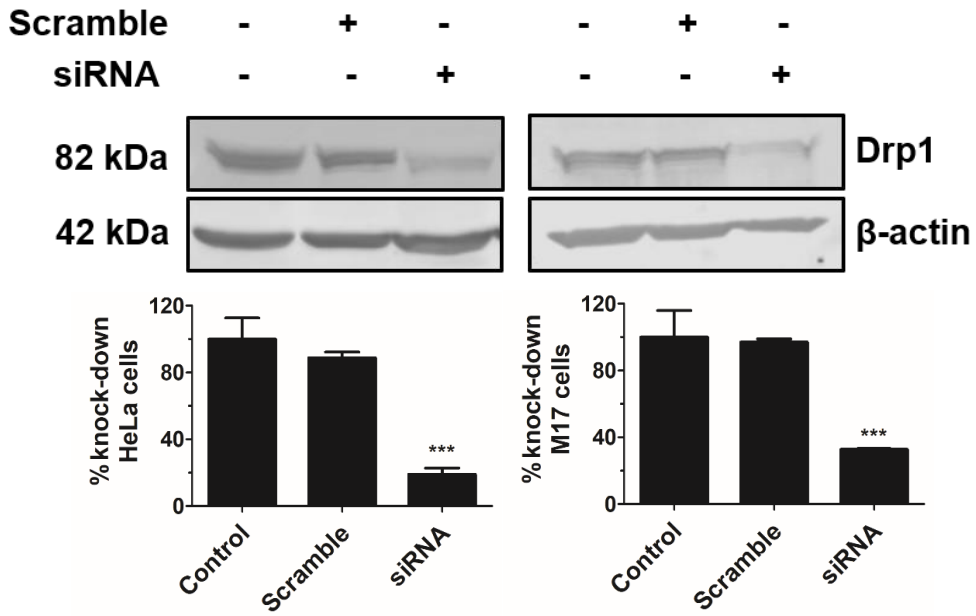

Figure 3.5 Efficiency of Drp1 knockdown mediated by siRNA. HeLa and M17 cells were transfected with 10 nM human siRNA and scramble for 48 h. 30 μg of protein were loaded/well. Western blot against Drp1 antibody was used to confirm knockdown efficiency compared to control and scramble cells. β-actin was used as loading control. Blots were visualized on an Odysey CLx machine and optical density measured using Li-Cor Image Studio software. Data are shown as mean ± SEM (n=4 independent experiments). One Way Anova with Tukey's post-hoc analysis ***: $P < 0.001$ compared to control and scramble cells.

To assess the effects of Drp1 inhibition on autophagy flux following Mn treatment, cells were processed for immunostaining. HeLa cells were transfected with either siRNA scramble or Drp1 siRNA for 24 h and then treated with 62.5 μM $MnCl_2$ for another 24 h. Results clearly indicate that Drp1 knockdown attenuated the autophagy impairment induced by $MnCl_2$ treatment as evidenced by a significant reduction in the number of autophagosomes (from 41.35 ± 0.91 to 27.21 ± 2.08) and increased autolysosomes (from 3.73 ± 0.66 to 16.84 ± 0.94), respectively. In fact, the number of autophagosomes and autolysosomes per cell were restored to a level that were no longer considered statistically different to control cells (autophagosomes, 22.74 ± 1.91; autolysosomes, 33.57 ± 4.43) (**Figure 3.6**).

Similar results were achieved in M17 cells co-transfected with Drp1 siRNA and LC3-cherry plasmid, treated with 125 μM $MnCl_2$ and then stained for p62. Data show that Drp1 inhibition reduced the Mn-induced accumulation of LC3 (from 140.98 ± 3.45 to 75.79 ± 1.77) and p62 (from 154.64 ± 3.42 to 62.14 ± 0.55) puncta to control (LC3, 55.10 ± 5.63; p62, 50.88 ± 3.87) and siRNA (LC3, 61.64 ± 1.88; p62, 47.03 ±1.51) levels. CQ was used as a positive control for autophagy blockade and induced a potent increase in both LC3 (243.17 ± 17.12) and p62 (258.84 ± 25.01) puncta (**Figure 3.7**).

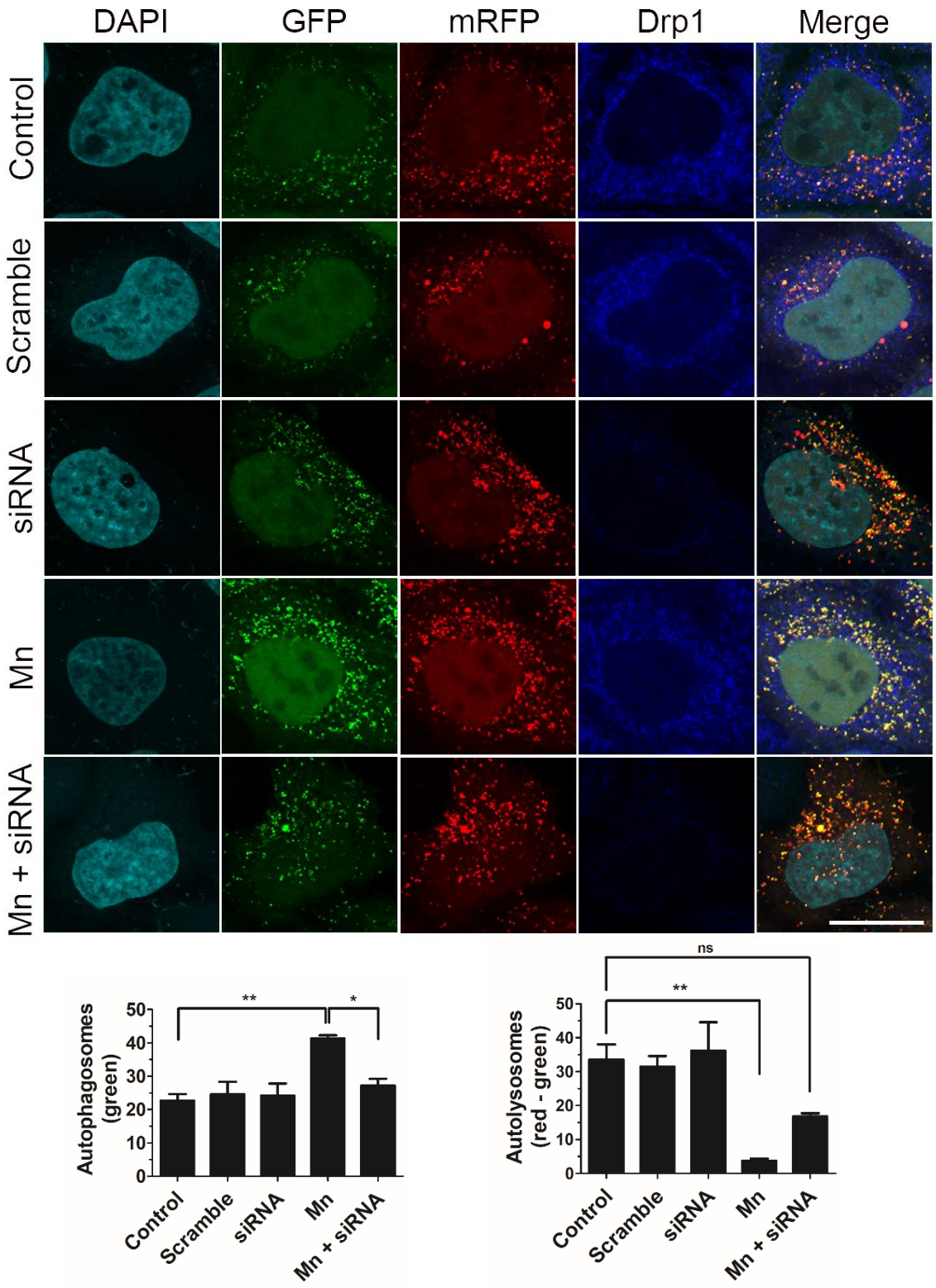

Figure 3.6 Drp1 inhibition attenuates autophagy blockade induced by Mn treatment in HeLa cells. HeLa mRFP-GFP-LC3 expressing cells were transfected with 10 nM human Drp1 siRNA or scramble. 24 h post-transfection cells were treated with $MnCl_2$ (62.5 μM) and stained for Drp1 (blue channel). The number of autophagosomes (green puncta) and autolysosomes (red minus green puncta) per cell was quantified in at least 30 cells per condition, for triplicate experiments. Data are shown as mean ± SEM (n=3 independent experiments). One Way Anova with Tukey's post-hoc analysis *: $P < 0.05$; **: $P < 0.01$. Scale bar 20 μm.

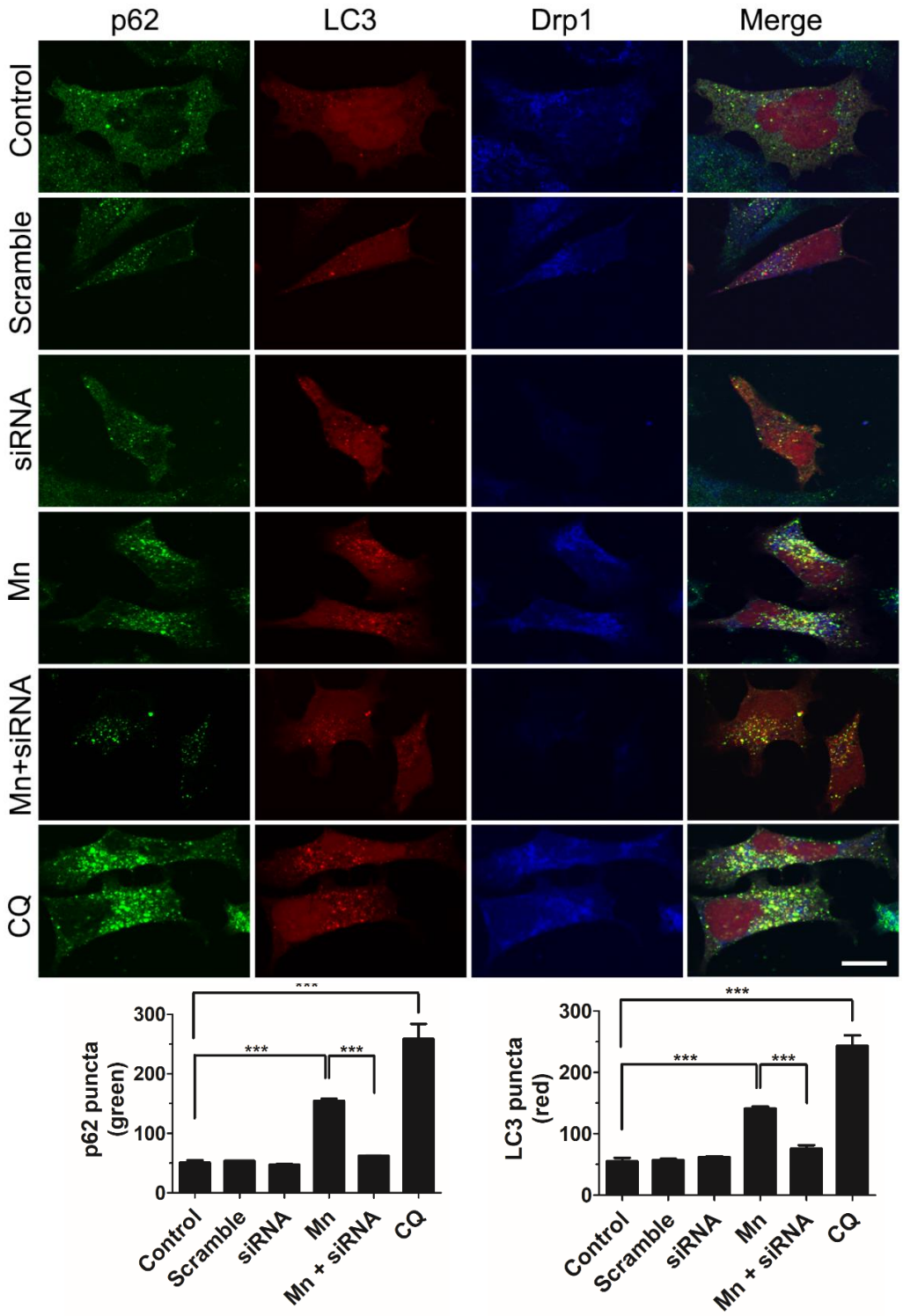

Figure 3.7 Inhibition of Drp1 attenuates autophagy blockade induced by Mn in M17 neuroblastoma cells. M17 cells were transfected with human Drp1 siRNA (10 nM) represented in the blue staining and LC3-cherry (red). 24 h post-transfection cells were treated with $MnCl_2$ (125 µM) for another 24 h, then stained for p62. ImageJ was used to quantify the amount of green and red vesicles, representing respectively p62 and LC3 puncta. The number of puncta per cell was determined by counting at least 20 LC3-cherry positive cells for each condition, for triplicate experiments. Data are shown as mean ± SEM (n=3 independent experiments). One Way Anova with Tukey's post-hoc analysis **: $P < 0.01$; ***: $P < 0.001$. Scale bar 20 µm.Scale bar 20 µm.

To fortify this data, LC3-II (the only well-characterised protein specifically localised to autophagic structures throughout the process from phagophore to lysosomal degradation) and p62 protein levels were assessed via WB in M17 cells (**Figure 3.8 A-C**). An increment in both LC3-II and p62 levels was detected when cells were exposed to 125 µM $MnCl_2$ for 24 h, indicative of a late blockade in the autophagy pathway Inhibition of Drp1 promoted a significant reduction of LC3-II and p62 levels in Mn-exposed cells that was no longer considered significant when compared to control cells. In addition, no changes in LC3-I protein levels were detected amongst groups (**Figure 3.8 D**). The LC3-II/LC3-I ratio was analysed to further investigate the relative expression of both proteins. Results showed that both Mn and CQ treatment caused an increase in LC3-II/LC3-I ratio, which was reduced by inhibiting Drp1 in Mn-treated cells (**Figure 3.8 E**). Overall, these results concur with the immunostaining data of both cell lines: inhibition of Drp1 improves autophagy function impaired by Mn treatment.

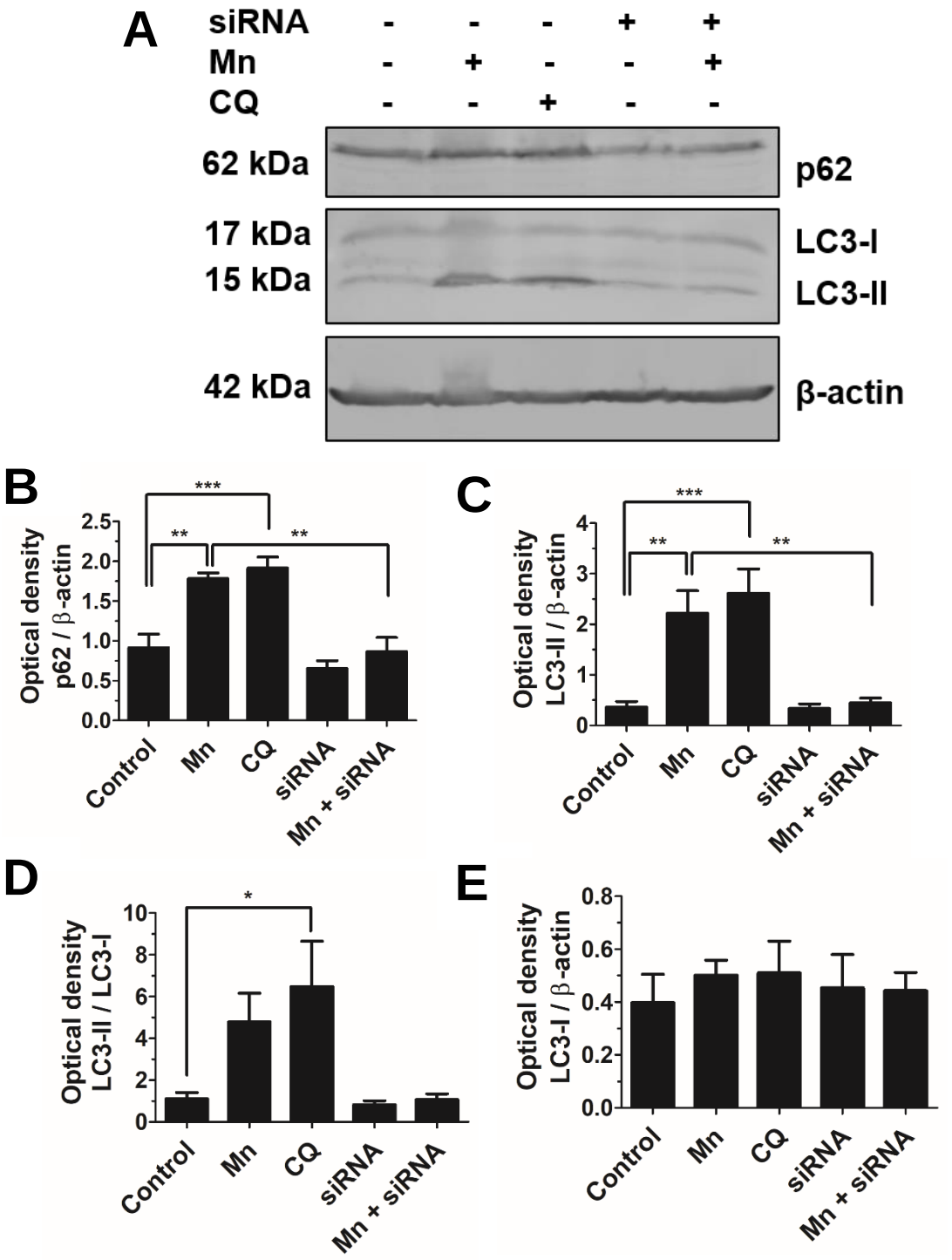

Figure 3.8 Drp1 inhibition is protective against Mn-induced autophagy. (**A**) WB of M17 cells transfected for 24 h with human Drp1 (10 nM) and/or then treated with either $MnCl_2$ (125 μM) or CQ (10 μM) for another 24 h. Cell pellets from one well of a 6-well plate were subjected to SDS-PAGE and probed with the indicated antibodies. (**B**) P-62, (**C**) LC3-II (**D**) LC3-I and (**E**) LC3-II/LC3-I levels were quantified using β-actin as a loading control. Blots were visualized on an Odysey CLx machine and optical density measured using Li-Cor Image Studio software. Data are shown as mean ± SEM (n=4 independent experiments). One Way Anova with Tukey's post-hoc analysis *: $P < 0.05$; **: $P < 0.01$; ***: $P < 0.001$ Note that the band running just below LC3-I at approximately 17.5 kDa may be a processing intermediate of LC3-I, detectable in freshly prepared samples.

First described by Cassidy et al. (2008), mdivi-1 is a cell permeable quinazolinone that inhibits Drp1 function in both yeast and mammalian cells. As many previous studies, including those from our research group, have reported that the beneficial effects of mdivi-1 in multiple PD models, I tested whether 10 μM mdivi-1, as previously described by Cui et al. (2010) could also confer protection against Mn toxicity and rescue the autophagy flux in HeLa cells.

Efficiency of mdivi-1 on Drp1 inhibition was not directly tested in this thesis, however this inhibitor has been widely reported to produce effects consistent with blocking mitochondrial fission (Smith and Gallo, 2017) and blocking GTPase function of human Drp1 (Numadate et al., 2014, Manczak et al., 2018) with an IC50 of approximately 13 μM (Numadate et al., 2014) and my lab has previously shown that mdivi-1 treatment could reduce excessive fission (Cui et al., 2010, Rappold et al., 2014, Bido et al., 2017, Fan et al., 2019).

Co-treatment with $MnCl_2$ and mdivi-1 significantly reduced the numbers of autophagosomes (19.10 ± 1.05) compared to Mn treated cells alone (25.60 ± 1.48), however, the number of autophagosomes remained significantly higher when compared to control cells (8.61 ± 0.96). On the other hand, the number of autolysosomes were significantly increased (16.13 ± 0.75) in cells co-treated with mdivi-1 and $MnCl_2$ compared to cells treated with $MnCl_2$ alone (4.80 ± 0.30) (**Figure 3.9**) and were no longer significantly different when compared to control cells (19.01 ± 0.37). Taken together these results suggest that the blockade in the autophagy flux caused by Mn exposure could be rescued by pharmacologically inhibiting Drp1. Of note, mdivi-1 treatment alone increased the number of autophagosomes (15.40 ± 1.46) as compared to the control group, further suggesting that mdivi-1 activates autophagy.

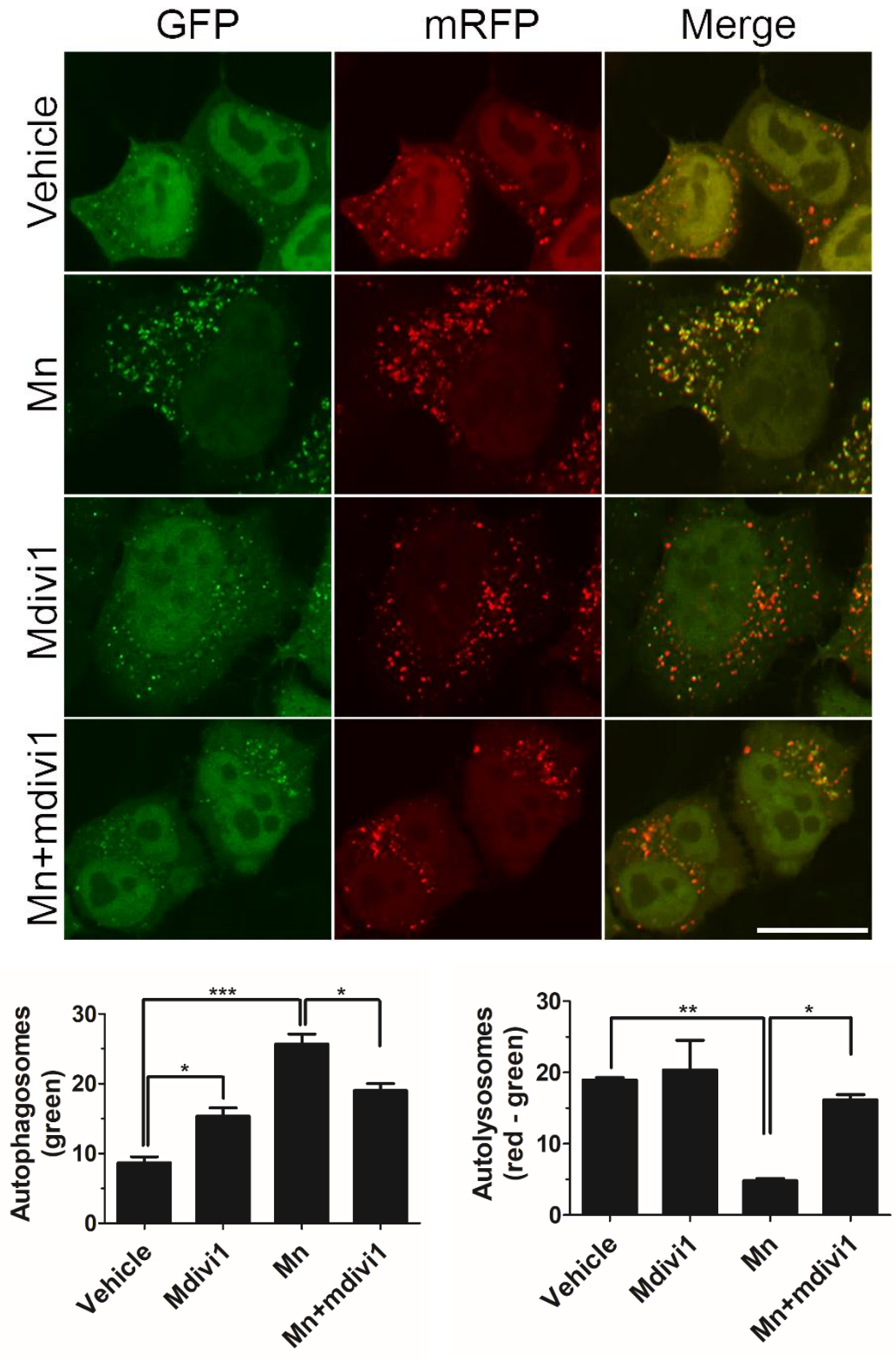

Figure 3.9 Mdivi-1 improves autophagy blockade induced by Mn treatment. HeLa mRFP-GFP-LC3 expressing cells were co-treated with $MnCl_2$ (62.5 μM) and mdivi-1 (10 μM) or control vehicle (DMSO) for 24 h. The numbers of autophagosomes (green puncta) and autolysosomes (red minus green puncta) per cell were quantified in approximately 30 cells per experiment, for triplicate experiments. Data are shown as mean ± SEM (n=3 independent experiments). One Way Anova with Tukey's post-hoc analysis *: $P < 0.05$; **: $P < 0.01$; ***: $P < 0.001$. Scale bar 20 μm.

3.2.4 Interplay between Mn and α-synuclein

In order to further investigate the effect of Mn-induced autophagy dysfunction and to explore a potential interaction between Mn and α-synuclein, the inducible human WT α-synuclein expressing N27 cell line, previously generated in our lab (Cui et al., 2010), was used. In the presence of Ponastrone A (PonA), an ecdysone analogue inducer, the expression of human WT α-synuclein was induced (**Figure 3.10**).

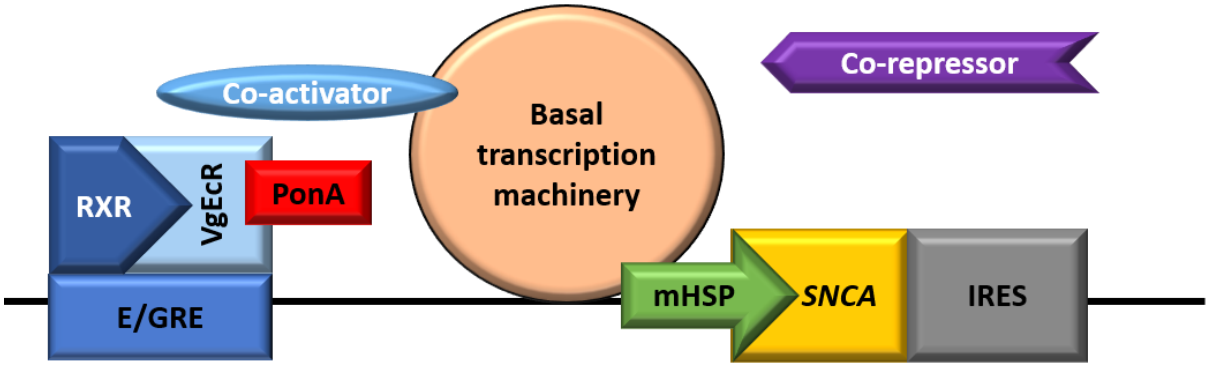

Figure 3.10 Inducible overexpression of human α-synuclein in rat DAergic N27 neuronal cells. Stable cells containing a vector that constitutively expresses the ecdysone receptor (VgEcR) and the retinoid X receptor (RXR) were generated. These cells were subsequently stably transfected with a second vector that contains the ecdysone-responsive element (E/GRE) and a multiple cloning site for the insertion of the human WT α-synuclein (*SNCA*) gene. The VgEcR-retinoid X receptor heterodimer binds to the E/GRE. In the presence of PonA, an ecdysone analogue inducer, the co-repressors are released from VgEcR, and the co-activators are recruited, resulting in *SNCA* gene activation via the minimal heat shock promoter (mHSP). IRES, internal ribosome entry site.

Previous WB results from our lab, using a human α-synuclein antibody, showed that α-synuclein overexpression in N27 cells was time and dose dependent after induction with PonA alone (Fan et al. data not yet published). The optimal induction conditions were determined to be 48 h treatment of 20 μM of PonA. A representative image of α-synuclein expression, following 48 h of PonA treatment, is described in **Figure 3.11 A**. To assess the effects of Mn on α-synuclein aggregation, N27 cells were exposed to Mn with PonA for 48 h; chloroquine (CQ), an inhibitor of lysosomal degradation, was used as a positive control.

Proteinase K treatment was then used to measure the number of insoluble α-synuclein positive aggregates as proteinase K resistance is a property of mature aggregated proteins. A significant increase in the number of α-synuclein insoluble aggregates in PonA induced cells (9.35 ± 0.40) was detected when compared to the non-induced (vehicle) cells (0.78 ± 0.31) (**Figure 3.11 D-E)**. This observation demonstrates the ability of our model to produce more mature α-synuclein containing aggregates. Treatment of cells with 125 μM $MnCl_2$ for 48 h (during PonA induction) induced a further increase in the number of α-synuclein aggregates per cell (19.46 ± 3.00) (**Figure 3.11 D-E**). Inhibition of Drp1, via siRNA, reduced the number of α-synuclein insoluble aggregates in PonA induced cells alone (1.02 ± 0.36) or in combination with Mn treatment (6.98 ± 0.75), no longer statistically different to vehicle cells. Drp1 knockdown efficiency was verified via WB (**Figure 3.11 B**).To determine the time-dependent nature of this effect, N27 cells were exposed to Mn and/or PonA for 24 h. As evidenced by the graph (**Figure 3.11 C**), 24 h incubation had no significant effect on α-synuclein in cells treated with either PonA alone (2.25 ±0.19) or with $MnCl_2$ and PonA together (2.34 ± 0.20), images not shown. In addition, exposure to $MnCl_2$ alone (1.80 ± 0.12), without PonA treatment, did not alter/induce α-synuclein expression (images not shown). On the contrary to Mn effects on α-synuclein expression after 24 and 48 h treatment, CQ treatment induced an increase in α-synuclein aggregates that was always stronger than Mn and statistically different compared to vehicle cells at 48 (24.86 ± 2.34) and 24 h (4.90 ± 0.52).

These findings indicate that there is a clear increase in number of proteinase K-resistant α-synuclein aggregates following 48 h exposure to Mn when compared to vehicle and α-synuclein overexpressing cells alone. Drp1inhibition reduced the amount of protein aggregates to normal levels. Given the time point and the effects of an autophagy inhibitor on α-synuclein aggregation, these results may suggest that α-synuclein aggregation could be the result of autophagy blockade.

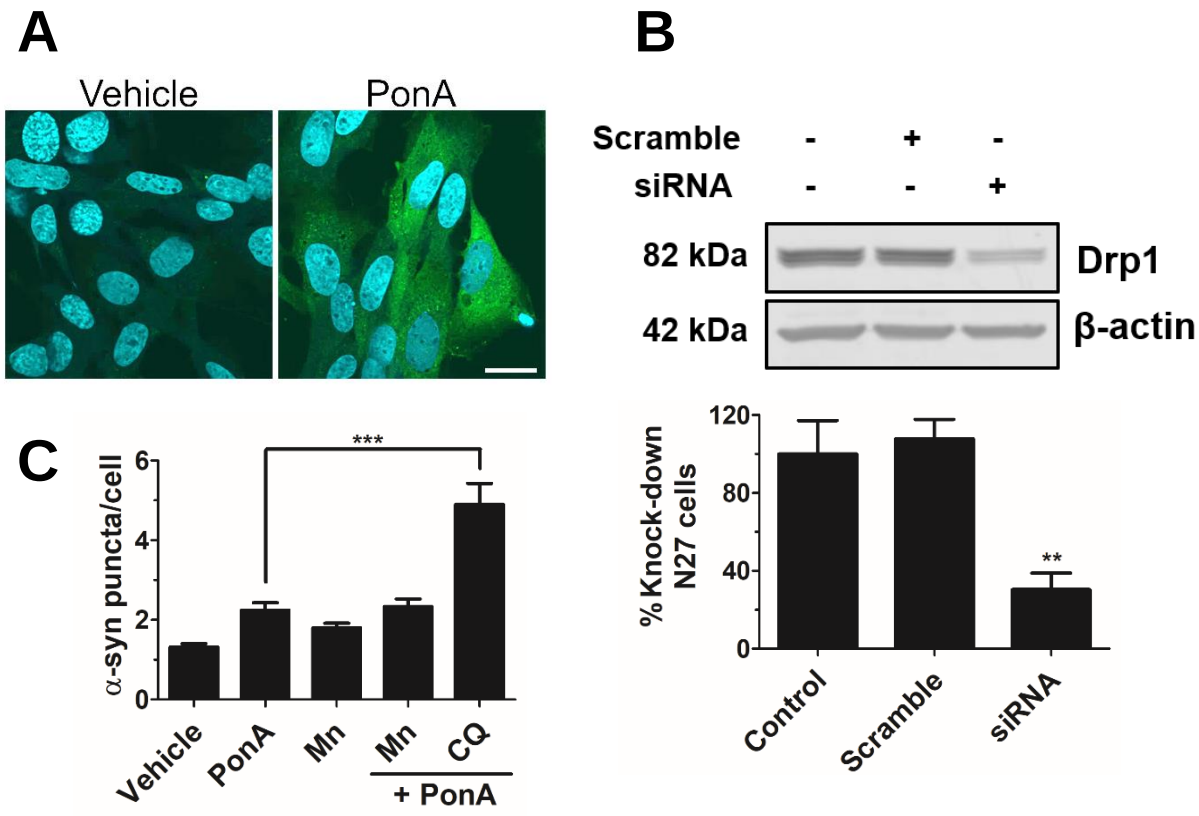

Figure 3.11 Drp1 inhibition attenuates α-synuclein aggregation, induced by Mn in N27 cells. (**A**) Representative image of α-synuclein induction (soluble aggregates), following 48 h of PonA treatment. Scale bar 20 μm. (**B**) Efficiency of Drp1 knock-down mediated by siRNA in N27 cells. Cells were transfected with 10 nM human siRNA and scramble for 48 h. 30 μg of protein were loaded/well. WB against Drp1 antibody was used to confirm knock-down efficiency compared to control and scramble. β-actin was used as loading control. Blots were visualized on an Odysey CLx machine and optical density measured using Li-Cor Image Studio software. **: $P < 0.01$ compared to control and scramble cells. Data are shown as mean ± SEM (n=3 independent experiments). (**C**) The graph represents insoluble α-synuclein puncta post Proteinase K treatment. α-synuclein overexpression was induced (20 μM PonA) alone or in combination with Mn (125 μM) or CQ (10 μM) for 24 h, along with Mn treatment alone. Data are shown as mean ± SEM (n=3 independent experiments). One Way Anova with Tukey's post-hoc analysis. No statistical difference was found between vehicle and Mn treated groups. ***: $P < 0.001$. (**D**) N27 cells were transfected with rat Drp1 siRNA (10 nM) or scramble control. 24 h post-transfection α-synuclein overexpression was induced (20 μM PonA) alone or in combination with Mn (125 μM) or CQ (10 μM) for 48 h. Post fixation, cells were incubated with either PBS (data not shown) or Proteinase K and then processed for ICC using an antibody particularly effective at identifying higher order structures of the protein (Millipore, AB5038). Images show insoluble α-synuclein aggregates. Scale bar 20 μm. (**E**) ImageJ was used to quantify the α-synuclein-positive puncta per cell in at least 30 cells for each condition, for triplicate experiments. Data are shown as mean ± SEM (n=3 independent experiments). One Way Anova with Tukey's post-hoc analysis *: $P < 0.05$; **: $P < 0.01$; ***: $P < 0.001$.

Figure continues on next page

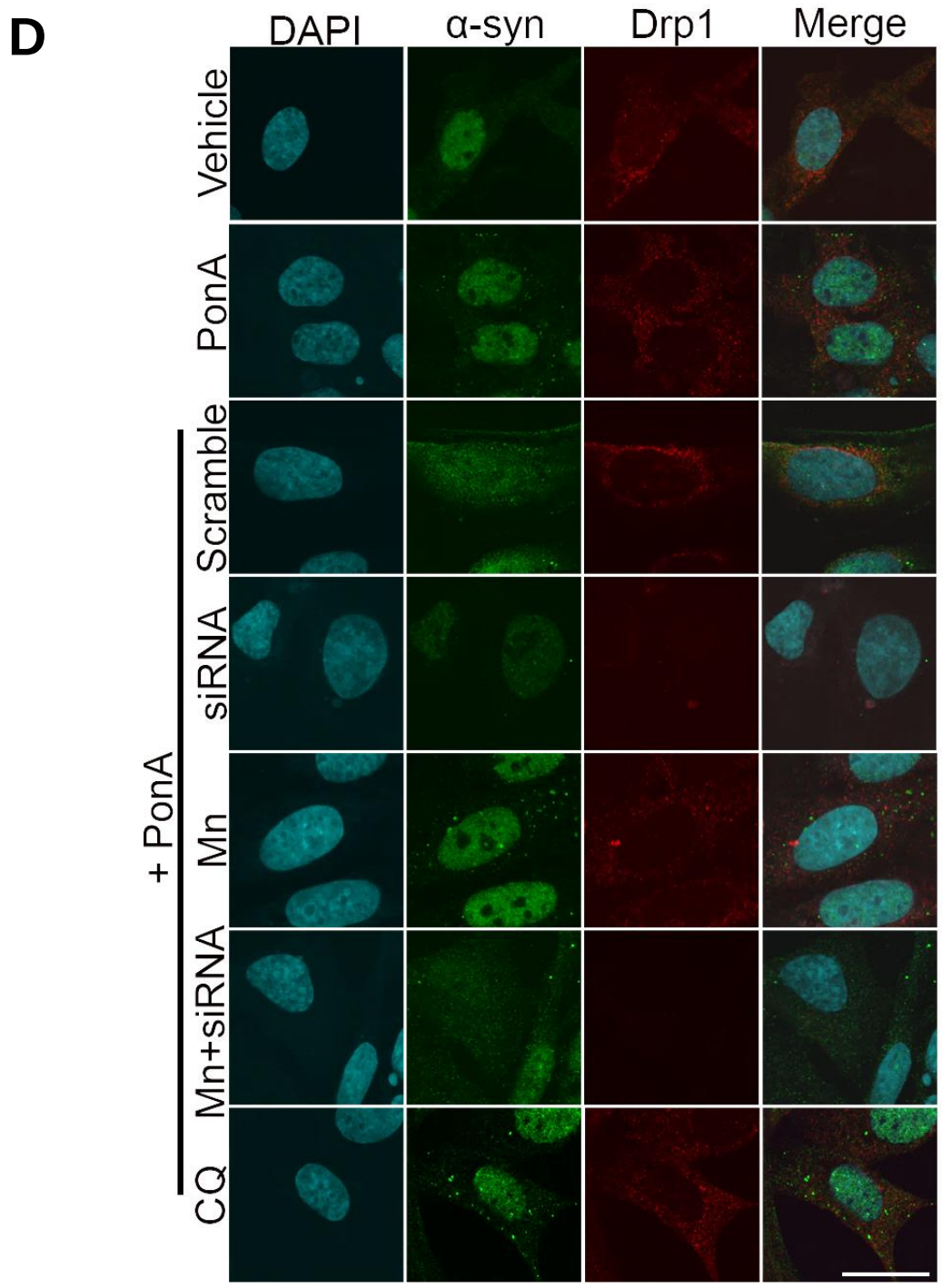
D
DAPI
α-syn
Drp1
Merge
Vehicle
PonA
Scramble
siRNA
Mn
Mn+siRNA
CQ
+ PonA
E
α-syn puncta/cell
30
20
10
0
**
**
*
***
***
Vehicle
PonA
Scramble
siRNA
Mn
Mn + siRNA
CQ
+ PonA

To investigate this further, N27 cells were transfected with LC3-cherry plasmid and Drp1 siRNA (as previously done in M17 cells), treated with $MnCl_2$ and/or PonA for 24 h and then processed for p62, Drp1 and α-synuclein staining (**Figure 3.12**). CQ was used as a positive control for autophagy blockade. Mn alone caused an increase in both LC3 (39.72 ± 0.76) and p62 (54.30 ± 4.73) puncta compared to vehicle cells (LC3, 18.06 ± 1.12; p62, 27.46 ± 0.99), indicating a blockade in the autophagy pathway. Again, inhibition of Drp1 improved Mn-induced accumulation of LC3 (25.02 ± 2.06) and p62 (33.55 ± 2.36) puncta (**Figure 3.12 A and C**). These results are consistent with both HeLa (**Figure 3.6**) and M17 (**Figure 3.7**) cells. Upon co-treatment of PonA and Mn, the number of LC3 (48.83 ± 3.54) and p62 (71.16 ± 8.33) puncta increased to levels that were statistically different to cells exposed to PonA (LC3, 33.23 ± 1.31; p62, 46 ± 2.20) and Mn alone (LC3, 39.72 ± 0.76; p62 54.30 ± 4.73). These results indicate that α-synuclein alone blocked autophagy, as did Mn, however had a greater effect when combined (PonA + Mn). Consistently, CQ treatment had a stronger effect and induced a greater accumulation of both LC3 (87.36 ± 8.41) and p62 (114.48 ± 11.55) puncta compared to any other treatment. Drp1 knockdown significantly reduced LC3 and p62 puncta in both PonA induced cells (LC3, 21.43 ± 1.73; p62, 29.69 ± 1.78) and cells co-treated with PonA and Mn (LC3, 26.75 ± 0.5; p62, 33.16 ± 1.35), to a level that was not statistically different to vehicle cells (LC3, 17.35 ± 0.71; p62, 25.57 ± 0.57) (**Figure 3.12 B and D**).

Overall this data suggest that autophagy dysfunction induced by Mn-exposure occurs prior to α-synuclein aggregation and that Drp1 inhibition ameliorates these Mn-induced changes.

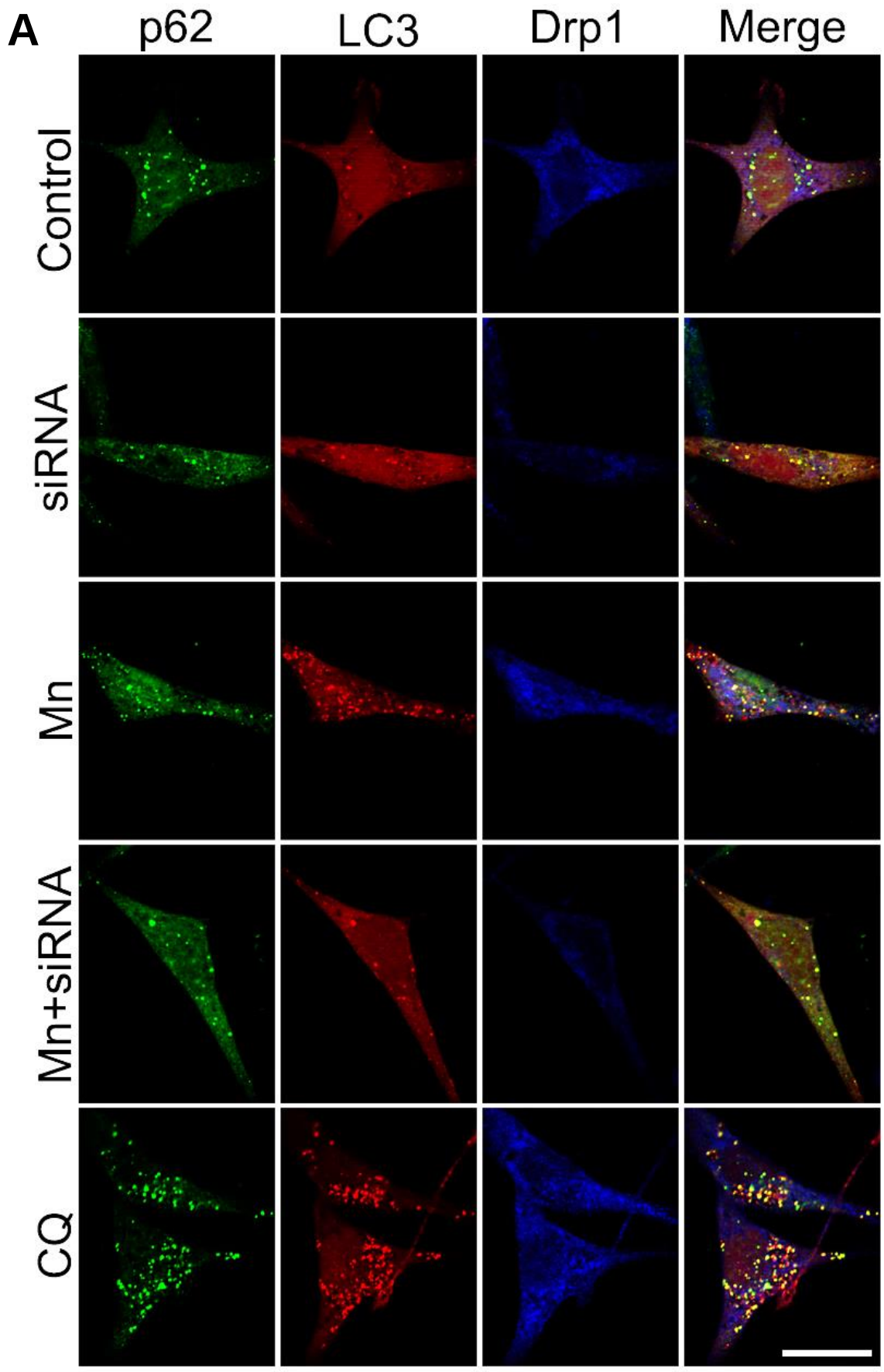

Figure continues on next page

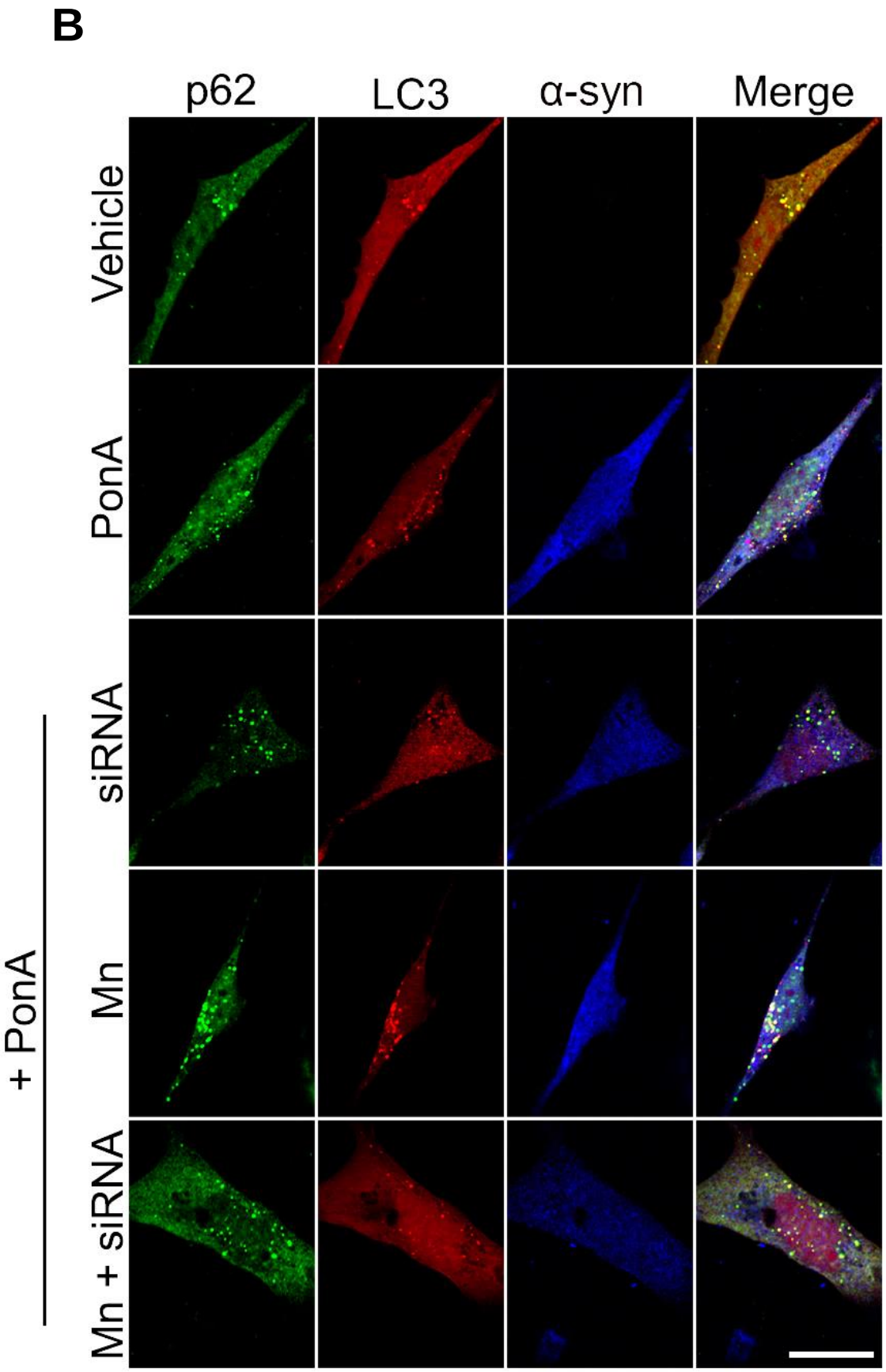

Figure continues on next page

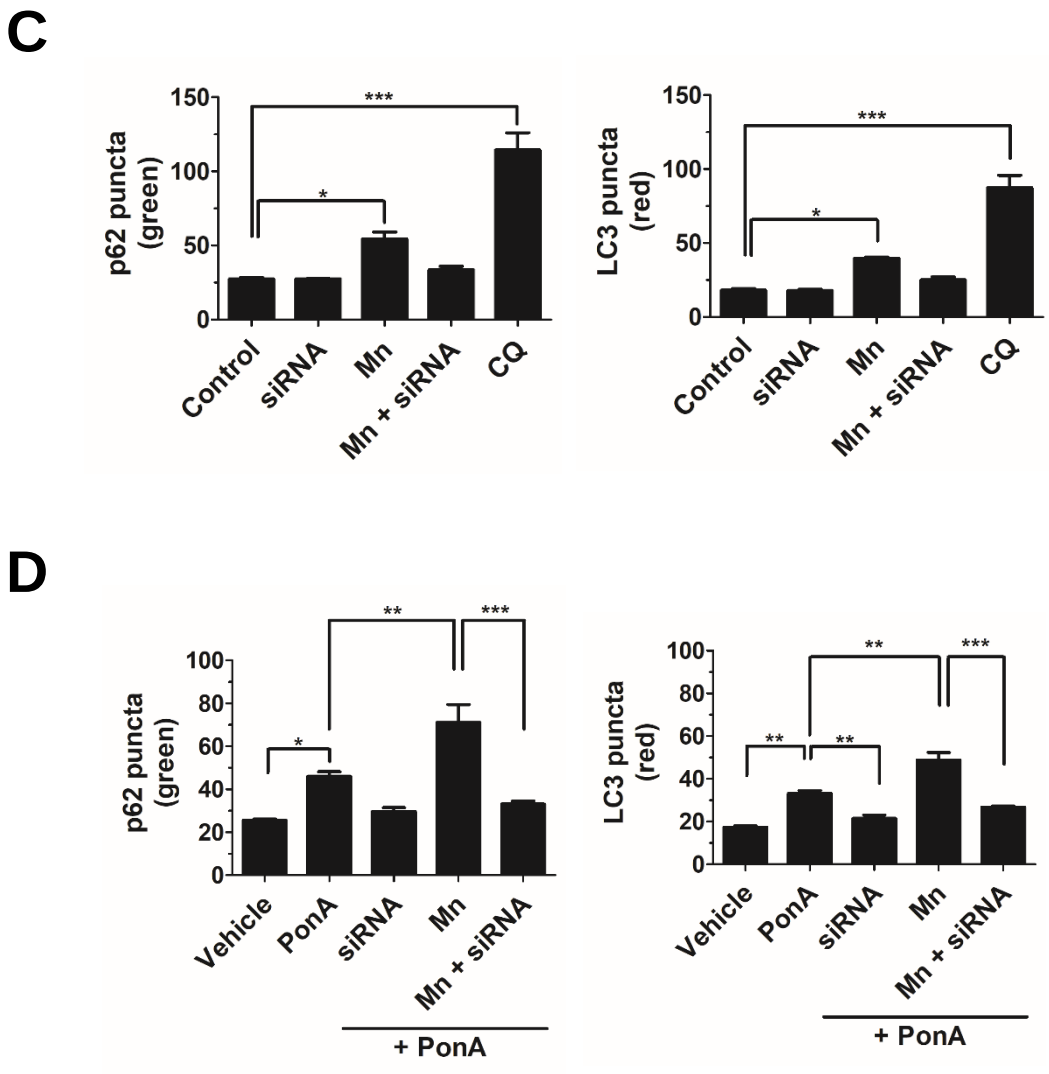

Figure 3.12 Inhibition of Drp1 attenuates autophagy blockade induced by Mn in N27 DAergic cells. N27 cells were transfected with human Drp1 siRNA (10 nM) represented in the blue staining and LC3-cherry (red). 24 h post-transfection cells were treated for another 24 h with (**A**) $MnCl_2$ (125 μM) and (**B**) $MnCl_2$ (125 μM) and/or PonA (20 μM). CQ (10 μM) was used as a positive control. Following imaging, ImageJ was used to count the amount of green and red vesicles, representing respectively p62 and LC3 puncta. The number of puncta per cell in (**C**) Mn-treated alone and (**D**) co-treated with Mn and/or PonA was determined by counting at least 20 LC3-cherry positive cells for each condition, for triplicate experiments. Data are shown as mean ± SEM (n=3 independent experiments). One Way Anova with Tukey's post-hoc analysis *: $P < 0.05$; **: $P < 0.01$; ***: $P < 0.001$ Scale bar 20 μm.

3.2.5 Effects of Mn on mitochondrial function and morphology

As previously stated, Mn toxicity has been widely associated with mitochondrial dysfunction. There is no evidence, however on whether mitochondrial dysfunction precedes autophagy dysfunction or *vice versa* and whether these impairments are the cause or the consequence of neurotoxicity. To address this issue, both M17 and N27 cells were treated with the same concentration of $MnCl_2$ (125 μM) that induced autophagy blockade and α-synuclein aggregation and evaluated for multiple measures of mitochondrial function and morphology.

Mitochondrial respiration was assessed in both cell lines by measuring the oxygen consumption rate (OCR), using the seahorse XF^e96 Extracellular Flux Analyser, following 24 h of $MnCl_2$ treatment (**Figure 3.13**). The herbicide PQ was used as a positive control to induce mitochondrial dysfunction (Cocheme and Murphy, 2008). The assay reported multiple key parameters, including basal respiration, ATP-linked respiration and spare respiratory capacity (SRC, ability of cells to meet an energetic demand, indicative of cell fitness). Results clearly showed that Mn exposure led to no changes in any measured paraments at this concentration in both M17 and N27 cells.

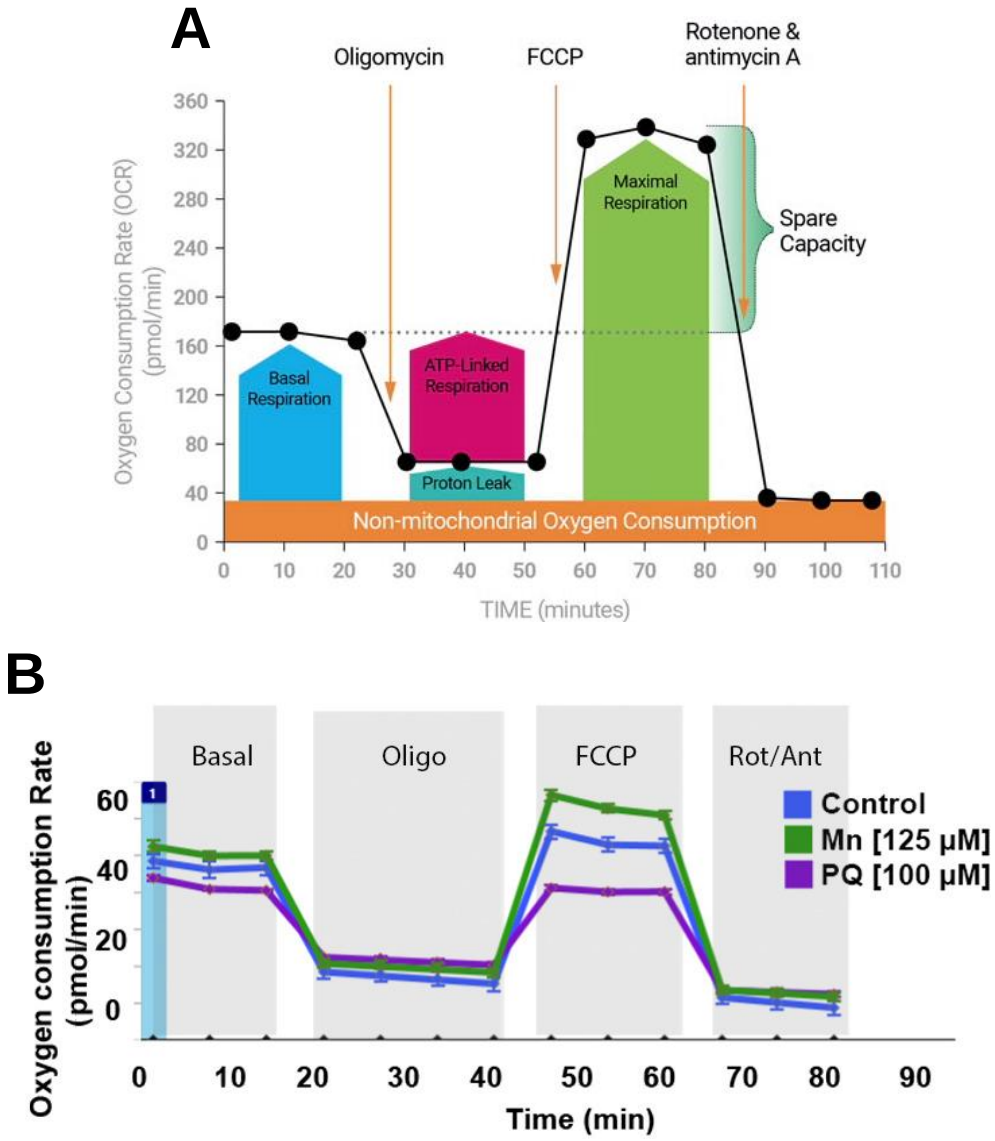

Figure continues on next page

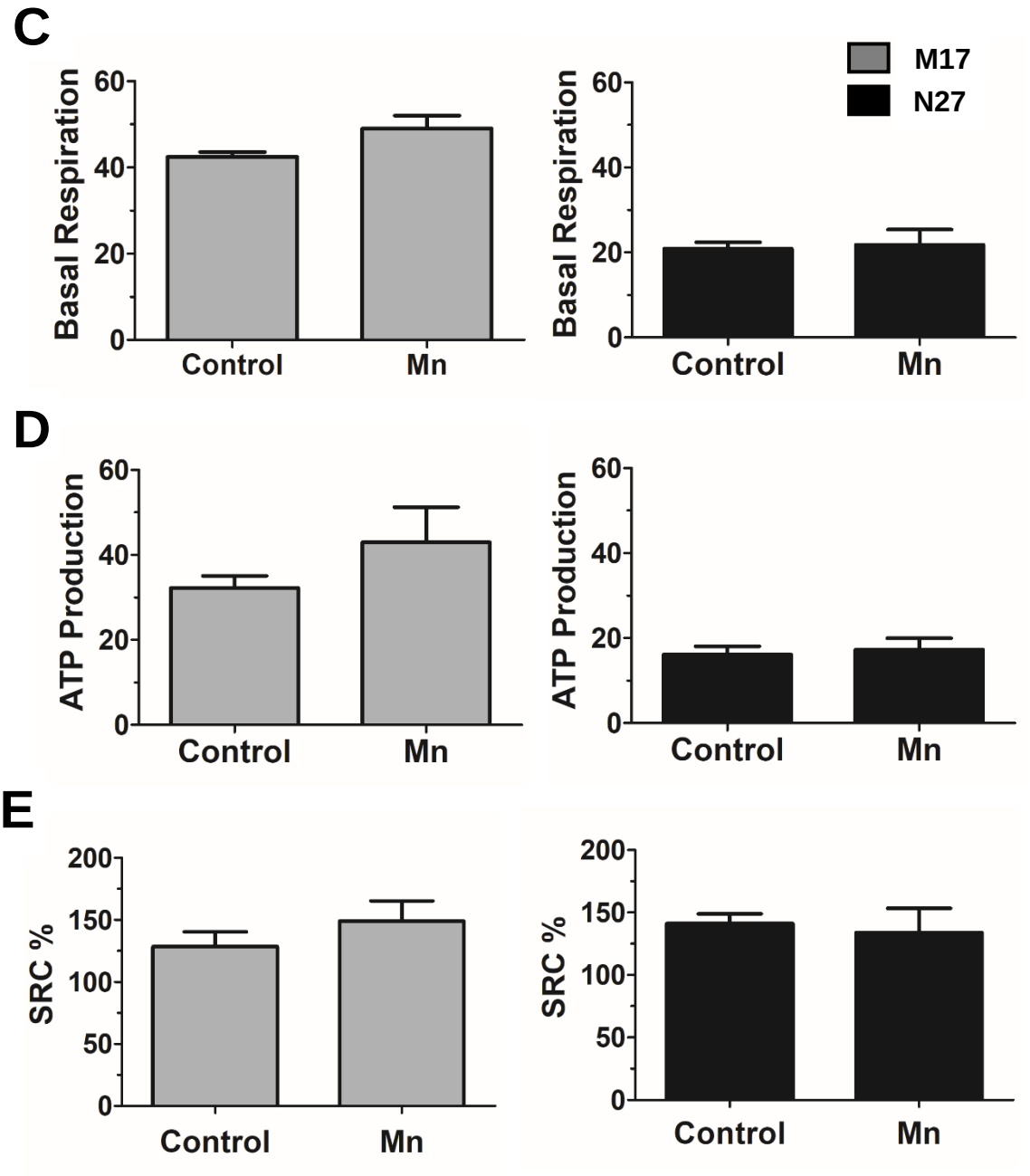

Figure 3.13 Mn does not impair mitochondrial function at a concentration that blocks autophagy. (**A**) Agilent Seahorse XF Cell Mito Stress Test profile of the key parameters of mitochondrial respiration. (**B**) Representative example of the kinetics OCR response in N27 and M17 cells exposed to Mn and PQ treatment. M17 and N27 cells were plated in XF^{e}96 tissue culture plate and treated with $MnCl_2$ (125 µM) for 24 h. Mitochondrial respiration was assessed by measuring OCR using the XF^{e}96 Extracellular Flux Analyzer. Sequential injections of oligomycin (to inhibit oxygen consumption mediated by ATP synthase), FCCP (an uncoupler to induce maximal OCR), Rotenone/Antimycin (to inhibit complex I and III, respectively). Effects of Mn on (**C**) Basal respiration, (**D**) ATP Production, (**E**) Spare Respiratory Capacity (SRC). Data are shown as mean ± SEM (n=3 to 4 independent experiments, with 6 wells per group, per experiment). Unpaired two-tailed Student's *t* test found no statistic significant difference when comparing control to Mn-exposed cells. The seahorse assay was performed and analysed by Dr Rebecca Z Fan.

To further corroborate these results, flow cytometry was used to measure membrane potential (Δψm) in live cells using TMRM, following Mn treatment in both M17 and N27 cells. The uncoupler carbonyl cyanide 4-(trifluoromethoxy) phenylhydrazone (FCCP) was used as a positive control to collapse membrane potential. As expected, FCCP significantly collapsed Δψm, as shown by a curve shift to the left (**Figure 3.14 A**), however, when cells were exposed to Mn, no changes were detected in either cell type (**Figure 3.14 B**).

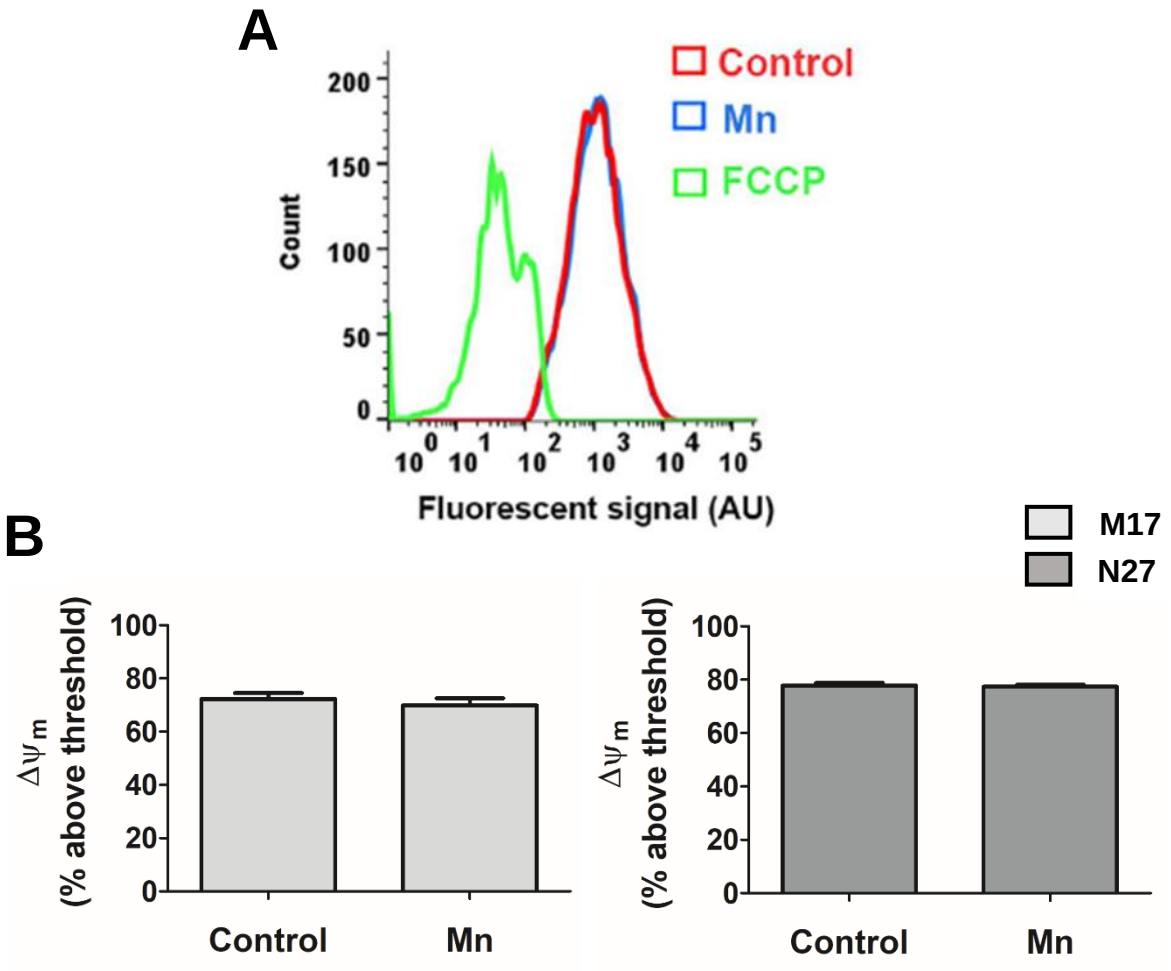

Figure 3.14 Mn does not affect mitochondrial membrane potential at a concentration that blocks autophagy. (**A**) Representative example of the fluorometric response of N27 and M17 cells exposed to Mn and FCCP. M17 and N27 cells were treated with Mn (125 µM) for 24 h. TMRM (50 nM) was applied for measuring mitochondrial membrane potential. Cells were incubated with TMRM for 20 min in dark and fluorescence signal was quantified using BD FACS Melody™ Cell Sorter. Uncoupler FCCP (20 µM) was used as a positive control to collapse membrane potential. (**B**) Δψm in M17 and N27 cells. Data are shown as mean ± SEM (n=3 independent experiments). Unpaired two-tailed Student's *t* test showed no statistic significant difference between control and Mn treated cells. Flow cytometry was performed and analysed by Dr Rebecca Z Fan.

Alaimo et al. (2014) previously suggested that high concentrations of $MnCl_2$ (750 µM) caused an imbalance in the equilibrium of fusion/fission proteins, which resulted in mitochondrial fragmentation. To verify these results, N27 cells were exposed to $MnCl_2$ for 24 h and mitochondrial morphology was determined following TOM20 immunostaining. Results clearly showed no changes in mitochondrial morphology in Mn-exposed cells (**Figure 3.15**). Mitochondrial perimeter measurements were binned to produce a histogram with a normal distribution. Mn treatment did not produce a change in any of the perimeter bins nor did it produce a shift in the normal distribution. Mitochondrial fragmentation would shift the distribution to the left, with more mitochondria in the smaller bins as shown by Cui et al. (2010).

As no changes in either mitochondrial function or morphology were detected using the same timepoint and concentration of $MnCl_2$ (125 µM) that impaired autophagy, a higher concentration of $MnCl_2$ (250 µM) was used to assess changes in mitochondrial function in N27 cells. The seahorse XF^e96 Extracellular Flux Analyser was used again following 24 h of $MnCl_2$ (250 µM) treatment. Results clearly indicated that this higher concentration of Mn could indeed affect mitochondrial respiration as evidenced by reductions in basal respiration, ATP-linked respiration and spare respiratory capacity when compared to control cells (**Figure 3.16**).

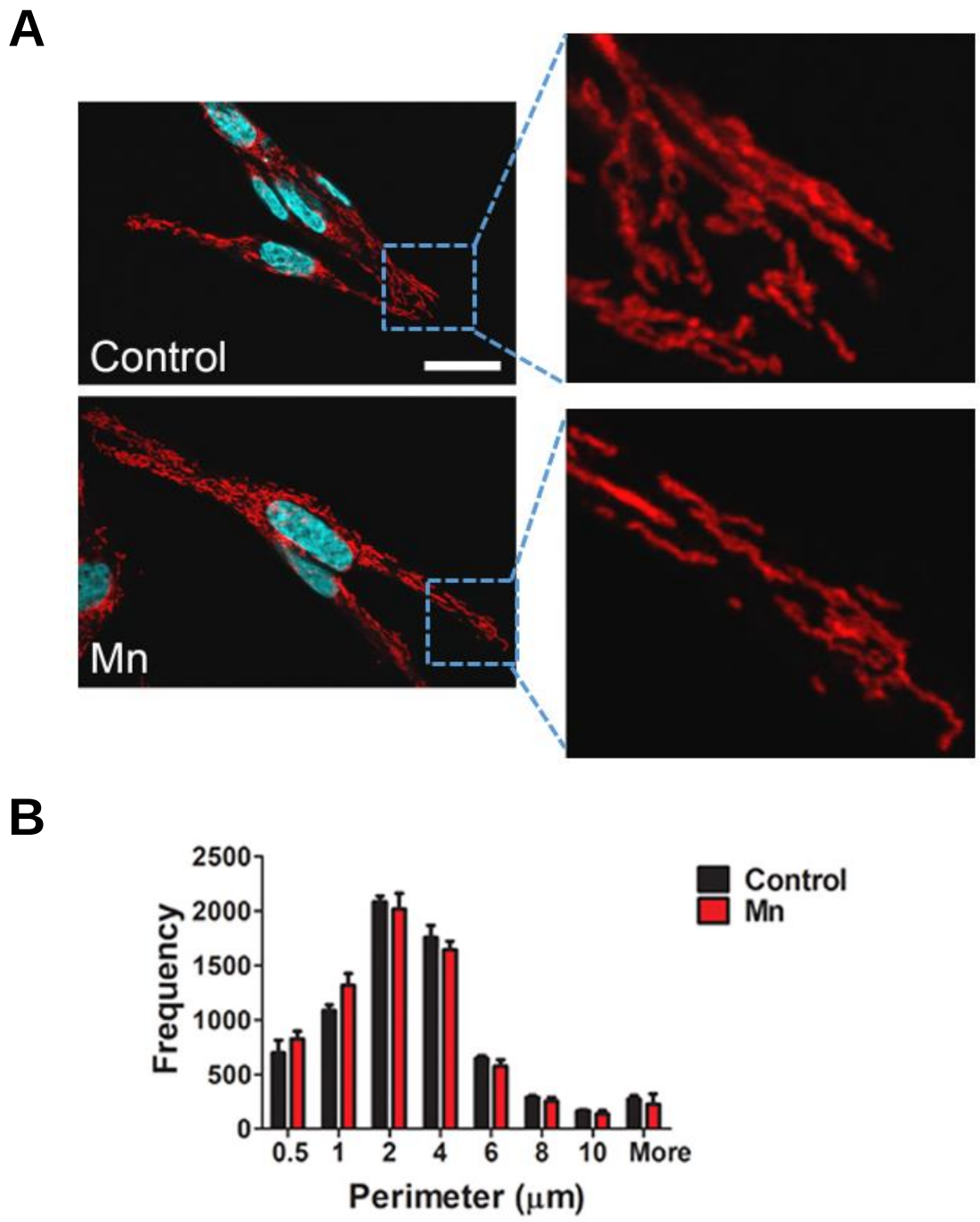

Figure 3.15 No evident changes in mitochondrial morphology in Mn-exposed cells. (**A**) Mitochondrial morphology of N27 cells treated with 125 μM $MnCl_2$ for 24 h. TOM20 was used to stain mitochondria (red). (**B**) Mitochondrial length and number was measured using ImageJ. Data represent the mean ± SEM (n=3 independent experiments), grouped into different size bins and analysed by Unpaired two-tailed Student's *t* test. No statistic significant difference was found between control and Mn treated cells. Scale bar 20 μm.

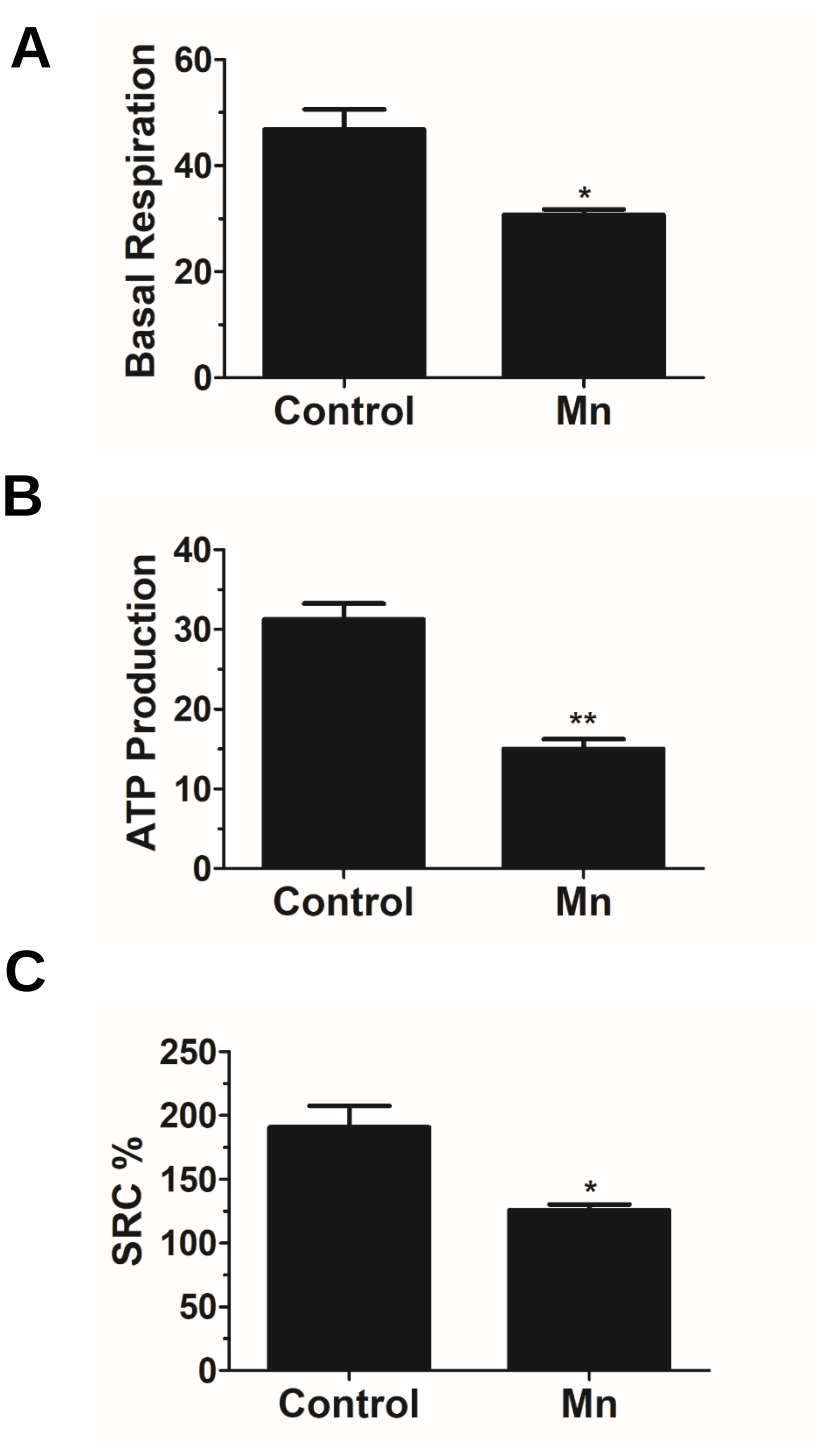

Figure 3.16 A higher concentration of Mn impairs mitochondrial function. N27 cells were plated in XF^{e}96 tissue culture plate and treated with $MnCl_2$ (250 µM) for 24 h. Mitochondrial respiration was assessed by measuring OCR using the XFe96 Extracellular Flux Analyzer. Sequential injections of oligomycin (to inhibit oxygen consumption mediated by ATP synthase), FCCP (an uncoupler to induce maximal OCR), Rotenone/Antimycin (to inhibit complex I and III, respectively). Effects of Mn on (**A**) Basal respiration, (**B**) ATP Production, (**C**) Spare Respiratory Capacity (SRC). Data represent mean ± SEM, n=3 independent experiments. Unpaired two-tailed Student's *t* test *: $P < 0.05$; **: $P < 0.01$ compared to control. The seahorse assay was performed and analysed by Dr Rebecca Z Fan.

3.2.6 Protective effect of Drp1 knockdown against Mn-induced neurotoxicity

As inhibition of Drp1 had a protective role in alleviating impaired autophagy and protein aggregation caused by Mn, I sought to assess the effects of Drp1 knockdown on cell viability in cells exposed to Mn for 24 h. As previously described in **Figure 3.1**, increasing concentrations of Mn produced a gradual decline in cell viability, reaching significance at 250 µM (~ 50 % death). At this concentration Drp1 knockdown significantly increased cell viability. At lower concentrations, although no significant difference was established, a trend is visible and clearly indicates that Drp1 inhibition increases cell viability (**Figure 3.17**).

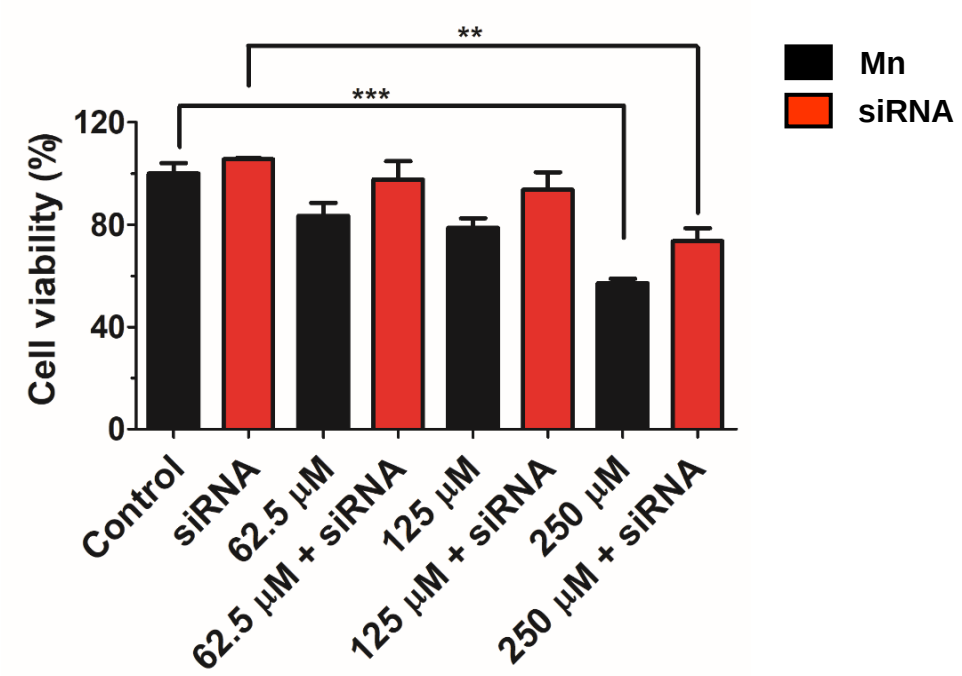

Figure 3.17 Inhibition of Drp1 via siRNA reduces cell death induced by Mn in DAergic cells. N27 cells were transfected with 10 nM rat Drp1 siRNA. 24 h post-transfection, cells were exposed to different concentrations of $MnCl_2$ (62.5, 125 and 250 µM) for another 24 h. Cell viability was performed using the Calcein assay. Values are relative to the untreated control group and they are represented as mean ± SEM (n=4 independent experiments, with 6 wells per group, per experiment). One Way Anova with Tukey's post-hoc analysis * $P < 0.05$, *** $P < 0.001$.

3.3 Discussion

Mn toxicity has been studied since it was first described by Couper in 1837 (Couper, 1837) and despite being recognised for impairing homeostasis and mitochondrial function (Sriram et al., 2010), the primary mechanism of Mn toxicity still remains to be fully elucidated.

Using sub-lethal doses of $MnCl_2$ I demonstrate that Mn is able to acutely impair autophagy flux in multiple cell lines. Results in **Figure 3.1** indicate that all the cell lines were affected by Mn exposure in a dose-dependent fashion and that high concentrations of Mn are detrimental and toxic for cells. Autophagic flux refers to the dynamic process of autophagy, which involves the inclusion of cargo within the autophagosome, the delivery of cargo to lysosomes and its subsequent degradation and release of the resulting macromolecules back into the cytosol (Klionsky et al., 2016). Results shown in **Figure 3.3** and **Figure 3.4** indicate that Mn exposure blocks autophagic flux in multiple cellular models. Mn impairs autophagy by promoting the accumulation of autophagosomes and reducing the number of autolysosomes in HeLa mRFP-GFP-LC3 expressing cells. The dual colour analysis using HeLa mRFP-GFP-LC3 expressing cells enables a direct estimation of both autophagy induction and flux. Further, both LC3 and p62 levels were elevated in M17 cells following $MnCl_2$ treatment.

An observed increase in LC3 levels, following Mn exposure, has previously been attributed to an increase in autophagy (Gorojod et al., 2015, Tai et al., 2016) however, this discrepancy highlights a common experimental flaw when assessing autophagy. Many past studies have solely used LC3 expression as an indication of autophagy levels, however this alone is not sufficient to make an accurate conclusion regarding autophagic capacity. Whilst it is true that an increased level of LC3 correlates to an increased number of autophagosomes, this could be caused by a blockage in autophagic clearance downstream from autophagosome formation. It is therefore imperative to measure other aspects of the autophagy pathway in addition to LC3.

P62 is an adapter protein that binds to cargo within the autophagosome (Komatsu et al., 2007, Pankiv et al., 2007, Bjorkoy et al., 2009) and enables their clearance in the lysosome. Since p62 itself is removed during autophagy, its amount inversely correlates with autophagic activity. If the autophagy flux is normal then no changes in p62 levels should be observed, however if lysosomal fusion is inhibited p62 will accumulate in addition to LC3. By measuring both LC3 and p62 expression patterns, in addition to the use of the HeLa cell model as a further measure of autophagy, I can confidently state that autophagy flux is impaired following exposure to Mn. It has previously been stated that when autophagy is suppressed at any step after complete closure of the autophagosome, only autophagosomes accumulate, while autolysosomes decrease (Mizushima et al., 2010). Although it is not clear where in the autophagy pathway Mn exposure causes a blockade, it appears to suppress the downstream steps of the autophagy pathway (e.g. autophagosome – lysosome fusion) or organelle trafficking as shown in **Figure 3.3** where Mn causes the accumulation of non-fused autophagosomes and reduces autolysosome formation. Of note, all figures with the HeLa mRFP-GFP-LC3 expressing cells display a GFP nuclear staining signal, which may be caused by an artefact of the stable cell line. This seems to correlate with the expression level of the reporter signal within each cell.

Although the results obtained in HeLa and M17 are similar, as they both indicate an impairment in the late stage of the autophagy pathway induced by Mn treatment, the concentrations at which Mn cause a blockade are different. Given the viability data, in which HeLa cells exhibit less sensitivity to Mn compared to M17 cells, the lowest concentration of $MnCl_2$ (62.5 µM) significantly impairs autophagy in HeLa but not in M17 cells, in which autophagy is blocked following 125 µM $MnCl_2$ treatment. The discrepancies given by these results could be related to the following reasons: 1) The mRFP-GFP-LC3 tandem fluorescent probe is stably over-expressed in HeLa cells and these cells may exhibit an exaggerated autophagy response to

stress. 2) The mRFP-GFP-LC3 assay is highly sensitive, as it is dependent on pH changes, and directly measures the number of autophagosome and autolysosomes, without any staining needed. 3) M17 cells were transiently transfected and then stained, providing less transfection efficiency and variable protein expression compared to HeLa cells and therefore display increased variability across experiments.

Autophagy is a fundamental process for the cell as it recycles cellular constituents, eliminates damaged organelles and protein aggregates. Neurons rely highly on this process particularly as the brain ages (Son et al., 2012). Therefore, it is not surprising that mutations in genes regulating autophagy can cause different neurodegenerative diseases. In AD, Huntington's disease, amyotrophic lateral sclerosis and PD defects can occur at different stages of the autophagy pathway and therefore have diverse implications for pathogenesis and eventually therapy (Son et al., 2012). Results from this study support previous studies that show that Mn has a detrimental effect on autophagy (Wang et al., 2017, Chen et al., 2018a). It still remains elusive, however, whether Mn can directly or indirectly impact autophagy as Mn may affect other cellular processes linked to autophagy. Regardless of this it is becoming clear that Mn can interact with proteins directly implicated in different neurodegenerative disorders by promoting their pathology and possibly accelerating the progression of the disease.

Previous studies have identified a link between autophagy dysfunction and accelerated α-synuclein aggregation (Dehay et al., 2012b, Usenovic et al., 2012, Bae et al., 2015), and also showed that by promoting autophagy, α-synuclein accumulation could be attenuated (Spencer et al., 2009, Decressac et al., 2013, Hoffmann et al., 2019). To further study gene-environment interactions in PD pathology, N27 cells overexpressing α-synuclein were exposed to Mn for 24 and 48 h. Results shown in **Figure 3.11** suggest that 48 h of $MnCl_2$ treatment is sufficient to exacerbate α-synuclein aggregation *in vitro*. No effects were exhibited after 24 h of α-synuclein induction via PonA treatment. Further, when autophagy was assessed in N27

overexpressing cells treated with $MnCl_2$ for 24 h (**Figure 3.12**), an exacerbated effect on the autophagy pathway was observed compared to cells overexpressing α-synuclein or exposed to Mn alone. These results may indicate that an increase in α-synuclein aggregation is a consequence of autophagy blockade induced by Mn exposure, as no significant changes in the number of α-synuclein aggregates was observed following 24 h of $MnCl_2$ treatment. In addition, the use of an autophagy inhibitor, CQ, supports the idea that interfering with the autophagy pathway might regulate α-synuclein aggregation. In fact, the number of α-synuclein positive aggregates caused by CQ exposure was higher compared to cells induced by PonA treatment alone or in combination with Mn at 24 and 48 h. Of note, the newly developed method for the detection of α-synuclein oligomers, through life-time imaging (Roberts et al., 2015), might have been a valuable tool to monitor the progression and the effect of α-synuclein accumulation.

Prior studies have shown that Mn-treated cells displayed increased α-synuclein aggregation (Uversky et al., 2001, Cai et al., 2010, Li et al., 2010). In addition, Harischandra et al. (2019) showed that Mn exposure could promote misfolded α-synuclein secretion in exosomal vesicles, between neurons and microglia, subsequently inducing proinflammatory and neurodegenerative responses, in both cells and mice. These results could indicate a possible mechanism that involves the exosome-mediated, cell-to-cell transmission of α-synuclein following Mn exposure. To my knowledge, however, this is the first time that the relationship between Mn and α-synuclein was studied in relation to autophagy. Results from the current study suggest that Mn could be involved in PD pathogenesis not only by exerting its previously reported toxic effects, but additionally by promoting α-synuclein aggregation and autophagy dysfunction.

To investigate the possibility that Mn exposure could impair autophagy through mitochondrial dysfunction, mitochondrial respiration, membrane potential and morphology were assessed in

Mn-treated cells using the same concentration that caused impairment in the autophagy pathway and promoted the induction of α-synuclein aggregation. Surprisingly, neither mitochondrial function (**Figure 3.13** and **3.14**) nor mitochondrial morphology (**Figure 3.15**) were altered following $MnCl_2$ treatment, despite a significant inhibitory effect on autophagy flux. This possibly indicates that the autophagy pathway is a primary target of Mn neurotoxicity, prior to any potential alterations in mitochondrial function. Results from the current study are not consistent with prior studies, the majority of which show that Mn can induce mitochondrial impairment. Most of the studies conducted on mitochondrial dysfunction caused by Mn were performed in primary astrocytes/astrocyte-like cells (Milatovic et al., 2007, Gonzalez et al., 2008, Yin et al., 2008, Alaimo et al., 2013, Alaimo et al., 2014). These cells are known for having much greater affinity to Mn compared to neurons (Aschner et al., 1992), therefore it is not surprising that the effects of Mn displayed in astrocytes are more elevated in comparisons to neuronal cells. Additionally, the sub-lethal concentrations of Mn used in the current study were chosen following cell viability assay, whilst previous studies used concentrations of Mn that caused over 40% cell death (Gonzalez et al., 2008, Yin et al., 2008, Yoon et al., 2011, Alaimo et al., 2014, Sarkar et al., 2018). Other studies associated Mn neurotoxicity with mitochondrial dysfunction at longer timepoints than the current study (Malecki, 2001, Rao and Norenberg, 2004). The methods used to assess mitochondrial function and morphology were based on work previously published by our lab (Cui et al., 2010, Rappold et al., 2014, Fan et al., 2019) and collaborators (Chen et al., 2015a). Despite this, assessing mitochondrial morphology, using fixed samples, has its limitations: 1) Mitochondrial function and morphology are not always linked (Knott et al., 2008, Chen et al., 2005). Thus, to directly evaluate mitochondrial function, I assessed oxidative phosphorylation (**Figure 3.13**) and membrane potential (**Figure 3.14**) using live cells. At a non-cytotoxic concentration, I did not detect functional alterations in mitochondria. 2) Mitochondrial morphology does not measure

other dynamic features such as movement and the equilibrium of fission and fusion. Live cell imaging could be performed either by tagging mitochondrial proteins with fluorescent proteins or by adding specific mitochondrial targeting sequences to fluorescent proteins (Okamoto et al., 2001). Of note, mitochondrial morphology performed in the current study relied on a single threshold value to be applied to all images for analysis. This could be limiting as the threshold value used not always be accurate for all images and this could potentially cause the loss of useful information. Positive controls for in vitro experiments should have been used as well. In particular, it would have been important to have N27 cells with PonA (expressed α-synuclein) to display mitochondrial fragmentation, as previously shown by Fan et al. (2019). Additionally, only mitochondrial length was assessed in this thesis, whilst degree of branching or form factor could have also apported additional data to support the results.

Interestingly, when a greater concentration of $MnCl_2$ (250 µM) was used to assess any changes in mitochondrial function, at 24 h, a substantial drop in mitochondrial respiration compared to untreated cells was observed (**Figure 3.16**). This concentration of Mn caused approximately 40% cell death at 24 h. Effects on mitochondrial function at this high concentration are therefore likely to be caused by the induction of cell death pathways and are an indirect consequence of Mn-induced cell death. This may partly explain conflicting results from prior studies which used higher concentrations of Mn to investigate changes in mitochondrial dynamics (Alaimo et al., 2013, Alaimo et al., 2014) or in mitochondrial function (Milatovic et al., 2007, Sarkar et al., 2018, Gonzalez et al., 2008). The results obtained in the current study, however, are limited to a single time-point (24 h). It is possible that 125 µM $MnCl_2$ may induce mitochondrial impairment following 48 or 72 h of exposure. In addition, given the ability of α-synuclein to impair mitochondria (Rocha et al., 2018, Vicario et al., 2018, Mullin and Schapira, 2013) and interact with Mn (Peres et al., 2016a), it would be interesting to investigate whether Mn could add to the pathologic effects of α-synuclein on mitochondria.

Despite the lack of mitochondrial dysfunction, pharmacological and genetic inhibition of Drp1 was found to be protective against Mn-induced changes in autophagy and α-synuclein aggregation. Results in the present study show that mdivi-1 alleviated Mn-induced block in autophagy flux evidenced by a reduction in autophagosomes and increase in autolysosomes (**Figure 3.9**). Interestingly, mdivi-1 treatment alone was sufficient to improve autophagic capacity of the cell. Mdivi-1 alone promoted an increase in the number of autophagosomes whilst the number of autolysosomes remained comparable to control cells. When combined with Mn treatment, mdivi-1 restored the numbers of autolysosomes to a level that was not statistically different to untreated cells, while maintaining a high number of autophagosomes. These results suggest that mdivi-1 may target multiple locations of the autophagy pathway as it was able to promote autophagosome formation, indicative of autophagy induction, and restore autolysosomal impairment caused by Mn.

Recently, the ability of mdivi-1 to inhibit Drp1 and impact mitochondrial fission was challenged by Bordt et al. (2017). Their evidence showed that mdivi-1 did not acutely elongate mitochondria (indicative of fission inhibition) in both primary neurons and COS-7 cells. Additionally, mdivi-1 impaired complex I through a Drp1-dependent mechanism at high concentrations. The use of high doses of mdivi-1 (≥ 25 μM) used in the latter study may have had an off-target effect on cells, as these same results have not been verified at lower doses. Given the potential concerns raised by this study and the possible off-target effects of mdivi-1, I also inhibited Drp1 via siRNA knockdown to corroborate the results obtained with mdivi-1. Immunostaining (**Figure 3.7**) and WB (**Figure 3.8**) results showed that Drp1 inhibition is protective against Mn effects on autophagy as evidenced by the restored number of both autophagosomes and autolysosome in HeLa cells and the levels of LC3 and p62 in M17 cells. Whilst assessing interactions between Mn and α-synuclein in N27 overexpressing cells, inhibition of Drp1 ameliorated the autophagic blockade caused by cells overexpressing α-

synuclein alone or co-treated with Mn. In addition, Drp1 inhibition significantly reduced the number of protein aggregates in cells exposed to α-synuclein and Mn concurrently or independently. Taken together, these data suggest a new role for Drp1 in the modulation of autophagy, which warrants further study. Additionally, Drp1 knockdown alone did not have an effect on the number of autophagosomes unlike mdivi-1. These results suggest an additional mechanism of action for mdivi-1. To my knowledge this is the first time that inhibition of Drp1, *via* small molecule and gene silencing, is protective against Mn-induced toxicity as well as combined Mn and α-synuclein toxicity *in vitro*.

When assessing the effects on cell viability of Drp1 knockdown in Mn-treated cells results showed a trend of improvement in cell survival, although no significance was demonstrated when comparing to untreated cells (**Figure 3.17**). The exact mechanisms whereby Drp1 inhibition may produce these effects is unknown and warrants further study, however it is possible that an increase in proteostasis mechanisms (e.g. autophagy, which is shown in this study) may influence the cell viability and cell cycle. However, these results support previous studies that have suggested that inhibition of Drp1 confers protection against cell death. Using a selective peptide inhibitor of Drp1 (P110), Qi et al. (2013) showed increased neuronal cell viability, with reduced apoptosis and autophagic cell death in a PD cell culture model, suggesting that Drp1 inhibitors might be useful for the treatment of diseases.

Understanding, specifically, where Mn blocks autophagy, might help us understand why Drp1 inhibition can rescue the subsequent autophagy blockade. Although mitochondria and autophagy are separate pathways that respond differently to changes in the cellular environment such as energy, nutrient availability and stress, there is existing evidence on a reciprocal crosstalk between them. This interplay seems to be evolutionarily conserved and defects in one of these elements could simultaneously impair the other, resulting in increased risk of developing various human diseases, including PD. Autophagy is critical for cellular

homeostasis, thus it is not surprising that its loss or dysregulation indirectly compromises mitochondrial integrity.

There is increasing evidence that link mitochondrial dynamics to autophagy. Purnell and Fox (2013) established that ATG7 knockdown or chemical inhibition of autophagy (using CQ, bafilomycin, E64D and pepstatin) increased Drp1 levels, whilst autophagy induction reduced Drp1 levels. These results suggest that Drp1 levels are quite sensitive to autophagy induction. A very recent study discovered the formation of stable mitochondria–lysosome membrane contact sites (Wong et al., 2018). They propose that contact formation is stimulated by the active lysosomal GTP-bound Rab7, whilst contact untethering is mediated by the mitochondrial TBC1D15 protein (a Rab7 GTPase-activating protein), recruited to the mitochondria by FIS1. Lysosomal Rab7 hydrolysis is therefore induced and results in the disconnection of GDP-bound Rab7 from the membrane. Wong et al. (2018) also investigated whether mitochondria–lysosome contacts could regulate mitochondrial dynamics. Time-lapse images displayed lysosomes contacting mitochondria at the site of mitochondrial division before fission in cells expressing LAMP1–mGFP (lysosomes) and mApple–TOM20 (mitochondria). In addition, mitochondrial TBC1D15, recruited by FIS1, promoted Rab7 GTP hydrolysis at mitochondria–lysosome contacts regulating both lysosomal morphology and mitochondrial fission. Additionally, Itoh et al. (2018) identified a previously uncharacterized isoform of Drp1, termed $Drp1_{ABCD}$ (as it contains four alternative exons A, B, C, D), highly expressed in the brain. $Drp1_{ABCD}$ appeared to be located, in addition to the mitochondria, at lysosomes (co-localisation with LAMP1), late endosomes (co-localisation with Rab7) and the plasma membrane (co-localisation with CAAX-mCherry). Interestingly, immunostaining with LAMP1, Drp1 and TOM20 antibodies revealed that $Drp1_{ABCD}$ was localised at interfaces between mitochondria and lysosomes/late endosomes. Additionally, $Drp1_{ABCD}$ location appeared to be dependent on the presence of both exons A and B in the GTPase domain (Itoh

et al., 2018). These results further suggest an interaction between Drp1 and the endosomal-lysosomal system. Although not directly linked to the autophagy pathway, Koseoglu et al. (2013) associated Drp1 with exocytosis, further strengthening the idea of Drp1 being able to interact with circular vesicle structures. Results from the current and previous studies suggest that Drp1 may be having a direct role in autophagy, by affecting lysosomal function or trafficking, rather than solely in mitochondrial dynamics; to confirm this, however, further in-depth studies are required.

In conclusion, this study provides a detailed description of the effects of Mn on autophagy flux in neuronal and non-neuronal cells and begins to explore the synergistic interaction between Mn and α-synuclein in the context of PD. In addition, results show that blocking Drp1 function may confer protection against the pathological effects caused by Mn, highlighting its importance in regulating the autophagy pathway and suggesting a novel mechanism involving Drp1 and autophagy. Given these results, it is important to note that Mn and Drp1 might not necessarily have the same target but converge at the autophagy pathway, this interaction however warrants further investigation. However, this study not only shows that Mn causes autophagy impairment in multiple cell lines but also, and more importantly, that this occurs without any mitochondrial complications. In fact, no changes in mitochondrial function and morphology were displayed at the concentration and time point used to block autophagy. This study is the first, to my knowledge, to examine the effects of Mn exposure on mitochondrial function, autophagy flux and α-synuclein aggregation concurrently. I demonstrate that the autophagy pathway is primarily affected, followed by α-synuclein aggregation, whilst mitochondrial function remains unaffected. Despite this, the inhibition of Drp1 improved the effects of Mn on these pathways. The discovery that the pathogenic and protective mechanisms of Mn and Drp1 inhibition, respectively, intersect at the autophagic pathway is novel and suggestive of a therapeutic target.

Chapter 4

Investigating the effects of subcutaneous delivery of Manganese on autophagy and mitochondria in mice

4.1 Introduction

In vitro studies have been an important resource for the elucidation of Mn mechanisms of action: accumulation in the mitochondria, disruption of calcium homeostasis (Gavin et al., 1999), ROS formation (Zhang et al., 2004) and inhibition of ATP production (Gunter et al., 2006). More recently, studies performed in rodents have confirmed the above *in vitro* results and have contributed to new discoveries. Cordova et al. (2012) investigated altered cellular mechanisms in the striatum of developing rats (postnatal day 8 to 12) intraperitoneally injected with Mn. Results showed that acute exposure to Mn causes impairments of complex I and II of the ETC, increased ROS and caspase activity. Intracerebral injection of Mn in the striatum induces mitochondrial swelling and dilatation of the ER in TH-positive neurons (Mo et al., 2016). MitoPark mice orally exposed to Mn display an accelerated disease progression and worsening of olfactory function compared to littermate controls. Mn treatment additionally causes striatal DA depletion, TH neuron loss, mitochondrial dysfunction, inflammatory response and protein aggregation (Langley et al., 2018). The above evidence indicates that acute Mn exposure induces mitochondrial impairment.

On the other hand, not much is known about the effects of Mn on autophagy function *in vivo* and what is available still remains controversial. Zhang et al. (2013) examined the short (4–12 h) and long-term (1–28 days) effects of Mn on DAergic neurons and autophagy following a single intrastriatal injection of Mn in rats. Their TEM results revealed an increased number of autophagosomes and swollen mitochondria, along with dysfunctional lysosomes containing dense particulate materials. WB results exhibited increased levels of Beclin 1 protein expression and LC3-II following short exposure to Mn. When assessing the long-term effects of Mn injection, results showed a significant and time-dependent (1, 7, 14, and 28 days) decrease of both Beclin 1 and LC3-II levels (Zhang et al., 2013). This group suggested an induction of autophagy following acute exposure and inhibition of autophagy after long-term

exposure to Mn. Autophagy dysfunction was also observed in the SN of mice injected intraperitoneally with $MnCl_2$, for 2 weeks (Chen et al., 2018a). On the contrary, an induction in autophagy was detected in mice injected intraperitoneally with $MnCl_2$ 5 times a week, for 4 weeks (Liu et al., 2018). In this study, $MnCl_2$ exposure caused a-synuclein oligomerisation, accompanied by increased formation of autophagic vacuoles. Results showed that Mn exposure increased Beclin-1 protein expression, increased the ratio of LC3-II to LC3-I, with a significant decrease in p62 expression in Mn-treated mice (Liu et al., 2018).

Results from the previous chapter have elucidated a new potential role for Mn neurotoxicity, in which Mn seems to first impair the autophagy pathway and then promote protein aggregation. Inhibition of Drp1, using both pharmacological and genetic interventions, improved the autophagy blockade and α-synuclein aggregation caused by the metal. The aim of this chapter is to investigate both mitochondrial and autophagy changes *in vivo* following acute Mn exposure in CAG-RFP-EGFP-LC3, $Drp1^{+/-}$ and WT mice. As Mn has been previously linked to idiopathic PD, the current work mainly focused on DAergic neurons and Mn ability to affect them. Inhibition of Drp1 represents a therapeutic strategy that has been demonstrated to be effective in multiple models of neurodegeneration. In the current chapter I aim to explore the potential effects of manipulating Drp1 in TH neurons *in vivo* and restore autophagy function. To this end, I assess whether global heterozygous Drp1 knock-out mice (Wakabayashi et al., 2009) and LC3 mice transduced with $Drp1^{K38A}$, a mutant of the Drp1 gene with dominant negative abilities (Smirnova et al., 2001, Zhu et al., 2004), can attenuate Mn-induced changes.

4.2 Results

4.2.1 Acute effects of Mn on autophagy flux in CAG-RFP-EGFP-LC3 mice

Many studies have attempted to address the effects of Mn exposure on cellular mechanisms in rodents. Despite the absence of a 'clinically representable' model for Mn toxicity I investigated the effects of $MnCl_2$ treatment on autophagy and mitochondria in both TH- and GAD67-positive neurons following acute exposure to Mn as previously described (Dodd et al., 2005, Khalid et al., 2011).

To assess the effects of Mn exposure on autophagy flux, I used a reporter mouse that harboured the same characteristics as the stably expressing mRFP-GFP-LC3 HeLa cells (see **Figure 3.2**). These autophagy reporter mice were generated by Li et al. (2014b) to ubiquitously express the tandem RFP-EGFP-LC3 under the CAG promoter. They were maintained by breeding with C57BL/6 inbred mice to establish a colony of heterozygous mice, which were viable and fertile (**Figure 4.1 A**). Three month old CAG-RFP-EGFP-LC3 transgenic mice (hereby LC3 mice) were given to up to three subcutaneous injections of 50 mg/kg of $MnCl_2$ every three days (0, 3, 6) and were sacrificed 24 h after each injection (day 1, 4 and 7). Prior each injection mice were monitored for weight loss, however no changes in bodyweight of either control or treated mice were observed (data not shown).

This study focused on the effects of Mn associated with PD, therefore changes in the autophagy pathway were assessed in TH-positive neurons of the SNpc. Assessment of autophagy was carried out blindly. Results showed that, only after three subcutaneous injections of $MnCl_2$, autophagy flux was significantly impaired in TH-positive neurons. Compared to the vehicle group (autophagosomes, 2.72 ± 0.23; autolysosomes, 3.87 ± 0.30), Mn-exposed animals exhibited a greater amount of autophagosomes (7.34 ± 0.46) and a reduced number of autolysosomes (1.48 ± 0.48) (**Figure 4.1 B**). Single (autophagosomes, 6.07 ± 0.83;

autolysosomes, 2.36 ± 0.14) or two (autophagosomes, 4.99 ± 0.76; autolysosomes, 2.28 ± 0.78) injections of Mn had an effect on the autophagy pathway as autophagosomes increased, whilst autolysosomes decreased (images not shown), as evidenced by the graph. These results, however, were not significantly different to vehicle levels, therefore the regimen of three subcutaneous injections of $MnCl_2$ was applied to all subsequent experiments.

Many studies have confirmed that Mn primarily accumulates in the GP, a region that is rich in GABA projections. GABA is synthesised by two glutamic acid decarboxylases: GAD67 and GAD65, respectively encoded by the *Gad1* and *Gad2* genes (Pinal and Tobin, 1998). GAD67 is responsible for over 90% of basal GABA synthesis (Fenalti et al., 2007) and was therefore used as a marker for GABAergic neurons. When autophagy flux was investigated in GAD67-positive neurons of the GP the results were consistent with those obtained in TH-positive neurons. Mn treatment caused an increase in the number and size of autophagosomes (12.45 ± 0.78) and a reduction in the number of autolysosomes (0.60 ± 0.28), compared to vehicle mice autophagosomes, 6.20 ± 0.18; autolysosomes, 1.71 ± 0.09). Again, results were indicative of autophagy blockade (**Figure 4.2**).

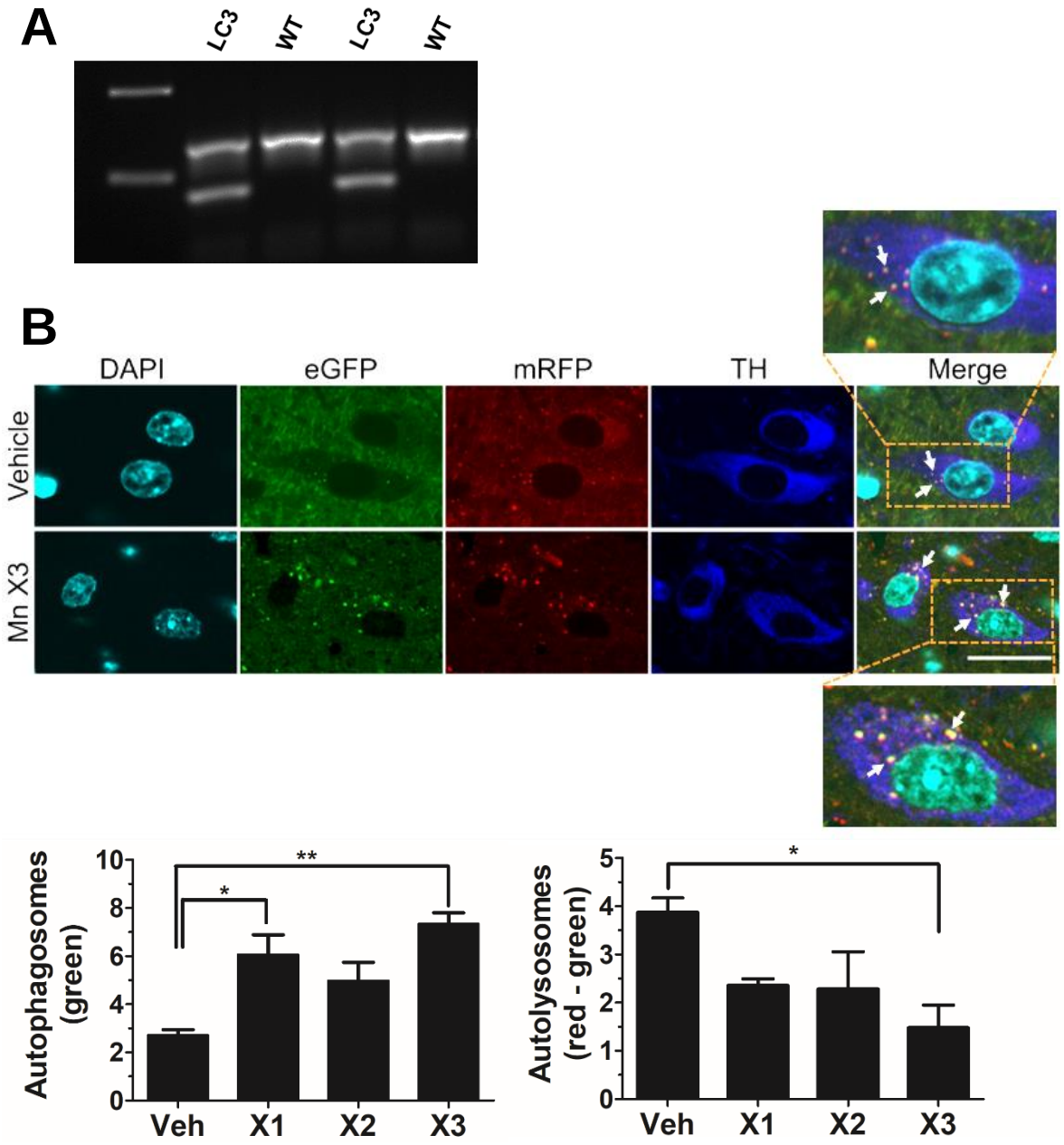

Figure 4.1 Mn blocks autophagy in TH-positive neurons of LC3 mice. (**A**) Gel electrophoresis of PCR products from DNA samples collected from LC3 pups and WT littermates prior to weaning. The WT allele produces a 324 bp product whilst the mutant allele also produces a 208 bp product. (**B**) Animals were injected with either $MnCl_2$ or H_2O (50mg/kg) every 3 days (0, 3, 6) for 3 doses and sacrificed 24 h after each injection (day 1, 4, 7). 30 µm nigral sections were stained with a TH antibody (blue). The red puncta (arrows in the upper panel) indicate functional autophagy as the green signal is quenched by the low pH of lysosomes, which fuse with autophagosomes and form autolysosomes. The yellow puncta (arrows in the Mn X3 panel) represent accumulated autophagosomes due to the colocalization of RFP and GFP signals, indicative of impaired autophagy. The numbers of autophagosomes (green vesicles) and autolysosomes (red vesicles minus green vesicles) were quantified in at least 30 TH-positive neurons, from multiple brain sections per condition. Data represent mean ± SEM (n=3 animals per group, 1 female and 2 males). One Way Anova with Tukey's post-hoc analysis * $P<0.05$ ** $P<0.01$ compared to the vehicle group. Scale bar 20 µm. Arrows indicate LC3 puncta.

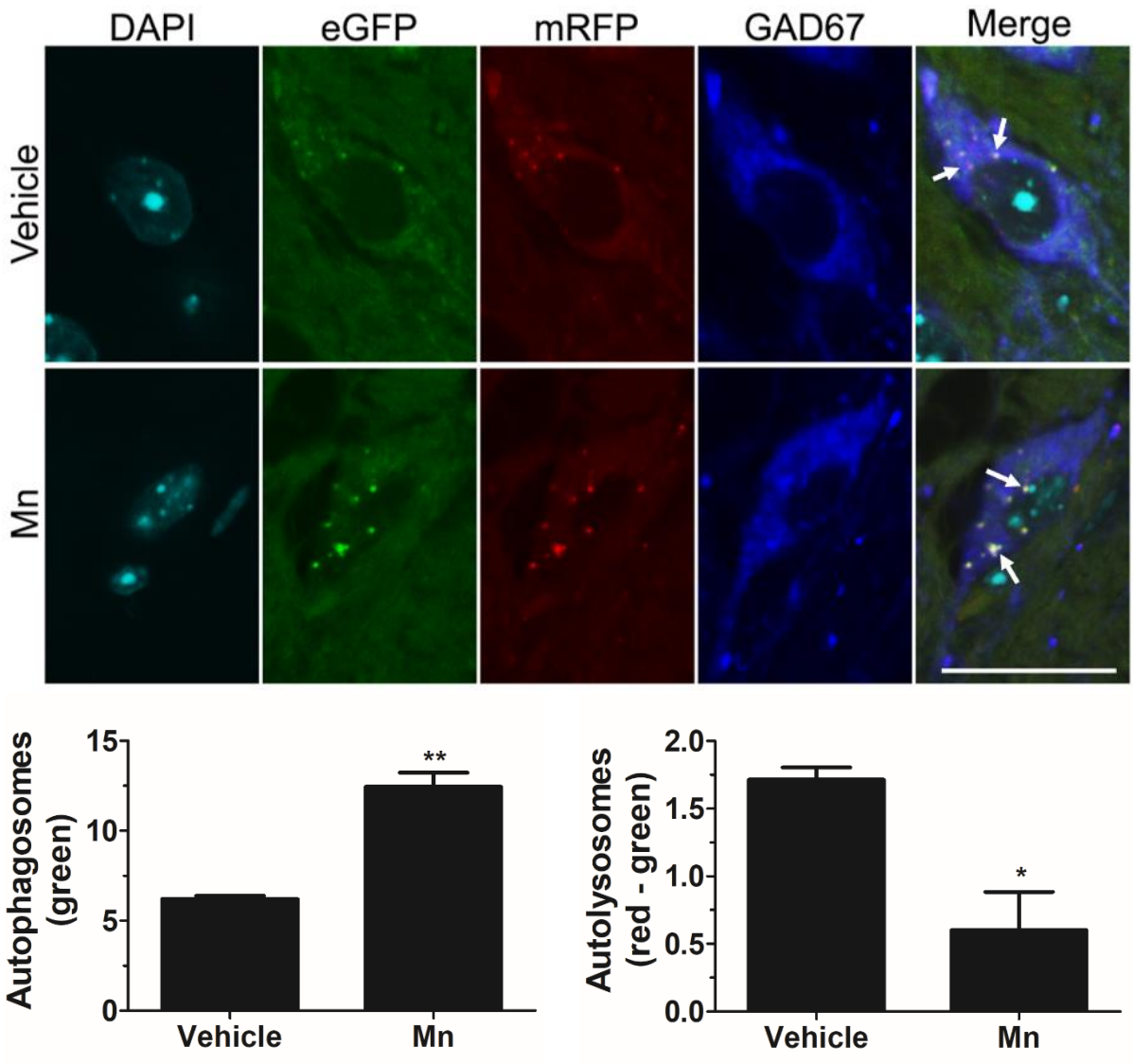

Figure 4.2 Mn blocks autophagy in GABAergic neurons of LC3 mice. LC3 mice were injected with either $MnCl_2$ or H_2O (50mg/kg) every 3 days for 3 doses and sacrificed on day 7. 30 µm striatal sections were stained with GAD67 antibody (blue). The numbers of autophagosomes (green vesicles) and autolysosomes (red vesicles minus green vesicles) were quantified in at least 25 GAD67-positive neurons from multiple brain sections, per condition. Data represent mean ± SEM (n=3 animals per group, 1 female and 2 males). Unpaired two-tailed Student's *t* test * P<0.05 ** P<0.01 compared to the vehicle group. Scale bar 20 µm. Arrows indicate LC3 puncta.

4.2.2 Acute exposure to Mn does not impact mitochondrial morphology

In vitro results suggested that Mn targeted the autophagy pathways prior to altering mitochondrial function and morphology; it was imperative to confirm this in an *in vivo* model. To do so, WT C57BL/6 mice were exposed to Mn and then mitochondrial morphology was investigated in both TH- and GAD67-positive neurons. The average length of mitochondria in each neuron was automatically determined using ImageJ as previously described (Chen et al., 2015a). The skeletonised mitochondria are representative of actual mitochondrial images. TH-positive neurons (**Figure 4.3 A**) exhibited an intact mitochondrial network with an unfragmented morphology in both Mn- and vehicle-treated groups. In addition, no statistical difference was observed as evidenced by the similar average mitochondria length in Mn (12.75 ± 0.57) and vehicle (10.85 ± 0.56) groups. GAD67-positve neurons appeared normal, with a slight, although not significant, reduction in mitochondrial length in the Mn-exposed (15.60 ± 1.11) group compared to vehicle (20.07 ± 1.73), however, the mitochondrial network appeared intact (**Figure 4.3 B**). When performing a power analysis on the G*Power Software using differences between groups and standard deviations as reported above, results suggest a n=6 may produce statistical significance.

Taken together, these results indicate that sub-acute exposure of Mn impairs autophagy flux without affecting the mitochondrial morphology of both TH- and GAD67-positive neurons.

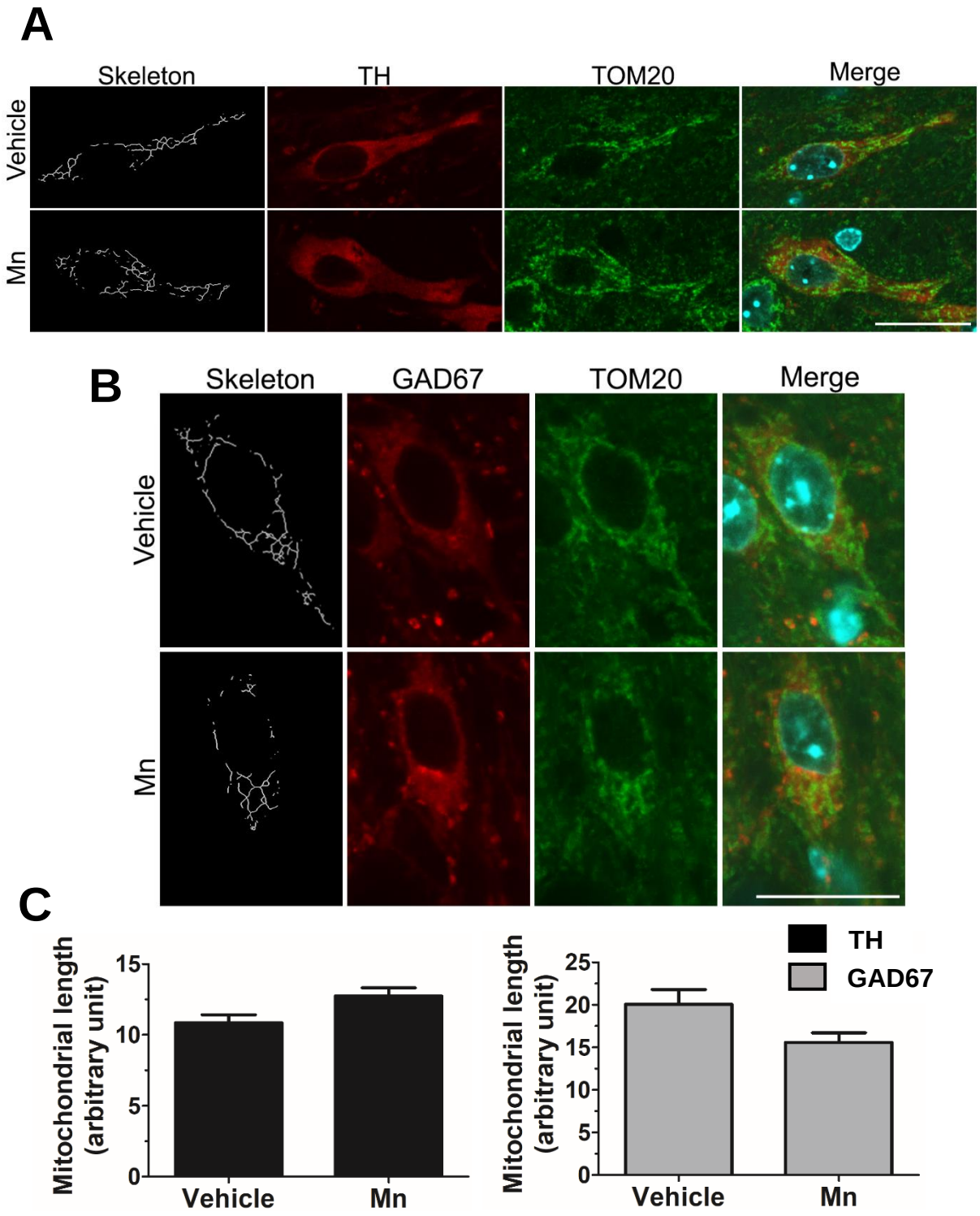

Figure 4.3 Sub-acute Mn expose does not alter mitochondrial morphology *in vivo*. WT mice were injected with either $MnCl_2$ or H_2O (50mg/kg) every 3 days for 3 doses and scarified on the day 7. 30 µm nigral and striatal sections were stained for TOM20 to assess mitochondrial morphology in (**A**) TH- and (**B**) GAD67-positive neurons (red), respectively. (**C**) Mitochondrial length was quantified in at least 20 TH- and GAD67-positive neurons from multiple brain sections per condition, using ImageJ. Data represent mean ± SEM (n=3 animals per group, 3 males). Unpaired two-tailed Student's *t* test found no statistical difference between vehicle and Mn-treated group. Scale bar 20 µm.

4.2.3 Investigating the effects of inhibiting Drp1 to restore Mn-induced changes on autophagy flux in TH-positive neurons

Experiments performed *in vitro* showed that by blocking Drp1 the autophagy impairment caused by Mn treatment could be improved. To this end, I utilised a Drp1 knockout mouse model to investigate whether changes in mitochondrial dynamics could restore autophagy function. $Drp1^{+/-}$ heterozygous mice were bred with WT C57BL/6 mice to establish a colony of heterozygous mice (**Figure 4.4 A**). $Drp1^{+/-}$ mice express a partially reduced level of Drp1 and are viable, in contrast to $Drp1^{-/-}$ homozygous mice that die during embryonic development (Wakabayashi et al., 2009). Similarly to their $Drp1^{+/+}$ littermates (hereby WT), $Drp1^{+/-}$ mice are fertile, normal in size, and did not display any physical or behavioural abnormalities. Prior to exposing both WT and $Drp1^{+/-}$ mice to $MnCl_2$, as for previous experiments, $Drp1^{+/-}$ mice were characterised to accurately establish and quantify Drp1 levels via immunostaining, WB and qPCR for gene expression. A reduction of ~ 40% Drp1 protein levels was obtained via WB (**Figure 4.4 B**), whilst qPCR results displayed over 60% reduced Drp1 gene expression levels (**Figure 4.4 D**) in $Drp1^{+/-}$ mice compared to littermates. **Figure 4.4 C** shows a representative image of Drp1 reduction in TH-positive neurons of $Drp1^{+/-}$ mice.

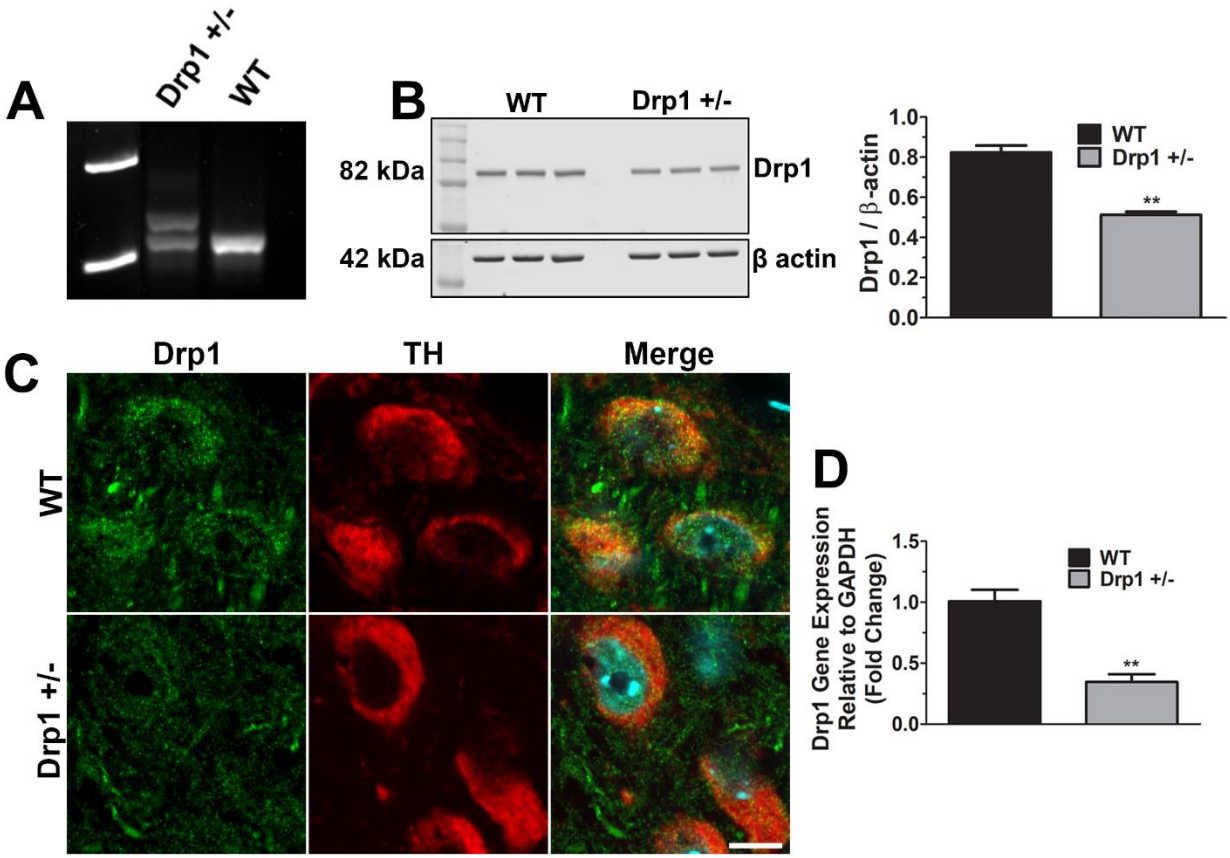

Figure 4.4 Characterisation of the global Drp1 heterozygous mouse strain (Drp1$^{+/-}$). (**A**) Gel electrophoresis of PCR products from DNA samples collected from Drp1$^{+/-}$ pups and WT littermates prior to weaning. The WT allele produces a 268 bp product, whilst the knock-out allele also produces a 312 bp product. (**B**) Drp1 protein expression in WT and Drp1$^{+/-}$ mice was quantified using WB. Whole brains were dissected and one hemisphere was homogenised in RIPA buffer. 15 µg of protein was loaded on a 10% Bis-Tris gel, transferred onto a PVDF membrane and stained for both Drp1 and the loading control β-actin; each lane of the gel represents one animal. Blots were visualized on an Odysey CLx machine and optical density measured using Li-Cor Image Studio software. Unpaired two-tailed Student's t test, **P < 0.01 compared to WT mice. Data are shown as mean ± SEM (n=3 separate animals). (**C**) Representative image of 30 µm SNpc brain sections stained with Drp1 (green) and TH (red) antibodies (n=1). Scale bar 10 µm. (**D**) The other hemisphere was homogenised in Trizol reagent and RNA isolated by phase separation. 1 µg of RNA was reverse transcribed, and relative gene expression of Drp1 measured by qPCR, using TaqMan based detection chemistry, with GAPDH as a reference gene. Comparisons were made using Unpaired two-tailed Student's t test, **P < 0.01 compared to WT mice. Data are shown as mean ± SEM (n=3 separate animals). qPCR was performed and analysed by Dr Martin Helley.

Following Drp1$^{+/-}$ mice characterisation, 12 animals in total, 3 per group (Drp1$^{+/-}$ or WT) were subcutaneously injected with either 50mg/kg of vehicle (H_2O) or $MnCl_2$ every 72 h for 3 doses and sacrificed on day 7. Blindly, autophagy was assessed in TH-positive neurons using LC3 and p62 antibodies and the number of puncta were quantified using ImageJ, as previously described. LC3 and p62 staining appeared diffuse in the vehicle groups of both WT (LC3, 112.32 ± 4.23; p62, 115.95 ± 5.14) and Drp1$^{+/-}$ (LC3 100.51 ± 0.52; p62, 106.90 ± 4.63) mice. The punctate pattern of the Mn-exposed group appeared to be more accumulated with clearly increased numbers of both LC3 (133.70 ± 5.35) and p62 (211.63 ± 30.17) puncta, suggesting a blockade in autophagy, and therefore confirming the results obtained in the LC3 mice.

In the Drp1$^{+/-}$ Mn-exposed mice, however, no significant changes were identified in the autophagy markers (LC3, 144.38 ± 4.79; p62, 212.22 ±18.01) when comparing to the Mn-treated WT group (**Figure 4.5**). These results suggest that a reduction of ~ 40% of Drp1 protein is not sufficient to clear the accumulated LC3 and p62 vesicles caused by Mn treatment and therefore, cannot improve autophagy impairment.

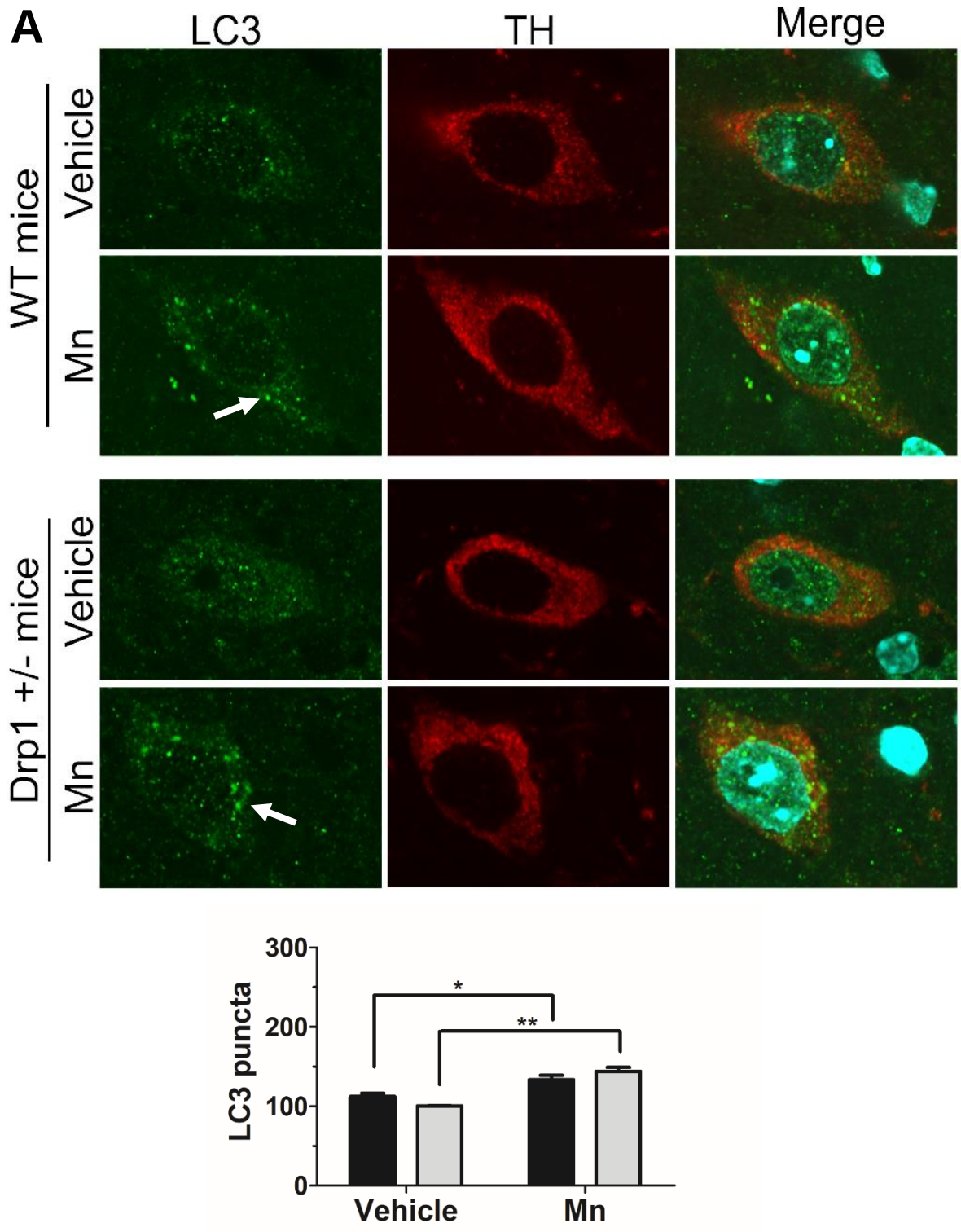

Figure continues on next page

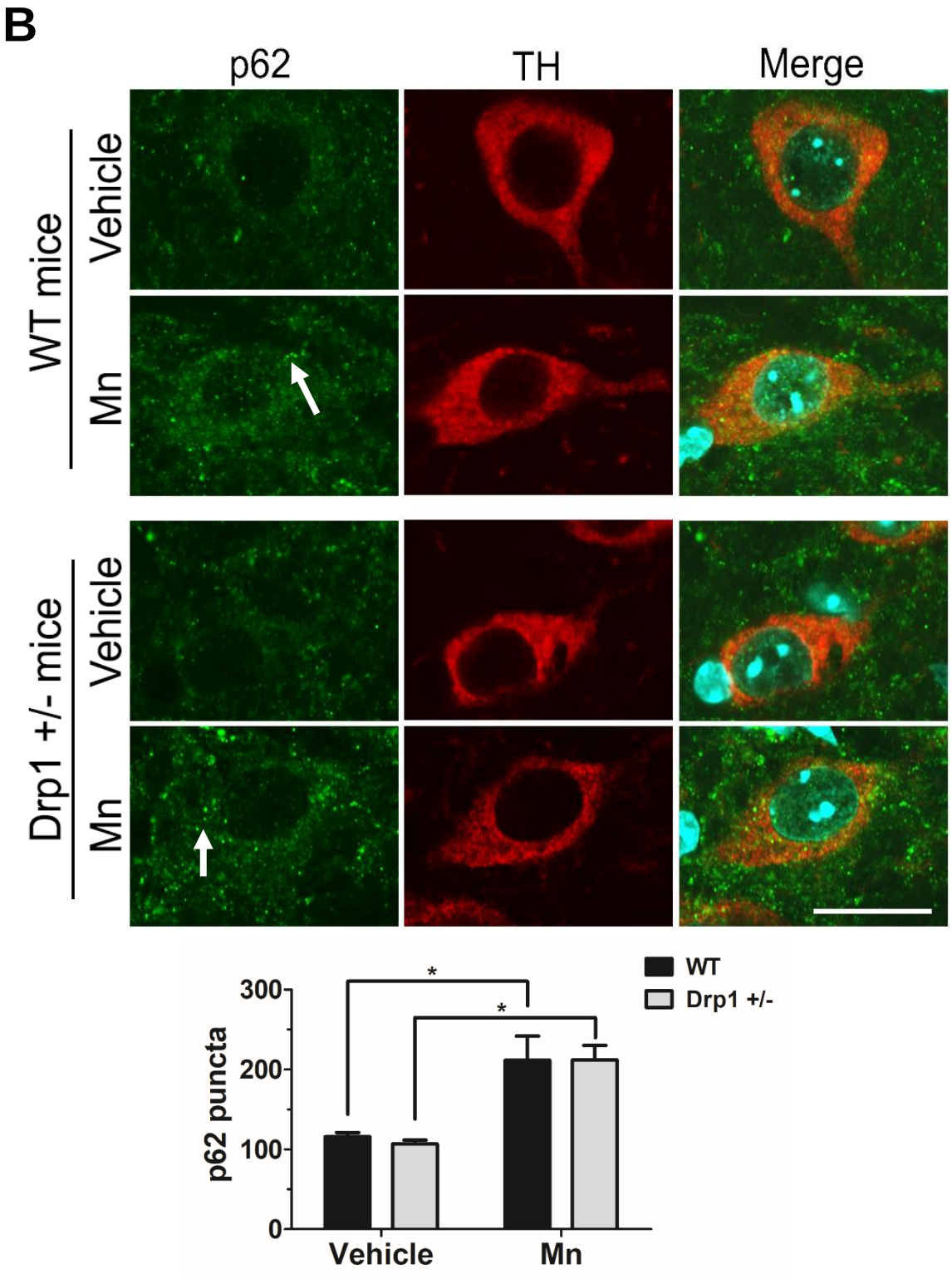

Figure 4.5 Heterozygous KO of Drp1 does not impact Mn-dependent changes in autophagy flux. WT and Drp1$^{+/-}$ mice were injected with either $MnCl_2$ or H_2O (50mg/kg) every 3 days for 3 doses and scarified on day 7. Nigral sections (30 µm) were stained for (**A**) LC3 and (**B**) p62 to assess autophagy flux in TH-positive neurons (red). LC3 and p62 puncta were blindly quantified in at least 20 neurons from multiple brain sections per condition, using ImageJ. Data represent mean ± SEM (n=3 animals per group). One Way Anova with Tukey's post-hoc analysis: * P<0.05 ** P<0.01 Scale bar 20 µm. Arrows indicate LC3 and p62 puncta, respectively.

The global Drp1$^{+/-}$ mice did not confer protection against the effects of Mn treatment on the autophagy pathway. Thus, I sought to assess whether using recombinant adeno-associated virus serotype 2/9 (rAAV2/9) vectors, to manipulate Drp1 function in SNpc neurons, could improve autophagy blockade caused by Mn treatment in LC3 mice.

To inhibit Drp1 function, rAAV2/9 was used to deliver Drp1^{K38A} (rAAV2/9-Drp1^{K38A}). K38A is a mutant form of the Drp1 gene with well-characterised dominant negative effects (Smirnova et al., 2001) and my laboratory has used this mutant successfully *in vitro* (Cui et al., 2010) and *in vivo* (Rappold et al., 2014) studies. The decision to using rAAV2/9 was based on several considerations: 1) AAV9 was proven to have high neuronal transduction rates in TH-positive neurons of the SNpc under control of the human synapsin (hSYN1) promoter to drive GFP expression (McLean et al., 2014, Bido et al., 2017). 2) rAAV2/9 displayed a high transduction efficiency in the brain (Chakrabarty et al., 2013). 3) Homozygous germline deletion of the Drp1 gene in mice is embryonically lethal, precluding the use of a complete knockout mouse.

The GTP-hydrolysis defective mutant K38A consists of a lysine-to-alanine mutation in one GTP-binding element of Drp1. Although K38A is deficient in hydrolysis, it is still capable of binding GTP and can stimulate Drp1 to bind and tubulate membranes. In addition, the expression of this mutant can induce the formation of large cytoplasmic structures (Pitts et al., 1999, Yoon et al., 2001). To monitor the expression of the Drp1-K38A protein, the rAAV-Drp1^{K38A} was engineered to express the HA (Human influenza hemagglutinin) tag, which facilitates its detection and to harbour a neuronal promoter (SYN1) for neuronal selectivity. A total of 8 mice were stereotactically injected with rAAV2-Drp1^{K38A} or H_2O (sham surgery) delivered to the SNpc of the right or left hemisphere, respectively (AP: -3.1, ML: ± 1.3, DV: -4.2, relative to the Bregma).

Six weeks after the injection (to allow sufficient time for protein expression in the DAergic neurons), 4 mice were subcutaneously injected with H_2O (vehicle) and 4 mice with $MnCl_2$ (**Figure 4.6**). The number of autophagosomes and autolysosomes was assessed, blindly, in TH-positive neurons of both hemispheres, to confirm that the delivery of the construct was successful. The surgery was successful in most animals as evidenced by clear K38A-positive inclusions. However, the expression of rAAV2/9-Drp1^{K38A} in the SNpc of two of the Mn-exposed mice, was not specific to TH neurons, therefore the ipsilateral sections of these mice could not be used. This made statistical analysis impossible when comparing vehicle (n=4) and Mn-treated (n=2) animals. Transduction efficiency in nigral DA neurons was calculated by quantifying TH-positive neurons transduced with Drp1-K38A (HA-tagged). The transduction efficiency rate was ~ 60%.

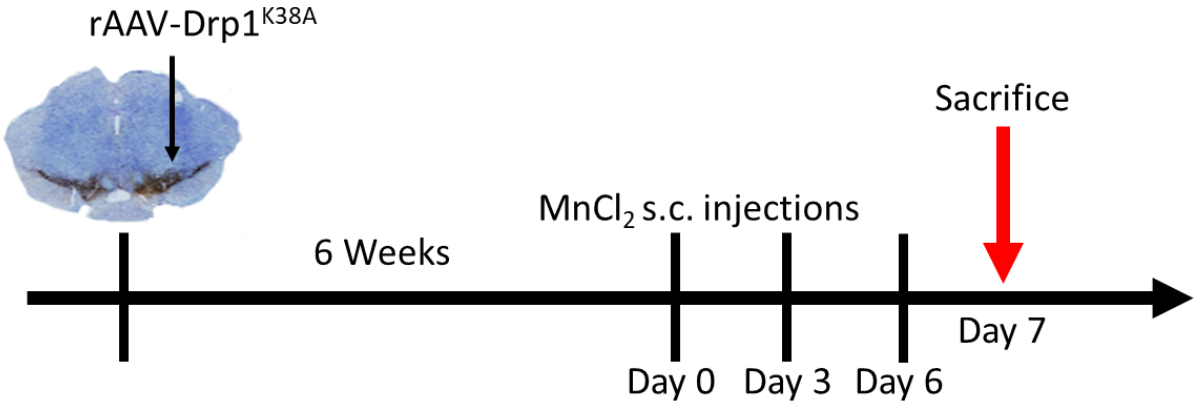

Figure 4.6 Schematic illustration of stereotactic infusion of rAAV-Drp1^{K38A} and experimental design. Six weeks old LC3 mice were unilaterally injected in the SNpc (right hemisphere) with rAAV2/9-Drp1K38A (1 x 109 U/µL). A sham surgery using 1 µL of sterile H2O was performed on the left hemisphere as a control. Six weeks post-surgery mice were injected with 50 mg/kg MnCl2 or H2O every 72 h for 3 doses and sacrificed 24 h after the last injection (day 7).

Overall, results confirmed a blockade in autophagy in Mn-treated sections, as evidence by an increase in the number of autophagosomes (12.96 ± 1.03) and a reduction in the number of autolysosomes (0.55 ± 0.21) compared to vehicle-treated (autophagosomes, 7.55 ± 0.79; autolysosomes, 2.9 ± 0.3) mice. Inhibition of Drp1 using rAAV2/9-Drp1^{K38A} displayed similar numbers of autophagosomes (8.02 ± 0.65) and autolysosomes (3.56 ± 0.73) compared to the vehicle. Interestingly, preliminary results show that the addition of the dominant negative Drp1^{K38A} might reduce the number of autophagosomes (9.71 ± 0.08) and increase autolysosomes (2.99 ± 0.59) in Mn-treated mice. Despite the lack of enough Mn + Drp1^{K38A} mice necessary for statistical analysis, a trend is visible and suggests that the use of a dominant negative form of Drp1, which blocks Drp1 physiological function more than what is achieved with the Drp1$^{+/-}$ mice, might be protective against Mn-induced changes in the autophagy flux (**Figure 4.7 A-B**).

A

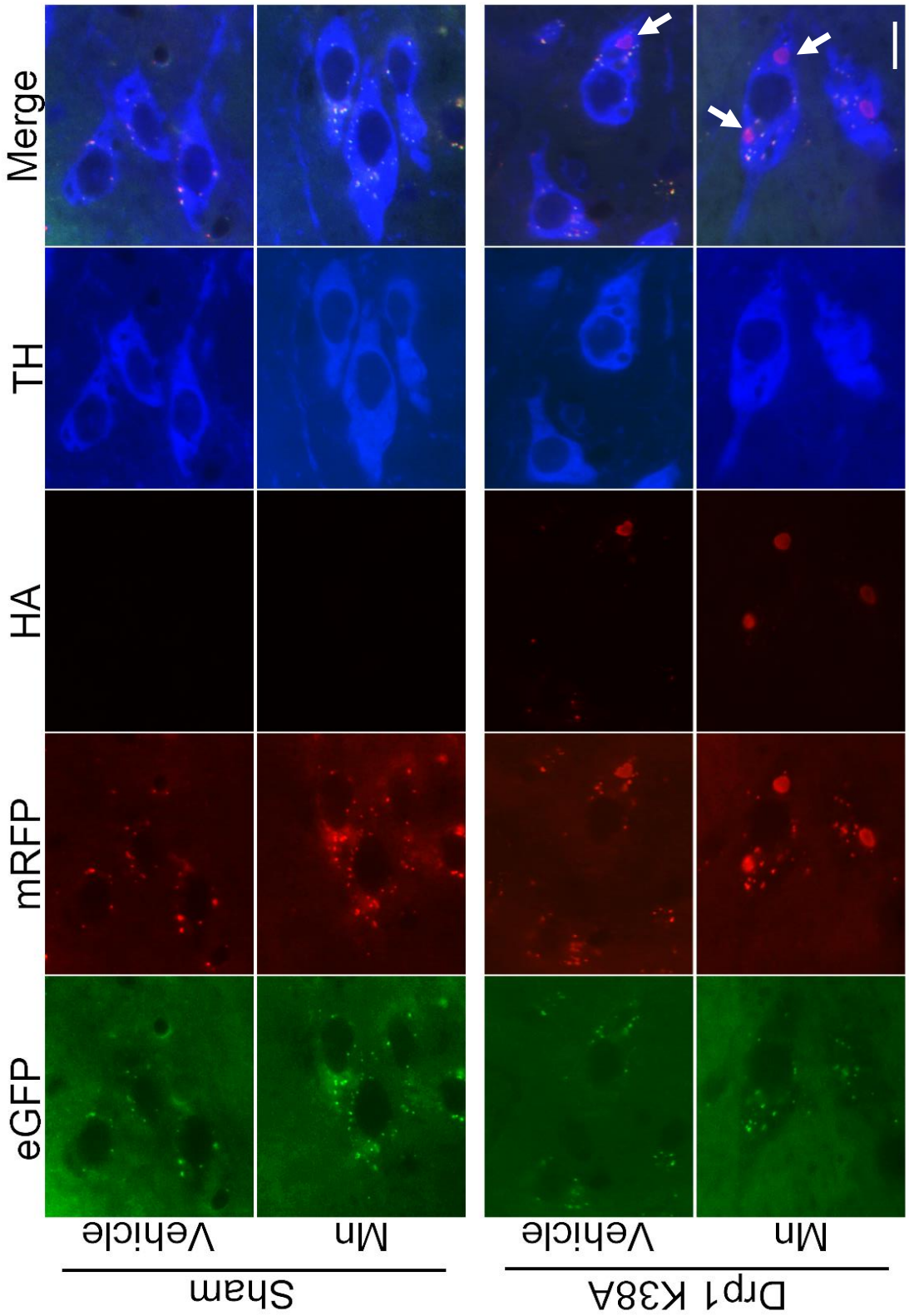

Figure continues on next page

B

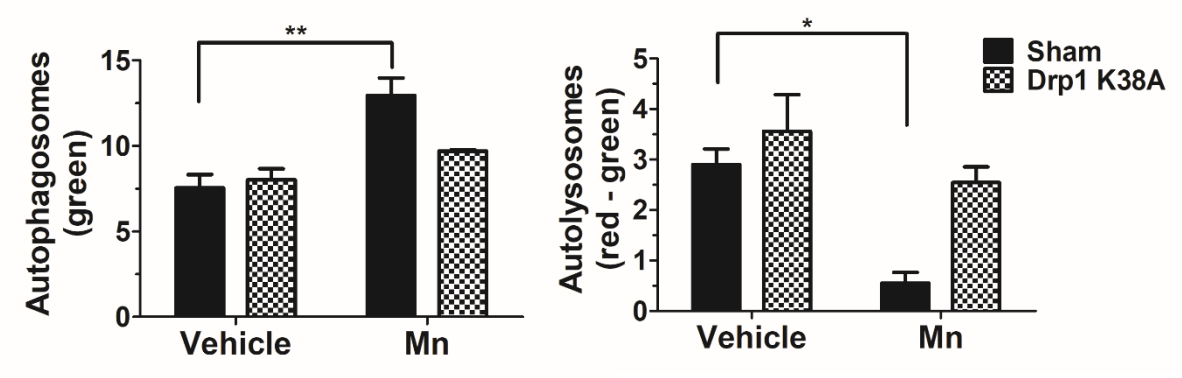

Figure 4.7 Drp1-K38A might improve autophagy impairment in TH-positive neurons. (**A**) The number of autophagosomes (green vesicles) and autolysosomes (red vesicles minus green vesicles) were quantified in 25-30 TH-positive neurons (blue staining) per condition. The expression of $Drp1^{K38A}$ was confirmed by staining with a HA antibody (red, 633 channel). Arrows indicate HA-positive aggregates caused by K38A. The merge image shows autophagy in TH-positive neurons. (**B**) Data represent mean ± SEM (2 males and 2 females in the Mn-treated group; 1 male and 3 females in the vehicle group). One Way Anova with Tukey's post-hoc analysis: * $P<0.05$ ** $P<0.01$ compared to the vehicle group (no statistics was performed for the Mn-treated K38A group as only n=2 due to lack of expression of $Drp1^{K38A}$ in TH neurons). Scale bar 10 µm. Stereotactic surgery was performed by Dr Rebecca Z Fan. Arrows indicate $Drp1^{K38A}$ inclusions.

4.3 Discussion

Previous *in vivo* studies have shown controversial results in relation to Mn effects on the autophagy pathway. In particular, some have shown autophagy induction (Zhang et al., 2013, Liu et al., 2018) whilst others reported autophagy blockade following Mn exposure (Zhang et al., 2013, Chen et al., 2018a). These differences could be related to differences in the duration of exposure and/or routes of administration and the methods of assessments.

I used a newly generated strain of autophagy reporter mice that ubiquitously expresses (RFP)-EGFP-LC3 fusion protein under the CAG promoter (Li et al., 2014b) to assess the effects of autophagy changes following Mn exposure. These mice were created to advance the understanding of the dynamics of the autophagy pathway under stress conditions. Autophagosomes can be distinguished from autolysosomes according to the differential pH sensitivity of RFP (pK_a 4.5), stable in acidic pH, and EGFP (pK_a 5.9), which is quenched in the acidic lysosomal environment following fusion of autophagosomes with lysosomes (Kimura et al., 2007, Zhou et al., 2012, Lin et al., 2014). These mice have been previously used to investigate the dynamics of renal epithelial cell autophagy, by measuring autophagy flux under starvation and ischemic injury (Li et al., 2014b). This is, the first attempt, to the best of my knowledge, at measuring autophagy changes in neurons, following Mn exposure in this mouse model.

The major concerns for a representative model of acute Mn toxicity were the choice of the adequate dose that could promote its accumulation in the basal ganglia, the administration route and the reduction of systemic side effects. I opted for multiple subcutaneous injections of $MnCl_2$ (50 mg/kg), previously described by Dodd et al. (2005), which caused a significant increase in basal ganglia Mn concentration, accompanied by a significant but not severe decrease in locomotor behaviour (Dodd et al., 2005).

In the current study, three injections of 50 mg/kg $MnCl_2$ over 7 days induced changes in autophagy flux, with a reduction in the number of autolysosomes and a substantial accumulation of autophagosomes in TH-positive neurons, indicative of dysfunctional autophagy. No significant changes in autophagy flux were detected following one or two injections of Mn, suggesting that, although Mn can reach the brain and start to accumulate after a single or two injections (Dodd et al., 2005), measurable toxic effects on the autophagy pathway do not manifest until the third dose. Overall these results suggest that acute exposure to $MnCl_2$ causes a late suppression (autophagosome-lysosome fusion) of the autophagy pathway as shown in **Figure 4.1**.

It is difficult to compare my data to what is available in the literature as the evidence on *in vivo* effects of Mn on autophagy in the SN is scarce and exposure paradigms vary between studies. My results, however, are in line with Zhang et al. (2013), who showed that a single intrastriatal injection of $MnCl_2$ could disrupt and block the autophagy pathway. TEM data displayed increased autophagosome numbers and dysfunctional lysosomes containing dense granules compared with control animals. It should be noted that the quantification of relative numbers of autophagosomes and autolysosomes observed by TEM can help discriminate between activation and blockade of autophagy, however it does not does provide direct insight into lysosomal degradation of autophagic substrates and is therefore not classified as an 'autophagic flux' assay (Mizushima et al., 2010). Chen et al. (2018a) investigated the role of autophagy in microglia inflammation following Mn-exposure (intraperitoneal injection of 100 mg/kg $MnCl_2$, every third day for two weeks) and detected an increase in both ATG5 and Beclin-1 protein levels, implying that Mn induced autophagy dysfunction in microglia. Again, although consistent with our results, Chen et al. (2018a) assessed the early stages of autophagosome formation, without measuring autophagic substrates levels to evaluate autophagic flux. The

current study provides a more thorough assessment of autophagy flux in TH-positive neurons, following Mn treatment, which has not been fully assessed in the past literature.

As previously mentioned, Mn is known to preferentially accumulate in the GP, a region rich in GABA projections. Many studies have associated Mn exposure to alterations in GABA levels, metabolism and motor impairments, however this is the first assessment of autophagic changes following Mn exposure in GABAergic neurons. My results, again, indicated that three subcutaneous injections of 50 mg/kg $MnCl_2$ over 7 days, in LC3 mice, caused an autophagy flux impairment in GAD67-positive neurons (**Figure 4.2**). This autophagy blockade induced by Mn could potentially promote other known features of Mn toxicity, including α-synuclein aggregation, mitochondrial dysfunction, oxidative stress, neuroinflammation and apoptosis, generating a loop of neurotoxicity.

One of the pitfalls of the CAG-RFP-EGFP-LC3 model is the fact that the EGFP signal is dependent on the enzymatic degradation and the speed at which lysosome quenches its fluorescence (Mizushima et al., 2010). This may cause the presence of EGFP fluorescence in autolysosomes, limiting the use of yellow puncta (red plus green) to identify autophagosomes and red puncta to identify autolysosomes. To address this possibility, additional immunostaining of LAMP1 with the RFP fluorescence could have helped to distinguish autolysosomes (containing LAMP1) from autophagosomes (containing no LAMP1) as previously performed by Li et al. (2014b). However, by assessing changes in LC3 and p62 staining in WT mice, following Mn treatment, I confirmed the results obtained in the LC3 mice.

As autophagy flux was impaired in TH- and GABA-positive neurons following Mn exposure, the next step was to assess whether mitochondria were also affected. Due to the difficulty of monitoring mitochondrial function *in vivo*, only mitochondrial morphology was assessed in WT mice exposed to three subcutaneous injections of 50 mg/kg $MnCl_2$ over 7 days. My results

did not reveal any changes in mitochondrial morphology following immunostaining with TOM20 in both vehicle and Mn-exposed animals. TH- and GAD67-positive neurons exhibited normally distributed filamentous mitochondria that did not appear fragmented, following Mn treatment, as evidenced by the skeleton image in **Figure 4.3**. Although these results are indicative of an unaltered mitochondrial structure, the effects on mitochondrial function following this dose-regimen are not known. Therefore, although Mn seems to induce changes in the autophagy flux without causing the destabilisation of the mitochondrial network, it is imperative to confirm that mitochondrial function remains unaffected. In fact, the majority of the work investigating the effects of Mn on mitochondria *in vivo*, were all assessed in relation to mitochondrial respiratory chain complex activity and ROS production (Zhang et al., 2003b, Cordova et al., 2012). Results showed that both acute (Cordova et al., 2012) and prolonged (Zhang et al., 2003b) exposure to Mn promoted ROS production and caspase activity, in addition to inhibiting the mitochondrial respiratory chain. Particularly, Cordova et al. (2012) reported no morphological changes, cellular degeneration or death in mice exposed to Mn. Although not specific to mitochondrial morphology, their results suggest that changes in mitochondrial function can occur without any morphological alterations. It is thus possible that mitochondrial dysfunction is present in mice exposed to Mn in the current study. TEM may help to assess the microstructure of mitochondria and provide further insight on the effects of Mn on mitochondria.

Direct inhibition of autophagy has previously been shown to impair mitochondrial oxygen consumption and energy production (Guo et al., 2011, Liang et al., 2012). Mutations in the *GBA* gene are well known to cause Gaucher disease (GD), the most common lysosomal storage disorder (resulting in reduced enzyme (GCase) activity, accumulation of substrate (glucocerebroside) within lysosomes, and impaired lysosomal activity) and to increase the susceptibility of developing PD (Brady et al., 1965, Westbroek et al., 2011, Murphy et al.,

2014). Osellame et al. (2013) discovered that primary neurons and astrocytes from a mouse model of neuronopathic GD harboured defective autophagic and proteasomal machineries that induced the accumulation of α-synuclein aggregates and promoted mitochondrial dysfunction, ultimately leading to neuronal cell death. Similar results were obtained by Jinn et al. (2017), who showed that deficiency of the lysosomal K^+ channel transmembrane protein 175 (TMEM175) impaired lysosomal capacity to clear autophagosomes, thus blocking the completion of autophagy. TMEM175 deficiency lead to reduced mitochondrial energetic capacity. It is possible that $MnCl_2$ is impairing the autophagy pathway prior to inducing mitochondrial dysfunction and that continuous exposure to Mn would eventually cause mitochondrial impairment. The other possibility is that mitochondrial function is indeed impaired, but to a level that is not affecting morphology. This said, further experiments assessing mitochondrial function, including the use of the seahorse XF analyser on purified mitochondria or synaptosomes, are needed to confirm these hypotheses.

Although the exact mechanism of action of Mn neurotoxicity is not fully known, results from this chapter suggest that Mn is affecting autophagy at the later stage, either by causing a disruption in the fusion of the autophagosomes with the lysosomes or at the lysosomal level itself. Suzuki et al. (1983) first described an interplay between Mn and lysosomes following a single intraperitoneal injection of Mn in mice. Their results indicated that most of the absorbed Mn in the brain was found in mitochondria and lysosome-rich fractions separated by density gradient centrifugation. In particular, lysosomes took up Mn to a greater extent than mitochondria when compared to controls. Similar results were obtained in rats overexposed to the metal, which displayed Mn-rich particles in pancreatic lysosomes (Okamoto et al., 1997). Recently, Gorojod et al. (2017) provided further insight into the interplay between the Mn and lysosomes, following intrastriatal administration of $MnCl_2$ in rats. Results showed that Mn exposure caused lysosomal membrane permeabilization and cathepsin upregulation. In

particular, cathepsin D levels were increased in striatal and SN neurons, accompanied with a marked reduction of immunoreactive cells. This evidence supports results from my study to suggest that Mn-exposure could indeed first target the autophagy pathway, as shown by the current *in vivo* data.

In recent years, targeting mitochondrial dynamics, either by blocking mitochondrial fission or promoting mitochondrial fusion, has been reported to be protective in several models of neurodegeneration and has been highlighted as a potential therapeutic (Cui et al., 2010, Qi et al., 2013, Rappold et al., 2014, Filichia et al., 2016, Kandimalla et al., 2016, Manczak et al., 2016, Bido et al., 2017). Mitochondrial dynamics, however, requires balance in order to maintain optimal mitochondrial function. *In vitro* results, from the previous chapter, showed that inhibiting Drp1 improved autophagy impairment caused by Mn-overexposure despite the absence of mitochondrial dysfunction. In the current chapter, $Drp1^{+/-}$ mice and WT littermates were exposed to $MnCl_2$, to investigate whether a partial reduction of Drp1 could be protective against Mn-induced changes in autophagy in TH-positive neurons. Previous studies have revealed that heterozygous knockdown of Drp1 could decrease fission activity and enhance fusion machinery compared to WT mice (Manczak et al., 2012). Additionally, $Drp1^{+/-}$ mice displayed reduced oxidative stress compare to WT mice and presented no mitochondrial or synaptic deficiencies. Based on these observations, it was hypothesised that a partial reduction of Drp1 could be beneficial against Mn-induced neurotoxicity. WT mice, again, displayed an impaired autophagic pathway, following Mn-exposure, as evidence by the accumulation of both LC3 and p62 proteins in TH-positive neurons. LC3 and p62 are degraded during autophagy; therefore, their amounts provide an estimate of the autophagic activity. Mn-exposure caused an incrementation of both proteins, as evidenced by the number of puncta and indicative of increased amount of autophagosomes and reduced degradation of autolysosomes. Surprisingly, LC3 and p62 levels were unchanged in $Drp1^{+/-}$ mice compared to WT littermates,

suggesting that heterozygous inhibition of Drp1 was not able to restore Mn-induced autophagy deficits (**Figure 4.5**). Partial reduction of Drp1 function has previously been shown to be protective in two models of neurodegeneration (Kandimalla et al., 2016, Manczak et al., 2016), however this was not the case for Mn toxicity. It is important to note that these previous models (Kandimalla et al., 2016, Manczak et al., 2016) involved mitochondrial dysfunction, whilst data from the previous chapter suggest a novel role for Drp1, separate from mitochondrial dynamics. It is possible that these two separate roles have varying sensitivity to Drp1 inhibition. One potential explanation for these discrepancies may be related to the amount of reduced Drp1 required to rescue the autophagic dysfunction induced by Mn. It is possible that the Mn regimen used in this study is too acute and high for this partial Drp1 reduction to confer protection. Future studies are needed to assess whether protection would be observed in these mutant animals when a more chronic and low dose of Mn is used. On the other hand, a partial inhibition of Drp1 may not be enough to overcome the blockade in the autophagy pathway induced by Mn and that a major reduction in Drp1 function is needed to restore autophagy flux.

To test the above hypothesis, LC3 mice were stereotactically injected with rAAV HA-tagged-Drp1^{K38A} (a dominant negative mutant of Drp1) to the SNpc and then exposed to Mn. Although preliminary (n=2), these results suggested that a more severe inhibition of Drp1 could reduce the number of accumulated autophagosomes, whilst increasing the number of autolysosomes, ameliorating autophagy flux in TH-positive neurons of Mn-exposed mice (**Figure 4.7**). Germline deletion of mitochondrial fission/fusion genes has previously been shown to be detrimental (Davies et al., 2007, Ishihara et al., 2009, Wakabayashi et al., 2009, Kageyama et al., 2012). The use of a dominant negative form of Drp1 did not completely ablate Drp1 function and the expression of K38A alone did not affect autophagy measurements. Smirnova et al. (2001) previously stated that only ~ 3% of total Drp1 is required by the mitochondria to maintain its physiological functions. It is possible that by producing a strong inhibitory effect

on Drp1 function, K38A is still allowing the mitochondria to perform normally, whilst improving Mn-induced changes to autophagy flux.

In the future, it would be worthwhile to apply other approaches for blocking Drp1 function. A possibility would be the packaging of the rAAV with shRNA to knockdown Drp1 expression or the administration of P110 peptide. Additionally, the effects of blocking mitochondrial fission have only been assessed up to eight weeks *in vivo* (Rappold et al., 2014) and for Drp1 blockade to be considered as a potentially viable clinical strategy for PD the long-term impact of manipulating mitochondrial dynamics must be evaluated. This assessment will be crucial for the evaluation of any possible adverse effects not seen within the time frames of my studies.

Although novel, the current study has some limitations. For systemic injections targeting the brain, $MnCl_2$ can be injected intravenously, intraperitoneally, or subcutaneously. All have been widely used, and there is no major evidence in the literature that suggest that one route is preferential or causes more toxicity than the others. A considerable drawback of using systemic injections, however, is that prior to entering the brain, Mn reaches the liver (Mn is absorbed into the mesenteric blood supply and directly carried to the liver), heart, and kidneys, increasing the risk of acute toxic effects, such as cardiac, renal, and liver failure. The choice of injecting $MnCl_2$ subcutaneously was decided in regard to the slower rate of absorption compared to other routes, providing a more sustained effect. Although inhalation or ingestion of Mn may be more representative of human exposure compared to subcutaneous injections, it should be assessed in a chronic setting.

When comparing this study to those in the literature it is difficult to make direct comparisons as different doses, routes of administration and time frames were used when assessing autophagy changes following Mn-exposure. Unfortunately, this is a disadvantage of using an acute model of Mn toxicity. Assessment of the acute toxic potential of $MnCl_2$ is required to

determine the effects that occur during accidental or deliberate short-term exposure to the metal and will serve as a guide in selecting the appropriate dose for long-term toxicity studies. However, acute models do not mimic the progression of the disease and therefore do not represent a direct model for a continuous, low exposure to the metal, which is seen in the human setting. In fact, most of the evidence on Mn intoxication derive from both occupational and environmental exposures (O'Neal and Zheng, 2015). Therefore, results from the current study might shed more light on the early effects of acute Mn toxicity. However the gradual accumulation of Mn in the brain will be addressed in the next chapter.

In conclusion, the current study indicates that Mn is causing an inhibition of the autophagy pathway in both DAergic and GABAergic neurons, without inducing any changes in mitochondrial morphology. Preliminary results also indicate that six weeks of gene therapy with $Drp1^{K38A}$ directly injected in the SNpc could potentially confer neuroprotection against acute Mn toxicity. Collectively these studies provide further insight into the pathogenic mechanisms of Mn toxicity in relation to PD and support previously reported *in vitro* data describing a novel regulatory function for Drp1 in the autophagy pathway. These results suggest that targeting the autophagy pathway may have a therapeutic effect on Mn-induced neurotoxicity.

Chapter 5

Assessment of cellular mechanisms of Manganese toxicity in six month old *SLC39A14*$^{-/-}$ mice

5.1 Introduction

Parkinsonism induced by Mn neurotoxicity can vary between individuals according to their disease onset, severity and symptoms and could be caused by a combination of genetic susceptibility and/or environmental factors (including occupational exposure); this chapter will focus on the neurotoxic insults induced by gradual accumulation of physiological Mn.

Whilst Mn neurotoxicity was first recognised in 1837 (Couper, 1837), the first genetic disorder of Mn metabolism, *SLC30A10*, was reported in 2012 (Quadri et al., 2012, Tuschl et al., 2012). Recently, two new genetic mutations have been described - mutations in *SLC39A14* (increased Mn accumulation and toxicity), *SLC39A8* (Mn and Zn deficiency). Current evidence on these three inherited disorders of Mn metabolism have helped to increase the understanding of Mn homeostasis and consequent neurotoxicity. Despite this, little is known about changes in intracellular mechanisms caused by chronic accumulation of Mn.

The aim of this chapter is to better understand the impacts of chronic Mn accumulation on the autophagy pathway and mitochondrial morphology using six month old *SLC39A14*$^{-/-}$ mice as a model. These mice have previously been shown to have elevated Mn levels in the brain. As evidence from rodents, non-human primates and patients show that both the GP (Yamada et al., 1986, Lucchini et al., 2000, Dorman et al., 2006b) and the SNpc (Hauser et al., 1994, Cersosimo and Koller, 2006, Park et al., 2007, Stanwood et al., 2009, Robison et al., 2012) are targeted by Mn, I addressed Mn-induced cellular changes in TH- and GAD67-positive neurons in this chapter.

5.2 Results

5.2.1 Effects of chronic Mn accumulation on striatal density and TH levels

SLC39A14$^{-/-}$ mice are viable and do not present any morphological abnormalities at birth (Hojyo et al., 2011, Aydemir et al., 2012). Young (eight weeks) *SLC39A14*$^{-/-}$ mice display high brain Mn levels of approximately 10-fold higher than age-matched WT control mice (Xin et al., 2017, Jenkitkasemwong et al., 2018) and, by six months of age, start to show signs of dystonia, accompanied by a reduced ability to coordinate their movements compared to littermates. These symptoms are similar to the PD-like motor deficits observed in patients that harbour a *SLC39A14* mutation (Tuschl et al., 2016). Based on these results, it was decided to assess changes in autophagy and mitochondrial morphology in six month old *SLC39A14*$^{-/-}$. When kept on a normal (10 ppm) or high (2400 ppm) Mn diet for 30 and 7 days, respectively, *SLC39A14*$^{-/-}$ mice exhibited elevated Mn concentrations in several tissues, including brain (Jenkitkasemwong et al., 2018). For the following experiments, all mice were fed with a standard chow diet, containing 130 ppm Mn, throughout the whole six months. Both homozygous (*SLC39A14*$^{-/-}$; KO) and litter-matched control (*SLC39A14*$^{+/+}$*;* WT) mice were used and genotyped a described in **Figure 5.1 A**. For most of the following experiments 6 WT (4 males and 2 females) and 5 KO (3 males and 2 females) were used.

As previously described by Xin et al. (2017), PD-like motor impairments were observed in six month old KO mice, however these were not explicitly measured in the current study. The first aim was to address possible changes in TH levels in the SN and striatum. To this end, WT and KO striatal sections were stained for TH using DAB based detection to assess any damage or loss of striatal terminals. TH staining revealed widespread transduction of DAergic fibres throughout the striatum of both groups. No difference in TH optical density was detected in striatal DAergic innervation of both WT and KO mice (**Figure 5.1 B–D)**. To further

corroborate these results, TH protein levels, were assessed in the ventral midbrain of WT and KO mice by WB (**Figure 5.1 E**). No statistical difference was identified between KO and WT, suggesting that DAergic neurons and terminals are not affected in mice lacking the SLC39A14 transporter.

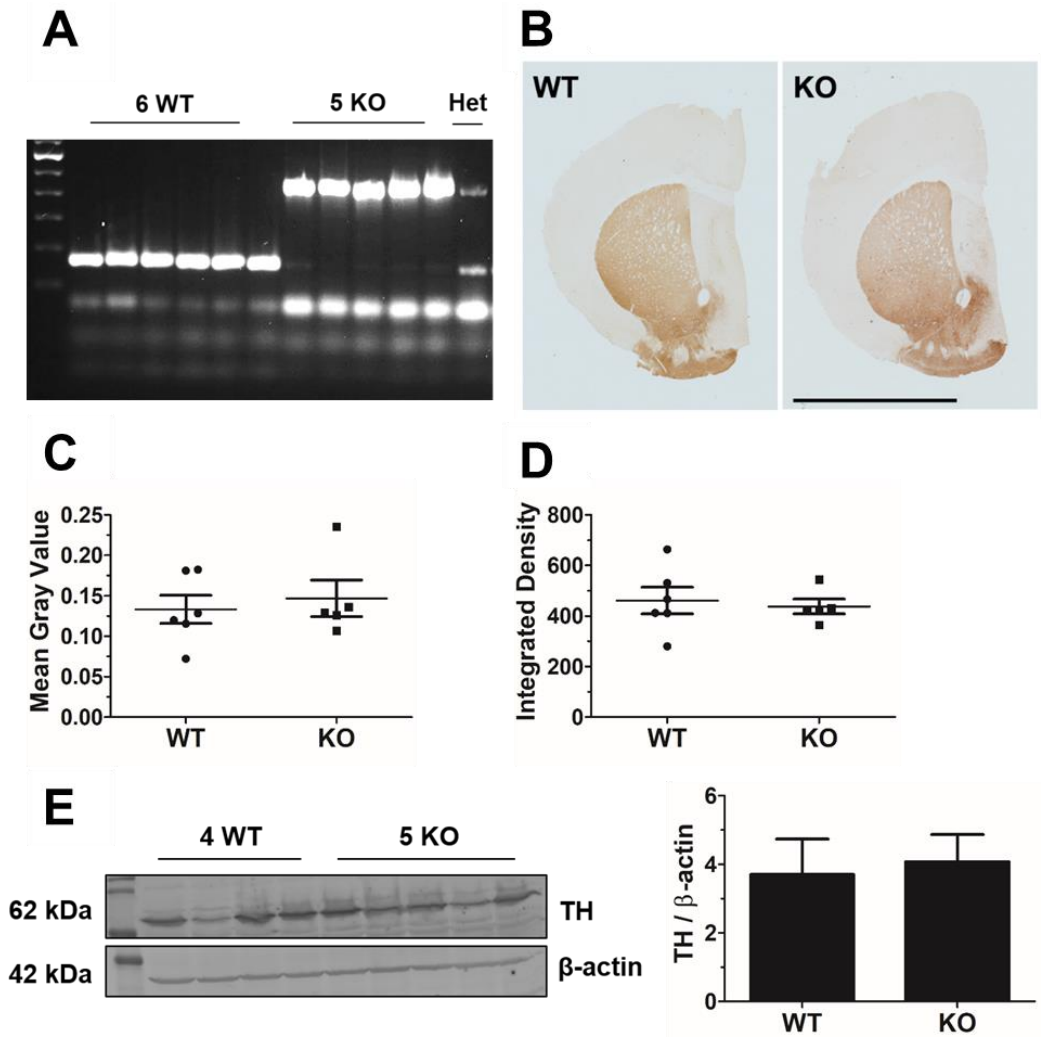

Figure 5.1 Six month old *SLC39A14*$^{-/-}$ mice do not exhibit detectable changes in striatal density and TH protein levels. (**A**) Gel electrophoresis of PCR products from DNA samples collected from WT (*SLC39A14*$^{+/+}$), KO (*SLC39A14*$^{-/-}$) and Het (*SLC39A14*$^{+/-}$) mice. The WT allele produces a 164 bp product, the mutant allele produces a 469 bp product, whilst the Het allele produces both. (**B**) 30 µm striatal sections from WT and KO mice were immunostained with a TH antibody (brown, diaminobenzidine chromogen). Scale bar 3500 µm. ImageJ was used to calculate (**C**) the mean gray value and (**D**) the integrated density of both groups. Unpaired two-tailed Student's *t* test displayed no statistical difference between groups. (**E**) From ventral midbrain regions, 30 µg of protein from 4 WT and 5 KO mice were loaded on a 12% polyacrylamide gels and WB was performed using a TH antibody. TH levels were quantified using β-actin as a loading control. Blots were visualized on an Odysey CLx machine and optical density measured using Li-Cor Image Studio software. Data represent mean ± SEM (WT n=4; KO n=5 animals per group). Unpaired two-tailed Student's *t* test displayed no statistical difference between WT and KO animals.

5.2.2 Autophagic changes in DAergic and GABAergic neurons of *SLC39A14*$^{-/-}$ mice

Next, changes in the autophagy pathway were assessed in nigral sections of TH-positive neurons using LC3 and p62 antibodies, following immunostaining. An increased number of LC3 and p62 puncta was observed in TH-positive neurons of KO mice compared to WT. In WT animals, the staining pattern of LC3 and p62 was largely diffuse, with a reduced number of visible puncta. Following Mn treatment, the diffuse staining pattern of LC3 and p62 visibly changed to a more punctate pattern (**Figure 5.2 A-D**). The number of LC3 (179.37 ± 12.59) and p62 (350.07 ± 10.41) puncta per cell in KO mice was statistically different from LC3 (52.69 ± 12.09) and p62 (162.89 ± 20.01) puncta in WT animals, indicating a blockade in autophagy flux. Interestingly, the average size of both LC3 (0.041 ± 0.001) and p62 (0.047 ± 0.002) were enlarged in KO mice in comparison to WT (LC3, 0.031 ± 0.0008; p62, 0.036 ± 0.0015) (**Figure 5.2 E-F**). This could be the result of an increase in accumulated proteins, unable to be degraded due to a block in autophagy flux.

The GP has been shown to be one of the earliest brain regions in which MRI imaging exhibit a hyperintensive signal caused by Mn intoxication (Guilarte et al., 2006b). To this end, autophagy changes were also investigated in GAD67-positive neurons located in the GP. Results were similar as those obtained in TH-positive neurons. LC3 (88.65 ± 4.43) and p62 (68.63 ± 10.36) staining appeared diffuse with fewer puncta in WT mice, whilst an accumulation in both LC3 (112.85 ± 5.77) and p62 (180.46 ± 13.21) puncta was observed in KO mice (**Figure 5.3 A-D**). Again, these results showed an impairment in autophagy caused by lack of *SLC39A14* and therefore Mn overload. When assessing changes in LC3 and p62 puncta size between WT and KO mice, LC3 (WT and KO, 0.38 ± 0.001) puncta displayed no

significant changes between the two groups, whilst p62 staining in KO (0.37 ± 0.002) mice exhibited evident larger puncta compared to WT (0.31 ± 0.0008) mice (**Figure 5.3 E-F**).

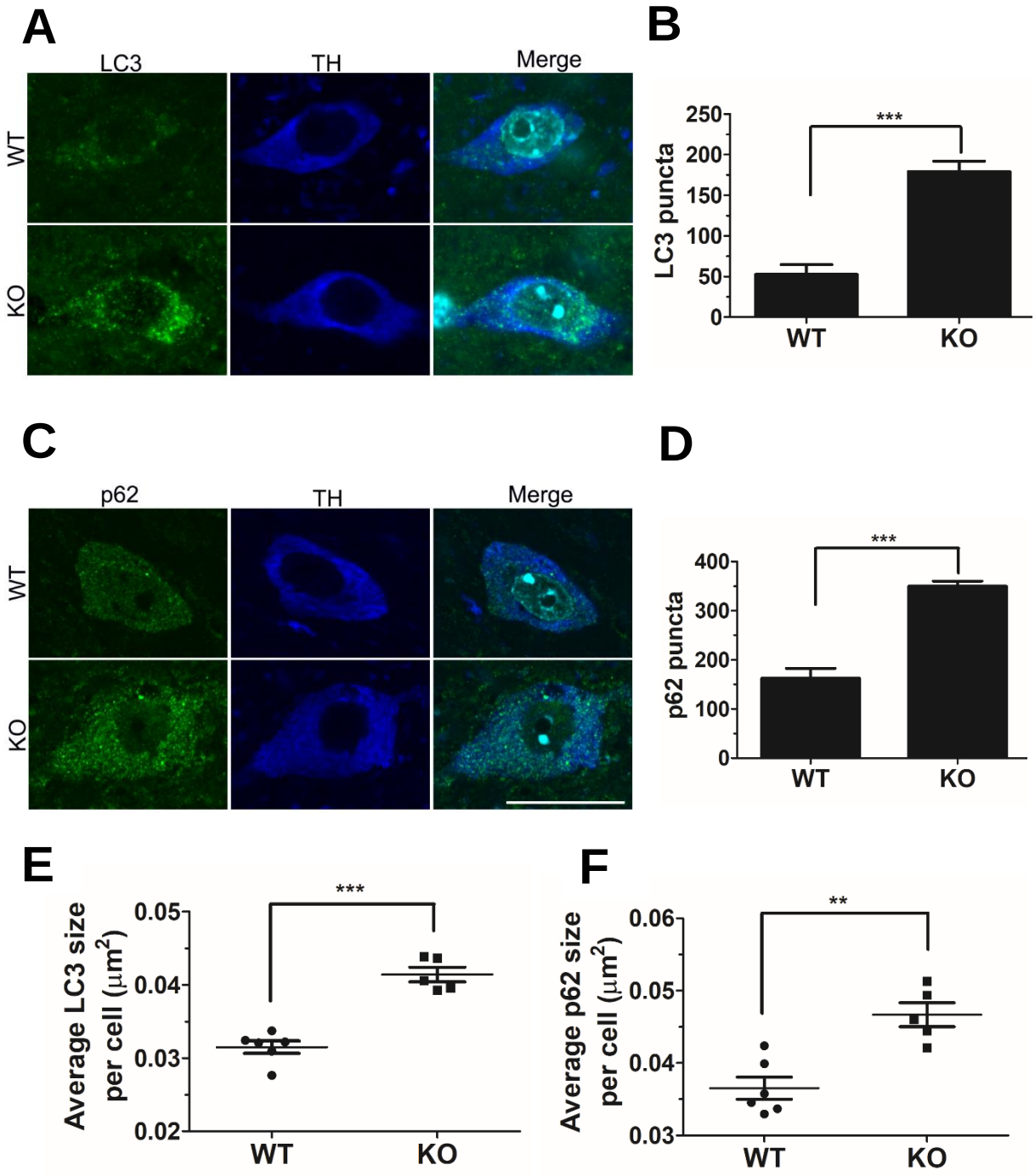

Figure 5.2 The autophagy pathway is impaired in TH-positive neurons of six month old *SLC39A14*$^{-/-}$ mice. Following perfusion and sectioning, 30 µm nigral sections were stained for (**A**) LC3 and (**B**) p62 to assess autophagy changes in TH-positive neurons (blue). (**C**) LC3 and (**D**) p62 puncta/cell were counted in at least 20 neurons from multiple brain sections per condition, using ImageJ. Average size of (**E**) LC3 and (**F**) p62 puncta per TH-positive cells. Data represent mean ± SEM (WT n=6; KO n=5). Unpaired two-tailed Student's *t* test: ** P<0.001 *** P<0.001. Scale bar 20 µm.

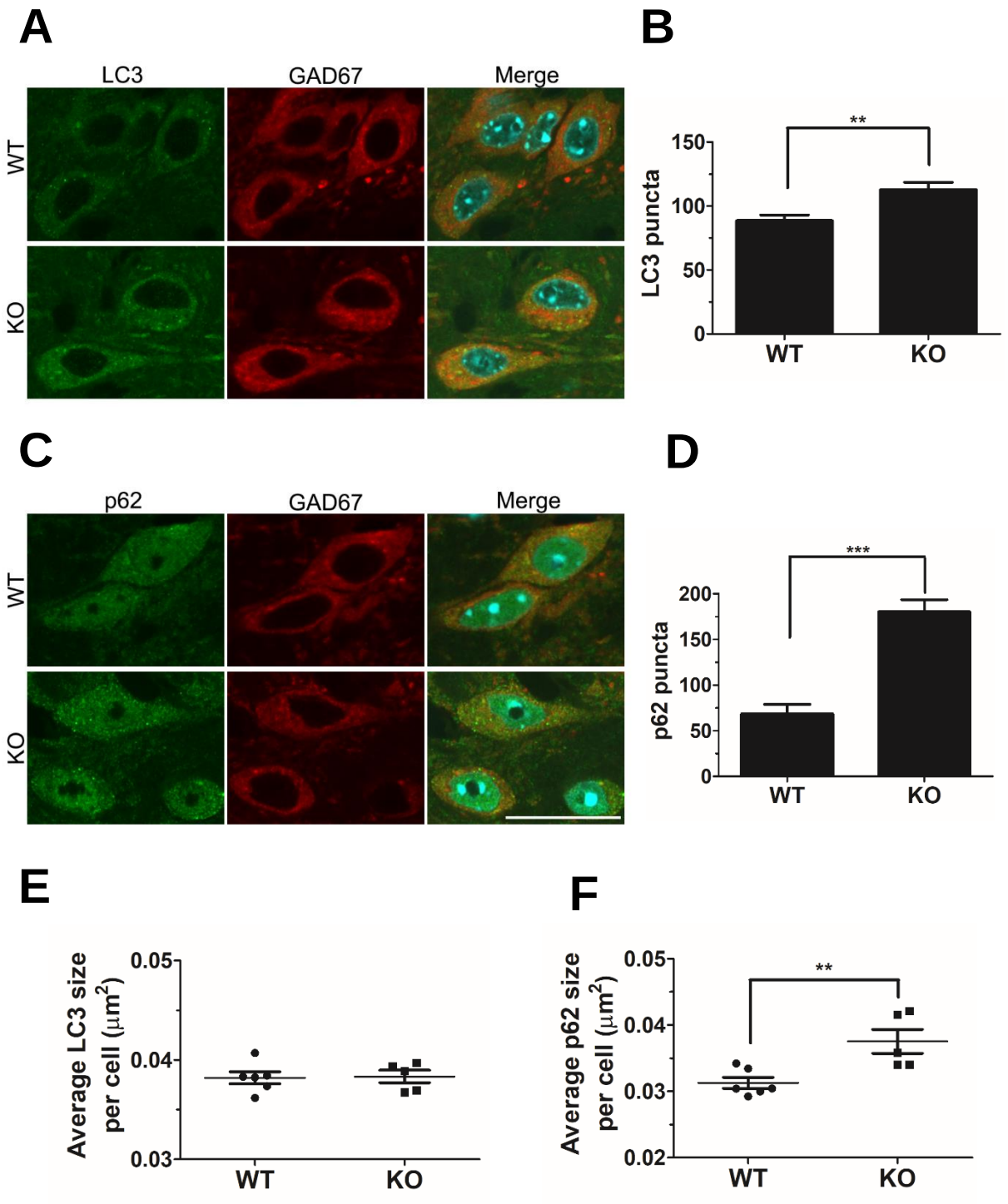

Figure 5.3 The autophagy pathway is impaired in GABAergic neurons of six month old *SLC39A14*$^{-/-}$ mice. Striatal sections (30 µm) were co-immunostained for GAD67 plus (**A**) LC3 and (**B**) p62 to assess autophagy flux in GABA neurons (blue) in the GP. (**C**) LC3 and (**D**) p62 puncta/cell were quantified in at least 20 neurons from multiple brain sections per condition, using ImageJ. Average size of (**E**) LC3 and (**F**) p62 puncta per GAD67-positive cells. Data represent mean ± SEM (WT n=6; KO n=5). Unpaired two-tailed Student's *t* test: ** P<0.01 *** P<0.001. Scale bar 20 µm.

5.2.3 Assessment of morphological changes in the mitochondria of DAergic and GABAergic neurons of *SLC39A14*$^{-/-}$ mice

Having found an impairment in autophagy flux in a genetic model of Mn accumulation, it was imperative to assess changes in mitochondrial function and morphology. However, due to lack of samples and difficulty in assessing mitochondrial function, WT and KO mice nigral and striatal sections were immunostained with TOM20 to investigate potential morphological changes caused by brain Mn accumulation. In both TH- (**Figure 5.4 A**) and GAD67-positive (**Figure 5.4 B**) neurons from the SN and GP regions, respectively, the mitochondrial network of WT (TH, 22.44 ± 2.09; GAD67, 21.21 ± 2.44) and KO (TH, 26.90 ± 2.07; GAD67, 20.65 ± 1.09) groups appeared integral, with no evident fragmentation or changes in mitochondrial length (**Figure 5.4 C**). Additionally an unpaired two-tailed Student's *t* test revealed no statistical difference of average mitochondria length between the two groups.

Taken together, these results indicate that chronic accumulation of Mn in *SLC39A14*$^{-/-}$ mice induces autophagy impairment in both TH- and GAD67-positive neurons, without causing observable changes in mitochondrial morphology.

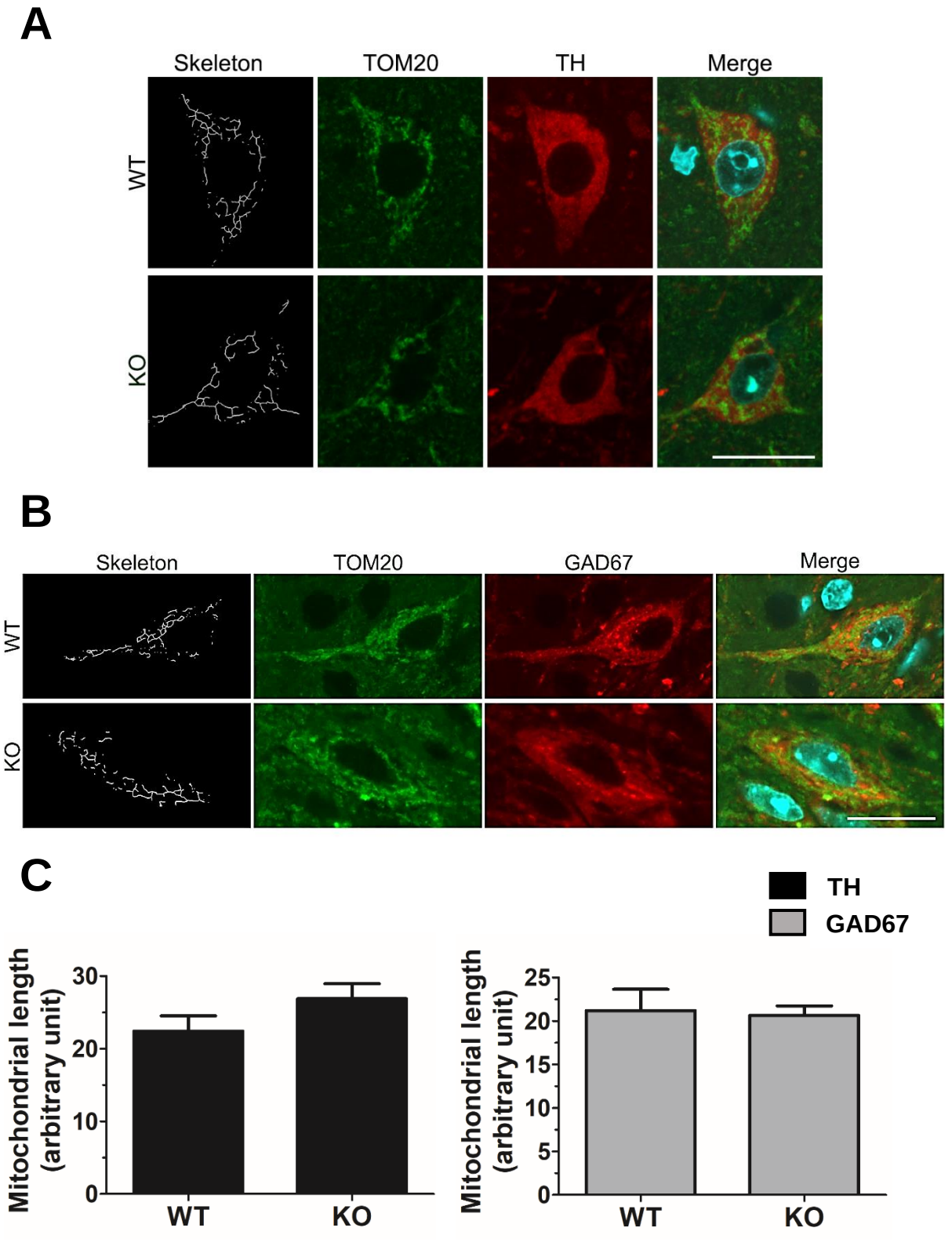

Figure 5.4 No evident alterations in mitochondrial morphology in *SLC39A14*$^{-/-}$ mice. Nigral and striatal sections (30 µm) were stained for TOM20 to assess mitochondrial morphology in (**A**) TH- and (**B**) GAD67-positive neurons (red). (**C**) Mitochondrial length was quantified in at least 20 TH- and GAD67-positive neurons per condition, using ImageJ. Data represent mean ± SEM (WT n=6; KO n=5 animals per group). Unpaired two-tailed Student's *t* test displayed no statistical difference between WT and KO animals. Scale bar 20 µm.

5.3 Discussion

In the current chapter, I report that chronic accumulation of Mn, caused by a homozygous deletion of the ZIP14 transporter, impairs the autophagy pathway in the SNpc of six month old *SLC39A14*$^{-/-}$ mice.

PD and Mn-induced parkinsonism share some similarities in their pathophysiological mechanisms and motor symptoms, however many clinical and pathologic manifestations differ between these two disorders (Kwakye et al., 2015). Degeneration of DAergic neurons of the SNpc represent the major feature of PD, whereas, a loss of DAergic neurons has not been a consistent feature in autopsy samples from humans or non-human primates exposed to Mn (Perl and Olanow, 2007, Burton and Guilarte, 2009, Guilarte, 2010). Neuroimaging data from some occupational Mn exposed cases have shown reduced levels of DAT (Kim et al., 2002, Huang et al., 2003), however other studies have revealed no effects of Mn exposure on DAT levels in the caudate and putamen (Guilarte et al., 2008, Sikk et al., 2010). Discrepancies in these results could be related to the unique genetic and environmental makeup of a patient, causing the disease to present as a spectrum.

The discovery of the ZIP14 Mn-specific transporter (Tuschl et al., 2016), has provided insight into Mn transport and elucidated further mechanisms underlying Mn-related diseases (Aydemir et al., 2017, Jenkitkasemwong et al., 2018). Despite this, the effects of Mn accumulation in basal ganglia circuitry have not been fully elucidated. To this end, I first investigated alterations in TH levels in both the SN and the striatum in six month old mice. Data shown in **Figure 5.1** indicate no apparent change in TH levels in the SN or the striatum of KO mice compared to WT. Of note, striatal OD measures TH protein expression but it does not distinguish between alterations in TH protein expression and the number of TH-positive fibres. However, this is a standard and well-established technique that our lab has published on extensively (Cui et al.,

2009, Rappold et al., 2011, Rappold et al., 2014). This method does allow distinction of the background and specific signal. As shown in **Figure 5.1B**, the TH immunoreactivity is very faint in regions such as the cortex, corpus colosum and septal nucleus when compared to nearby regions high in TH protein such as the striatum, nucleus accumbens and olfactory tubercle. The background intensity was subtracted from the specific signal when striatal OD was quantified. Based on experience in our and other labs, a loss of nigral DAergic neurons does result in a reduction in striatal TH immunoreactivity, which is a reflection of TH positive fibres.

Overall my results could suggest that the locomotor deficits described by several groups (Xin et al., 2017, Jenkitkasemwong et al., 2018) are not associated with the loss of DAergic neurons within the nigrostriatal pathway. This evidence is consistent with Guilarte et al. (2008) who showed that the nigrostriatal DAergic system is dysfunctional but intact in non-human primates chronically exposed to Mn, therefore suggesting that the neuropathology of chronic Mn exposure differs from that observed in idiopathic PD.

As demonstrated in Chapter 4, acute exposure to Mn caused a blockade in the autophagy pathway, without affecting mitochondrial morphology. To further investigate possible alterations in cellular mechanisms caused by chronic Mn accumulation in *SLC39A14*$^{-/-}$ mice, autophagic and mitochondrial markers were again used. As the GP represents the major site of Mn accumulation in the brain, changes in autophagy and mitochondrial morphology were assessed in both TH- and GAD67-positive neurons in the SN and GP, respectively. Results in **Figure 5.2** and **5.3** show an accumulation of both LC3 and p62 in the SNpc and GP of *SLC39A14*$^{-/-}$ mice. This was evidenced by an increased number of LC3 and p62 puncta in both TH- and GAD67-positive neurons. Additionally, LC3 and p62 puncta size was enlarged compared to WT mice in TH-positive neurons, whilst only p62 puncta size incremented in GAD67-positive neurons of KO. Although not clear, these results could indicate that Mn has effects on multiple levels of the autophagy pathway. For example, an increase in

autophagosome size could suggest a deficit in autophagosome maturation. This result however is preliminary and warrants further study, including the ultrastructural examination of autophagic vesicles in the presence of Mn.

Previous studies have additionally shown that autophagy impairment caused formation of p62 aggregates (Komatsu et al., 2007) and that p62-positive inclusions can contain endogenous α-synuclein (Sato et al., 2018). However, to demonstrate direct sequestration of aggregates by autophagosomes, immuno-TEM is required. In particular, these aggregates could be representative of α-synuclein. Verina et al. (2013) previously showed that moderate exposure to Mn promoted α-synuclein aggregation in neuronal and glial cells in the frontal cortex of non-human primates. As previously discussed in section 3.2.4, an increase in α-synuclein aggregation occurred consequently to autophagy dysfunction induced by Mn in N27 DAergic cells. It would be interesting, in the future, to assess whether these p62-positive aggregates co-localise with α-synuclein in DAergic and GABAergic neurons of *SLC39A14*$^{-/-}$ mice and perform a time course to investigate whether protein aggregation occurs prior to autophagy blockade or *vice versa*.

As discussed, prior to the discovery of SLC39A14 being implicated in Mn influx (Tuschl et al., 2016), SLC39A14 was known for only transporting Zn (Taylor et al., 2005). Therefore, although this is the first time that changes in the autophagy pathway were assessed in *SLC39A14*$^{-/-}$ mice, previous results from Aydemir et al. (2016), whilst assessing the effects of Zn on glucose metabolism, showed that liver endosomes of *SLC39A14*$^{-/-}$ mice displayed impaired cathepsin D activity, thus suggesting an indirect link between Mn and lysosomes. This study supports results from multiple chapters in which Mn accumulation causes a late stage block in the autophagy pathway.

Furthermore, Aydemir et al. (2016) examined the association between SLC39A14 and mitochondrial function. In addition to localising to mitochondria, SLC39A14 is involved in ATP synthesis. Interestingly, by evaluating the amount of ATP in total and mitochondrial fractions from *SLC39A14*$^{-/-}$ mice total liver ATP concentrations were reduced, whereas no changes were detected in mitochondrial ATP concentrations (Aydemir et al., 2016). It is of important note that the latter study assessed changes in mitochondrial metabolism in the liver, therefore it is possible that the brain, being more sensitive to Mn overload, might react differently. Results from the current study, however, show no changes in mitochondrial morphology in TH- and GAD67-positive neurons *SLC39A14*$^{-/-}$ mice. TOM20 staining shown in **Figure 5.4** revealed an intact mitochondrial network between the two groups in both nigral and striatal regions. These results support those from the above study, suggesting that a deficiency in the SLC39A14 transporter in six month old mice does not affect mitochondrial morphology and rather causes an impairment in the autophagy pathway. As previously stated in section 4.3, it is important to note that this study has the limitation of not assessing mitochondrial function in full. Given the scarce tissue availability for my PhD study, mitochondrial respiration and ultrastructure by TEM were not evaluated and therefore it is imperative to do so in future studies to fully ascertain that Mn overload does not affect mitochondrial function in *SLC39A14*$^{-/-}$ mice.

To conclude, this study provides evidence, for the first time, of a role for the autophagy pathway in chronic Mn overload in mice lacking the ZIP14 transporter. Results show that chronic Mn accumulation causes autophagy impairment without affecting mitochondrial morphology nor causing DAergic neuron cell death in six month old *SLC39A14*$^{-/-}$ mice. These preliminary findings expand our understanding of Mn effects on cellular mechanisms in *SLC39A14*$^{-/-}$ mice and highlight its importance in neurodegenerative disease processes. In addition, they support findings from previous chapters and suggest that the autophagy pathway

is impaired in a chronic model of Mn neurotoxicity. These results emphasise the importance of conducting future experiments to fully understand the mechanisms by which Mn is inducing these cellular changes. Some key future investigations include 1) assessing changes in the autophagy pathway, mitochondrial function and protein aggregation at multiple timepoints (3 – 12 month old mice); 2) investigating whether improving autophagy could have a positive effect on motor symptoms. This might shed light on understanding how Mn dyshomeostasis/toxicity might contribute to PD pathology and provide new paths for drug discovery to combat diseases associated with Mn toxicity.

Chapter 6
General discussion and future perspectives

6.1 General discussion

Heavy metals are known for causing neurotoxicity and are of major concern due to their long-lasting and possible irreversible nature; particularly, elevated Mn levels can accumulate in the basal ganglia and cause a PD-like syndrome referred to as Manganism. Since genes involved in early and late onset of PD and Mn overload potentially disrupt similar cellular processes in the basal ganglia, it is possible that PD symptoms may overlap with Mn toxicity. As previously discussed by Roth et al. (2014), there are four key themes that correlate PD and Mn neurotoxicity: oxidative stress triggered by mitochondrial dysfunction, abnormal vesicular trafficking, α-synuclein aggregation and impaired proteostasis. The association of Mn with each of these processes further implicates its potential risk of promoting the onset of parkinsonism. Prior research has implicated Mn in causing mitochondrial impairment (Gavin et al., 1992, Gunter et al., 2010, Gunter et al., 2012, Martinez-Finley et al., 2013) and promoting α-synuclein aggregation (Uversky et al., 2001, Bates et al., 2015), whereas evidence on the effects of Mn on the autophagy pathway are controversial and not fully understood (Zhang et al., 2013, Gorojod et al., 2015, Ma et al., 2017, Zhou et al., 2018). Moreover, none of these intracellular processes have been studied concurrently and therefore it is not clear which one precedes the other. Unravelling this could pose great value to both our further understanding of Mn-induced neurotoxicity and possible benefits to disease therapy. To this end, the present study set out to investigate how exposure to Mn affects cellular mechanisms, in both *in vitro* and *in vivo* models, with the following core aims:

- To investigate the effects of Mn on autophagy, mitochondria and α-synuclein aggregation.
- To assess whether inhibition of Drp1 may be protective against Mn-induced changes on intracellular PD-associated processes.

- To explore any autophagic and mitochondrial changes in the newly developed *SLC39A14* knockout (*SLC39A14*$^{-/-}$) mouse model.

Autophagy is a dynamic process that encompasses autophagosome formation with cargo capture and consequent shuttling to the lysosomes, whereupon the two vesicles fuse, yielding autolysosomes which will degrade the contents and recycle them. Completion of this process is termed 'autophagy flux'. Two methods were used to accurately assess changes in autophagy flux induced by Mn exposure: 1) mRFP-GFP-LC3 expressing cells/neurons, which provide a useful system to distinguish between non-degraded autophagosomes and autolysosomes, 2) the combination of LC3 (autophagosome marker) and p62 (autophagy substrate) markers in either WB or immunostaining studies.

Results in the current study demonstrate that Mn impairs autophagy flux by promoting autophagosomes accumulation and reduction of autolysosomes both *in vitro* and *in vivo*. Additionally, the effect of Mn on autophagy flux was exacerbated in cells overexpressing WT human α-synuclein, indicating an interplay between Mn and α-synuclein and further suggesting a link between Mn and PD. A recent study showed that increased autophagosome synthesis, which cannot be processed at the lysosomal level, are futile for the cells as responsible for depleting energy and nutrition, ultimately contributing to the cell's demise (Button et al., 2017). Although Mn mechanism of action on the autophagy pathway is still not fully understood, I suggest Mn could be either directly affecting autolysosome formation, lysosomal function or indirectly targeting the autophagy pathways through a different mechanism.

Consequently to autophagy blockade, Mn exposure increased α-synuclein aggregation in cells overexpressing α-synuclein. α-synuclein accumulation has previously been associated with impaired functioning of protein degradation mechanisms (Xilouri et al., 2013, Ebrahimi-Fakhari et al., 2012), autophagy being one of the key pathways. On the other hand, reduced

autophagic function was shown to promote intracellular accumulation of proteins and neurodegeneration (Hara et al., 2006, Komatsu et al., 2006). The reliance of neurons on a functional autophagic pathway is supported by observations that the brain is particularly vulnerable to lysosomal disorders, especially during aging (Nixon, 2013).

Unlike previous studies assessing the effects of Mn on mitochondria, I did not find any significant morphologic alterations or functional changes in the mitochondria of cells and neurons exposed to Mn, unless the dose of Mn used was increased to a level that caused over 40% cell death. Given Mn physiological role in mitochondrial homeostasis, the majority of the studies focused on Mn toxicity and assessed changes in mitochondrial metabolism, ROS and recently mitochondrial morphology (Alaimo et al., 2013, Alaimo et al., 2014, Martinez-Finley et al., 2013). Most of the prior evidence has pointed to mitochondria being the major target of Mn toxicity. These assessments, however, were not performed in conjunction with changes in other cellular pathways, using sub-toxic concentrations. I, therefore, suggest that Mn is primarily causing autophagy impairment, resulting in α-synuclein aggregation, whilst mitochondrial function and morphology (not affected at the studied timepoint) may cause a decline in intracellular ATP or elevation in ROS production at a later time point. This could be, in fact, expected since autophagy is responsible for clearing intracellular toxins and damaged organelles that generate oxidative stress (Lemasters, 2005). As the autophagy machinery helps to clear damaged mitochondria, if autophagy is dysfunctional/impaired there will be an increase in dysfunctional mitochondria, unable to be cleared. In addition, as the material used to generate the initial membrane of the autophagosomes has been shown to be attributed to several organelles, including mitochondria (Hailey et al., 2010), it is possible that the accumulated number of autophagosomes, caused by Mn, will potentially induce mitochondrial stress and promote ROS production over time. It has been reported that in the mitochondria Mn alters oxidative phosphorylation and that Mn^{3+} is more potent than Mn^{2+} in

producing ROS (Ali et al., 1995, Chen et al., 2001). Since the enhanced ability of trivalent Mn to cause oxidative stress has been confirmed in rats injected with either $MnCl_2$ (Mn^{2+}) or $Mn(OAc)_3$ (Mn^{3+}) (Ali et al., 1995), it is possible that low concentrations of $MnCl_2$, used in the current study, were not potent enough to induce oxidative stress and affect mitochondrial function. Overall our findings suggest a novel mechanism of action for Mn toxicity (**Figure 6.1)**. Mn overexposure appears to first promote autophagy impairment and consequently α-synuclein aggregation.

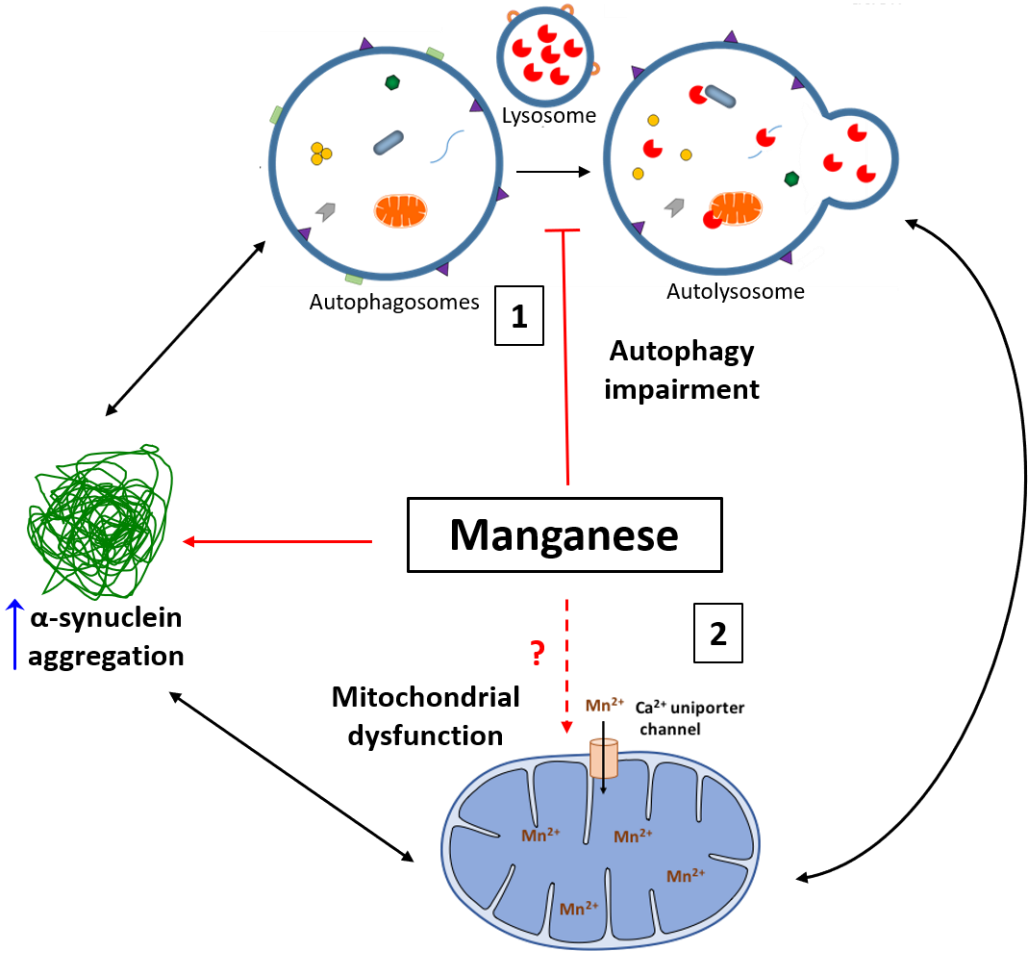

Figure 6.1 Proposed model of Mn-induced changes on cellular mechanisms. Given results obtained from the current study I propose a novel mechanism of action of Mn neurotoxicity. The red lines represent the effects of Mn, whereas the black arrows show the effects of each pathway on the others. Mn primarily affects the autophagy pathways by causing a late stage block, with increased number of autophagosomes and reduced autolysosomes. This impairment induces protein aggregation, without affecting mitochondrial morphology nor function, unless Mn concentrations are increased to a level that is detrimental for the cell. The question mark represents the possibility of future mitochondrial dysfunction that may appear with continuous exposure to the metal.

In the current study I used different strategies to inhibit Drp1 and assess its effects on cells exposed to Mn alone or combined to α-synuclein. Whilst inhibition of Drp1, via siRNA and mdivi-1, ameliorated autophagic impairment induced by Mn, their effects on the autophagy pathway appeared different. siRNA mediated knockdown of Drp1 attenuated the accumulation of autophagosomes caused by Mn and/or α-synuclein and promoted the increase in the number of autolysosomes. Mdivi-1 alone promoted autophagosome formation, indicative of autophagy induction (significantly different to control cells), however in combination with Mn it maintained a high number of autophagosomes whilst increasing the number of autolysosomes. It appears that mdivi-1 is possibly targeting multiple sites of the autophagy pathway or having off target effects. These results, however, suggest the inhibition of Drp1 improved autophagy flux either by promoting autophagosome-lysosome fusion or restoring lysosomal function.

The evidence available in the literature suggests that Mn can accumulate in lysosomes (Suzuki et al., 1983, Okamoto et al., 1997) and affect the enzymatic capacity of cathepsins (Fan et al., 2010, Gorojod et al., 2017). Specific Drp1 isoforms, abundant in the brain, have been shown to locate to lysosomes and late endosomes (Itoh et al., 2018) as well as mitochondria (Smirnova et al., 1998). Additionally, mitochondria can interact dynamically with lysosomes and these contacts were proven to be different from those targeting damaged mitochondria into lysosomes for degradation (Wong et al., 2018). Given the ability of Mn to impair lysosomes and Drp1 to interact with endosomal-lysosomal pathways, it is possible that inhibiting Drp1 is restoring autophagy defects in Mn-exposed cells/neurons through lysosomes. Interestingly, heterozygous deletion of Drp1 in mice did not confer protection against Mn-induced changes in autophagy flux, whilst preliminary results from mice transduced with $Drp1^{K38A}$ displayed potential restoration of autophagy flux. These results indicate that heterozygous knockout of Drp1 cannot exert protective effects against Mn-induced changes in autophagy, whilst the use of a dominant negative form of Drp1, that allows sufficient fission for the maintenance of

normal physiological function, could be protective and represents a potential new target against Mn-induced neurotoxicity. Based on the current study and those from previous groups, which indicate a non-canonical function of Drp1 signalling (possibly within the lysosomes), I suggest a novel role for Drp1 in the regulation of the autophagy pathway, which will warrant more in-depth studies.

Although the protective mechanism of Drp1 inhibition on the autophagy pathways is novel, the interplay between mitochondria and autophagy has been previously shown to be crucial for maintaining homeostasis in eukaryotic cells. Komatsu et al. (2005) showed that ATG7 knockout mice exhibit deformed mitochondria, and accumulated ubiquitin-positive aggregates. Similarly, mitochondrial swelling and oxidative stress have been reported in liver-specific ATG7 knockout and systematically ATG5-deficient mice (Inami et al., 2011, Takamura et al., 2011). In addition, independently to their role in autophagosome formation, defects in the ATG12-ATG3 complex, cause an increase in mitochondrial mass, affecting mitochondrial homeostasis (Radoshevich et al., 2010). Conversely, mitochondria have been shown to play key roles in regulating nonselective autophagy. ROS are essential for autophagy and specifically regulate the activity of ATG4 (a cysteine protease that regulates autophagy through the processing and deconjugating of ATG8 to the autophagosomal membrane) (Scherz-Shouval et al., 2007). Mitochondria were shown to serve as a membrane source for autophagosome formation and cells lacking *Mfn2* did not form autophagosomes (Hailey et al., 2010). Recently, Thomas et al. (2018) reported that phenformin (inhibitor of mitochondrial complex I) or genetic defects in complex I (Rodenburg, 2016), impaired autophagy, suggesting the requirement of mitochondrial complex I (or perhaps mitochondrial function in general) in the autophagy pathway. This evidence not only shows an evolutionarily conserved interplay between mitochondria and autophagy, but also indicates that defects in one of these elements could simultaneously affect the other.

In addition to restoring autophagy flux impaired by Mn both *in vitro* and *in vivo*, Drp1 inhibition was also neuroprotective against Mn-induced cell death and also ameliorated α-synuclein aggregation. As α-synuclein aggregation was suggested to be the result of autophagy dysfunction, I speculate that protein aggregation was rescued by restoring autophagy flux. This suggestion has been previously confirmed (Moors et al., 2017, Fowler and Moussa, 2018, Arotcarena et al., 2019). In fact, following the discovery of accumulated autophagic vacuoles in the SN of post-mortem patients with PD (Anglade et al., 1997), an extensive amount of recently identified genetic factors, including α-synuclein, was proven to be involved in or to interact with the autophagy pathway (Gan-Or et al., 2015). Given the evidence for a role of autophagy deregulation in PD and the identification of autophagy as key player in degrading α-synuclein, a decade ago pioneering studies have explored the possibility of autophagy-enhancing strategies as disease-modifying therapy to reduce α-synuclein aggregation in PD (Moors et al., 2017). Indeed, the use of rapamycin or lithium, promoted α-synuclein clearance and reduced neurodegeneration both *in vitro* and *in vivo* (Webb et al., 2003, Crews et al., 2010, Xiong et al., 2011, Hou et al., 2015). Additionally, direct targeting of lysosomes has emerged as an attractive strategy for manipulating autophagy in neurodegenerative diseases, as evidence suggests that strategies that solely promote autophagosome synthesis may be deleterious for the cell (Button et al., 2017). These studies include: the use of acidic nanoparticles to restore lysosomal function (Baltazar et al., 2012, Bourdenx et al., 2016), the direct targeting of specific lysosomal enzymes, such as GCase, to stimulate α-synuclein clearance (Sardi et al., 2011, Rocha et al., 2015) and overexpression of TFEB, a master gene for lysosomal biogenesis, for alleviating α-synuclein pathology and rescue midbrain DA neurons (Decressac et al., 2013). These examples give precedence and credence to my suggestion: promoting or restoring autophagy activity could represent a promising and relevant therapy for protein accumulation-based neurodegenerative diseases.

How is Drp1 inhibition improving Mn-inducted cytotoxicity? Recently, Zhang et al. (2019) investigated the role of Mn exposure in autophagy regulation. Their results showed that 24 h 100 µM $MnCl_2$ suppresses TFEB activity, causing autophagy dysfunction and mitochondrial pathology in primary astrocytes. These results were validated *in vivo*, using the same acute Mn treatment regime adopted in the current thesis. Overexpression of TFEB partially restored Mn-induced autophagy dysfunction (Zhang et al., 2019). These findings suggest an interplay between compromised autophagic and mitochondrial function in Mn toxicity and identify TFEB as a potential therapeutic target for Mn-induced toxicity. Interestingly, Fan et al. (2019) utilised three complementary approaches to investigate the protective role of Drp1 inhibition in cells overexpressing human WT α-synuclein. They discovered that reduction of Drp1 function could inhibit mTOR (mammalian target of rapamycin) activity, to an equivalent extent as rapamycin, and attenuate autophagy impairment caused by α-synuclein. mTOR kinase is involved in conveying nutrient-sensing signals to lysosomes, thus paring lysosomal functions to cellular energy demands (Dunlop and Tee, 2014, Rabanal-Ruiz and Korolchuk, 2018). To accomplish this, mTOR phosphorylates TFEB to modulate its localisation, transcriptional activity, stability and cellular abundance (Puertollano et al., 2018). Upon mTOR inhibition, dephosphorylated TFEB translocates to the nucleus and upregulates the activity of its targets genes, many of which are involved in lysosomal biogenesis and function (Palmieri et al., 2011, Settembre et al., 2012).

Given the above information, I propose that Drp1 inhibition reduces mTOR activity and thus promotes TFEB expression to a level that improves autophagy dysregulation caused by Mn exposure. It is thus possible that Drp1 inhibition confers neuroprotection through the autophagy-lysosomal pathway. This proposed effect of Drp1 inhibition on the autophagy pathway is illustrated in **Figure 6.2**.

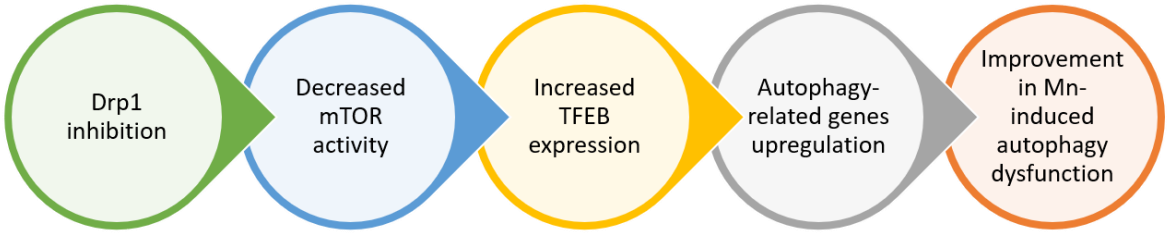

Figure 6.2 Proposed effect of Drp1 inhibition on autophagy dysregulation promoted by Mn treatment. Inhibition of Drp1 deregulates mTOR activity, which in turn alters TFEB phosphorylation status, thus affecting its levels. Increase in TFEB levels upregulates autophagy-related genes and potentially restores Mn-induced autophagy changes.

Lastly, I investigated the effects of chronic accumulation of Mn in a newly developed mouse model of Mn neurotoxicity. My results indicated that impaired uptake of Mn in *SLC39A14*$^{-/-}$ mice, which promotes Mn to accumulate in multiple tissues (particularly in the bone and brain) (Jenkitkasemwong et al., 2018), causes autophagy flux impairment in DAergic and GABAergic neurons of six month old mice without affecting the mitochondrial network. It is possible that mitochondrial dysfunction is not associated with any perturbations in mitochondrial morphology, thus further studies are needed to assess mitochondrial function. These results are in line with those achieved in mice subcutaneously injected with $MnCl_2$, further implicating Mn involvement in negatively impacting the autophagy pathway. It would be interesting to investigate whether the autophagy-induced changes in neurons are also observed in astrocytes and where this proteostasis dysfunction occurs first. However, this is the first time that a more in-depth mechanistic study has been performed in this new genetic model of chronic Mn deposition. These findings expand our understanding of chronical Mn neurotoxicity, particularly given the lack of satisfactory treatment for Mn neurotoxicity. Our results could be of further interest in the clinical setting as patients acutely or chronically exposed to Mn will probably display autophagy impairment in nigral and striatal neurons, in addition to

astrogliosis. This knowledge could potentially help target those neurons and reduce the risk of promoting α-synuclein oligomerization and enhance cellular toxicity.

In summary, the major findings and contributions of the present study to the area of Mn research report that:

- Autophagy is an initial target of Mn neurotoxicity, rather than mitochondria.
- Consequently to autophagy dysfunction, Mn exposure promotes α-synuclein aggregation *in vitro*.
- α-synuclein and Mn can independently block autophagy flux but have a greater effect when combined.
- Drp1 inhibition, via small molecule or siRNA, alleviates impaired autophagy, protein aggregation and cell death induced by Mn *in vitro*.
- Preliminary results show that stereotactic delivery of $Drp1^{K38A}$ in the SNpc of mice, is protective against acute Mn-induced changes in autophagy flux.
- Six month old *SLC39A14*$^{-/-}$ mice exhibited an impairment in the autophagy pathway in both DAergic and GABAergic neurons, caused by a gradual accumulation of physiological Mn in the brain.

Collectively the results included in this thesis provide further insight into the pathogenic mechanism of Mn and its potential role in PD pathogenesis. PD has previously been associated with the accumulation of intracytoplasmic aggregates and autophagy impairment. Mn accumulation could therefore represent a potential risk for PD by affecting the autophagy pathway and promoting α-synuclein aggregation. Inhibition of Drp1 was discovered to be restorative against autophagy and protein aggregation changes caused by the metal, suggesting a new role for Drp1. Given Drp1's potential role in the autophagy pathway, I hypothesise that targeting Drp1 may represent a novel method to modulate the autophagy pathway with

particular relevance for neurodegenerative diseases. Despite several limitations, I believe that the results presented in the current study are an important assessment at multiple cellular pathways and represent a starting point from which a more comprehensive and detailed analysis could be performed in the future.

6.2 Future perspectives

Across most neurodegenerative disorders, proteostasis has been widely studied given that many of these diseases, including PD, display protein aggregation and dysfunctional UPS or autophagy as part of their cellular pathology. Given the role of Mn in PD pathogenesis and the results obtained in the current study, a more in-depth understanding of Mn's mechanism of action in the autophagy pathway is needed and will enable the identification of possible methods for effective therapeutic strategies. Although results from the current study suggest a late-stage block caused by Mn overexposure, it is important to investigate multiple sites of the autophagy pathway to fully ascertain this. Additionally, as the autophagy pathway represents one of the major proteolytic systems that maintain cellular protein homeostasis, it would be interesting to assess whether Mn also affects CMA and UPS pathways both in the presence and absence of α-synuclein.

A particularly novel finding in the current study is that the inhibition of Drp1 improved the observed autophagic deficits and protein aggregation in multiple cell lines and in mice caused by Mn. As the exact function of Drp1 in the autophagy pathway is currently not known it is important to understand how and where in the autophagy pathway Drp1 is ameliorating Mn-induced neurotoxicity. Using different Drp1 isoforms, colocalization studies with various autophagy markers could be performed, in addition to deleting ATG proteins and evaluating changes in Drp1 levels to better comprehend this mitochondria-autophagy interplay. Whilst blocking Drp1 function inhibits mitochondrial fission, would promoting fusion, produce a similar effect on autophagy or are these results only specific to Drp1? Xue et al. (2018) demonstrated that Mfn2 could promote LC3-II expression and downregulate p62 expression in pancreatic cancer cells. It would be interesting to assess whether overexpressing the fusion protein Mfn2 could also ameliorate Mn-induced changes. Furthermore, as Drp1 is mainly known for being implicated in mitochondrial fission, would prolonged Mn exposure impair

mitophagy? A recent study showed that, contrarily to the thought of Drp1 being essential for mitophagy (Gomes et al., 2011, Rambold et al., 2011), Drp1 knockout cells could recruit Parkin to elongated mitochondrial networks and enhance mitophagy (Burman et al., 2017).

The current study clearly shows that Mn promotes the aggregation of α-synuclein following autophagy impairment. Aggregation and spread of a misfolded α-synuclein represent a hallmark of PD pathogenesis. A recent study demonstrated that Mn exposure could promote the transfer of α-synuclein between neurons and microglia, causing neuroinflammatory and neurodegenerative responses in both cell culture and animal models (Harischandra et al., 2019). These results indicate that Mn is contributing to PD-associated propagation of both α-synuclein and neuroinflammation involving neuronal and microglial interactions. It would be interesting to assess whether inhibiting Drp1 or overexpressing Mfn2 may prevent this α-synuclein release and spread.

Another key finding of the current study was the ability of low concentrations of Mn (at 24 h) to primarily block autophagy flux, without affecting mitochondrial function or morphology *in vitro*. Future experiments are needed to investigate Mn effects on PD-processes over a longer time frame. In addition, my i*n vivo* studies focused on morphological changes, without assessing mitochondrial function following acute and chronic exposure to the metal. It is imperative to establish whether Mn indeed impairs mitochondrial function, independently to mitochondrial morphology, via EM and seahorse assay.

Assessment of autophagic function, mitochondrial morphology and neuroinflammation in *SLC39A14*$^{-/-}$ mice has increased our knowledge of the effects of Mn following deletion of the newly discovered SLC39A14 influx Mn transporter. Although novel, further research is needed to fully characterise this genetic model of Mn neurotoxicity. In particular performing stereology both in the GP and the SN would be key to support results obtained in the current

study and definitely demonstrate whether Mn can promote neuronal cell death. I performed immunostaining using specific markers for microglial activation and astrocytic response, however, an assessment of cytokine/chemokine expression, that are upregulated during neuroinflammation, would give further insight into the effect of Mn on glial cell functions and tissue microenvironment in general.

Previous studies have shown impaired DA release in animals exposed to Mn (Guilarte et al., 2006a, Guilarte et al., 2008, Khalid et al., 2011). Particularly, Khalid et al. (2011) used the same injection strategy adopted in Chapter 4 to acutely expose mice to $MnCl_2$ and showed altered striatal DA release in these mice. It would be interesting to replicate this data in both WT and LC3 mice as well as investigate whether *SLC39A14*$^{-/-}$ mice could display similar deficits, performing HPLC or *in vivo* microdialysis. As previously reported by Rappold et al. (2014) inhibition of Drp1 restored pre-existing DA release deficits in *PINK1*$^{-/-}$ and MPTP mice, the same strategy could therefore be used to ameliorate possible DA release deficits in *SLC39A14*$^{-/-}$ and WT/LC3 mice exposed to Mn.

Finally, the long-term impact of blocking Drp1 should be evaluated in order to assess potential detrimental effects of this therapy. To achieve this aim, Drp1 expression could be reduced using WT mice stereotactically expressing dominant negative Drp1 forms over 12 to 18 months. Neuropathological parameters including cell loss (stereology), DA release (HPLC), and synaptic function (immunostaining of synaptic markers, synaptosome isolation) will need investigation.

These proposed experiments, in combination with those detailed in the current study, will allow for a more in-depth understanding of Mn mechanisms of action, its interaction with α-synuclein in the development of PD and the specific role of Drp1 in the setting of neurodegeneration.

Chapter 7
Appendices

7.1 Appendix A - Additional introduction

7.1.1 Rotenone

Rotenone, a potent non-competitive mitochondrial complex I inhibitor derived from the *Leguminosa* plant family (Soloway, 1976), is a naturally cytotoxic compound used as a pesticide/piscicide and associated with increased risk of developing PD (Tanner et al., 2011, Kamel, 2013). Rotenone is highly lipophilic and does not require specific transporters to cross the blood-brain barrier (BBB) (Higgins and Greenamyre, 1996). Moreover, due to its relatively short half-life (~ 3 days) (Hisata, 2002), the most likely route of exposure is through low chronic exposure to the pesticide. Rotenone impairs mitochondrial function by inhibiting the ETC, through direct inhibition of complex I (NADH–dehydrogenase). This inhibition leads to a reduction in ATP production and electron leakage that can generate ROS such as superoxide, subsequently causing a reduction in glutathione levels and ultimately leading to oxidative stress (Schuler and Casida, 2001, Sherer et al., 2003). Rotenone has also been shown to induce rapid mitochondrial fragmentation in primary cortical neurons, within two hours of treatment (Barsoum et al., 2006b). This neurotoxicity was averted by promoting mitochondrial fusion with Mfn1 and blocking Drp1 with Drp1-K38A (Barsoum et al., 2006b). Recent studies have demonstrated that rotenone can also be involved in altering mitochondrial transport and protein interactions within neurons (Choi et al., 2011, Di Maio et al., 2016). Although *in vivo* models of rotenone toxicity display variable neuropathology, rotenone has been shown to cause selective nigrostriatal neurodegeneration with the presence of α-synuclein-positive cytoplasmic inclusions and a neuroinflammatory component, which resulted in motor impairments (Betarbet et al., 2000, Cannon et al., 2009).

7.1.2 Paraquat

Paraquat (PQ) is a non-selective herbicide that interferes with photosynthesis and produces ROS, resulting in the damage of plant membranes proteins (Breckenridge et al., 2013). It is also commonly used to control pests in a variety crop (Bromilow, 2004). PQ is a molecule that exists as a divalent cation (PQ^{2+}) and undergoes redox cycling with cellular diaphorases such as NADPH oxidase and nitric oxide synthase (NOS) to generate a monovalent cation (PQ^{+}). From this redox cycle, superoxide is produced, which can generate ROS and result in cellular toxicity (Day et al., 1999). PQ requires the L-neutral amino acid transporter to enter the brain (Shimizu et al., 2001, McCormack and Di Monte, 2003). Once in the brain PQ^{+} can enter cells via the dopamine transporter (DAT) and the organic cation transporter-3 (OCT-3) (Rappold et al., 2011), a bidirectional transporter that is highly expressed in astrocytes and in γ-aminobutyric acid (GABA) producing neurons in nigrostriatal regions (Cui et al., 2009, Gasser et al., 2009). Although PQ is not a complex I inhibitor, this seems to be the preferred site in which PQ induces superoxide formation (Richardson et al., 2005, Cochemé and Murphy, 2008). Consistent with the role of promoting oxidative stress, a recent study showed that PD patients, who had been previously exposed to the pesticide, exhibited mitochondria DNA damage (Sanders et al., 2017). Along with mitochondrial dysfunction, several other studies reported that oxidative stress induced by PQ led to inhibition of basal autophagy in PC12 cells and primary astrocytes (Janda et al., 2015, Zhou et al., 2017).

Systematic injections of PQ in WT mice were reported to induce motor deficits and loss of DAergic neurons in the SNpc (~20-25%). The effects of PQ appeared to be specific as GABAergic neurons in the SNpc and striatum, DAergic neurons in the VTA and glutamatergic neurons in the hippocampus remained unaffected. Interestingly, although the damage induced by PQ affected DAergic cell bodies, no significant depletion of striatal DA was observed (Thiruchelvam et al., 2000, McCormack et al., 2002, Tieu, 2011). It has been suggested that,

due to an increase in TH activity following PQ administration, the increased DA synthesis may counteract the effects of terminal damage and help restore tissue levels of the neurotransmitter. When co-administered with manganese ethylenebisdithiocarbamate (Maneb), the loss of DAergic SNpc neurons is more severe and a slight reduction of striatal DA was visible, although this was not statistically significant (Thiruchelvam et al., 2000). In contrast to WT mice, mice lacking the organic cation transporter-3 (*Slc22a3*), displayed enhanced striatal damage when exposed to PQ, likely due to a reduced buffering capacity by non-DAergic cells, allowing PQ to damage DAergic terminals (Rappold et al., 2011). Additionally, PQ treatment in rodents induced neuroinflammation, α-synuclein up-regulation and aggregation, reminiscent of LBs in PD (Manning-Bog et al., 2002a, Wu et al., 2005, Fernagut et al., 2007, Purisai et al., 2007). Despite inconsistent data from *in vivo* studies, evidence from epidemiological and mechanistic studies corroborate the theory of PQ increasing the risk of developing PD.

7.1.3 The roles of Rabs, SNAREs and tethering factors (Figure 7.1)

Rab proteins are known to confine to specific membranes and recruit effector proteins. These include cargo adaptors, motor proteins and tethering proteins to help SNARE proteins with the fusion machinery upon arrival of the vesicular cargo (Stenmark, 2009, Zhen and Stenmark, 2015). Rab proteins are activated by specific guanine nucleotide exchange factors (GEFs) that promote GTP binding. Upon binding GTP, Rabs alter their conformation to interact with their effector proteins. In contrast, Rabs are inactivated by specific GTPase-activating proteins (GAPs) that hydrolyse GTP to GDP, which cause a disconnection between Rabs and effector proteins and extraction from the membranes (Nakamura and Yoshimori, 2017).

Rab7, localised on late endosomes and lysosomes is essential for endocytic membrane trafficking from late endosome to lysosome and has been suggested to be important for

autophagosome–lysosome fusion (Rab7 knockdown leads to an accumulation of late autophagic vacuoles) and subsequent digestion (Gutierrez et al., 2004, Jäger et al., 2004). Interestingly, UV radiation resistance-associated (UVRAG) and Run domain Beclin-1 interacting and cysteine-rich containing protein (Rubicon), two components of the PI3K-III complex, take part in endocytic transport, autophagosome maturation and/or autophagosome–lysosome fusion via Rab7 (Liang et al., 2008, Matsunaga et al., 2009, Zhong et al., 2009, Tabata et al., 2010). These proteins have opposite effects: UVRAG induces autophagosome–lysosome fusion by binding to VPS16 (a subunit of the homotypic fusion and protein sorting (HOPS) complex), which stimulates Rab7 GTPase activity (Liang et al., 2008), whereas Rubicon inhibits it by physically interacting with UVRAG and binding to VPS34, thus suppressing its lipid kinase activity and autophagy maturation (Sun et al., 2011).

More than 60 SNAREs are involved in fusion processes of mammalian cells. Functionally, SNAREs are organized into v-SNAREs located on donor vesicles and t-SNAREs on target vesicles. Structurally, SNAREs are classified into Q-SNAREs (with a Q amino acid residue) and R-SNAREs (with a R amino acid residue) (Nakamura and Yoshimori, 2017). Studies have shown that upon starvation, the Q-SNARE syntaxin 17 (STX17) is recruited from the cytosol to mature autophagosomes, where it interacts with the Q-SNARE SNAP29 and the lysosomal R-SNARE VAMP8 to promote autophagosome–lysosome fusion (Itakura et al., 2012). Further evidence has also implicated STX17 to be involved in the formation of the isolation membrane at the ER-mitochondria contact site (Hamasaki et al., 2013). The ER-resident STX17 protein, upon starvation, binds to and recruits ATG14L to initiate autophagosome formation (Hamasaki et al., 2013).

Membrane tethers are implicated in docking and fusion by bridging opposing membranes and by stimulating the formation of SNARE complexes. The HOPS complex, acting as a tethering factor, mediates autophagosome–lysosome fusion by interacting with STX17 (Jiang et al., 2014). Ectopic P granules protein 5 (EPG5), originally discovered in a *C. elegans* genetic screen, represents another Rab7 effector and tethering factor required for fusion specificity of autophagosomes with endosomes/lysosomes (Tian et al., 2010, Wang et al., 2016b). By interacting with Rab7 and R-SNARE VAMP7/VAMP8 proteins, EPG5 can be recruited to late endosomes/lysosomes. EPG5 also interacts with LC3 through its LC3-interacting region (LIR) motif and with Q-SNARE complexes on autophagosomes (Wang et al., 2016b).

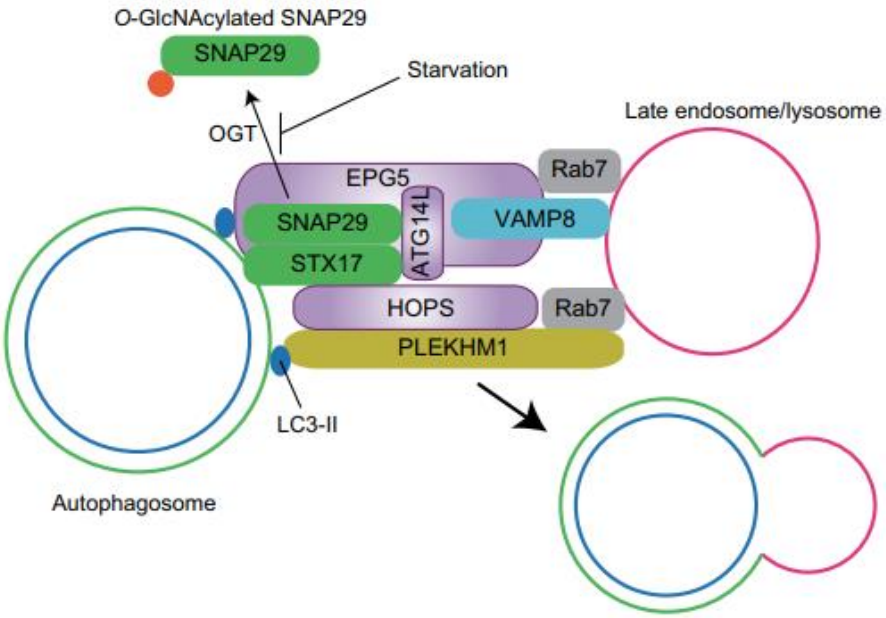

Figure 7.1 Fusion of autophagosome and lysosome – the roles of Rabs, SNAREs and tethering factors. Following recruitment to the late endosomes/lysosomes, together with Rab7 and VAMP-8, EPG5 tethers late endosomes/lysosomes by binding to LC3 and STX17–SNAP29. This induces the assembly of the trans-SNARE complex for fusion. On the other hand, ATG14L binds to STX17 and to a binary complex formed between STX17 and SNAP29 (STX17–SNAP29) on autophagosomes, facilitating its interaction with VAMP8 to promote autophagosome–lysosome fusion. This suggests that ATG14L acts earlier than EPG5. PLEKHM1 is an adaptor protein that interacts with Rab7, HOPS–SNARE complexes and LC3 proteins to enable autophagosome–lysosome fusion. EPG5, ATG14L and the HOPS complex act as tethering factors, although their exact relationship is not fully understood. O-GlcNAcylated SNAP-29, generated by O-linked β-N-acetylglucosamine (O-GlcNAc) transferase (OGT), does not have a high binding affinity for its partner SNAREs. This modification is suppressed by starvation, and a reduction in O-GlcNAcylated SNAP-29 levels triggers the assembly of SNAP-29-containing trans-SNARE complexes, thus stimulating autophagy. Adopted from Nakamura and Yoshimori (2017)

7.2 Appendix B – Supplementary results

7.2.1 Effects of paraquat on autophagy and α-synuclein aggregation

In addition to Mn, several studies have suggested that exposure to pesticides, such as paraquat (PQ), can increase the risk of developing PD (Liou et al., 1997, Tanner et al., 2011, Wang et al., 2011a). Despite extensive research in PQ's mechanism of action, not much is known of its effect on the autophagy pathway. Previous evidence has shown that PQ can block autophagy flux by promoting an increase in both LC3 and p62 levels in PC12 cells (Zhou et al., 2017), however the concentration of the pesticide used was particularly high (4 mM). I therefore first performed a cell viability assay on both HeLa mRFP-GFP-LC3 and inducible N27 cells treated for 24 and 48 h with increasing concentrations (25 – 1600 µM) of PQ (**Figure 7.2**). PQ caused a decrease in cell viability in a time-dependent fashion in both cell lines, however contrarily to Mn, HeLa cells were more sensitive to PQ compared to N27 cells.

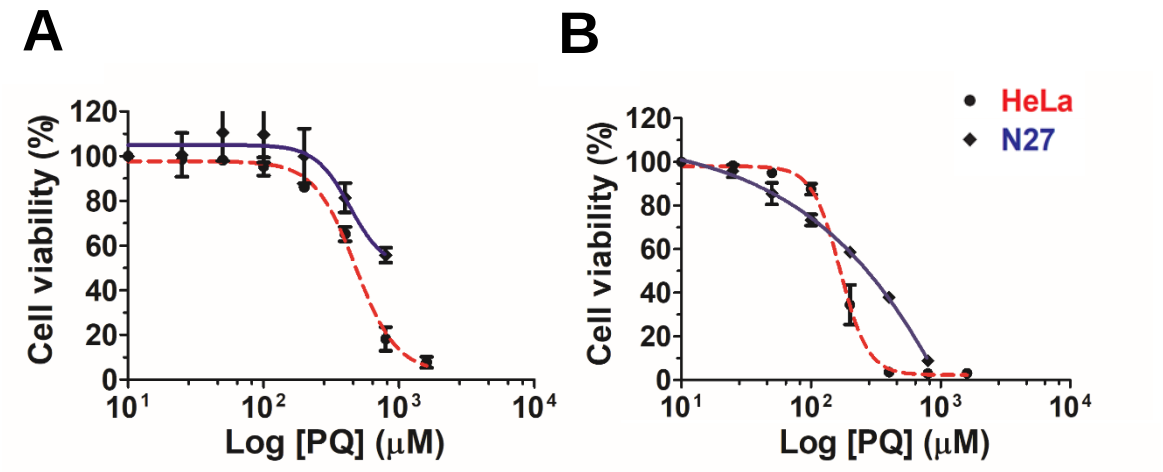

Figure 7.2 PQ reduces cell viability in a dose-dependent fashion. HeLa and N27 cells were cultured in 96-well plates and exposed to varying concentrations of PQ (25 – 1600 µM) for (**A**) 24 and (**B**) 48 h. Values are relative to 100% for the untreated group and they are represented as mean ± SEM (n=3 independent experiments).

Following cell viability, HeLa cells were exposed to several concentrations of PQ (all shown to have little effect on cell viability at 24 h) to assess changes in autophagy flux, as previously described in section 3.2.2. Following PQ treatment, the number of autophagosomes significantly increased, whilst autolysosomes decreased compared to control cells (**Figure 7.3**). Similarly to Mn, these results are indicative of autophagy dysfunction. As all PQ concentrations caused a statistically significant blockade in autophagy flux, 50 μM PQ was chosen as the preferred concentration for future experiments.

Given the effects of PQ on autophagy flux and the previous results obtained with Mn, I evaluated whether Drp1 inhibition could restore autophagy flux blocked caused by PQ in HeLa cells. Knockdown of Drp1 (via siRNA) attenuated autophagy impairment by reducing the number of autophagosomes and increasing the number of autolysosomes to a level that was no longer statistically different to control cells (**Figure 7.4**).

In addition, as previous studies described and up-regulation and aggregation of α-synuclein in mice exposed to PQ (Manning-Bog et al., 2002b), I assessed whether inhibiting Drp1 could reduce α-synuclein aggregation promoted by the pesticide in inducible N27 cells overexpressing WT human α-synuclein (**Figure 7.5**). 48 h induction by PonA alone produced a significant increase in the number of proteinase K-positive puncta in comparison to control cells. Treatment of cells with 50 μM PQ for 48 h (during PonA induction) promoted a further increase in the number of α-synuclein aggregates per cell. As for Mn (**Figure 3.11**), inhibition of Drp1, via siRNA, completely rescued α-synuclein aggregation in cells expressing α-synuclein alone or combined with PQ.

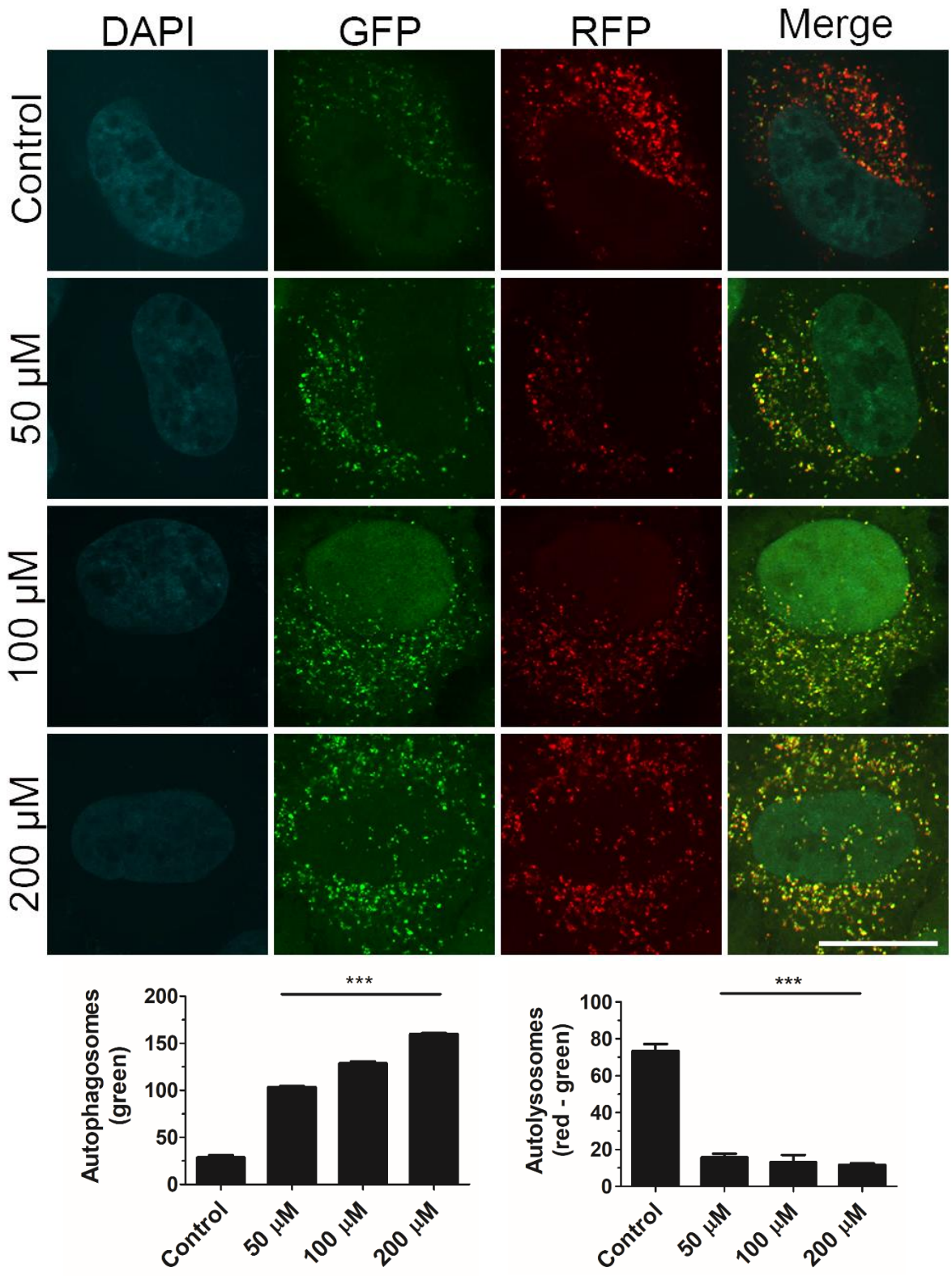

Figure 7.3 PQ inhibits autophagy flux in HeLa cells. mRFP-GFP-LC3 stably expressing HeLa cells were treated with PQ at different concentrations (50 – 200 µM) for 24 h. The numbers of autophagosomes (green vesicles) and autolysosomes (red vesicles minus green vesicles) per cell were quantified in at least 30 cells per condition, for triplicate experiments. Data are shown as mean ± SEM (n=3 independent experiments). One Way Anova with Tukey's post-hoc analysis ***: $P < 0.001$ compared to control cells. Scale bar 20 µm.

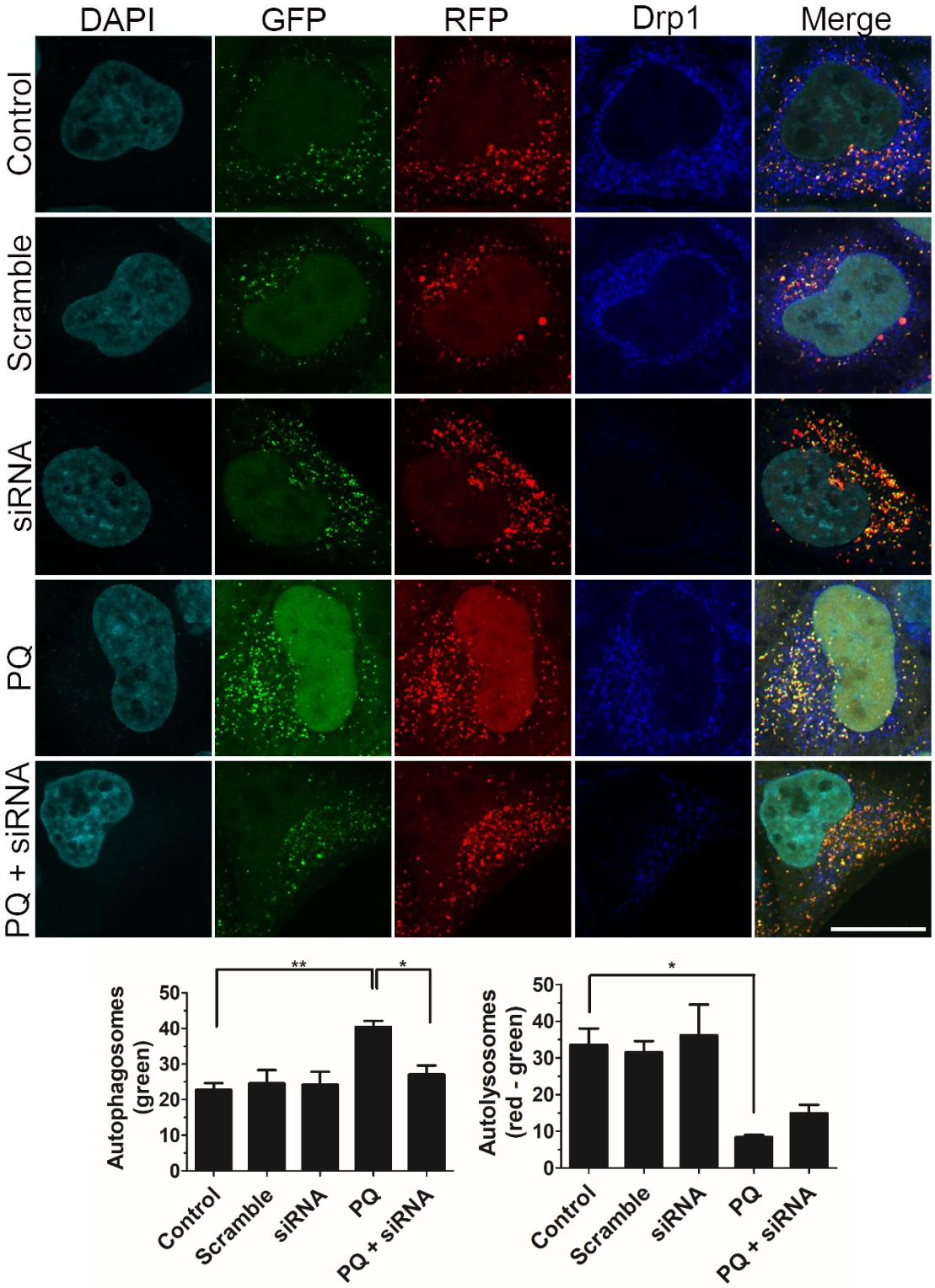

Figure 7.4 Drp1 inhibition attenuates autophagy blockade induced by PQ treatment in HeLa cells. HeLa mRFP-GFP-LC3 expressing cells were transfected with 10 nM human Drp1 siRNA (blue channel) or scramble. 24 h post-transfection cells were treated with PQ (50 μM). The numbers of autophagosomes (green puncta) and autolysosomes (red minus green puncta) was quantified in at least 30 cells per condition, for triplicate experiments. Data are shown as mean ± SEM (n=3 independent experiments). One Way Anova with Tukey's post-hoc analysis **: $P < 0.05$; **: $P < 0.01$. Scale bar 20 μm.

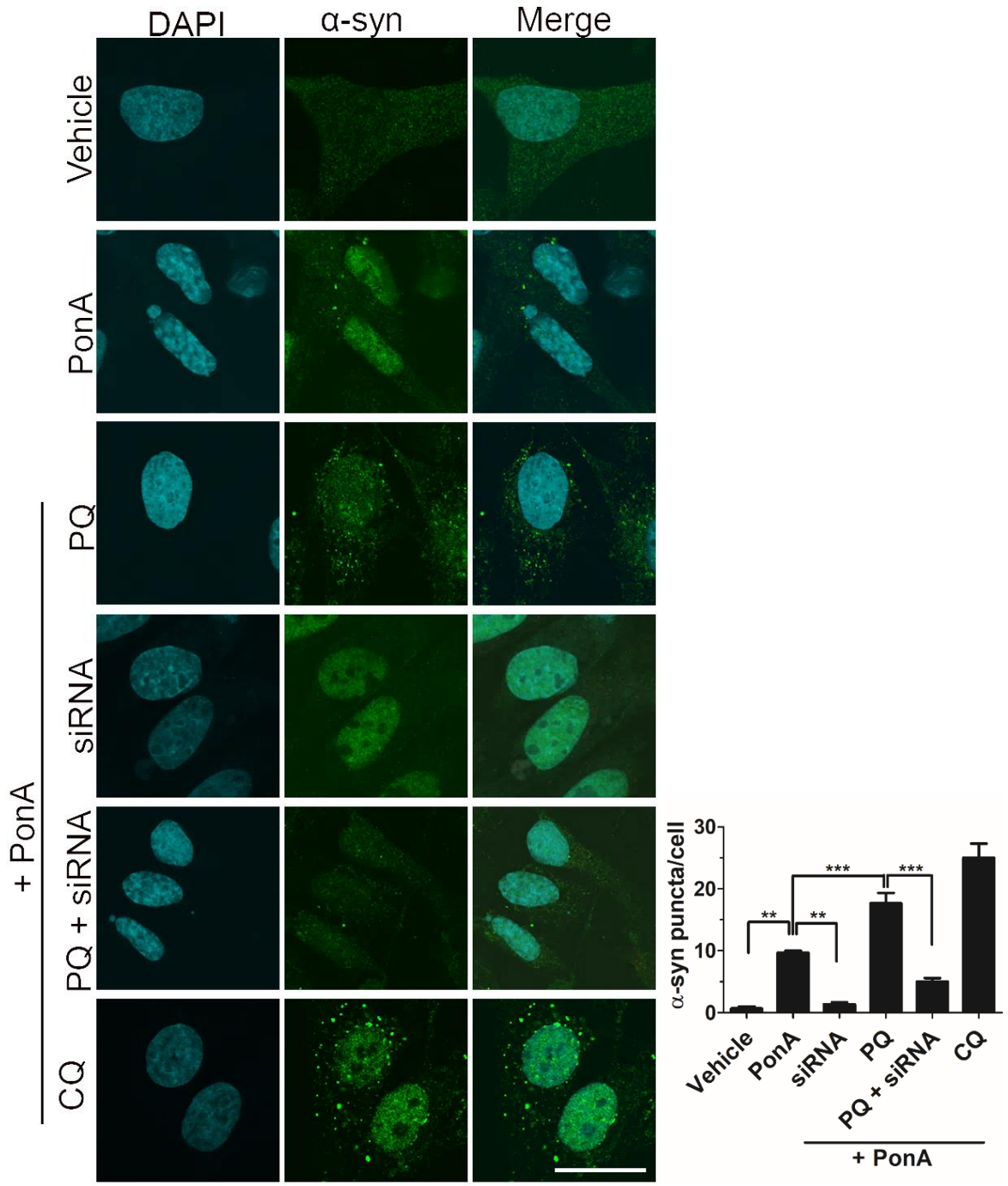

Figure 7.5 PQ induces α-synuclein aggregation, improved by inhibition of Drp1 in N27 cells. N27 cells were transfected with rat Drp1 siRNA (10 nM). 24 h post-transfection α-synuclein overexpression was induced (20 μM PonA) in combination with PQ (50 μM) or CQ (10 μM) for 48 h. Post fixation, cells were incubated with either PBS (data not shown) or Proteinase K and then processed for ICC using an antibody (Millipore, AB5038) particularly effective at identifying higher order structures of the protein. Images show insoluble α-synuclein aggregates. ImageJ was used to quantify the α-synuclein-positive puncta. Data are shown as mean ± SEM (n=3 independent experiments). One Way Anova with Tukey's post-hoc analysis **: $P < 0.01$; ***: $P < 0.001$. Scale bar 20 μm.

As previously discussed in section 3.2.5, PQ was used as a positive control to induce mitochondrial dysfunction when assessing the effects of Mn on mitochondria, however the data was not shown. PQ caused a significant reduction in mitochondrial respiratory capacity compared to untreated cells (**Figure 7.6**). These results indicate that PQ exposure reduces the cell's ability to respond to energetic demand, therefore promoting mitochondrial dysfunction.

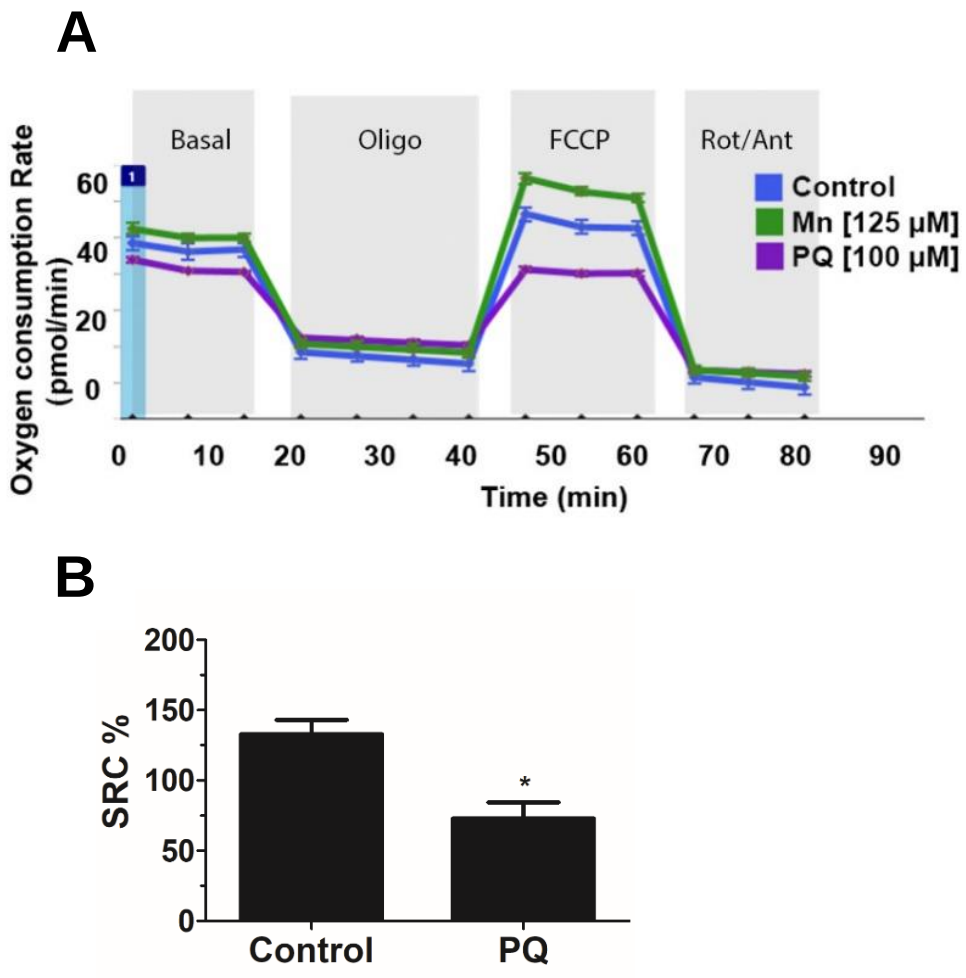

Figure 7.6 Effects of PQ treatment on mitochondrial respiration. (**A**) Representative example of kinetic OCR response of N27 and M17 cells to Mn and PQ treatment. M17 and N27 cells were plated in XF^{e}96 tissue culture plate and treated with $MnCl_2$ (125 µM) and PQ (100 µM) for 24 h. Mitochondrial respiration was assessed by measuring OCR using the XFe96 Extracellular Flux Analyzer. Sequential injections of oligomycin (to inhibit oxygen consumption mediated by ATP synthase), FCCP (an uncoupler to induce maximal OCR), Rotenone/Antimycin (to inhibit complex I and III, respectively). (**B**) Effects of PQ on Spare Respiratory Capacity (SRC). Data are shown as mean ± SEM (n=3/4 independent experiments). Unpaired two-tailed Student's *t* test *: $P < 0.05$ when comparing control to PQ-exposed cells. The seahorse assay was performed and analysed by Dr Rebecca Z Fan.

Overall these results indicate that PQ blocks autophagy flux, impairs mitochondrial function and promotes α-synuclein aggregation *in vitro*. Inhibition of Drp1 ameliorated autophagic impairment and α-synuclein aggregation induced by PQ.

Although results from this supplementary chapter suggest that PQ is having an impact on both mitochondrial function and autophagy flux, in comparison to Mn, the concentrations used for the seahorse assay were higher (100 µM) than the lowest dose (50 µM) used in the autophagy flux assay. Whilst my results show that 100 µM PQ does indeed block autophagy flux and also induce mitochondrial dysfunction, this cannot be said for the lowest concentration of PQ used in this study. In fact, it is possible that 50 µM PQ is altering autophagy flux without affecting mitochondrial function (as for Mn) and therefore more studies are needed to address this issue.

Despite this, the effects of Drp1 inhibition on the autophagy pathway and protein aggregation are in line with the results obtained in Chapter 3 and confirm the possibility for a new regulatory role for Drp1 in the autophagy pathway.

7.2.2 Evaluation of astrocyte and microglia activation in the SNpc of *SLC39A14*$^{-/-}$ mice

Moreno et al. (2009) have previously established that Mn exposure can induce neuroinflammation in glial cells. Astrocytes and microglia are essential within the CNS and can adopt, in response to foreign or endogenous signals, an activated phenotype which leads to the release of pro-inflammatory mediators. In particular, glial cells represent an important target of Mn in the brain, as they are involved in sequestering the metal and activating inflammatory signalling pathways harmful for neurons through overproduction of ROS, NOS and inflammatory cytokines (Zhao et al., 2009, Verina et al., 2011, Tjalkens et al., 2017).

Aschner et al. (1992) showed that Mn preferentially accumulates in astrocytes given their expression of high-capacity transporters and that Mn concentrations in astrocytes can be 50-folds greater compared to neurons. Additionally, given their key role in maintenance of cellular homeostasis, astrocytes regulate extracellular glutamate levels that can be disrupted by Mn and cause an inflammatory response (Tjalkens et al., 2017).

The main focus of this chapter was to investigate the effects of chronic accumulation of Mn in *SLC39A14*$^{-/-}$ mice in the SNpc. As astrocytes can be morphologically characterised by the expression of the intermediate filament proteins glial fibrillary acidic protein (GFAP), immunostaining against GFAP in the SNpc was used to label astrocytes and assess any changes between WT and KO mice. The total area of stained astrocytes appeared increased in KO mice (10.54 ± 0.68) compared to WT (5.89 ± 0.31) (**Figure 7.7 A-B**), suggesting that chronic Mn accumulation induces inflammatory response in astrocytes. In contrast to WT, KO mice displayed a moderate/severe reactive astrogliosis in which most astrocytes display cellular

hypertrophy with some overlap of astrocyte processes, which may result in potential disruption of individual astrocyte domains.

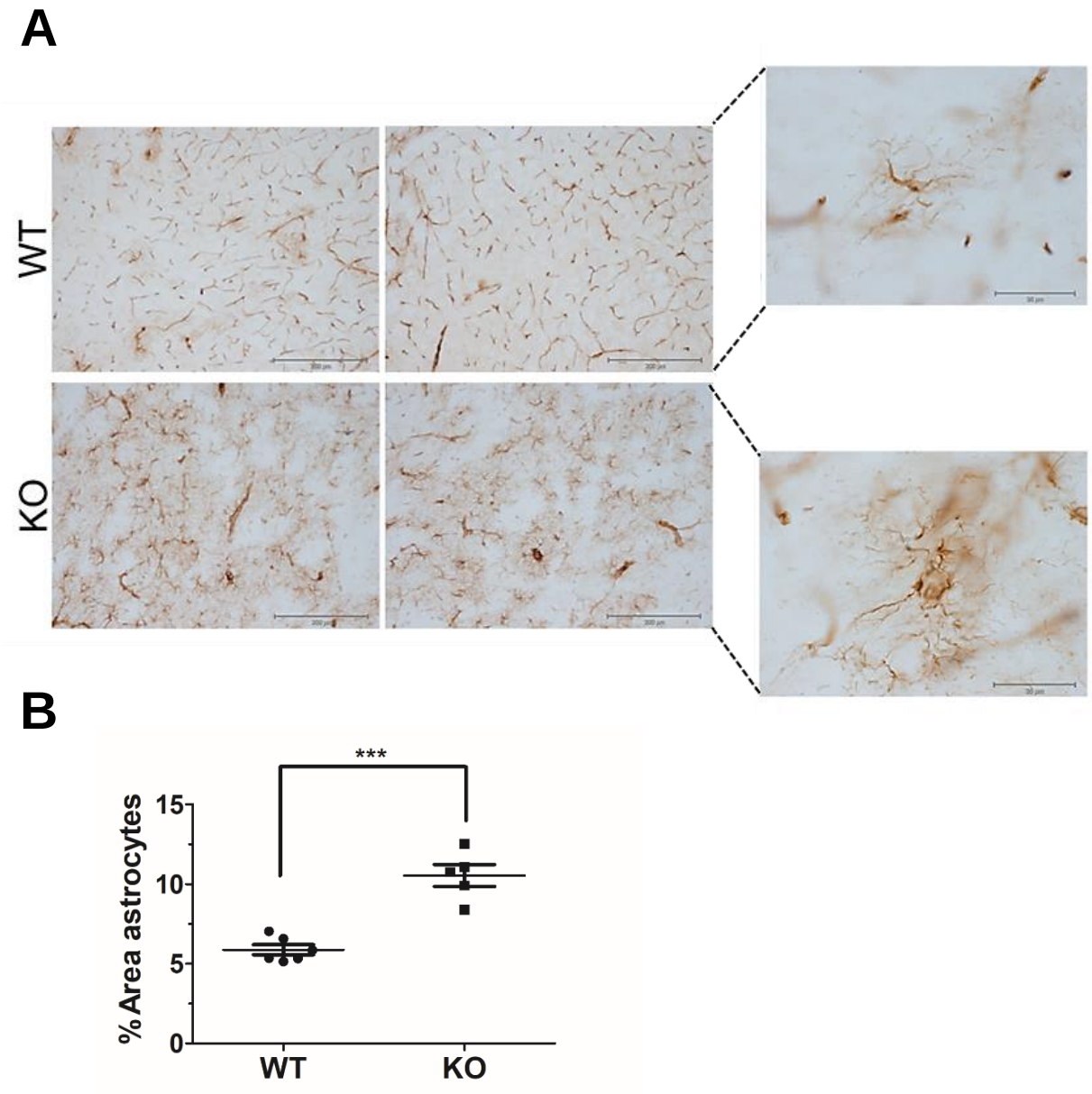

Figure 7.7 *SLC39A14*$^{-/-}$ mice display activated astrocytes in the SNpc. Nigral sections (30 µm) were immunostained with GFAP to assess changes in astrocytic morphology in (**A**) WT and KO mice. The representative images are 20X and 100X zoom, respectively. (**B**) Quantification of % area of GFAP positive staining in WT and KO mice. Data represent mean ± SEM (WT n=6; KO n=5 animals per group). Unpaired two-tailed Student's *t* test. *** P<0.001 compared to the WT group.

In the current study, Iba1 was used as a microglia marker to investigate microglial activation in cells lacking SLC39A14. In both WT and KO animals, Iba1-positive cells were evenly distributed throughout the SNpc (**Figure 7.8 A**).

Cells appeared small with fine ramified processes typical of resting microglia. Statistical analysis revealed that the density of Iba1-positive cells was not altered in KO (10.48 ± 0.83) when compared to WT mice (9.81 ± 1.11), suggesting there was no association between microglia reactivity and the level of Mn in KO mice (**Figure 7.8 B**). Sholl analysis (assessment of the morphological changes in relation to the radial distance from the soma) of microglial cells did not reveal any variations in morphological characteristics and no overall group differences were detected (**Figure 7.8 C-D**). Overall, these results indicate that *SLC39A14*$^{-/-}$ mice display a marked increase in astrocyte activation without impacting microglial morphology, at this stage of aging.

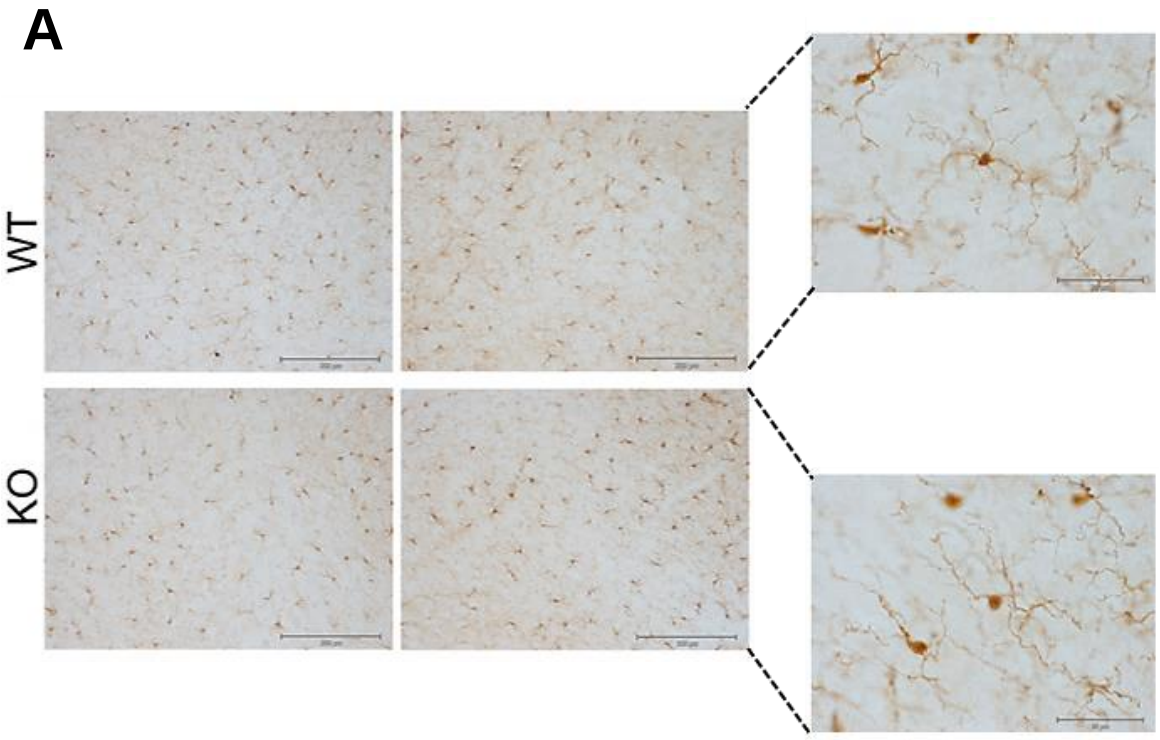

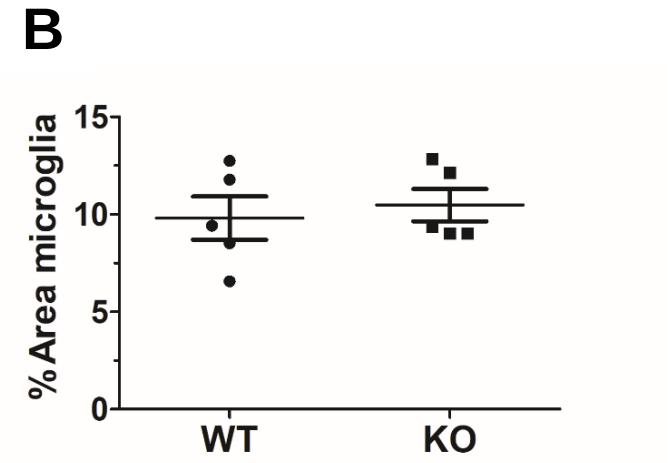

Figure continues on next page

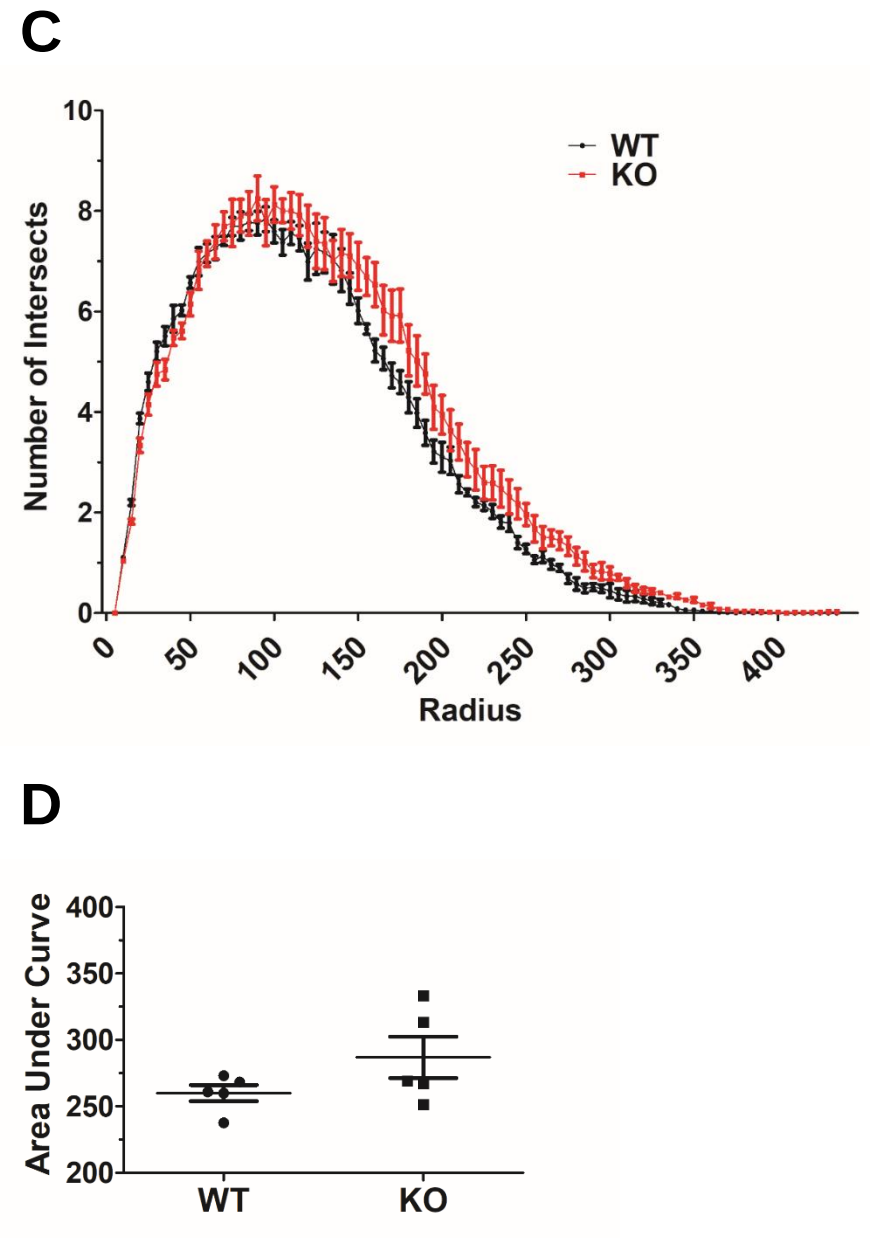

Figure 7.8 Microglial morphology is not altered in the SNpc of *SLC39A14*$^{-/-}$ mice. Nigral sections (30 µm) were immunostained with Iba1 to assess microglial morphology in (**A**) WT and KO mice. The representative images are 20X and 100X zoom, respectively. (**B**) Quantification of % area of Iba1 positive staining in WT and KO mice. Data represent mean ± SEM (WT n=5; KO n=5 animals per group). Unpaired two-tailed Student's *t* test displayed no statistical difference between WT and KO animals. (**C**) Analysis of microglial morphology using Sholl Analysis. The graph represents the average number of intersections per cell at defined radial lengths. Data represent mean ± SEM (WT n=5; KO n=5 animals per group). (**D**) The area under the curve from the Sholl analysis was also calculated for each animal. Data represent mean ± SEM (WT n=5; KO n=5 animals per group). Unpaired two-tailed Student's *t* test displayed no statistical difference between WT and KO mice.

Increasing evidence have associated Mn exposure to neuroinflammation, including both microglia and astrocytes (Moreno et al., 2009, Verina et al., 2011, Krishna et al., 2014, Wang et al., 2017, Chen et al., 2018a, Langley et al., 2018). When assessing changes in astrocytic morphology, results displayed astroglial activation in the SN of KO mice compared to WT, evidenced by an increased total astrocytic volume. Although the regions in which astrocyte activation was observed may differ, my data agrees with prior studies (Kern et al., 2010, Peres et al., 2015, Sarkar et al., 2018), which report increased GFAP expression following Mn exposure. One of the hallmarks of Mn toxicity, in addition to the neuronal degeneration in the GP and in some cases the SN, is the mild-to-moderate proliferation of astrocytes (Yamada et al., 1986). Astrocytes have been suggested to be particularly susceptible to Mn neurotoxicity given the propensity of Mn to accumulate within them (Aschner et al., 1992). Within the brain, the enzyme glutamine synthetase is known to be exclusively expressed in astrocytes and to be responsible for converting glutamate to glutamine (Martinez-Hernandez et al., 1977). One of the proposed mechanisms of action of Mn accumulation in astrocytes is the impairment of glutamate/glutamine transporters (Erikson and Aschner, 2002, Sidoryk-Wegrzynowicz et al., 2009), which disrupts synaptic homeostasis and elicit neurotoxicity. Previous studies have also reported the ability of astrocytes to release inflammatory cytokines and nitric oxide (NO) during Mn exposure (Liu et al., 2006, Moreno et al., 2008, Moreno et al., 2009), indicative of an enhanced neuroinflammatory response. Results from the current study suggest that chronic Mn induces astrogliosis in conjunction with autophagy impairment in neurons and could possibly promote neuroinflammatory cytokines production. It would be interesting, in the future, to investigate changes in neuroinflammatory cytokines and autophagic alterations in astrocytes caused by chronic Mn accumulation.

The involvement of microglia-mediated inflammation in PD pathology was first described by McGeer et al. (1988) and confirmed by many others (Imamura et al., 2003, Gerhard et al., 2006,

Mount et al., 2007, Doorn et al., 2014, Grozdanov et al., 2014). Prior studies have also suggested a potential role for microglia in mediating Mn-induced neurodegeneration (Zhao et al., 2009, Verina et al., 2011). I therefore sought to investigate the chronic effects of Mn on microglial cells of the SN of *SLC39A14*$^{-/-}$ mice compared to WT. Iba1-labelled microglia displayed remarkably consistent morphologies between KO and WT in both the total % of area and morphological assessments (Sholl analysis). Progressive neuronal loss can activate and recruit microglia or *vice versa*, therefore it may not be surprising that no microglial response was observed in mice that did not display any changes in TH levels. In fact, when Zhao et al. (2009) described an increase in the number of activated microglia, up-regulation of iNOS, TNFα and IL-1β in the SNpc of rats intrastriatally injected with Mn, they also detected a clear reduction in TH-positive cells. In addition, increased levels of inflammatory cytokines were reported in mice intraperitoneally injected with 100 mg/kg $MnCl_2$ for two weeks (Chen et al., 2018a). Previous studies have shown an association between *SLC39A14*$^{-/-}$ mice and acute inflammation (Aydemir et al., 2017). This was evidenced by an upregulation of TNF-α, increase in NF-κB protein and TSPO in the brains of these deficient mice (Aydemir et al., 2017). Results from the current chapter could differ from previous reports for several reasons: 1) Differences in age of mice and exposure paradigm (slow chronic increase of Mn *vs* acute high dose). 2) The brain region assessed in the current study was the SN, whilst Aydemir et al. (2017) used whole brain. 3) I assessed changes in microglial morphology in contrast to specific cytokines activated by an inflammatory stimulus. 4) It is possible that this inflammatory response was elicited by astrocytes (due to slight and not drastic increase in inflammatory cytokines), not microglia and therefore no changes were observed in Iba1 staining performed in the current study.

Overall, these results are preliminary and warrant further study as a stereological quantification of both microglia and astrocytes is required.

7.3 Appendix C - Publication

Publication: Helley, M. P., Pinnell, J., **Sportelli, C.** and Tieu, K. 2017. Mitochondria: A Common Target for Genetic Mutations and Environmental Toxicants in Parkinson's Disease. Frontiers in genetics, 8, 177.

Parkinson’s disease (PD) is a devastating neurological movement disorder. Since its first discovery 200 years ago, genetic and environmental factors have been identified to play a role in PD development and progression. Although genetic studies have been the predominant driving force in PD research over the last few decades, currently only a small fraction of PD cases can be directly linked to monogenic mutations. The remaining cases have been attributed to other risk associated genes, environmental exposures and gene–environment interactions, making PD a multifactorial disorder with a complex aetiology. However, enormous efforts from global research have yielded significant insights into pathogenic mechanisms and potential therapeutic targets for PD. This review will highlight mitochondrial dysfunction as a common pathway involved in both genetic mutations and environmental toxicants linked to PD.

Please note full texts have not been included due to copyright restrictions.

8. References

ABBOTT, N. J. & FRIEDMAN, A. 2012. Overview and introduction: the blood-brain barrier in health and disease. *Epilepsia,* 53 Suppl 6**,** 1-6.

ADE, K. K., JANSSEN, M. J., ORTINSKI, P. I. & VICINI, S. 2008. Differential tonic GABA conductances in striatal medium spiny neurons. *J Neurosci,* 28**,** 1185-97.

AHMED, I., LIANG, Y., SCHOOLS, S., DAWSON, V. L., DAWSON, T. M. & SAVITT, J. M. 2012. Development and characterization of a new Parkinson's disease model resulting from impaired autophagy. *The Journal of neuroscience : the official journal of the Society for Neuroscience,* 32**,** 16503-16509.

AHN, B. H., RHIM, H., KIM, S. Y., SUNG, Y. M., LEE, M. Y., CHOI, J. Y., WOLOZIN, B., CHANG, J. S., LEE, Y. H., KWON, T. K., CHUNG, K. C., YOON, S. H., HAHN, S. J., KIM, M. S., JO, Y. H. & MIN, D. S. 2002. alpha-Synuclein interacts with phospholipase D isozymes and inhibits pervanadate-induced phospholipase D activation in human embryonic kidney-293 cells. *J Biol Chem,* 277**,** 12334-42.

AKUNDI, R. S., HUANG, Z., EASON, J., PANDYA, J. D., ZHI, L., CASS, W. A., SULLIVAN, P. G. & BUELER, H. 2011. Increased mitochondrial calcium sensitivity and abnormal expression of innate immunity genes precede dopaminergic defects in Pink1-deficient mice. *PLoS One,* 6**,** e16038.

ALAIMO, A., GOROJOD, R. M., BEAUQUIS, J., MUÑOZ, M. J., SARAVIA, F. & KOTLER, M. L. 2014. Deregulation of Mitochondria-Shaping Proteins Opa-1 and Drp-1 in Manganese-Induced Apoptosis. *PLOS ONE,* 9**,** e91848.

ALAIMO, A., GOROJOD, R. M., MIGLIETTA, E. A., VILLARREAL, A., RAMOS, A. J. & KOTLER, M. L. 2013. Manganese induces mitochondrial dynamics impairment and apoptotic cell death: a study in human Gli36 cells. *Neurosci Lett,* 554**,** 76-81.

ALI, S. F., DUHART, H. M., NEWPORT, G. D., LIPE, G. W. & SLIKKER, W. 1995. Manganese-induced reactive oxygen species: Comparison between Mn+2 and Mn+3. *Neurodegeneration,* 4**,** 329-334.

ALVAREZ-ERVITI, L., RODRIGUEZ-OROZ, M. C., COOPER, J. & ET AL. 2010. Chaperone-mediated autophagy markers in parkinson disease brains. *Archives of Neurology,* 67**,** 1464-1472.

ANDERSON, C. M. & SWANSON, R. A. 2000. Astrocyte glutamate transport: review of properties, regulation, and physiological functions. *Glia,* 32**,** 1-14.

ANDERSON, J. G., FORDAHL, S. C., COONEY, P. T., WEAVER, T. L., COLYER, C. L. & ERIKSON, K. M. 2008. Manganese exposure alters extracellular GABA, GABA receptor and transporter protein and mRNA levels in the developing rat brain. *Neurotoxicology,* 29**,** 1044-1053.

ANDERSON, J. P., WALKER, D. E., GOLDSTEIN, J. M., DE LAAT, R., BANDUCCI, K., CACCAVELLO, R. J., BARBOUR, R., HUANG, J., KLING, K., LEE, M., DIEP, L., KEIM, P. S., SHEN, X., CHATAWAY, T., SCHLOSSMACHER, M. G., SEUBERT, P., SCHENK, D., SINHA, S., GAI, W. P. & CHILCOTE, T. J. 2006. Phosphorylation of Ser-129 is the dominant pathological modification of alpha-synuclein in familial and sporadic Lewy body disease. *J Biol Chem,* 281**,** 29739-52.

ANGELI, S., BARHYDT, T., JACOBS, R., KILLILEA, D. W., LITHGOW, G. J. & ANDERSEN, J. K. 2014. Manganese disturbs metal and protein homeostasis in Caenorhabditis elegans. *Metallomics,* 6**,** 1816-23.

ANGLADE, P., VYAS, S., JAVOY-AGID, F., HERRERO, M. T., MICHEL, P. P., MARQUEZ, J., MOUATT-PRIGENT, A., RUBERG, M., HIRSCH, E. C. & AGID, Y.

1997. Apoptosis and autophagy in nigral neurons of patients with Parkinson's disease. *Histol Histopathol,* 12**,** 25-31.

ANTONY, P. M. A., DIEDERICH, N. J., KRÜGER, R. & BALLING, R. 2013. The hallmarks of Parkinson's disease. 280**,** 5981-5993.

APPEL-CRESSWELL, S., VILARINO-GUELL, C., ENCARNACION, M., SHERMAN, H., YU, I., SHAH, B., WEIR, D., THOMPSON, C., SZU-TU, C., TRINH, J., AASLY, J. O., RAJPUT, A., RAJPUT, A. H., JON STOESSL, A. & FARRER, M. J. 2013. Alpha-synuclein p.H50Q, a novel pathogenic mutation for Parkinson's disease. *Mov Disord,* 28**,** 811-3.

ARAWAKA, S., SATO, H., SASAKI, A., KOYAMA, S. & KATO, T. 2017. Mechanisms underlying extensive Ser129-phosphorylation in α-synuclein aggregates. *Acta Neuropathologica Communications,* 5**,** 48.

ARCHER, S. L. 2013. Mitochondrial Dynamics — Mitochondrial Fission and Fusion in Human Diseases. *New England Journal of Medicine,* 369**,** 2236-2251.

AROTCARENA, M. L., TEIL, M. & DEHAY, B. 2019. Autophagy in Synucleinopathy: The Overwhelmed and Defective Machinery. *Cells,* 8.

ASCHNER, J. L. & ASCHNER, M. 2005. Nutritional aspects of manganese homeostasis. *Mol Aspects Med,* 26**,** 353-62.

ASCHNER, M. & GANNON, M. 1994. Manganese (Mn) transport across the rat blood-brain barrier: saturable and transferrin-dependent transport mechanisms. *Brain Res Bull,* 33**,** 345-9.

ASCHNER, M., GANNON, M. & KIMELBERG, H. K. 1992. Manganese uptake and efflux in cultured rat astrocytes. *J Neurochem,* 58**,** 730-5.

AU, C., BENEDETTO, A., ANDERSON, J., LABROUSSE, A., ERIKSON, K., EWBANK, J. J. & ASCHNER, M. 2009. SMF-1, SMF-2 and SMF-3 DMT1 orthologues regulate and are regulated differentially by manganese levels in C. elegans. *PLoS One,* 4**,** e7792.

AYDEMIR, T. B., CHANG, S.-M., GUTHRIE, G. J., MAKI, A. B., RYU, M.-S., KARABIYIK, A. & COUSINS, R. J. 2012. Zinc transporter ZIP14 functions in hepatic zinc, iron and glucose homeostasis during the innate immune response (endotoxemia). *PloS one,* 7**,** e48679-e48679.

AYDEMIR, T. B., KIM, M. H., KIM, J., COLON-PEREZ, L. M., BANAN, G., MARECI, T. H., FEBO, M. & COUSINS, R. J. 2017. Metal Transporter Zip14 (Slc39a14) Deletion in Mice Increases Manganese Deposition and Produces Neurotoxic Signatures and Diminished Motor Activity. *J Neurosci,* 37**,** 5996-6006.

AYDEMIR, T. B., TROCHE, C., KIM, M. H. & COUSINS, R. J. 2016. Hepatic ZIP14-mediated Zinc Transport Contributes to Endosomal Insulin Receptor Trafficking and Glucose Metabolism. *J Biol Chem,* 291**,** 23939-23951.

BAE, E.-J., YANG, N. Y., LEE, C., LEE, H.-J., KIM, S., SARDI, S. P. & LEE, S.-J. 2015. Loss of glucocerebrosidase 1 activity causes lysosomal dysfunction and α-synuclein aggregation. *Experimental & molecular medicine,* 47**,** e153-e153.

BAE, E. J., YANG, N. Y., SONG, M., LEE, C. S., LEE, J. S., JUNG, B. C., LEE, H. J., KIM, S., MASLIAH, E., SARDI, S. P. & LEE, S. J. 2014. Glucocerebrosidase depletion enhances cell-to-cell transmission of α-synuclein. *Nat Commun,* 5**,** 4755.

BALOH, R. H., SCHMIDT, R. E., PESTRONK, A. & MILBRANDT, J. 2007. Altered Axonal Mitochondrial Transport in the Pathogenesis of Charcot-Marie-Tooth Disease from Mitofusin 2 Mutations. *The Journal of Neuroscience,* 27**,** 422.

BALTAZAR, G. C., GUHA, S., LU, W., LIM, J., BOESZE-BATTAGLIA, K., LATIES, A. M., TYAGI, P., KOMPELLA, U. B. & MITCHELL, C. H. 2012. Acidic nanoparticles are trafficked to lysosomes and restore an acidic lysosomal pH and degradative function to compromised ARPE-19 cells. *PLoS One,* 7**,** e49635.

BANERJEE, K., SINHA, M., PHAM CLE, L., JANA, S., CHANDA, D., CAPPAI, R. & CHAKRABARTI, S. 2010. Alpha-synuclein induced membrane depolarization and loss of phosphorylation capacity of isolated rat brain mitochondria: implications in Parkinson's disease. *FEBS Lett,* 584**,** 1571-6.

BAPTISTA, M. J., O'FARRELL, C., DAYA, S., AHMAD, R., MILLER, D. W., HARDY, J., FARRER, M. J. & COOKSON, M. R. 2003. Co-ordinate transcriptional regulation of dopamine synthesis genes by alpha-synuclein in human neuroblastoma cell lines. *J Neurochem,* 85**,** 957-68.

BARBEAU, A. 1984. Manganese and extrapyramidal disorders (a critical review and tribute to Dr. George C. Cotzias). *Neurotoxicology,* 5**,** 13-35.

BARHOUMI, R., FASKE, J., LIU, X. & TJALKENS, R. B. 2004. Manganese potentiates lipopolysaccharide-induced expression of NOS2 in C6 glioma cells through mitochondrial-dependent activation of nuclear factor kappaB. *Brain Res Mol Brain Res,* 122**,** 167-79.

BARSOUM, M. J., YUAN, H., GERENCSER, A. A., LIOT, G., KUSHNAREVA, Y., GRÄBER, S., KOVACS, I., LEE, W. D., WAGGONER, J., CUI, J., WHITE, A. D., BOSSY, B., MARTINOU, J.-C., YOULE, R. J., LIPTON, S. A., ELLISMAN, M. H., PERKINS, G. A. & BOSSY-WETZEL, E. 2006a. Nitric oxide-induced mitochondrial fission is regulated by dynamin-related GTPases in neurons. *The EMBO Journal,* 25**,** 3900-3911.

BARSOUM, M. J., YUAN, H., GERENCSER, A. A., LIOT, G., KUSHNAREVA, Y., GRÄBER, S., KOVACS, I., LEE, W. D., WAGGONER, J., CUI, J., WHITE, A. D., BOSSY, B., MARTINOU, J. C., YOULE, R. J., LIPTON, S. A., ELLISMAN, M. H., PERKINS, G. A. & BOSSY-WETZEL, E. 2006b. Nitric oxide-induced mitochondrial fission is regulated by dynamin-related GTPases in neurons. *EMBO J,* 25**,** 3900-11.

BARTELS, T., CHOI, J. G. & SELKOE, D. J. 2011. α-Synuclein occurs physiologically as a helically folded tetramer that resists aggregation. *Nature,* 477**,** 107-110.

BATES, C. A., FU, S., YSSELSTEIN, D., ROCHET, J. C. & ZHENG, W. 2015. Expression and Transport of alpha-Synuclein at the Blood-Cerebrospinal Fluid Barrier and Effects of Manganese Exposure. *Admet dmpk,* 3**,** 15-33.

BAUMURATOV, A. S., ANTONY, P. M., OSTASZEWSKI, M., HE, F., SALAMANCA, L., ANTUNES, L., WEBER, J., LONGHINO, L., DERKINDEREN, P., KOOPMAN, W. J. & DIEDERICH, N. J. 2016. Enteric neurons from Parkinson's disease patients display ex vivo aberrations in mitochondrial structure. *Sci Rep,* 6**,** 33117.

BENDER, A., DESPLATS, P., SPENCER, B., ROCKENSTEIN, E., ADAME, A., ELSTNER, M., LAUB, C., MUELLER, S., KOOB, A. O., MANTE, M., PHAM, E., KLOPSTOCK, T. & MASLIAH, E. 2013. TOM40 mediates mitochondrial dysfunction induced by α-synuclein accumulation in Parkinson's disease. *PLoS One,* 8**,** e62277.

BENDER, A., KRISHNAN, K. J., MORRIS, C. M., TAYLOR, G. A., REEVE, A. K., PERRY, R. H., JAROS, E., HERSHESON, J. S., BETTS, J., KLOPSTOCK, T., TAYLOR, R. W. & TURNBULL, D. M. 2006. High levels of mitochondrial DNA deletions in substantia nigra neurons in aging and Parkinson disease. *Nat Genet,* 38**,** 515-7.

BENNETT, M. C., BISHOP, J. F., LENG, Y., CHOCK, P. B., CHASE, T. N. & MOURADIAN, M. M. 1999. Degradation of alpha-synuclein by proteasome. *J Biol Chem,* 274**,** 33855-8.

BENTO, C. F., ASHKENAZI, A., JIMENEZ-SANCHEZ, M. & RUBINSZTEIN, D. C. 2016. The Parkinson's disease-associated genes ATP13A2 and SYT11 regulate autophagy via a common pathway. *Nature Communications,* 7**,** 11803.

BERNHEIMER, H., BIRKMAYER, W., HORNYKIEWICZ, O., JELLINGER, K. & SEITELBERGER, F. 1973. Brain dopamine and the syndromes of Parkinson and

Huntington Clinical, morphological and neurochemical correlations. *Journal of the Neurological Sciences,* 20**,** 415-455.

BERTINET, D. B., TINIVELLA, M., BALZOLA, F. A., DE FRANCESCO, A., DAVINI, O., RIZZO, L., MASSARENTI, P., LEONARDI, M. A. & BALZOLA, F. 2000. Brain manganese deposition and blood levels in patients undergoing home parenteral nutrition. *JPEN J Parenter Enteral Nutr,* 24**,** 223-7.

BETARBET, R., SHERER, T., MACKENZIE, G., GARCIA-OSUNA, M., PANOV, A. & GREENAMYRE, J. 2000. Chronic systemic pesticide exposure reproduces features of Parkinson's disease. *Nature Neuroscience,* 3**,** 1301-1306.

BIANCHI, R., ADAMI, C., GIAMBANCO, I. & DONATO, R. 2007. S100B binding to RAGE in microglia stimulates COX-2 expression. 81**,** 108-118.

BIDO, S., SORIA, F. N., FAN, R. Z., BEZARD, E. & TIEU, K. 2017. Mitochondrial division inhibitor-1 is neuroprotective in the A53T-α-synuclein rat model of Parkinson's disease. *Sci Rep,* 7**,** 7495.

BINDOFF, L. A., BIRCH-MACHIN, M., CARTLIDGE, N. E., PARKER, W. D., JR. & TURNBULL, D. M. 1989. Mitochondrial function in Parkinson's disease. *Lancet,* 2**,** 49.

BINOLFI, A., RASIA, R. M., BERTONCINI, C. W., CEOLIN, M., ZWECKSTETTER, M., GRIESINGER, C., JOVIN, T. M. & FERNÁNDEZ, C. O. 2006. Interaction of alpha-synuclein with divalent metal ions reveals key differences: a link between structure, binding specificity and fibrillation enhancement. *J Am Chem Soc,* 128**,** 9893-901.

BJORKLUND, A. & DUNNETT, S. B. 2007. Dopamine neuron systems in the brain: an update. *Trends Neurosci,* 30**,** 194-202.

BJORKOY, G., LAMARK, T., PANKIV, S., OVERVATN, A., BRECH, A. & JOHANSEN, T. 2009. Monitoring autophagic degradation of p62/SQSTM1. *Methods Enzymol,* 452**,** 181-97.

BLAUWENDRAAT, C., NALLS, M. A. & SINGLETON, A. B. 2020. The genetic architecture of Parkinson's disease. *Lancet Neurol,* 19**,** 170-178.

BLUM-DEGEN, D., MULLER, T., KUHN, W., GERLACH, M., PRZUNTEK, H. & RIEDERER, P. 1995. Interleukin-1 beta and interleukin-6 are elevated in the cerebrospinal fluid of Alzheimer's and de novo Parkinson's disease patients. *Neurosci Lett,* 202**,** 17-20.

BOLAND, B., KUMAR, A., LEE, S., PLATT, F. M., WEGIEL, J., YU, W. H. & NIXON, R. A. 2008. Autophagy induction and autophagosome clearance in neurons: relationship to autophagic pathology in Alzheimer's disease. *The Journal of neuroscience : the official journal of the Society for Neuroscience,* 28**,** 6926-6937.

BORDT, E. A., CLERC, P., ROELOFS, B. A., SALADINO, A. J., TRETTER, L., ADAM-VIZI, V., CHEROK, E., KHALIL, A., YADAVA, N., GE, S. X., FRANCIS, T. C., KENNEDY, N. W., PICTON, L. K., KUMAR, T., UPPULURI, S., MILLER, A. M., ITOH, K., KARBOWSKI, M., SESAKI, H., HILL, R. B. & POLSTER, B. M. 2017. The Putative Drp1 Inhibitor mdivi-1 Is a Reversible Mitochondrial Complex I Inhibitor that Modulates Reactive Oxygen Species. *Dev Cell,* 40**,** 583-594.e6.

BORGSTAHL, G. E., PARGE, H. E., HICKEY, M. J., BEYER, W. F., HALLEWELL, R. A. & TAINER, J. A. 1992. The structure of human mitochondrial manganese superoxide dismutase reveals a novel tetrameric interface of two 4-helix bundles. *Cell,* 71**,** 107-18.

BORNHORST, J., CHAKRABORTY, S., MEYER, S., LOHREN, H., BRINKHAUS, S. G., KNIGHT, A. L., CALDWELL, K. A., CALDWELL, G. A., KARST, U., SCHWERDTLE, T., BOWMAN, A. & ASCHNER, M. 2014. The effects of pdr1, djr1.1 and pink1 loss in manganese-induced toxicity and the role of alpha-synuclein in C. elegans. *Metallomics,* 6**,** 476-90.

BORNHORST, J., WEHE, C. A., HÜWEL, S., KARST, U., GALLA, H.-J. & SCHWERDTLE, T. 2012. Impact of manganese on and transfer across blood-brain and blood-cerebrospinal fluid barrier in vitro. *The Journal of biological chemistry,* 287**,** 17140-17151.

BOUABID, S., TINAKOUA, A., LAKHDAR-GHAZAL, N. & BENAZZOUZ, A. 2016. Manganese neurotoxicity: behavioral disorders associated with dysfunctions in the basal ganglia and neurochemical transmission. *J Neurochem,* 136**,** 677-691.

BOURDENX, M., DANIEL, J., GENIN, E., SORIA, F. N., BLANCHARD-DESCE, M., BEZARD, E. & DEHAY, B. 2016. Nanoparticles restore lysosomal acidification defects: Implications for Parkinson and other lysosomal-related diseases. *Autophagy,* 12**,** 472-83.

BOUSSET, L., PIERI, L., RUIZ-ARLANDIS, G., GATH, J., JENSEN, P. H., HABENSTEIN, B., MADIONA, K., OLIERIC, V., BOCKMANN, A., MEIER, B. H. & MELKI, R. 2013. Structural and functional characterization of two alpha-synuclein strains. *Nat Commun,* 4**,** 2575.

BOWLER, R. M., GOCHEVA, V., HARRIS, M., NGO, L., ABDELOUAHAB, N., WILKINSON, J., DOTY, R. L., PARK, R. & ROELS, H. A. 2011. Prospective study on neurotoxic effects in manganese-exposed bridge construction welders. *Neurotoxicology,* 32**,** 596-605.

BOYCOTT, KYM M., BEAULIEU, CHANDREE L., KERNOHAN, KRISTIN D., GEBRIL, OLA H., MHANNI, A., CHUDLEY, ALBERT E., REDL, D., QIN, W., HAMPSON, S., KÜRY, S., TETREAULT, M., PUFFENBERGER, ERIK G., SCOTT, JAMES N., BEZIEAU, S., REIS, A., UEBE, S., SCHUMACHER, J., HEGELE, ROBERT A., MCLEOD, D. R., GÁLVEZ-PERALTA, M., MAJEWSKI, J., RAMAEKERS, VINCENT T., NEBERT, DANIEL W., INNES, A. M., PARBOOSINGH, JILLIAN S. & ABOU JAMRA, R. 2015. Autosomal-Recessive Intellectual Disability with Cerebellar Atrophy Syndrome Caused by Mutation of the Manganese and Zinc Transporter Gene SLC39A8. *The American Journal of Human Genetics,* 97**,** 886-893.

BRAAK, H., DEL TREDICI, K., RÜB, U., DE VOS, R. A., JANSEN STEUR, E. N. & BRAAK, E. 2003a. Staging of brain pathology related to sporadic Parkinson's disease. *Neurobiol Aging,* 24**,** 197-211.

BRAAK, H., RÜB, U., GAI, W. P. & DEL TREDICI, K. 2003b. Idiopathic Parkinson's disease: possible routes by which vulnerable neuronal types may be subject to neuroinvasion by an unknown pathogen. *Journal of Neural Transmission,* 110**,** 517-536.

BRAAK, H., SASTRE, M. & DEL TREDICI, K. 2007. Development of alpha-synuclein immunoreactive astrocytes in the forebrain parallels stages of intraneuronal pathology in sporadic Parkinson's disease. *Acta Neuropathol,* 114**,** 231-41.

BRADY, R. O., KANFER, J. & SHAPIRO, D. 1965. THE METABOLISM OF GLUCOCEREBROSIDES. I. PURIFICATION AND PROPERTIES OF A GLUCOCEREBROSIDE-CLEAVING ENZYME FROM SPLEEN TISSUE. *J Biol Chem,* 240**,** 39-43.

BRAIDY, N., GAI, W. P., XU, Y. H., SACHDEV, P., GUILLEMIN, G. J., JIANG, X. M., BALLARD, J. W., HORAN, M. P., FANG, Z. M., CHONG, B. H. & CHAN, D. K. 2014. Alpha-synuclein transmission and mitochondrial toxicity in primary human foetal enteric neurons in vitro. *Neurotox Res,* 25**,** 170-82.

BRECKENRIDGE, C. B., STURGESS, N. C., BUTT, M., WOLF, J. C., ZADORY, D., BECK, M., MATHEWS, J. M., TISDEL, M. O., MINNEMA, D., TRAVIS, K. Z., COOK, A. R., BOTHAM, P. A. & SMITH, L. L. 2013. Pharmacokinetic, neurochemical, stereological and neuropathological studies on the potential effects of paraquat in the

substantia nigra pars compacta and striatum of male C57BL/6J mice. *NeuroToxicology,* 37**,** 1-14.

BROCHARD, V., COMBADIÈRE, B., PRIGENT, A., LAOUAR, Y., PERRIN, A., BERAY-BERTHAT, V., BONDUELLE, O., ALVAREZ-FISCHER, D., CALLEBERT, J., LAUNAY, J.-M., DUYCKAERTS, C., FLAVELL, R. A., HIRSCH, E. C. & HUNOT, S. 2009. Infiltration of CD4+ lymphocytes into the brain contributes to neurodegeneration in a mouse model of Parkinson disease. *The Journal of Clinical Investigation,* 119**,** 182-192.

BRODACKI, B., STASZEWSKI, J., TOCZYLOWSKA, B., KOZLOWSKA, E., DRELA, N., CHALIMONIUK, M. & STEPIEN, A. 2008. Serum interleukin (IL-2, IL-10, IL-6, IL-4), TNFalpha, and INFgamma concentrations are elevated in patients with atypical and idiopathic parkinsonism. *Neurosci Lett,* 441**,** 158-62.

BROMILOW, R. H. 2004. Paraquat and sustainable agriculture. *Pest Manag Sci,* 60**,** 340-9.

BUELL, A. K., GALVAGNION, C., GASPAR, R., SPARR, E., VENDRUSCOLO, M., KNOWLES, T. P. J., LINSE, S. & DOBSON, C. M. 2014. Solution conditions determine the relative importance of nucleation and growth processes in α-synuclein aggregation. 111**,** 7671-7676.

BUHLMAN, L., DAMIANO, M., BERTOLIN, G., FERRANDO-MIGUEL, R., LOMBÈS, A., BRICE, A. & CORTI, O. 2014. Functional interplay between Parkin and Drp1 in mitochondrial fission and clearance. *Biochim Biophys Acta,* 1843**,** 2012-26.

BURMAN, J. L., PICKLES, S., WANG, C., SEKINE, S., VARGAS, J. N. S., ZHANG, Z., YOULE, A. M., NEZICH, C. L., WU, X., HAMMER, J. A. & YOULE, R. J. 2017. Mitochondrial fission facilitates the selective mitophagy of protein aggregates. *J Cell Biol,* 216**,** 3231-3247.

BURRE, J., SHARMA, M. & SUDHOF, T. C. 2012. Systematic mutagenesis of alpha-synuclein reveals distinct sequence requirements for physiological and pathological activities. *J Neurosci,* 32**,** 15227-42.

BURRE, J., SHARMA, M., TSETSENIS, T., BUCHMAN, V., ETHERTON, M. R. & SUDHOF, T. C. 2010. Alpha-synuclein promotes SNARE-complex assembly in vivo and in vitro. *Science,* 329**,** 1663-7.

BURTE, F., DE GIROLAMO, L. A., HARGREAVES, A. J. & BILLETT, E. E. 2011. Alterations in the mitochondrial proteome of neuroblastoma cells in response to complex 1 inhibition. *J Proteome Res,* 10**,** 1974-86.

BURTON, N. C. & GUILARTE, T. R. 2009. Manganese neurotoxicity: lessons learned from longitudinal studies in nonhuman primates. *Environ Health Perspect,* 117**,** 325-32.

BUTLER, B., SAHA, K., RANA, T., BECKER, J. P., SAMBO, D., DAVARI, P., GOODWIN, J. S. & KHOSHBOUEI, H. 2015. Dopamine Transporter Activity Is Modulated by alpha-Synuclein. *J Biol Chem,* 290**,** 29542-54.

BUTTON, R. W., LIN, F., ERCOLANO, E., VINCENT, J. H., HU, B., HANEMANN, C. O. & LUO, S. 2014. Artesunate induces necrotic cell death in schwannoma cells. *Cell Death Dis,* 5**,** e1466.

BUTTON, R. W., LUO, S. & RUBINSZTEIN, D. C. 2015. Autophagic activity in neuronal cell death. *Neurosci Bull,* 31**,** 382-94.

BUTTON, R. W., ROBERTS, S. L., WILLIS, T. L., HANEMANN, C. O. & LUO, S. 2017. Accumulation of autophagosomes confers cytotoxicity. *J Biol Chem,* 292**,** 13599-13614.

CAI, T., YAO, T., ZHENG, G., CHEN, Y., DU, K., CAO, Y., SHEN, X., CHEN, J. & LUO, W. 2010. Manganese induces the overexpression of alpha-synuclein in PC12 cells via ERK activation. *Brain Res,* 1359**,** 201-7.

CANNON, J. R. & GREENAMYRE, J. T. 2013. Gene-environment interactions in Parkinson's disease: specific evidence in humans and mammalian models. *Neurobiol Dis,* 57**,** 38-46.

CANNON, J. R., TAPIAS, V. M., NA, H. M., HONICK, A. S., DROLET, R. E. & GREENAMYRE, J. T. 2009. A highly reproducible rotenone model of Parkinson's disease. *Neurobiology of Disease,* 34**,** 279-290.

CARMONA, A., ZOGZAS, C. E., ROUDEAU, S., PORCARO, F., GARREVOET, J., SPIERS, K. M., SALOME, M., CLOETENS, P., MUKHOPADHYAY, S. & ORTEGA, R. 2019. SLC30A10 Mutation Involved in Parkinsonism Results in Manganese Accumulation within Nanovesicles of the Golgi Apparatus. *ACS Chem Neurosci,* 10**,** 599-609.

CARTONI, R. & MARTINOU, J. C. 2009. Role of mitofusin 2 mutations in the physiopathology of Charcot-Marie-Tooth disease type 2A. *Exp Neurol,* 218**,** 268-73.

CASAREJOS, M. J., MENENDEZ, J., SOLANO, R. M., RODRIGUEZ-NAVARRO, J. A., GARCIA DE YEBENES, J. & MENA, M. A. 2006. Susceptibility to rotenone is increased in neurons from parkin null mice and is reduced by minocycline. *J Neurochem,* 97**,** 934-46.

CASSIDY-STONE, A., CHIPUK, J. E., INGERMAN, E., SONG, C., YOO, C., KUWANA, T., KURTH, M. J., SHAW, J. T., HINSHAW, J. E., GREEN, D. R. & NUNNARI, J. 2008. Chemical inhibition of the mitochondrial division dynamin reveals its role in Bax/Bak-dependent mitochondrial outer membrane permeabilization. *Dev Cell,* 14**,** 193-204.

CAUDLE, W. M., GUILLOT, T. S., LAZO, C. R. & MILLER, G. W. 2012. Industrial toxicants and Parkinson's disease. *Neurotoxicology,* 33**,** 178-88.

CELSI, F., PIZZO, P., BRINI, M., LEO, S., FOTINO, C., PINTON, P. & RIZZUTO, R. 2009. Mitochondria, calcium and cell death: a deadly triad in neurodegeneration. *Biochim Biophys Acta,* 1787**,** 335-44.

CERRI, S., MUS, L. & BLANDINI, F. 2019. Parkinson's Disease in Women and Men: What's the Difference? *Journal of Parkinson's disease,* 9**,** 501-515.

CERSOSIMO, M. G. & KOLLER, W. C. 2006. The diagnosis of manganese-induced parkinsonism. *Neurotoxicology,* 27**,** 340-6.

CERVANTES-CERVANTES, M. P., CALDERÓN-SALINAS, J. V., ALBORES, A. & MUÑOZ-SÁNCHEZ, J. L. 2005. Copper increases the damage to DNA and proteins caused by reactive oxygen species. *Biol Trace Elem Res,* 103**,** 229-48.

CHAKRABARTY, P., ROSARIO, A., CRUZ, P., SIEMIENSKI, Z., CEBALLOS-DIAZ, C., CROSBY, K., JANSEN, K., BORCHELT, D. R., KIM, J. Y., JANKOWSKY, J. L., GOLDE, T. E. & LEVITES, Y. 2013. Capsid serotype and timing of injection determines AAV transduction in the neonatal mice brain. *PLoS One,* 8**,** e67680.

CHANG, C.-R., MANLANDRO, C. M., ARNOULT, D., STADLER, J., POSEY, A. E., HILL, R. B. & BLACKSTONE, C. 2010. A lethal de novo mutation in the middle domain of the dynamin-related GTPase Drp1 impairs higher order assembly and mitochondrial division. *The Journal of biological chemistry,* 285**,** 32494-32503.

CHEN, H. & CHAN, D. C. 2010. Physiological functions of mitochondrial fusion. *Ann N Y Acad Sci,* 1201**,** 21-5.

CHEN, H., CHOMYN, A. & CHAN, D. C. 2005. Disruption of fusion results in mitochondrial heterogeneity and dysfunction. *J Biol Chem,* 280**,** 26185-92.

CHEN, H., DETMER, S. A., EWALD, A. J., GRIFFIN, E. E., FRASER, S. E. & CHAN, D. C. 2003. Mitofusins Mfn1 and Mfn2 coordinately regulate mitochondrial fusion and are essential for embryonic development. *The Journal of Cell Biology,* 160**,** 189.

CHEN, H., MCCAFFERY, J. M. & CHAN, D. C. 2007a. Mitochondrial Fusion Protects against Neurodegeneration in the Cerebellum. *Cell,* 130**,** 548-562.
CHEN, H., VERMULST, M., WANG, Y. E., CHOMYN, A., PROLLA, T. A., MCCAFFERY, J. M. & CHAN, D. C. 2010. Mitochondrial Fusion Is Required for mtDNA Stability in Skeletal Muscle and Tolerance of mtDNA Mutations. *Cell,* 141**,** 280-289.
CHEN, J.-Y., TSAO, G. C., ZHAO, Q. & ZHENG, W. 2001. Differential Cytotoxicity of Mn(II) and Mn(III): Special Reference to Mitochondrial [Fe-S] Containing Enzymes. *Toxicology and Applied Pharmacology,* 175**,** 160-168.
CHEN, J., SU, P., LUO, W. & CHEN, J. 2018a. Role of LRRK2 in manganese-induced neuroinflammation and microglial autophagy. *Biochem Biophys Res Commun,* 498**,** 171-177.
CHEN, L. & FEANY, M. B. 2005. α-Synuclein phosphorylation controls neurotoxicity and inclusion formation in a Drosophila model of Parkinson disease. *Nature Neuroscience,* 8**,** 657.
CHEN, L., JIN, J., DAVIS, J., ZHOU, Y., WANG, Y., LIU, J., LOCKHART, P. J. & ZHANG, J. 2007b. Oligomeric alpha-synuclein inhibits tubulin polymerization. *Biochem Biophys Res Commun,* 356**,** 548-53.
CHEN, L., XIE, Z., TURKSON, S. & ZHUANG, X. 2015a. A53T human alpha-synuclein overexpression in transgenic mice induces pervasive mitochondria macroautophagy defects preceding dopamine neuron degeneration. *J Neurosci,* 35**,** 890-905.
CHEN, P., BORNHORST, J. & ASCHNER, M. 2018b. Manganese metabolism in humans. *Front Biosci (Landmark Ed),* 23**,** 1655-1679.
CHEN, P., MIAH, M. R. & ASCHNER, M. 2016. Metals and Neurodegeneration. *F1000Res,* 5.
CHEN, R. H., WISLET-GENDEBIEN, S., SAMUEL, F., VISANJI, N. P., ZHANG, G., MARSILIO, D., LANGMAN, T., FRASER, P. E. & TANDON, A. 2013. alpha-Synuclein membrane association is regulated by the Rab3a recycling machinery and presynaptic activity. *J Biol Chem,* 288**,** 7438-49.
CHEN, S. W., DRAKULIC, S., DEAS, E., OUBERAI, M., APRILE, F. A., ARRANZ, R., NESS, S., ROODVELDT, C., GUILLIAMS, T., DE-GENST, E. J., KLENERMAN, D., WOOD, N. W., KNOWLES, T. P., ALFONSO, C., RIVAS, G., ABRAMOV, A. Y., VALPUESTA, J. M., DOBSON, C. M. & CREMADES, N. 2015b. Structural characterization of toxic oligomers that are kinetically trapped during alpha-synuclein fibril formation. *Proc Natl Acad Sci U S A,* 112**,** E1994-2003.
CHEN, Y., MCMILLAN-WARD, E., KONG, J., ISRAELS, S. J. & GIBSON, S. B. 2007c. Mitochondrial electron-transport-chain inhibitors of complexes I and II induce autophagic cell death mediated by reactive oxygen species. 120**,** 4155-4166.
CHESI, A., KILARU, A., FANG, X., COOPER, A. A. & GITLER, A. D. 2012. The Role of the Parkinson's Disease Gene PARK9 in Essential Cellular Pathways and the Manganese Homeostasis Network in Yeast. *PLOS ONE,* 7**,** e34178.
CHIANG, H. L., TERLECKY, S. R., PLANT, C. P. & DICE, J. F. 1989. A role for a 70-kilodalton heat shock protein in lysosomal degradation of intracellular proteins. *Science,* 246**,** 382-5.
CHICCO, A. J. & SPARAGNA, G. C. 2007. Role of cardiolipin alterations in mitochondrial dysfunction and disease. *Am J Physiol Cell Physiol,* 292**,** C33-44.
CHINTA, S. J., MALLAJOSYULA, J. K., RANE, A. & ANDERSEN, J. K. 2010. Mitochondrial α-synuclein accumulation impairs complex I function in dopaminergic neurons and results in increased mitophagy in vivo. *Neurosci Lett,* 486**,** 235-9.

CHOI, W.-S., PALMITER, R. D. & XIA, Z. 2011. Loss of mitochondrial complex I activity potentiates dopamine neuron death induced by microtubule dysfunction in a Parkinson's disease model. *The Journal of Cell Biology,* 1992**,** 873-882.

CHUNG, K. K., ZHANG, Y., LIM, K. L., TANAKA, Y., HUANG, H., GAO, J., ROSS, C. A., DAWSON, V. L. & DAWSON, T. M. 2001. Parkin ubiquitinates the alpha-synuclein-interacting protein, synphilin-1: implications for Lewy-body formation in Parkinson disease. *Nat Med,* 7**,** 1144-50.

CLAUS HENN, B., KIM, J., WESSLING-RESNICK, M., TÉLLEZ-ROJO, M. M., JAYAWARDENE, I., ETTINGER, A. S., HERNÁNDEZ-AVILA, M., SCHWARTZ, J., CHRISTIANI, D. C., HU, H. & WRIGHT, R. O. 2011. Associations of iron metabolism genes with blood manganese levels: a population-based study with validation data from animal models. *Environ Health,* 10**,** 97.

COCHEME, H. M. & MURPHY, M. P. 2008. Complex I is the major site of mitochondrial superoxide production by paraquat. *J Biol Chem,* 283**,** 1786-98.

COCHEMÉ, H. M. & MURPHY, M. P. 2008. Complex I is the major site of mitochondrial superoxide production by paraquat. *J Biol Chem,* 283**,** 1786-98.

CONWAY, K. A., HARPER, J. D. & LANSBURY, P. T. 1998. Accelerated in vitro fibril formation by a mutant α-synuclein linked to early-onset Parkinson disease. *Nature Medicine,* 4**,** 1318.

CONWAY, K. A., LEE, S. J., ROCHET, J. C., DING, T. T., WILLIAMSON, R. E. & LANSBURY, P. T., JR. 2000. Acceleration of oligomerization, not fibrillization, is a shared property of both alpha-synuclein mutations linked to early-onset Parkinson's disease: implications for pathogenesis and therapy. *Proceedings of the National Academy of Sciences of the United States of America,* 97**,** 571-576.

COOK, D. G., FAHN, S. & BRAIT, K. A. 1974. Chronic Manganese Intoxication. *JAMA Neurology,* 30**,** 59-64.

COON, S., STARK, A., PETERSON, E., GLOI, A., KORTSHA, G., POUNDS, J., CHETTLE, D. & GORELL, J. 2006. Whole-body lifetime occupational lead exposure and risk of Parkinson's disease. *Environmental health perspectives,* 114**,** 1872-1876.

COOPER, A. A., GITLER, A. D., CASHIKAR, A., HAYNES, C. M., HILL, K. J., BHULLAR, B., LIU, K., XU, K., STRATHEARN, K. E., LIU, F., CAO, S., CALDWELL, K. A., CALDWELL, G. A., MARSISCHKY, G., KOLODNER, R. D., LABAER, J., ROCHET, J. C., BONINI, N. M. & LINDQUIST, S. 2006. Alpha-synuclein blocks ER-Golgi traffic and Rab1 rescues neuron loss in Parkinson's models. *Science,* 313**,** 324-8.

CORDOVA, F. M., AGUIAR, A. S., JR., PERES, T. V., LOPES, M. W., GONÇALVES, F. M., REMOR, A. P., LOPES, S. C., PILATI, C., LATINI, A. S., PREDIGER, R. D. S., ERIKSON, K. M., ASCHNER, M. & LEAL, R. B. 2012. In vivo manganese exposure modulates Erk, Akt and Darpp-32 in the striatum of developing rats, and impairs their motor function. *PloS one,* 7**,** e33057-e33057.

COTZIAS, G. C. & GREENOUGH, J. J. 1958. The high specificity of the manganese pathway through the body. *J Clin Invest,* 37**,** 1298-305.

COUPER, J. 1837. On the effects of black oxide of manganese which inhaled into the lungs. *British Annals of Medicine, Pharmacy, Vital Statistics, and General Science,* 1**,** 41-42.

COVY, J. P. & GIASSON, B. I. 2011. α-Synuclein, leucine-rich repeat kinase-2, and manganese in the pathogenesis of Parkinson disease. *Neurotoxicology,* 32**,** 622-9.

CREMADES, N., COHEN, S. I. A., DEAS, E., ABRAMOV, A. Y., CHEN, A. Y., ORTE, A., SANDAL, M., CLARKE, R. W., DUNNE, P., APRILE, F. A., BERTONCINI, C. W., WOOD, N. W., KNOWLES, T. P. J., DOBSON, C. M. & KLENERMAN, D. 2012. Direct observation of the interconversion of normal and toxic forms of α-synuclein. *Cell,* 149**,** 1048-1059.

CREWS, L., SPENCER, B., DESPLATS, P., PATRICK, C., PAULINO, A., ROCKENSTEIN, E., HANSEN, L., ADAME, A., GALASKO, D. & MASLIAH, E. 2010. Selective molecular alterations in the autophagy pathway in patients with Lewy body disease and in models of alpha-synucleinopathy. *PLoS One,* 5**,** e9313.

CROSSGROVE, J. & ZHENG, W. 2004. Manganese toxicity upon overexposure. *NMR Biomed,* 17**,** 544-53.

CROSSGROVE, J. S., ALLEN, D. D., BUKAVECKAS, B. L., RHINEHEIMER, S. S. & YOKEL, R. A. 2003. Manganese distribution across the blood-brain barrier. I. Evidence for carrier-mediated influx of managanese citrate as well as manganese and manganese transferrin. *Neurotoxicology,* 24**,** 3-13.

CROSSGROVE, J. S. & YOKEL, R. A. 2004. Manganese distribution across the blood-brain barrier III. The divalent metal transporter-1 is not the major mechanism mediating brain manganese uptake. *Neurotoxicology,* 25**,** 451-60.

CROSSGROVE, J. S. & YOKEL, R. A. 2005. Manganese distribution across the blood-brain barrier. IV. Evidence for brain influx through store-operated calcium channels. *Neurotoxicology,* 26**,** 297-307.

CUERVO, A. M. & DICE, J. F. 1996. A receptor for the selective uptake and degradation of proteins by lysosomes. *Science,* 273**,** 501-3.

CUERVO, A. M. & DICE, J. F. 2000a. Age-related decline in chaperone-mediated autophagy. *J Biol Chem,* 275**,** 31505-13.

CUERVO, A. M. & DICE, J. F. 2000b. Regulation of Lamp2a Levels in the Lysosomal Membrane. *Traffic,* 1**,** 570-583.

CUERVO, A. M., STEFANIS, L., FREDENBURG, R., LANSBURY, P. T. & SULZER, D. 2004. Impaired degradation of mutant alpha-synuclein by chaperone-mediated autophagy. *Science,* 305**,** 1292-5.

CUI, M., ARAS, R., CHRISTIAN, W. V., RAPPOLD, P. M., HATWAR, M., PANZA, J., JACKSON-LEWIS, V., JAVITCH, J. A., BALLATORI, N., PRZEDBORSKI, S. & TIEU, K. 2009. The organic cation transporter-3 is a pivotal modulator of neurodegeneration in the nigrostriatal dopaminergic pathway. *Proceedings of the National Academy of Sciences,* 106**,** 8043.

CUI, M., TANG, X., CHRISTIAN, W. V., YOON, Y. & TIEU, K. 2010. Perturbations in mitochondrial dynamics induced by human mutant PINK1 can be rescued by the mitochondrial division inhibitor mdivi-1. *J Biol Chem,* 285**,** 11740-52.

DA SILVA, C. J., DA ROCHA, A. J., JERONYMO, S., MENDES, M. F., MILANI, F. T., MAIA, A. C., JR., BRAGA, F. T., SENS, Y. A. & MIORIN, L. A. 2007. A preliminary study revealing a new association in patients undergoing maintenance hemodialysis: manganism symptoms and T1 hyperintense changes in the basal ganglia. *AJNR Am J Neuroradiol,* 28**,** 1474-9.

DAGDA, R. K., CHERRA, S. J., KULICH, S. M., TANDON, A., PARK, D. & CHU, C. T. 2009. Loss of PINK1 function promotes mitophagy through effects on oxidative stress and mitochondrial fission. *J Biol Chem,* 284**,** 13843-55.

DAGDA, R. K., ZHU, J., KULICH, S. M. & CHU, C. T. 2008. Mitochondrially localized ERK2 regulates mitophagy and autophagic cell stress: implications for Parkinson's disease. *Autophagy,* 4**,** 770-82.

DAMIER, P., HIRSCH, E. C., ZHANG, P., AGID, Y. & JAVOY-AGID, F. 1993. Glutathione peroxidase, glial cells and Parkinson's disease. *Neuroscience,* 52**,** 1-6.

DAUER, W. & PRZEDBORSKI, S. 2003. Parkinson's Disease: Mechanisms and Models. *Neuron,* 39**,** 889-909.

DAVIDSON, W. S., JONAS, A., CLAYTON, D. F. & GEORGE, J. M. 1998. Stabilization of alpha-synuclein secondary structure upon binding to synthetic membranes. *J Biol Chem,* 273**,** 9443-9.

DAVIDSSON, L., CEDERBLAD, A., LONNERDAL, B. & SANDSTROM, B. 1989a. Manganese retention in man: a method for estimating manganese absorption in man. *Am J Clin Nutr,* 49**,** 170-9.

DAVIDSSON, L., LONNERDAL, B., SANDSTROM, B., KUNZ, C. & KEEN, C. L. 1989b. Identification of transferrin as the major plasma carrier protein for manganese introduced orally or intravenously or after in vitro addition in the rat. *J Nutr,* 119**,** 1461-4.

DAVIES, V. J., HOLLINS, A. J., PIECHOTA, M. J., YIP, W., DAVIES, J. R., WHITE, K. E., NICOLS, P. P., BOULTON, M. E. & VOTRUBA, M. 2007. Opa1 deficiency in a mouse model of autosomal dominant optic atrophy impairs mitochondrial morphology, optic nerve structure and visual function. *Hum Mol Genet,* 16**,** 1307-18.

DAVIS, E. J., FOSTER, T. D. & THOMAS, W. E. 1994. Cellular forms and functions of brain microglia. *Brain Res Bull,* 34**,** 73-8.

DAY, B. J., PATEL, M., CALAVETTA, L., CHANG, L. Y. & STAMLER, J. S. 1999. A mechanism of paraquat toxicity involving nitric oxide synthase. *Proc Natl Acad Sci U S A,* 96**,** 12760-5.

DE BRITO, O. M. & SCORRANO, L. 2008. Mitofusin 2 tethers endoplasmic reticulum to mitochondria. *Nature,* 456**,** 605.

DE DUVE, C., DE BARSY, T., POOLE, B., TROUET, A., TULKENS, P. & VAN HOOF, F. 1974. Commentary. Lysosomotropic agents. *Biochem Pharmacol,* 23**,** 2495-531.

DECRESSAC, M., MATTSSON, B., WEIKOP, P., LUNDBLAD, M., JAKOBSSON, J. & BJORKLUND, A. 2013. TFEB-mediated autophagy rescues midbrain dopamine neurons from alpha-synuclein toxicity. *Proc Natl Acad Sci U S A,* 110**,** E1817-26.

DEHAY, B., MARTINEZ-VICENTE, M., RAMIREZ, A., PERIER, C., KLEIN, C., VILA, M. & BEZARD, E. 2012a. Lysosomal dysfunction in Parkinson disease: ATP13A2 gets into the groove. *Autophagy,* 8**,** 1389-1391.

DEHAY, B., RAMIREZ, A., MARTINEZ-VICENTE, M., PERIER, C., CANRON, M. H., DOUDNIKOFF, E., VITAL, A., VILA, M., KLEIN, C. & BEZARD, E. 2012b. Loss of P-type ATPase ATP13A2/PARK9 function induces general lysosomal deficiency and leads to Parkinson disease neurodegeneration. *Proc Natl Acad Sci U S A,* 109**,** 9611-6.

DELEERSNIJDER, A., GERARD, M., DEBYSER, Z. & BAEKELANDT, V. 2013. The remarkable conformational plasticity of alpha-synuclein: blessing or curse? *Trends Mol Med,* 19**,** 368-77.

DENG, H., DODSON, M. W., HUANG, H. & GUO, M. 2008. The Parkinson's disease genes pink1 and parkin promote mitochondrial fission and/or inhibit fusion in Drosophila. *Proc Natl Acad Sci U S A,* 105**,** 14503-8.

DESAI, B. S., MONAHAN, A. J., CARVEY, P. M. & HENDEY, B. 2007. Blood-brain barrier pathology in Alzheimer's and Parkinson's disease: implications for drug therapy. *Cell Transplant,* 16**,** 285-99.

DESAI, V. G., FEUERS, R. J., HART, R. W. & ALI, S. F. 1996. MPP(+)-induced neurotoxicity in mouse is age-dependent: evidenced by the selective inhibition of complexes of electron transport. *Brain Res,* 715**,** 1-8.

DETTMER, U., NEWMAN, A. J., SOLDNER, F., LUTH, E. S., KIM, N. C., VON SAUCKEN, V. E., SANDERSON, J. B., JAENISCH, R., BARTELS, T. & SELKOE, D. 2015. Parkinson-causing α-synuclein missense mutations shift native tetramers to

monomers as a mechanism for disease initiation. *Nature communications,* 6**,** 7314-7314.

DEVI, L., RAGHAVENDRAN, V., PRABHU, B., AVADHANI, N. & ANANDATHEERTHAVARADA, H. 2008. Mitochondrial import and accumulation of alpha-synuclein impair complex I in human dopaminergic neuronal cultures and Parkinson disease brain. *Journal of Biological Chemistry,* 283**,** 9089-9100.

DEVINE, M. J. & KITTLER, J. T. 2018. Mitochondria at the neuronal presynapse in health and disease. *Nat Rev Neurosci,* 19**,** 63-80.

DI FONZO, A., CHIEN, H. F., SOCAL, M., GIRAUDO, S., TASSORELLI, C., ILICETO, G., FABBRINI, G., MARCONI, R., FINCATI, E., ABBRUZZESE, G., MARINI, P., SQUITIERI, F., HORSTINK, M. W., MONTAGNA, P., LIBERA, A. D., STOCCHI, F., GOLDWURM, S., FERREIRA, J. J., MECO, G., MARTIGNONI, E., LOPIANO, L., JARDIM, L. B., OOSTRA, B. A., BARBOSA, E. R., BONIFATI, V. & NETWORK, I. P. G. 2007. ATP13A2 missense mutations in juvenile parkinsonism and young onset Parkinson disease. *Neurology,* 68**,** 1557-62.

DI MAIO, R., BARRETT, P. J., HOFFMAN, E. K., BARRETT, C. W., ZHARIKOV, A., BORAH, A., HU, Z., MCCOY, J., CHU, C. T., BURTON, E. A., HASTINGS, T. G. & GREENAMYRE, J. T. 2016. a-Synuclein binds to TOM20 and inhibits mitochondrial protein import in Parkinson's disease. *Science Translational Medicine,* 8.

DIAZ-VELIZ, G., MORA, S., GOMEZ, P., DOSSI, M. T., MONTIEL, J., ARRIAGADA, C., ABOITIZ, F. & SEGURA-AGUILAR, J. 2004. Behavioral effects of manganese injected in the rat substantia nigra are potentiated by dicumarol, a DT-diaphorase inhibitor. *Pharmacol Biochem Behav,* 77**,** 245-51.

DICE, J. F. 1990. Peptide sequences that target cytosolic proteins for lysosomal proteolysis. *Trends Biochem Sci,* 15**,** 305-9.

DIOGENES, M. J., DIAS, R. B., ROMBO, D. M., VICENTE MIRANDA, H., MAIOLINO, F., GUERREIRO, P., NASSTROM, T., FRANQUELIM, H. G., OLIVEIRA, L. M., CASTANHO, M. A., LANNFELT, L., BERGSTROM, J., INGELSSON, M., QUINTAS, A., SEBASTIAO, A. M., LOPES, L. V. & OUTEIRO, T. F. 2012. Extracellular alpha-synuclein oligomers modulate synaptic transmission and impair LTP via NMDA-receptor activation. *J Neurosci,* 32**,** 11750-62.

DODD, C. A., WARD, D. L. & KLEIN, B. G. 2005. Basal Ganglia accumulation and motor assessment following manganese chloride exposure in the C57BL/6 mouse. *Int J Toxicol,* 24**,** 389-97.

DONATO, R. 2001. S100: a multigenic family of calcium-modulated proteins of the EF-hand type with intracellular and extracellular functional roles. *The International Journal of Biochemistry & Cell Biology,* 33**,** 637-668.

DOORN, K. J., MOORS, T., DRUKARCH, B., VAN DE BERG, W., LUCASSEN, P. J. & VAN DAM, A. M. 2014. Microglial phenotypes and toll-like receptor 2 in the substantia nigra and hippocampus of incidental Lewy body disease cases and Parkinson's disease patients. *Acta Neuropathol Commun,* 2**,** 90.

DORMAN, D. C., STRUVE, M. F., MARSHALL, M. W., PARKINSON, C. U., JAMES, R. A. & WONG, B. A. 2006a. Tissue manganese concentrations in young male rhesus monkeys following subchronic manganese sulfate inhalation. *Toxicol Sci,* 92**,** 201-10.

DORMAN, D. C., STRUVE, M. F., WONG, B. A., DYE, J. A. & ROBERTSON, I. D. 2006b. Correlation of brain magnetic resonance imaging changes with pallidal manganese concentrations in rhesus monkeys following subchronic manganese inhalation. *Toxicol Sci,* 92**,** 219-27.

DORSEY, E. R. & BLOEM, B. R. 2018. The Parkinson Pandemic—A Call to ActionThe Parkinson PandemicThe Parkinson Pandemic. *JAMA Neurology,* 75**,** 9-10.

DRIVER, J. A., LOGROSCINO, G., GAZIANO, J. M. & KURTH, T. 2009. Incidence and remaining lifetime risk of Parkinson disease in advanced age. *Neurology,* 72**,** 432-8.

DUCIC, T., CARBONI, E., LAI, B., CHEN, S., MICHALKE, B., LAZARO, D. F., OUTEIRO, T. F., BAHR, M., BARSKI, E. & LINGOR, P. 2015. Alpha-Synuclein Regulates Neuronal Levels of Manganese and Calcium. *ACS Chem Neurosci,* 6**,** 1769-79.

DUNLOP, E. A. & TEE, A. R. 2014. mTOR and autophagy: a dynamic relationship governed by nutrients and energy. *Semin Cell Dev Biol,* 36**,** 121-9.

DYDAK, U., JIANG, Y. M., LONG, L. L., ZHU, H., CHEN, J., LI, W. M., EDDEN, R. A., HU, S., FU, X., LONG, Z., MO, X. A., MEIER, D., HAREZLAK, J., ASCHNER, M., MURDOCH, J. B. & ZHENG, W. 2011. In vivo measurement of brain GABA concentrations by magnetic resonance spectroscopy in smelters occupationally exposed to manganese. *Environ Health Perspect,* 119**,** 219-24.

EBRAHIMI-FAKHARI, D., WAHLSTER, L. & MCLEAN, P. J. 2012. Protein degradation pathways in Parkinson's disease: curse or blessing. *Acta Neuropathol,* 124**,** 153-72.

EKSTRAND, M. I., TERZIOGLU, M., GALTER, D., ZHU, S., HOFSTETTER, C., LINDQVIST, E., THAMS, S., BERGSTRAND, A., HANSSON, F. S., TRIFUNOVIC, A., HOFFER, B., CULLHEIM, S., MOHAMMED, A. H., OLSON, L. & LARSSON, N.-G. 2007. Progressive parkinsonism in mice with respiratory-chain-deficient dopamine neurons. *Proceedings of the National Academy of Sciences of the United States of America,* 104**,** 1325-1330.

EL-AGNAF, O., BODLES-BRAKHOP, A., J. S. GUTHRIE, D., HARRIOTT, P. & BRENT IRVINE, G. 1998. *The n-terminal region of Non-A-beta Component of Alzheimers-disease amyloid is responsible for its tendency to assume beta-sheet and aggregate*.

ELDER, A., GELEIN, R., SILVA, V., FEIKERT, T., OPANASHUK, L., CARTER, J., POTTER, R., MAYNARD, A., ITO, Y., FINKELSTEIN, J. & OBERDORSTER, G. 2006. Translocation of inhaled ultrafine manganese oxide particles to the central nervous system. *Environ Health Perspect,* 114**,** 1172-8.

EMANUELE, M., ESPOSITO, A., CAMERINI, S., ANTONUCCI, F., FERRARA, S., SEGHEZZA, S., CATELANI, T., CRESCENZI, M., MAROTTA, R., CANALE, C., MATTEOLI, M., MENNA, E. & CHIEREGATTI, E. 2016. Exogenous Alpha-Synuclein Alters Pre- and Post-Synaptic Activity by Fragmenting Lipid Rafts. *EBioMedicine,* 7**,** 191-204.

EMMANOUILIDOU, E., STEFANIS, L. & VEKRELLIS, K. 2010. Cell-produced alpha-synuclein oligomers are targeted to, and impair, the 26S proteasome. *Neurobiol Aging,* 31**,** 953-68.

ERIKSON, K. & ASCHNER, M. 2002. Manganese causes differential regulation of glutamate transporter (GLAST) taurine transporter and metallothionein in cultured rat astrocytes. *Neurotoxicology,* 23**,** 595-602.

ERIKSON, K. M., JOHN, C. E., JONES, S. R. & ASCHNER, M. 2005. Manganese accumulation in striatum of mice exposed to toxic doses is dependent upon a functional dopamine transporter. *Environ Toxicol Pharmacol,* 20**,** 390-4.

ERIKSON, K. M., SHIHABI, Z. K., ASCHNER, J. L. & ASCHNER, M. 2002. Manganese accumulates in iron-deficient rat brain regions in a heterogeneous fashion and is associated with neurochemical alterations. *Biol Trace Elem Res,* 87**,** 143-56.

ERIKSSON, H., MAGISTE, K., PLANTIN, L. O., FONNUM, F., HEDSTROM, K. G., THEODORSSON-NORHEIM, E., KRISTENSSON, K., STALBERG, E. & HEILBRONN, E. 1987. Effects of manganese oxide on monkeys as revealed by a

combined neurochemical, histological and neurophysiological evaluation. *Arch Toxicol,* 61**,** 46-52.

FABRE, E., MONSERRAT, J., HERRERO, A., BARJA, G. & LERET, M. L. 1999. Effect of MPTP on brain mitochondrial H2O2 and ATP production and on dopamine and DOPAC in the striatum. *J Physiol Biochem,* 55**,** 325-31.

FAHRNER, J. A., LIU, R., PERRY, M. S., KLEIN, J. & CHAN, D. C. 2016. A novel de novo dominant negative mutation in DNM1L impairs mitochondrial fission and presents as childhood epileptic encephalopathy. *Am J Med Genet A,* 170**,** 2002-11.

FAN, R. Z., GUO, M., LUO, S., CUI, M. & TIEU, K. 2019. Exosome release and neuropathology induced by α-synuclein: new insights into protective mechanisms of Drp1 inhibition. *Acta Neuropathologica Communications,* 7**,** 184.

FAN, X., LUO, G., YANG, D., MING, M., LIU, H., PU, P. & LE, W. 2010. Critical role of lysosome and its associated protein cathepsin D in manganese-induced toxicity in cultured midbrain astrocyte. *Neurochemistry International,* 56**,** 291-300.

FARES, M. B., AIT-BOUZIAD, N., DIKIY, I., MBEFO, M. K., JOVICIC, A., KIELY, A., HOLTON, J. L., LEE, S. J., GITLER, A. D., ELIEZER, D. & LASHUEL, H. A. 2014. The novel Parkinson's disease linked mutation G51D attenuates in vitro aggregation and membrane binding of alpha-synuclein, and enhances its secretion and nuclear localization in cells. *Hum Mol Genet,* 23**,** 4491-509.

FAUCHEUX, B. A., BONNET, A. M., AGID, Y. & HIRSCH, E. C. 1999. Blood vessels change in the mesencephalon of patients with Parkinson's disease. *Lancet,* 353**,** 981-2.

FAUVET, B., MBEFO, M. K., FARES, M. B., DESOBRY, C., MICHAEL, S., ARDAH, M. T., TSIKA, E., COUNE, P., PRUDENT, M., LION, N., ELIEZER, D., MOORE, D. J., SCHNEIDER, B., AEBISCHER, P., EL-AGNAF, O. M., MASLIAH, E. & LASHUEL, H. A. 2012. alpha-Synuclein in central nervous system and from erythrocytes, mammalian cells, and Escherichia coli exists predominantly as disordered monomer. *J Biol Chem,* 287**,** 15345-64.

FENALTI, G., LAW, R. H., BUCKLE, A. M., LANGENDORF, C., TUCK, K., ROSADO, C. J., FAUX, N. G., MAHMOOD, K., HAMPE, C. S., BANGA, J. P., WILCE, M., SCHMIDBERGER, J., ROSSJOHN, J., EL-KABBANI, O., PIKE, R. N., SMITH, A. I., MACKAY, I. R., ROWLEY, M. J. & WHISSTOCK, J. C. 2007. GABA production by glutamic acid decarboxylase is regulated by a dynamic catalytic loop. *Nat Struct Mol Biol,* 14**,** 280-6.

FERNAGUT, P. O., HUTSON, C. B., FLEMING, S. M., TETREAUT, N. A., SALCEDO, J., MASLIAH, E. & CHESSELET, M. F. 2007. Behavioral and histopathological consequences of paraquat intoxication in mice: effects of alpha-synuclein over-expression. *Synapse,* 61**,** 991-1001.

FERNANDES, A., DE OLIVEIRA, E. F., DE REZENDE, I. C. V. & PONZONI, S. 2010. Manganese neurotoxic time course is not influenced by l-deprenyl systemic treatment: Influence of l-deprenyl in manganese neurotoxic time course. *Brain Research,* 1317**,** 277-285.

FIESEL, F. C., CAULFIELD, T. R., MOUSSAUD-LAMODIÈRE, E. L., OGAKI, K., DOURADO, D. F. A. R., FLORES, S. C., ROSS, O. A. & SPRINGER, W. 2015. Structural and Functional Impact of Parkinson Disease-Associated Mutations in the E3 Ubiquitin Ligase Parkin. *Human mutation,* 36**,** 774-786.

FILADI, R., GREOTTI, E., TURACCHIO, G., LUINI, A., POZZAN, T. & PIZZO, P. 2015. Mitofusin 2 ablation increases endoplasmic reticulum–mitochondria coupling. *Proceedings of the National Academy of Sciences,* 112**,** E2174-E2181.

FILICHIA, E., HOFFER, B., QI, X. & LUO, Y. 2016. Inhibition of Drp1 mitochondrial translocation provides neural protection in dopaminergic system in a Parkinson's disease model induced by MPTP. *Scientific Reports,* 6.

FITSANAKIS, V. A., ZHANG, N., ANDERSON, J. G., ERIKSON, K. M., AVISON, M. J., GORE, J. C. & ASCHNER, M. 2008. Measuring brain manganese and iron accumulation in rats following 14 weeks of low-dose manganese treatment using atomic absorption spectroscopy and magnetic resonance imaging. *Toxicol Sci,* 103**,** 116-24.

FITSANAKIS, V. A., ZHANG, N., AVISON, M. J., ERIKSON, K. M., GORE, J. C. & ASCHNER, M. 2011. Changes in dietary iron exacerbate regional brain manganese accumulation as determined by magnetic resonance imaging. *Toxicol Sci,* 120**,** 146-53.

FITZGERALD, K., MIKALUNAS, V., RUBIN, H., MCCARTHEY, R., VANAGUNAS, A. & CRAIG, R. M. 1999. Hypermanganesemia in patients receiving total parenteral nutrition. *JPEN J Parenter Enteral Nutr,* 23**,** 333-6.

FORDAHL, S. C., ANDERSON, J. G., COONEY, P. T., WEAVER, T. L., COLYER, C. L. & ERIKSON, K. M. 2010. Manganese exposure inhibits the clearance of extracellular GABA and influences taurine homeostasis in the striatum of developing rats. *Neurotoxicology,* 31**,** 639-46.

FORTE, G., ALIMONTI, A., PINO, A., STANZIONE, P., BRESCIANINI, S., BRUSA, L., SANCESARIO, G., VIOLANTE, N. & BOCCA, B. 2005. Metals and oxidative stress in patients with Parkinson's disease. *Ann Ist Super Sanita,* 41**,** 189-95.

FOWLER, A. J. & MOUSSA, C. E. H. 2018. Activating Autophagy as a Therapeutic Strategy for Parkinson's Disease. *CNS Drugs,* 32**,** 1-11.

FRIEDMAN, L. G., LACHENMAYER, M. L., WANG, J., HE, L., POULOSE, S. M., KOMATSU, M., HOLSTEIN, G. R. & YUE, Z. 2012. Disrupted autophagy leads to dopaminergic axon and dendrite degeneration and promotes presynaptic accumulation of α-synuclein and LRRK2 in the brain. *The Journal of neuroscience : the official journal of the Society for Neuroscience,* 32**,** 7585-7593.

FUJISHIRO, H., YOSHIDA, M., NAKANO, Y. & HIMENO, S. 2014. Interleukin-6 enhances manganese accumulation in SH-SY5Y cells: implications of the up-regulation of ZIP14 and the down-regulation of ZnT10. *Metallomics,* 6**,** 944-949.

FUJIWARA, H., HASEGAWA, M., DOHMAE, N., KAWASHIMA, A., MASLIAH, E., GOLDBERG, M. S., SHEN, J., TAKIO, K. & IWATSUBO, T. 2002. α-Synuclein is phosphorylated in synucleinopathy lesions. *Nature Cell Biology,* 4**,** 160.

FUKUSHIMA, T., TAN, X., LUO, Y. & KANDA, H. 2010. Relationship between blood levels of heavy metals and Parkinson's disease in China. *Neuroepidemiology,* 34**,** 18-24.

FUKUSHIMA, T., TAN, X., LUO, Y., WANG, P., SONG, J., KANDA, H., HAYAKAWA, T., KUMAGAI, T., KAKAMU, T., TSUJI, M., HIDAKA, T. & MORI, Y. 2013. Heavy metals in blood and urine and its relation to depressive symptoms in Parkinson's disease patients. *Fukushima J Med Sci,* 59**,** 76-80.

GALTER, D., WESTERLUND, M., CARMINE, A., LINDQVIST, E., SYDOW, O. & OLSON, L. 2006. LRRK2 expression linked to dopamine-innervated areas. *Ann Neurol,* 59**,** 714-9.

GAN-OR, Z., AMSHALOM, I., KILARSKI, L. L., BAR-SHIRA, A., GANA-WEISZ, M., MIRELMAN, A., MARDER, K., BRESSMAN, S., GILADI, N. & ORR-URTREGER, A. 2015. Differential effects of severe vs mild GBA mutations on Parkinson disease. *Neurology,* 84**,** 880-7.

GANDHI, S., WOOD-KACZMAR, A., YAO, Z., PLUN-FAVREAU, H., DEAS, E., KLUPSCH, K., DOWNWARD, J., LATCHMAN, D. S., TABRIZI, S. J., WOOD, N. W., DUCHEN, M. R. & ABRAMOV, A. Y. 2009. PINK1-associated Parkinson's

disease is caused by neuronal vulnerability to calcium-induced cell death. *Mol Cell,* 33**,** 627-38.

GARCIA, S. J., GELLEIN, K., SYVERSEN, T. & ASCHNER, M. 2006. A manganese-enhanced diet alters brain metals and transporters in the developing rat. *Toxicol Sci,* 92**,** 516-25.

GARRICK, M. D., SINGLETON, S. T., VARGAS, F., KUO, H. C., ZHAO, L., KNOPFEL, M., DAVIDSON, T., COSTA, M., PARADKAR, P., ROTH, J. A. & GARRICK, L. M. 2006. DMT1: which metals does it transport? *Biol Res,* 39**,** 79-85.

GASSER, P. J., ORCHINIK, M., RAJU, I. & LOWRY, C. A. 2009. Distribution of organic cation transporter 3, a corticosterone-sensitive monoamine transporter, in the rat brain. *Journal of Comparative Neurology,* 512**,** 529-555.

GATTO, N. M., DEAPEN, D., STOYANOFF, S., PINDER, R., NARAYAN, S., BORDELON, Y. & RITZ, B. 2014. Lifetime exposure to estrogens and Parkinson's disease in California teachers. *Parkinsonism Relat Disord,* 20**,** 1149-56.

GAUTIER, C. A., GIAIME, E., CABALLERO, E., NUNEZ, L., SONG, Z., CHAN, D., VILLALOBOS, C. & SHEN, J. 2012. Regulation of mitochondrial permeability transition pore by PINK1. *Mol Neurodegener,* 7**,** 22.

GAUTIER, C. A., KITADA, T. & SHEN, J. 2008. Loss of PINK1 causes mitochondrial functional defects and increased sensitivity to oxidative stress. *Proc Natl Acad Sci U S A,* 105**,** 11364-9.

GAVIN, C. E., GUNTER, K. K. & GUNTER, T. E. 1990. Manganese and calcium efflux kinetics in brain mitochondria. Relevance to manganese toxicity. *Biochem J,* 266**,** 329-34.

GAVIN, C. E., GUNTER, K. K. & GUNTER, T. E. 1992. Mn2+ sequestration by mitochondria and inhibition of oxidative phosphorylation. *Toxicol Appl Pharmacol,* 115**,** 1-5.

GAVIN, C. E., GUNTER, K. K. & GUNTER, T. E. 1999. Manganese and calcium transport in mitochondria: implications for manganese toxicity. *Neurotoxicology,* 20**,** 445-53.

GEGG, M. E., BURKE, D., HEALES, S. J., COOPER, J. M., HARDY, J., WOOD, N. W. & SCHAPIRA, A. H. 2012. Glucocerebrosidase deficiency in substantia nigra of parkinson disease brains. *Ann Neurol,* 72**,** 455-63.

GEGG, M. E., COOPER, J. M., CHAU, K. Y., ROJO, M., SCHAPIRA, A. H. & TAANMAN, J. W. 2010. Mitofusin 1 and mitofusin 2 are ubiquitinated in a PINK1/parkin-dependent manner upon induction of mitophagy. *Hum Mol Genet,* 19**,** 4861-70.

GEGG, M. E., COOPER, J. M., SCHAPIRA, A. H. & TAANMAN, J. W. 2009. Silencing of PINK1 expression affects mitochondrial DNA and oxidative phosphorylation in dopaminergic cells. *PLoS One,* 4**,** e4756.

GEISLER, S., HOLMSTROM, K. M., SKUJAT, D., FIESEL, F. C., ROTHFUSS, O. C., KAHLE, P. J. & SPRINGER, W. 2010a. PINK1/Parkin-mediated mitophagy is dependent on VDAC1 and p62/SQSTM1. *Nat Cell Biol,* 12**,** 119-31.

GEISLER, S., HOLMSTROM, K. M., TREIS, A., SKUJAT, D., WEBER, S. S., FIESEL, F. C., KAHLE, P. J. & SPRINGER, W. 2010b. The PINK1/Parkin-mediated mitophagy is compromised by PD-associated mutations. *Autophagy,* 6**,** 871-8.

GEORGE, J. M., JIN, H., WOODS, W. S. & CLAYTON, D. F. 1995. Characterization of a novel protein regulated during the critical period for song learning in the zebra finch. *Neuron,* 15**,** 361-72.

GERHARD, A., PAVESE, N., HOTTON, G., TURKHEIMER, F., ES, M., HAMMERS, A., EGGERT, K., OERTEL, W., BANATI, R. B. & BROOKS, D. J. 2006. In vivo imaging of microglial activation with [11C](R)-PK11195 PET in idiopathic Parkinson's disease. *Neurobiol Dis,* 21**,** 404-12.

GHOSH, D., MONDAL, M., MOHITE, G. M., SINGH, P. K., RANJAN, P., ANOOP, A., GHOSH, S., JHA, N. N., KUMAR, A. & MAJI, S. K. 2013. The Parkinson's Disease-Associated H50Q Mutation Accelerates α-Synuclein Aggregation in Vitro. *Biochemistry,* 52**,** 6925-6927.

GHOSH, D., SAHAY, S., RANJAN, P., SALOT, S., MOHITE, G. M., SINGH, P. K., DWIVEDI, S., CARVALHO, E., BANERJEE, R., KUMAR, A. & MAJI, S. K. 2014. The Newly Discovered Parkinson's Disease Associated Finnish Mutation (A53E) Attenuates α-Synuclein Aggregation and Membrane Binding. *Biochemistry,* 53**,** 6419-6421.

GIBB, W. R., SCOTT, T. & LEES, A. J. 1991. Neuronal inclusions of Parkinson's disease. *Mov Disord,* 6**,** 2-11.

GILKS, W. P., ABOU-SLEIMAN, P. M., GANDHI, S., JAIN, S., SINGLETON, A., LEES, A. J., SHAW, K., BHATIA, K. P., BONIFATI, V., QUINN, N. P., LYNCH, J., HEALY, D. G., HOLTON, J. L., REVESZ, T. & WOOD, N. W. 2005. A common LRRK2 mutation in idiopathic Parkinson's disease. *Lancet,* 365**,** 415-6.

GITLER, A. D., CHESI, A., GEDDIE, M. L., STRATHEARN, K. E., HAMAMICHI, S., HILL, K. J., CALDWELL, K. A., CALDWELL, G. A., COOPER, A. A., ROCHET, J. C. & LINDQUIST, S. 2009. Alpha-synuclein is part of a diverse and highly conserved interaction network that includes PARK9 and manganese toxicity. *Nat Genet,* 41**,** 308-15.

GOLDSTEIN, S., MEYERSTEIN, D. & CZAPSKI, G. 1993. The Fenton reagents. *Free Radic Biol Med,* 15**,** 435-45.

GOMES, L. C., BENEDETTO, G. D. & SCORRANO, L. 2011. During autophagy mitochondria elongate, are spared from degradation and sustain cell viability. *Nature Cell Biology,* 13**,** 589.

GOMEZ-LAZARO, M., BONEKAMP, N. A., GALINDO, M. F., JORDÁN, J. & SCHRADER, M. 2008. 6-Hydroxydopamine (6-OHDA) induces Drp1-dependent mitochondrial fragmentation in SH-SY5Y cells. *Free Radical Biology and Medicine,* 44**,** 1960-1969.

GÓMEZ-SUAGA, P., LUZÓN-TORO, B., CHURAMANI, D., ZHANG, L., BLOOR-YOUNG, D., PATEL, S., WOODMAN, P. G., CHURCHILL, G. C. & HILFIKER, S. 2012. Leucine-rich repeat kinase 2 regulates autophagy through a calcium-dependent pathway involving NAADP. *Hum Mol Genet,* 21**,** 511-25.

GONZALEZ-POLO, R. A., NISO-SANTANO, M., ORTIZ-ORTIZ, M. A., GOMEZ-MARTIN, A., MORAN, J. M., GARCIA-RUBIO, L., FRANCISCO-MORCILLO, J., ZARAGOZA, C., SOLER, G. & FUENTES, J. M. 2007. Inhibition of paraquat-induced autophagy accelerates the apoptotic cell death in neuroblastoma SH-SY5Y cells. *Toxicol Sci,* 97**,** 448-58.

GONZALEZ, L. E., JUKNAT, A. A., VENOSA, A. J., VERRENGIA, N. & KOTLER, M. L. 2008. Manganese activates the mitochondrial apoptotic pathway in rat astrocytes by modulating the expression of proteins of the Bcl-2 family. *Neurochemistry International,* 53**,** 408-415.

GOOD, C. H., HOFFMAN, A. F., HOFFER, B. J., CHEFER, V. I., SHIPPENBERG, T. S., BÄCKMAN, C. M., LARSSON, N.-G., OLSON, L., GELLHAAR, S., GALTER, D. & LUPICA, C. R. 2011. Impaired nigrostriatal function precedes behavioral deficits in a genetic mitochondrial model of Parkinson's disease. *FASEB journal : official publication of the Federation of American Societies for Experimental Biology,* 25**,** 1333-1344.

GORELL, J. M., JOHNSON, C. C., RYBICKI, B. A., PETERSON, E. L., KORTSHA, G. X., BROWN, G. G. & RICHARDSON, R. J. 1997. Occupational exposures to metals as risk factors for Parkinson's disease. *Neurology,* 48**,** 650-8.

GORELL, J. M., JOHNSON, C. C., RYBICKI, B. A., PETERSON, E. L., KORTSHA, G. X., BROWN, G. G. & RICHARDSON, R. J. 1999. Occupational exposure to manganese, copper, lead, iron, mercury and zinc and the risk of Parkinson's disease. *Neurotoxicology,* 20**,** 239-47.

GOROJOD, R. M., ALAIMO, A., ALCON, S. P., POMILIO, C., SARAVIA, F. & KOTLER, M. L. 2015. The autophagic- lysosomal pathway determines the fate of glial cells under manganese- induced oxidative stress conditions. *Free Radical Biology and Medicine,* 87**,** 237-251.

GOROJOD, R. M., ALAIMO, A., PORTE ALCON, S., SARAVIA, F. & KOTLER, M. L. 2017. Interplay between lysosomal, mitochondrial and death receptor pathways during manganese-induced apoptosis in glial cells. *Arch Toxicol,* 91**,** 3065-3078.

GREENBAUM, E. A., GRAVES, C. L., MISHIZEN-EBERZ, A. J., LUPOLI, M. A., LYNCH, D. R., ENGLANDER, S. W., AXELSEN, P. H. & GIASSON, B. I. 2005. The E46K mutation in alpha-synuclein increases amyloid fibril formation. *J Biol Chem,* 280**,** 7800-7.

GREGER, J. L. 1998. Dietary standards for manganese: overlap between nutritional and toxicological studies. *J Nutr,* 128**,** 368s-371s.

GROZDANOV, V., BLIEDERHAEUSER, C., RUF, W. P., ROTH, V., FUNDEL-CLEMENS, K., ZONDLER, L., BRENNER, D., MARTIN-VILLALBA, A., HENGERER, B., KASSUBEK, J., LUDOLPH, A. C., WEISHAUPT, J. H. & DANZER, K. M. 2014. Inflammatory dysregulation of blood monocytes in Parkinson's disease patients. *Acta Neuropathol,* 128**,** 651-63.

GRUBMAN, A., WHITE, A. R. & LIDDELL, J. R. 2014. Mitochondrial metals as a potential therapeutic target in neurodegeneration. *British journal of pharmacology,* 171**,** 2159-2173.

GUAN, J., PAVLOVIC, D., DALKIE, N., WALDVOGEL, H. J., O'CARROLL, S. J., GREEN, C. R. & NICHOLSON, L. F. 2013. Vascular degeneration in Parkinson's disease. *Brain Pathol,* 23**,** 154-64.

GUARDIA-LAGUARTA, C., AREA-GOMEZ, E., RÜB, C., LIU, Y., MAGRANÉ, J., BECKER, D., VOOS, W., SCHON, E. A. & PRZEDBORSKI, S. 2014. α-Synuclein is localized to mitochondria-associated ER membranes. *J Neurosci,* 34**,** 249-59.

GUARDIA-LAGUARTA, C., AREA-GOMEZ, E., SCHON, E. A. & PRZEDBORSKI, S. 2015. Novel subcellular localization for α-synuclein: possible functional consequences. *Frontiers in neuroanatomy,* 9**,** 17-17.

GUI, Y.-X., WANG, X.-Y., KANG, W.-Y., ZHANG, Y.-J., ZHANG, Y., ZHOU, Y., QUINN, T. J., LIU, J. & CHEN, S.-D. 2012. Extracellular signal-related kinase is involved in alpha-synuclein-induced mitochondrial dynamic disorders by regulating dynamin-like protein 1. *Neurobiology of Aging,* 33**,** 2841-2854.

GUILARTE, T. R. 2010. Manganese and Parkinson's Disease: A Critical Review and New Findings. *Environmental Health Perspectives,* 118**,** 1071-1080.

GUILARTE, T. R., BURTON, N. C., MCGLOTHAN, J. L., VERINA, T., ZHOU, Y., ALEXANDER, M., PHAM, L., GRISWOLD, M., WONG, D. F., SYVERSEN, T. & SCHNEIDER, J. S. 2008. Impairment of nigrostriatal dopamine neurotransmission by manganese is mediated by pre-synaptic mechanism(s): implications to manganese-induced parkinsonism. *J Neurochem,* 107**,** 1236-47.

GUILARTE, T. R., CHEN, M. K., MCGLOTHAN, J. L., VERINA, T., WONG, D. F., ZHOU, Y., ALEXANDER, M., ROHDE, C. A., SYVERSEN, T., DECAMP, E., KOSER, A.

J., FRITZ, S., GONCZI, H., ANDERSON, D. W. & SCHNEIDER, J. S. 2006a. Nigrostriatal dopamine system dysfunction and subtle motor deficits in manganese-exposed non-human primates. *Exp Neurol,* 202**,** 381-90.

GUILARTE, T. R. & GONZALES, K. K. 2015. Manganese-Induced Parkinsonism Is Not Idiopathic Parkinson's Disease: Environmental and Genetic Evidence. *Toxicological Sciences,* 146**,** 204-212.

GUILARTE, T. R., MCGLOTHAN, J. L., DEGAONKAR, M., CHEN, M.-K., BARKER, P. B., SYVERSEN, T. & SCHNEIDER, J. S. 2006b. Evidence for Cortical Dysfunction and Widespread Manganese Accumulation in the Nonhuman Primate Brain following Chronic Manganese Exposure: A 1H-MRS and MRI Study. *Toxicological Sciences,* 94**,** 351-358.

GUNTER, T. E., GAVIN, C. E., ASCHNER, M. & GUNTER, K. K. 2006. Speciation of manganese in cells and mitochondria: a search for the proximal cause of manganese neurotoxicity. *Neurotoxicology,* 27**,** 765-76.

GUNTER, T. E., GAVIN, C. E. & GUNTER, K. K. 2012. The Role of Mitochondrial Oxidative Stress and ATP Depletion in the Pathology of Manganese Toxicity. *In:* LI, Y. V. & ZHANG, J. H. (eds.) *Metal Ion in Stroke.* New York, NY: Springer New York.

GUNTER, T. E., GERSTNER, B., GUNTER, K. K., MALECKI, J., GELEIN, R., VALENTINE, W. M., ASCHNER, M. & YULE, D. I. 2013. Manganese transport via the transferrin mechanism. *Neurotoxicology,* 34**,** 118-27.

GUNTER, T. E., GERSTNER, B., LESTER, T., WOJTOVICH, A. P., MALECKI, J., SWARTS, S. G., BROOKES, P. S., GAVIN, C. E. & GUNTER, K. K. 2010. An analysis of the effects of Mn2+ on oxidative phosphorylation in liver, brain, and heart mitochondria using state 3 oxidation rate assays. *Toxicol Appl Pharmacol,* 249**,** 65-75.

GUO, J. L., COVELL, D. J., DANIELS, J. P., IBA, M., STIEBER, A., ZHANG, B., RIDDLE, D. M., KWONG, L. K., XU, Y., TROJANOWSKI, J. Q. & LEE, V. M. 2013. Distinct alpha-synuclein strains differentially promote tau inclusions in neurons. *Cell,* 154**,** 103-17.

GUO, J. L. & LEE, V. M. Y. 2014. Cell-to-cell transmission of pathogenic proteins in neurodegenerative diseases. *Nature medicine,* 20**,** 130-138.

GUO, J. T., CHEN, A. Q., KONG, Q., ZHU, H., MA, C. M. & QIN, C. 2008. Inhibition of vesicular monoamine transporter-2 activity in alpha-synuclein stably transfected SH-SY5Y cells. *Cell Mol Neurobiol,* 28**,** 35-47.

GUO, J. Y., CHEN, H. Y., MATHEW, R., FAN, J., STROHECKER, A. M., KARSLI-UZUNBAS, G., KAMPHORST, J. J., CHEN, G., LEMONS, J. M., KARANTZA, V., COLLER, H. A., DIPAOLA, R. S., GELINAS, C., RABINOWITZ, J. D. & WHITE, E. 2011. Activated Ras requires autophagy to maintain oxidative metabolism and tumorigenesis. *Genes Dev,* 25**,** 460-70.

GUTIERREZ, M. G., MUNAFÓ, D. B., BERÓN, W. & COLOMBO, M. I. 2004. Rab7 is required for the normal progression of the autophagic pathway in mammalian cells. *Journal of Cell Science,* 117**,** 2687.

GWIAZDA, R. H., LEE, D., SHERIDAN, J. & SMITH, D. R. 2002. Low cumulative manganese exposure affects striatal GABA but not dopamine. *Neurotoxicology,* 23**,** 69-76.

HA, C., RYU, J. & PARK, C. B. 2007. Metal ions differentially influence the aggregation and deposition of Alzheimer's beta-amyloid on a solid template. *Biochemistry,* 46**,** 6118-25.

HAILEY, D. W., RAMBOLD, A. S., SATPUTE-KRISHNAN, P., MITRA, K., SOUGRAT, R., KIM, P. K. & LIPPINCOTT-SCHWARTZ, J. 2010. Mitochondria Supply Membranes for Autophagosome Biogenesis during Starvation. *Cell,* 141**,** 656-667.

HAMASAKI, M., FURUTA, N., MATSUDA, A., NEZU, A., YAMAMOTO, A., FUJITA, N., OOMORI, H., NODA, T., HARAGUCHI, T., HIRAOKA, Y., AMANO, A. & YOSHIMORI, T. 2013. Autophagosomes form at ER-mitochondria contact sites. *Nature,* 495**,** 389-93.

HANSEN, C., ANGOT, E., BERGSTROM, A. L., STEINER, J. A., PIERI, L., PAUL, G., OUTEIRO, T. F., MELKI, R., KALLUNKI, P., FOG, K., LI, J. Y. & BRUNDIN, P. 2011. alpha-Synuclein propagates from mouse brain to grafted dopaminergic neurons and seeds aggregation in cultured human cells. *J Clin Invest,* 121**,** 715-25.

HARA, T., NAKAMURA, K., MATSUI, M., YAMAMOTO, A., NAKAHARA, Y., SUZUKI-MIGISHIMA, R., YOKOYAMA, M., MISHIMA, K., SAITO, I., OKANO, H. & MIZUSHIMA, N. 2006. Suppression of basal autophagy in neural cells causes neurodegenerative disease in mice. *Nature,* 441**,** 885-9.

HARISCHANDRA, D. S., JIN, H., ANANTHARAM, V., KANTHASAMY, A. & KANTHASAMY, A. G. 2015. alpha-Synuclein protects against manganese neurotoxic insult during the early stages of exposure in a dopaminergic cell model of Parkinson's disease. *Toxicol Sci,* 143**,** 454-68.

HARISCHANDRA, D. S., ROKAD, D., NEAL, M. L., GHAISAS, S., MANNE, S., SARKAR, S., PANICKER, N., ZENITSKY, G., JIN, H., LEWIS, M., HUANG, X., ANANTHARAM, V., KANTHASAMY, A. & KANTHASAMY, A. G. 2019. Manganese promotes the aggregation and prion-like cell-to-cell exosomal transmission of alpha-synuclein. *Sci Signal,* 12.

HARRIS, W. R. & CHEN, Y. 1994. Electron paramagnetic resonance and difference ultraviolet studies of Mn2+ binding to serum transferrin. *Journal of Inorganic Biochemistry,* 54**,** 1-19.

HASHIMOTO, M., HSU, L. J., ROCKENSTEIN, E., TAKENOUCHI, T., MALLORY, M. & MASLIAH, E. 2002. alpha-Synuclein protects against oxidative stress via inactivation of the c-Jun N-terminal kinase stress-signaling pathway in neuronal cells. *J Biol Chem,* 277**,** 11465-72.

HAUSER, R. A., ZESIEWICZ, T. A., ROSEMURGY, A. S., MARTINEZ, C. & OLANOW, C. W. 1994. Manganese intoxication and chronic liver failure. *Ann Neurol,* 36**,** 871-5.

HAWKES, C. H., DEL TREDICI, K. & BRAAK, H. 2007. Parkinson's disease: a dual-hit hypothesis. *Neuropathology and Applied Neurobiology,* 33**,** 599-614.

HEEMAN, B., VAN DEN HAUTE, C., AELVOET, S. A., VALSECCHI, F., RODENBURG, R. J., REUMERS, V., DEBYSER, Z., CALLEWAERT, G., KOOPMAN, W. J., WILLEMS, P. H. & BAEKELANDT, V. 2011. Depletion of PINK1 affects mitochondrial metabolism, calcium homeostasis and energy maintenance. *J Cell Sci,* 124**,** 1115-25.

HEGARTY, S. V., SULLIVAN, A. M. & O'KEEFFE, G. W. 2013. Midbrain dopaminergic neurons: A review of the molecular circuitry that regulates their development. *Developmental Biology,* 379**,** 123-138.

HELLEY, M. P., PINNELL, J., SPORTELLI, C. & TIEU, K. 2017. Mitochondria: A Common Target for Genetic Mutations and Environmental Toxicants in Parkinson's Disease. *Frontiers in genetics,* 8**,** 177-177.

HENRIKSSON, J. & TJALVE, H. 2000. Manganese taken up into the CNS via the olfactory pathway in rats affects astrocytes. *Toxicol Sci,* 55**,** 392-8.

HERNANDEZ, D. G., REED, X. & SINGLETON, A. B. 2016. Genetics in Parkinson disease: Mendelian versus non-Mendelian inheritance. *J Neurochem,* 139 Suppl 1**,** 59-74.

HERRERO HERNANDEZ, E., VALENTINI, M. C. & DISCALZI, G. 2002. T1-weighted hyperintensity in basal ganglia at brain magnetic resonance imaging: are different pathologies sharing a common mechanism? *Neurotoxicology,* 23**,** 669-74.

HIGGINS, D. S., JR. & GREENAMYRE, J. T. 1996. [3H]dihydrorotenone binding to NADH: ubiquinone reductase (complex I) of the electron transport chain: an autoradiographic study. *J Neurosci,* 16**,** 3807-16.

HILTON, D., STEPHENS, M., KIRK, L., EDWARDS, P., POTTER, R., ZAJICEK, J., BROUGHTON, E., HAGAN, H. & CARROLL, C. 2014. Accumulation of alpha-synuclein in the bowel of patients in the pre-clinical phase of Parkinson's disease. *Acta Neuropathol,* 127**,** 235-41.

HISATA, J. 2002. Final supplemental environmental impact statement. Lake and stream rehabilitation: rotenone use and health risks. *Washington State Department of Fish and Wildlife*.

HOFFMANN, A.-C., MINAKAKI, G., MENGES, S., SALVI, R., SAVITSKIY, S., KAZMAN, A., VICENTE MIRANDA, H., MIELENZ, D., KLUCKEN, J., WINKLER, J. & XIANG, W. 2019. Extracellular aggregated alpha synuclein primarily triggers lysosomal dysfunction in neural cells prevented by trehalose. *Scientific Reports,* 9**,** 544.

HOJYO, S., FUKADA, T., SHIMODA, S., OHASHI, W., BIN, B. H., KOSEKI, H. & HIRANO, T. 2011. The zinc transporter SLC39A14/ZIP14 controls G-protein coupled receptor-mediated signaling required for systemic growth. *PLoS One,* 6**,** e18059.

HORNING, K. J., CAITO, S. W., TIPPS, K. G., BOWMAN, A. B. & ASCHNER, M. 2015. Manganese Is Essential for Neuronal Health. *Annu Rev Nutr,* 35**,** 71-108.

HORNYKIEWICZ, O. & KISH, S. J. 1987. Biochemical pathophysiology of Parkinson's disease. *Adv Neurol,* 45**,** 19-34.

HOU, L., XIONG, N., LIU, L., HUANG, J., HAN, C., ZHANG, G., LI, J., XU, X., LIN, Z. & WANG, T. 2015. Lithium protects dopaminergic cells from rotenone toxicity via autophagy enhancement. *BMC Neurosci,* 16**,** 82.

HRISTOVA, V. A., BEASLEY, S. A., RYLETT, R. J. & SHAW, G. S. 2009. Identification of a novel Zn2+ -binding domain in the autosomal recessive juvenile Parkinson-related E3 ligase parkin. *Journal of Biological Chemistry,* 284**,** 14978-14986.

HSU, L. J., SAGARA, Y., ARROYO, A., ROCKENSTEIN, E., SISK, A., MALLORY, M., WONG, J., TAKENOUCHI, T., HASHIMOTO, M. & MASLIAH, E. 2000. alpha-synuclein promotes mitochondrial deficit and oxidative stress. *Am J Pathol,* 157**,** 401-10.

HUANG, C. C., WENG, Y. H., LU, C. S., CHU, N. S. & YEN, T. C. 2003. Dopamine transporter binding in chronic manganese intoxication. *J Neurol,* 250**,** 1335-9.

HUANG, E., ONG, W. Y. & CONNOR, J. R. 2004. Distribution of divalent metal transporter-1 in the monkey basal ganglia. *Neuroscience,* 128**,** 487-96.

HUANG, L. & TEPAAMORNDECH, S. 2013. The SLC30 family of zinc transporters – A review of current understanding of their biological and pathophysiological roles. *Molecular Aspects of Medicine,* 34**,** 548-560.

HUGHES, A. J., DANIEL, S. E., KILFORD, L. & LEES, A. J. 1992. Accuracy of clinical diagnosis of idiopathic Parkinson's disease: a clinico-pathological study of 100 cases. *J Neurol Neurosurg Psychiatry,* 55**,** 181-4.

IMAMURA, K., HISHIKAWA, N., SAWADA, M., NAGATSU, T., YOSHIDA, M. & HASHIZUME, Y. 2003. Distribution of major histocompatibility complex class II-positive microglia and cytokine profile of Parkinson's disease brains. *Acta Neuropathol,* 106**,** 518-26.

INAMI, Y., WAGURI, S., SAKAMOTO, A., KOUNO, T., NAKADA, K., HINO, O., WATANABE, S., ANDO, J., IWADATE, M., YAMAMOTO, M., LEE, M.-S., TANAKA, K. & KOMATSU, M. 2011. Persistent activation of Nrf2 through p62 in hepatocellular carcinoma cells. 193**,** 275-284.

INGERMAN, E., PERKINS, E. M., MARINO, M., MEARS, J. A., MCCAFFERY, J. M., HINSHAW, J. E. & NUNNARI, J. 2005. Dnm1 forms spirals that are structurally tailored to fit mitochondria. *J Cell Biol,* 170**,** 1021-7.

ISHIHARA, N., NOMURA, M., JOFUKU, A., KATO, H., SUZUKI, S. O., MASUDA, K., OTERA, H., NAKANISHI, Y., NONAKA, I., GOTO, Y., TAGUCHI, N., MORINAGA, H., MAEDA, M., TAKAYANAGI, R., YOKOTA, S. & MIHARA, K. 2009. Mitochondrial fission factor Drp1 is essential for embryonic development and synapse formation in mice. *Nat Cell Biol,* 11**,** 958-66.

ITAKURA, E., KISHI-ITAKURA, C. & MIZUSHIMA, N. 2012. The hairpin-type tail-anchored SNARE syntaxin 17 targets to autophagosomes for fusion with endosomes/lysosomes. *Cell,* 151**,** 1256-69.

ITOH, K., ADACHI, Y., YAMADA, T., SUZUKI, T. L., OTOMO, T., MCBRIDE, H. M., YOSHIMORI, T., IIJIMA, M. & SESAKI, H. 2018. A brain-enriched Drp1 isoform associates with lysosomes, late endosomes, and the plasma membrane. *Journal of Biological Chemistry,* 293**,** 11809-11822.

JÄGER, S., BUCCI, C., TANIDA, I., UENO, T., KOMINAMI, E., SAFTIG, P. & ESKELINEN, E.-L. 2004. Role for Rab7 in maturation of late autophagic vacuoles. *Journal of Cell Science,* 117**,** 4837.

JANDA, E., LASCALA, A., CARRESI, C., PARAFATI, M., APRIGLIANO, S., RUSSO, V., SAVOIA, C., ZIVIANI, E., MUSOLINO, V., MORANI, F., ISIDORO, C. & MOLLACE, V. 2015. Parkinsonian toxin-induced oxidative stress inhibits basal autophagy in astrocytes via NQO2/quinone oxidoreductase 2: Implications for neuroprotection. *Autophagy,* 11**,** 1063-1080.

JANSSEN, R. J. R. J., NIJTMANS, L. G., HEUVEL, L. P. V. D. & SMEITINK, J. A. M. 2006. Mitochondrial complex I: Structure, function and pathology. 29**,** 499-515.

JENKITKASEMWONG, S., AKINYODE, A., PAULUS, E., WEISKIRCHEN, R., HOJYO, S., FUKADA, T., GIRALDO, G., SCHRIER, J., GARCIA, A., JANUS, C., GIASSON, B. & KNUTSON, M. D. 2018. SLC39A14 deficiency alters manganese homeostasis and excretion resulting in brain manganese accumulation and motor deficits in mice. *Proceedings of the National Academy of Sciences,* 115**,** E1769.

JENSEN, L. T., CARROLL, M. C., HALL, M. D., HARVEY, C. J., BEESE, S. E. & CULOTTA, V. C. 2009. Down-regulation of a manganese transporter in the face of metal toxicity. *Mol Biol Cell,* 20**,** 2810-9.

JEONG, J. & EIDE, D. J. 2013. The SLC39 family of zinc transporters. *Molecular aspects of medicine,* 34**,** 612-619.

JIANG, P., GAN, M., YEN, S. H., MCLEAN, P. J. & DICKSON, D. W. 2017. Impaired endo-lysosomal membrane integrity accelerates the seeding progression of alpha-synuclein aggregates. *Sci Rep,* 7**,** 7690.

JIANG, P., NISHIMURA, T., SAKAMAKI, Y., ITAKURA, E., HATTA, T., NATSUME, T. & MIZUSHIMA, N. 2014. The HOPS complex mediates autophagosome–lysosome fusion through interaction with syntaxin 17. *Molecular Biology of the Cell,* 25**,** 1327-1337.

JIANG, Y., ZHENG, W., LONG, L., ZHAO, W., LI, X., MO, X., LU, J., FU, X., LI, W., LIU, S., LONG, Q., HUANG, J. & PIRA, E. 2007. Brain magnetic resonance imaging and manganese concentrations in red blood cells of smelting workers: search for biomarkers of manganese exposure. *Neurotoxicology,* 28**,** 126-35.

JIN, S. M., LAZAROU, M., WANG, C., KANE, L. A., NARENDRA, D. P. & YOULE, R. J. 2010. Mitochondrial membrane potential regulates PINK1 import and proteolytic destabilization by PARL. *J Cell Biol,* 191**,** 933-42.

JINN, S., DROLET, R. E., CRAMER, P. E., WONG, A. H.-K., TOOLAN, D. M., GRETZULA, C. A., VOLETI, B., VASSILEVA, G., DISA, J., TADIN-STRAPPS, M. & STONE, D. J. 2017. TMEM175 deficiency impairs lysosomal and mitochondrial function and increases α-synuclein aggregation. *Proceedings of the National Academy of Sciences of the United States of America,* 114**,** 2389-2394.

JOSEPHS, K. A., AHLSKOG, J. E., KLOS, K. J., KUMAR, N., FEALEY, R. D., TRENERRY, M. R. & COWL, C. T. 2005. Neurologic manifestations in welders with pallidal MRI T1 hyperintensity. *Neurology,* 64**,** 2033-9.

JUNN, E. & MOURADIAN, M. M. 2002. Human alpha-synuclein over-expression increases intracellular reactive oxygen species levels and susceptibility to dopamine. *Neurosci Lett,* 320**,** 146-50.

JURSA, T. & SMITH, D. R. 2009. Ceruloplasmin alters the tissue disposition and neurotoxicity of manganese, but not its loading onto transferrin. *Toxicol Sci,* 107**,** 182-93.

KAGEYAMA, Y., ZHANG, Z., RODA, R., FUKAYA, M., WAKABAYASHI, J., WAKABAYASHI, N., KENSLER, T. W., REDDY, P. H., IIJIMA, M. & SESAKI, H. 2012. Mitochondrial division ensures the survival of postmitotic neurons by suppressing oxidative damage. *The Journal of Cell Biology,* 197**,** 535.

KAMBE, T., HASHIMOTO, A. & FUJIMOTO, S. 2014. Current understanding of ZIP and ZnT zinc transporters in human health and diseases. *Cell Mol Life Sci,* 71**,** 3281-95.

KAMEL, F. 2013. Paths from Pesticides to Parkinson's. *Science,* 341**,** 722-723.

KAMER, K. J. & MOOTHA, V. K. 2015. The molecular era of the mitochondrial calcium uniporter. *Nature Reviews Molecular Cell Biology,* 16**,** 545.

KAMP, F., EXNER, N., LUTZ, A. K., WENDER, N., HEGERMANN, J., BRUNNER, B., NUSCHER, B., BARTELS, T., GIESE, A., BEYER, K., EIMER, S., WINKLHOFER, K. F. & HAASS, C. 2010. Inhibition of mitochondrial fusion by a-synuclein is rescued by PINK1, Parkin and DJ-1. *The EMBO Journal,* 29**,** 3571-3589.

KANDIMALLA, R., MANCZAK, M., FRY, D., SUNEETHA, Y., SESAKI, H. & REDDY, P. H. 2016. Reduced dynamin-related protein 1 protects against phosphorylated Tau-induced mitochondrial dysfunction and synaptic damage in Alzheimer's disease. *Hum Mol Genet,* 25**,** 4881-4897.

KANYO, Z. F., SCOLNICK, L. R., ASH, D. E. & CHRISTIANSON, D. W. 1996. Structure of a unique binuclear manganese cluster in arginase. *Nature,* 383**,** 554-7.

KAUFMANN, T. J., HARRISON, P. M., RICHARDSON, M. J., PINHEIRO, T. J. & WALL, M. J. 2016. Intracellular soluble alpha-synuclein oligomers reduce pyramidal cell excitability. *J Physiol,* 594**,** 2751-72.

KAWAMURA, R., IKUTA, H., FUKUZUMI, S., YAMADA, R., TSUBAKI, S., KODAMA, T. & KURATA, S. 1941. Intoxication by Manganese in Well Water. *Kitasato Archives of Experimental Medicine,* 18**,** 145-69.

KERN, C. H., STANWOOD, G. D. & SMITH, D. R. 2010. Preweaning manganese exposure causes hyperactivity, disinhibition, and spatial learning and memory deficits associated with altered dopamine receptor and transporter levels. *Synapse,* 64**,** 363-78.

KHALID, M., AOUN, R. A. & MATHEWS, T. A. 2011. Altered striatal dopamine release following a sub-acute exposure to manganese. *J Neurosci Methods,* 202**,** 182-91.

KILARSKI, L. L., PEARSON, J. P., NEWSWAY, V., MAJOUNIE, E., KNIPE, M. D., MISBAHUDDIN, A., CHINNERY, P. F., BURN, D. J., CLARKE, C. E., MARION, M. H., LEWTHWAITE, A. J., NICHOLL, D. J., WOOD, N. W., MORRISON, K. E., WILLIAMS-GRAY, C. H., EVANS, J. R., SAWCER, S. J., BARKER, R. A., WICKREMARATCHI, M. M., BEN-SHLOMO, Y., WILLIAMS, N. M. & MORRIS, H. R. 2012. Systematic review and UK-based study of PARK2 (parkin), PINK1,

PARK7 (DJ-1) and LRRK2 in early-onset Parkinson's disease. *Mov Disord*, 27**,** 1522-9.

KIM-HAN, J. S., ANTENOR-DORSEY, J. A. & O'MALLEY, K. L. 2011. The parkinsonian mimetic, MPP+, specifically impairs mitochondrial transport in dopamine axons. *J Neurosci*, 31**,** 7212-21.

KIM, J., BUCKETT, P. D. & WESSLING-RESNICK, M. 2013. Absorption of manganese and iron in a mouse model of hemochromatosis. *PLoS One*, 8**,** e64944.

KIM, Y., KIM, J. M., KIM, J. W., YOO, C. I., LEE, C. R., LEE, J. H., KIM, H. K., YANG, S. O., CHUNG, H. K., LEE, D. S. & JEON, B. 2002. Dopamine transporter density is decreased in parkinsonian patients with a history of manganese exposure: what does it mean? *Mov Disord*, 17**,** 568-75.

KIM, Y., PARK, J. K., CHOI, Y., YOO, C. I., LEE, C. R., LEE, H., LEE, J. H., KIM, S. R., JEONG, T. H., YOON, C. S. & PARK, J. H. 2005. Blood manganese concentration is elevated in iron deficiency anemia patients, whereas globus pallidus signal intensity is minimally affected. *Neurotoxicology*, 26**,** 107-11.

KIMURA, S., NODA, T. & YOSHIMORI, T. 2007. Dissection of the autophagosome maturation process by a novel reporter protein, tandem fluorescent-tagged LC3. *Autophagy*, 3**,** 452-60.

KINGWELL, K. 2017. Zeroing in on neurodegenerative α-synuclein. *Nature Reviews Drug Discovery*, 16**,** 371.

KITADA, T., ASAKAWA, S., HATTORI, N., MATSUMINE, H., YAMAMURA, Y., MINOSHIMA, S., YOKOCHI, M., MIZUNO, Y. & SHIMIZU, N. 1998. Mutations in the parkin gene cause autosomal recessive juvenile parkinsonism. *Nature*, 392**,** 605-608.

KLEIN, C. & LOHMANN-HEDRICH, K. 2007. Impact of recent genetic findings in Parkinson's disease. *Curr Opin Neurol*, 20**,** 453-64.

KLEIN, C., LOHMANN-HEDRICH, K., ROGAEVA, E., SCHLOSSMACHER, M. G. & LANG, A. E. 2007. Deciphering the role of heterozygous mutations in genes associated with parkinsonism. *Lancet Neurol*, 6**,** 652-62.

KLEIN, C. & WESTENBERGER, A. 2012. Genetics of Parkinson's Disease. *Cold Spring Harbor Perspectives in Medicine*.

KLIONSKY, D. J., ABDELMOHSEN, K., ABE, A., ABEDIN, M. J., ABELIOVICH, H., ACEVEDO AROZENA, A., ADACHI, H., ADAMS, C. M., ADAMS, P. D., ADELI, K., ADHIHETTY, P. J., ADLER, S. G., AGAM, G., AGARWAL, R., AGHI, M. K., AGNELLO, M., AGOSTINIS, P., AGUILAR, P. V., AGUIRRE-GHISO, J., AIROLDI, E. M., AIT-SI-ALI, S., AKEMATSU, T., AKPORIAYE, E. T., AL-RUBEAI, M., ALBAICETA, G. M., ALBANESE, C., ALBANI, D., ALBERT, M. L., ALDUDO, J., ALGÜL, H., ALIREZAEI, M., ALLOZA, I., ALMASAN, A., ALMONTE-BECERIL, M., ALNEMRI, E. S., ALONSO, C., ALTAN-BONNET, N., ALTIERI, D. C., ALVAREZ, S., ALVAREZ-ERVITI, L., ALVES, S., AMADORO, G., AMANO, A., AMANTINI, C., AMBROSIO, S., AMELIO, I., AMER, A. O., AMESSOU, M., AMON, A., AN, Z., ANANIA, F. A., ANDERSEN, S. U., ANDLEY, U. P., ANDREADI, C. K., ANDRIEU-ABADIE, N., ANEL, A., ANN, D. K., ANOOPKUMAR-DUKIE, S., ANTONIOLI, M., AOKI, H., APOSTOLOVA, N., AQUILA, S., AQUILANO, K., ARAKI, K., ARAMA, E., ARANDA, A., ARAYA, J., ARCARO, A., ARIAS, E., ARIMOTO, H., ARIOSA, A. R., ARMSTRONG, J. L., ARNOULD, T., ARSOV, I., ASANUMA, K., ASKANAS, V., ASSELIN, E., ATARASHI, R., ATHERTON, S. S., ATKIN, J. D., ATTARDI, L. D., AUBERGER, P., AUBURGER, G., AURELIAN, L., AUTELLI, R., AVAGLIANO, L., AVANTAGGIATI, M. L., AVRAHAMI, L., AWALE, S., AZAD, N., BACHETTI, T.,

BACKER, J. M., BAE, D.-H., BAE, J.-S., BAE, O.-N., BAE, S. H., BAEHRECKE, E. H., BAEK, S.-H., BAGHDIGUIAN, S., BAGNIEWSKA-ZADWORNA, A., et al. 2016. Guidelines for the use and interpretation of assays for monitoring autophagy (3rd edition). *Autophagy,* 12**,** 1-222.

KLIONSKY, D. J. & SCHULMAN, B. A. 2014. Dynamic regulation of macroautophagy by distinctive ubiquitin-like proteins. *Nature Structural &Amp; Molecular Biology,* 21**,** 336.

KNOTT, A. B., PERKINS, G., SCHWARZENBACHER, R. & BOSSY-WETZEL, E. 2008. Mitochondrial fragmentation in neurodegeneration. *Nat Rev Neurosci,* 9**,** 505-18.

KOCH, J., FEICHTINGER, R. G., FREISINGER, P., PIES, M., SCHRODL, F., IUSO, A., SPERL, W., MAYR, J. A., PROKISCH, H. & HAACK, T. B. 2016. Disturbed mitochondrial and peroxisomal dynamics due to loss of MFF causes Leigh-like encephalopathy, optic atrophy and peripheral neuropathy. *J Med Genet,* 53**,** 270-8.

KOLLER, W. C., LYONS, K. E. & TRULY, W. 2004. Effect of levodopa treatment for parkinsonism in welders. *Neurology,* 62**,** 730.

KOMATSU, M., WAGURI, S., CHIBA, T., MURATA, S., IWATA, J., TANIDA, I., UENO, T., KOIKE, M., UCHIYAMA, Y., KOMINAMI, E. & TANAKA, K. 2006. Loss of autophagy in the central nervous system causes neurodegeneration in mice. *Nature,* 441**,** 880-4.

KOMATSU, M., WAGURI, S., KOIKE, M., SOU, Y. S., UENO, T., HARA, T., MIZUSHIMA, N., IWATA, J., EZAKI, J., MURATA, S., HAMAZAKI, J., NISHITO, Y., IEMURA, S., NATSUME, T., YANAGAWA, T., UWAYAMA, J., WARABI, E., YOSHIDA, H., ISHII, T., KOBAYASHI, A., YAMAMOTO, M., YUE, Z., UCHIYAMA, Y., KOMINAMI, E. & TANAKA, K. 2007. Homeostatic levels of p62 control cytoplasmic inclusion body formation in autophagy-deficient mice. *Cell,* 131**,** 1149-63.

KOMATSU, M., WAGURI, S., UENO, T., IWATA, J., MURATA, S., TANIDA, I., EZAKI, J., MIZUSHIMA, N., OHSUMI, Y., UCHIYAMA, Y., KOMINAMI, E., TANAKA, K. & CHIBA, T. 2005. Impairment of starvation-induced and constitutive autophagy in Atg7-deficient mice. *J Cell Biol,* 169**,** 425-34.

KONDAPALLI, C., KAZLAUSKAITE, A., ZHANG, N., WOODROOF, H. I., CAMPBELL, D. G., GOURLAY, R., BURCHELL, L., WALDEN, H., MACARTNEY, T. J., DEAK, M., KNEBEL, A., ALESSI, D. R. & MUQIT, M. M. K. 2012. PINK1 is activated by mitochondrial membrane potential depolarization and stimulates Parkin E3 ligase activity by phosphorylating Serine 65. *Open Biology,* 2**,** 120080.

KONG, S. M., CHAN, B. K., PARK, J. S., HILL, K. J., AITKEN, J. B., COTTLE, L., FARGHAIAN, H., COLE, A. R., LAY, P. A., SUE, C. M. & COOPER, A. A. 2014. Parkinson's disease-linked human PARK9/ATP13A2 maintains zinc homeostasis and promotes α-Synuclein externalization via exosomes. *Hum Mol Genet,* 23**,** 2816-33.

KONTOPOULOS, E., PARVIN, J. D. & FEANY, M. B. 2006. Alpha-synuclein acts in the nucleus to inhibit histone acetylation and promote neurotoxicity. *Hum Mol Genet,* 15**,** 3012-23.

KORDOWER, J. H., CHU, Y., HAUSER, R. A., FREEMAN, T. B. & OLANOW, C. W. 2008. Lewy body-like pathology in long-term embryonic nigral transplants in Parkinson's disease. *Nat Med,* 14**,** 504-6.

KORTEKAAS, R., LEENDERS, K. L., VAN OOSTROM, J. C., VAALBURG, W., BART, J., WILLEMSEN, A. T. & HENDRIKSE, N. H. 2005. Blood-brain barrier dysfunction in parkinsonian midbrain in vivo. *Ann Neurol,* 57**,** 176-9.

KOSEOGLU, S., DILKS, J. R., PETERS, C. G., FITCH-TEWFIK, J. L., FADEL, N. A., JASUJA, R., ITALIANO, J. E., JR., HAYNES, C. L. & FLAUMENHAFT, R. 2013.

Dynamin-related protein-1 controls fusion pore dynamics during platelet granule exocytosis. *Arteriosclerosis, thrombosis, and vascular biology,* 33**,** 481-488.
KOWALTOWSKI, A. J., CASTILHO, R. F. & VERCESI, A. E. 1995. Ca(2+)-induced mitochondrial membrane permeabilization: role of coenzyme Q redox state. *Am J Physiol,* 269**,** C141-7.
KOWALTOWSKI, A. J., NAIA-DA-SILVA, E. S., CASTILHO, R. F. & VERCESI, A. E. 1998. Ca2+-stimulated mitochondrial reactive oxygen species generation and permeability transition are inhibited by dibucaine or Mg2+. *Arch Biochem Biophys,* 359**,** 77-81.
KRACHLER, M. & ROSSIPAL, E. 2000. Concentrations of trace elements in extensively hydrolysed infant formulae and their estimated daily intakes. *Ann Nutr Metab,* 44**,** 68-74.
KRAYTSBERG, Y., KUDRYAVTSEVA, E., MCKEE, A. C., GEULA, C., KOWALL, N. W. & KHRAPKO, K. 2006. Mitochondrial DNA deletions are abundant and cause functional impairment in aged human substantia nigra neurons. *Nat Genet,* 38**,** 518-20.
KREBS, N., LANGKAMMER, C., GOESSLER, W., ROPELE, S., FAZEKAS, F., YEN, K. & SCHEURER, E. 2014. Assessment of trace elements in human brain using inductively coupled plasma mass spectrometry. *J Trace Elem Med Biol,* 28**,** 1-7.
KRIEGER, D., KRIEGER, S., JANSEN, O., GASS, P., THEILMANN, L. & LICHTNECKER, H. 1995. Manganese and chronic hepatic encephalopathy. *Lancet,* 346**,** 270-4.
KRISHNA, S., DODD, C. A., HEKMATYAR, S. K. & FILIPOV, N. M. 2014. Brain deposition and neurotoxicity of manganese in adult mice exposed via the drinking water. *Arch Toxicol,* 88**,** 47-64.
KRUGER, R., KUHN, W., MULLER, T., WOITALLA, D., GRAEBER, M., KOSEL, S., PRZUNTEK, H., EPPLEN, J. T., SCHOLS, L. & RIESS, O. 1998. Ala30Pro mutation in the gene encoding alpha-synuclein in Parkinson's disease. *Nat Genet,* 18**,** 106-8.
KRUMAN, I. I. & MATTSON, M. P. 1999. Pivotal Role of Mitochondrial Calcium Uptake in Neural Cell Apoptosis and Necrosis. *Journal of Neurochemistry,* 72**,** 529-540.
KUMA, A., HATANO, M., MATSUI, M., YAMAMOTO, A., NAKAYA, H., YOSHIMORI, T., OHSUMI, Y., TOKUHISA, T. & MIZUSHIMA, N. 2004. The role of autophagy during the early neonatal starvation period. *Nature,* 432**,** 1032.
KUMUDINI, N., UMA, A., DEVI, Y. P., NAUSHAD, S. M., MRIDULA, R., BORGOHAIN, R. & KUTALA, V. K. 2014. Association of Parkinson's disease with altered serum levels of lead and transition metals among South Indian subjects. *Indian J Biochem Biophys,* 51**,** 121-6.
KUZUHARA, S., MORI, H., IZUMIYAMA, N., YOSHIMURA, M. & IHARA, Y. 1988. Lewy bodies are ubiquitinated. A light and electron microscopic immunocytochemical study. *Acta Neuropathol,* 75**,** 345-53.
KWAKYE, G. F., PAOLIELLO, M. M., MUKHOPADHYAY, S., BOWMAN, A. B. & ASCHNER, M. 2015. Manganese-Induced Parkinsonism and Parkinson's Disease: Shared and Distinguishable Features. *Int J Environ Res Public Health,* 12**,** 7519-40.
LANGLEY, M. R., GHAISAS, S., AY, M., LUO, J., PALANISAMY, B. N., JIN, H., ANANTHARAM, V., KANTHASAMY, A. & KANTHASAMY, A. G. 2018. Manganese exposure exacerbates progressive motor deficits and neurodegeneration in the MitoPark mouse model of Parkinson's disease: Relevance to gene and environment interactions in metal neurotoxicity. *Neurotoxicology,* 64**,** 240-255.
LANGSTON, J., BALLARD, P., TETRAD, J. & IRWIN, I. 1983. Chronic parkinsonism in humans due to a product of meperidine-analog synthesis. *Science,* 25**,** 979 -980.
LASHUEL, H. A., PETRE, B. M., WALL, J., SIMON, M., NOWAK, R. J., WALZ, T. & LANSBURY, P. T., JR. 2002. Alpha-synuclein, especially the Parkinson's disease-

associated mutants, forms pore-like annular and tubular protofibrils. *J Mol Biol,* 322**,** 1089-102.

LAWSON, L. J., PERRY, V. H., DRI, P. & GORDON, S. 1990. Heterogeneity in the distribution and morphology of microglia in the normal adult mouse brain. *Neuroscience,* 39**,** 151-70.

LAZAROU, M., JIN, S. M., KANE, L. A. & YOULE, R. J. 2012. Role of PINK1 binding to the TOM complex and alternate intracellular membranes in recruitment and activation of the E3 ligase Parkin. *Dev Cell,* 22**,** 320-33.

LECHPAMMER, M., CLEGG, M. S., MUZAR, Z., HUEBNER, P. A., JIN, L. W. & GOSPE, S. M., JR. 2014. Pathology of inherited manganese transporter deficiency. *Ann Neurol,* 75**,** 608-12.

LEE, E., YIN, Z., SIDORYK-WĘGRZYNOWICZ, M., JIANG, H. & ASCHNER, M. 2012. 15-Deoxy-Δ12,14-prostaglandin J_2 modulates manganese-induced activation of the NF-κB, Nrf2, and PI3K pathways in astrocytes. *Free Radic Biol Med,* 52**,** 1067-74.

LEE, H. J., CHO, E. D., LEE, K. W., KIM, J. H., CHO, S. G. & LEE, S. J. 2013. Autophagic failure promotes the exocytosis and intercellular transfer of alpha-synuclein. *Exp Mol Med,* 45**,** e22.

LEE, H. J., KHOSHAGHIDEH, F., PATEL, S. & LEE, S. J. 2004. Clearance of alpha-synuclein oligomeric intermediates via the lysosomal degradation pathway. *J Neurosci,* 24**,** 1888-96.

LEE, J. Y., NAGANO, Y., TAYLOR, J. P., LIM, K. L. & YAO, T. P. 2010. Disease-causing mutations in parkin impair mitochondrial ubiquitination, aggregation, and HDAC6-dependent mitophagy. *J Cell Biol,* 189**,** 671-9.

LEE, S., SATO, Y. & NIXON, R. A. 2011. Primary lysosomal dysfunction causes cargo-specific deficits of axonal transport leading to Alzheimer-like neuritic dystrophy. *Autophagy,* 7**,** 1562-3.

LEE, Y., STEVENS, D. A., KANG, S. U., JIANG, H., LEE, Y. I., KO, H. S., SCARFFE, L. A., UMANAH, G. E., KANG, H., HAM, S., KAM, T. I., ALLEN, K., BRAHMACHARI, S., KIM, J. W., NEIFERT, S., YUN, S. P., FIESEL, F. C., SPRINGER, W., DAWSON, V. L., SHIN, J. H. & DAWSON, T. M. 2017. PINK1 Primes Parkin-Mediated Ubiquitination of PARIS in Dopaminergic Neuronal Survival. *Cell Rep,* 18**,** 918-932.

LEITCH, S., FENG, M., MUEND, S., BRAITERMAN, L. T., HUBBARD, A. L. & RAO, R. 2011. Vesicular distribution of Secretory Pathway Ca(2)+-ATPase isoform 1 and a role in manganese detoxification in liver-derived polarized cells. *Biometals,* 24**,** 159-70.

LEMASTERS, J. J. 2005. Selective mitochondrial autophagy, or mitophagy, as a targeted defense against oxidative stress, mitochondrial dysfunction, and aging. *Rejuvenation Res,* 8**,** 3-5.

LEMKAU, L. R., COMELLAS, G., KLOEPPER, K. D., WOODS, W. S., GEORGE, J. M. & RIENSTRA, C. M. 2012. Mutant protein A30P α-synuclein adopts wild-type fibril structure, despite slower fibrillation kinetics. *The Journal of biological chemistry,* 287**,** 11526-11532.

LESAGE, S., ANHEIM, M., LETOURNEL, F., BOUSSET, L., HONORE, A., ROZAS, N., PIERI, L., MADIONA, K., DURR, A., MELKI, R., VERNY, C. & BRICE, A. 2013. G51D alpha-synuclein mutation causes a novel parkinsonian-pyramidal syndrome. *Ann Neurol,* 73**,** 459-71.

LEYVA-ILLADES, D., CHEN, P., ZOGZAS, C. E., HUTCHENS, S., MERCADO, J. M., SWAIM, C. D., MORRISETT, R. A., BOWMAN, A. B., ASCHNER, M. & MUKHOPADHYAY, S. 2014. SLC30A10 is a cell surface-localized manganese efflux

transporter, and parkinsonism-causing mutations block its intracellular trafficking and efflux activity. *J Neurosci,* 34**,** 14079-95.

LI, J., UVERSKY, V. N. & FINK, A. L. 2001. Effect of familial Parkinson's disease point mutations A30P and A53T on the structural properties, aggregation, and fibrillation of human alpha-synuclein. *Biochemistry,* 40**,** 11604-13.

LI, J., UVERSKY, V. N. & FINK, A. L. 2002. Conformational behavior of human alpha-synuclein is modulated by familial Parkinson's disease point mutations A30P and A53T. *Neurotoxicology,* 23**,** 553-67.

LI, J. Y., ENGLUND, E., HOLTON, J. L., SOULET, D., HAGELL, P., LEES, A. J., LASHLEY, T., QUINN, N. P., REHNCRONA, S., BJORKLUND, A., WIDNER, H., REVESZ, T., LINDVALL, O. & BRUNDIN, P. 2008. Lewy bodies in grafted neurons in subjects with Parkinson's disease suggest host-to-graft disease propagation. *Nat Med,* 14**,** 501-3.

LI, L., NADANACIVA, S., BERGER, Z., SHEN, W., PAUMIER, K., SCHWARTZ, J., MOU, K., LOOS, P., MILICI, A. J., DUNLOP, J. & HIRST, W. D. 2014a. Human A53T α-Synuclein Causes Reversible Deficits in Mitochondrial Function and Dynamics in Primary Mouse Cortical Neurons. *PLOS ONE,* 8**,** e85815.

LI, L., WANG, Z. V., HILL, J. A. & LIN, F. 2014b. New autophagy reporter mice reveal dynamics of proximal tubular autophagy. *J Am Soc Nephrol,* 25**,** 305-15.

LI, W., WEST, N., COLLA, E., PLETNIKOVA, O., TRONCOSO, J. C., MARSH, L., DAWSON, T. M., JAKALA, P., HARTMANN, T., PRICE, D. L. & LEE, M. K. 2005. Aggregation promoting C-terminal truncation of alpha-synuclein is a normal cellular process and is enhanced by the familial Parkinson's disease-linked mutations. *Proc Natl Acad Sci U S A,* 102**,** 2162-7.

LI, W. W., YANG, R., GUO, J. C., REN, H. M., ZHA, X. L., CHENG, J. S. & CAI, D. F. 2007. Localization of alpha-synuclein to mitochondria within midbrain of mice. *Neuroreport,* 18**,** 1543-6.

LI, Y., SUN, L., CAI, T., ZHANG, Y., LV, S., WANG, Y. & YE, L. 2010. alpha-Synuclein overexpression during manganese-induced apoptosis in SH-SY5Y neuroblastoma cells. *Brain Res Bull,* 81**,** 428-33.

LIANG, C., LEE, J. S., INN, K. S., GACK, M. U., LI, Q., ROBERTS, E. A., VERGNE, I., DERETIC, V., FENG, P., AKAZAWA, C. & JUNG, J. U. 2008. Beclin1-binding UVRAG targets the class C Vps complex to coordinate autophagosome maturation and endocytic trafficking. *Nat Cell Biol,* 10**,** 776-87.

LIANG, X., DE VERA, M. E., BUCHSER, W. J., ROMO DE VIVAR CHAVEZ, A., LOUGHRAN, P., BEER STOLZ, D., BASSE, P., WANG, T., VAN HOUTEN, B., ZEH, H. J., 3RD & LOTZE, M. T. 2012. Inhibiting systemic autophagy during interleukin 2 immunotherapy promotes long-term tumor regression. *Cancer Res,* 72**,** 2791-801.

LICHTEN, L. A. & COUSINS, R. J. 2009. Mammalian zinc transporters: nutritional and physiologic regulation. *Annu Rev Nutr,* 29**,** 153-76.

LICHTEN, L. A., LIUZZI, J. P. & COUSINS, R. J. 2009. Interleukin-1beta contributes via nitric oxide to the upregulation and functional activity of the zinc transporter Zip14 (Slc39a14) in murine hepatocytes. *Am J Physiol Gastrointest Liver Physiol,* 296**,** G860-7.

LIESA, M., PALACÍN, M. & ZORZANO, A. 2009. Mitochondrial Dynamics in Mammalian Health and Disease. *Physiological Reviews,* 89**,** 799-845.

LILL, C. M., ROEHR, J. T., MCQUEEN, M. B., KAVVOURA, F. K., BAGADE, S., SCHJEIDE, B. M., SCHJEIDE, L. M., MEISSNER, E., ZAUFT, U., ALLEN, N. C., LIU, T., SCHILLING, M., ANDERSON, K. J., BEECHAM, G., BERG, D.,

BIERNACKA, J. M., BRICE, A., DESTEFANO, A. L., DO, C. B., ERIKSSON, N., FACTOR, S. A., FARRER, M. J., FOROUD, T., GASSER, T., HAMZA, T., HARDY, J. A., HEUTINK, P., HILL-BURNS, E. M., KLEIN, C., LATOURELLE, J. C., MARAGANORE, D. M., MARTIN, E. R., MARTINEZ, M., MYERS, R. H., NALLS, M. A., PANKRATZ, N., PAYAMI, H., SATAKE, W., SCOTT, W. K., SHARMA, M., SINGLETON, A. B., STEFANSSON, K., TODA, T., TUNG, J. Y., VANCE, J., WOOD, N. W., ZABETIAN, C. P., YOUNG, P., TANZI, R. E., KHOURY, M. J., ZIPP, F., LEHRACH, H., IOANNIDIS, J. P., BERTRAM, L., CONSORTIUM, A. G. E. O. P. S. D., CONSORTIUM, I. P. S. D. G., CONSORTIUM, P. S. D. G. & 2), W. T. C. C. C. 2012. Comprehensive research synopsis and systematic meta-analyses in Parkinson's disease genetics: The PDGene database. *PLoS Genet,* 8**,** e1002548.

LIN, F., WANG, Z. V. & HILL, J. A. 2014. Seeing is believing: dynamic changes in renal epithelial autophagy during injury and repair. *Autophagy,* 10**,** 691-3.

LIN, W., VANN, D. R., DOULIAS, P. T., WANG, T., LANDESBERG, G., LI, X., RICCIOTTI, E., SCALIA, R., HE, M., HAND, N. J. & RADER, D. J. 2017. Hepatic metal ion transporter ZIP8 regulates manganese homeostasis and manganese-dependent enzyme activity. *J Clin Invest,* 127**,** 2407-2417.

LIOU, H. H., TSAI, M. C., CHEN, C. J., JENG, J. S., CHANG, Y. C., CHEN, S. Y. & CHEN, R. C. 1997. Environmental risk factors and Parkinson's disease: a case-control study in Taiwan. *Neurology,* 48**,** 1583-8.

LIU, C., YAN, D. Y., TAN, X., MA, Z., WANG, C., DENG, Y., LIU, W., YANG, T. Y., XU, Z. F. & XU, B. 2018. Effect of the cross-talk between autophagy and endoplasmic reticulum stress on Mn-induced alpha-synuclein oligomerization. *Environ Toxicol,* 33**,** 315-324.

LIU, G., ZHANG, C., YIN, J., LI, X., CHENG, F., LI, Y., YANG, H., UEDA, K., CHAN, P. & YU, S. 2009a. alpha-Synuclein is differentially expressed in mitochondria from different rat brain regions and dose-dependently down-regulates complex I activity. *Neurosci Lett,* 454**,** 187-92.

LIU, H.-F., HO, P. W.-L., LEUNG, G. C.-T., LAM, C. S.-C., PANG, S. Y.-Y., LI, L., KUNG, M. H.-W., RAMSDEN, D. B. & HO, S.-L. 2017. Combined LRRK2 mutation, aging and chronic low dose oral rotenone as a model of Parkinson's disease. *Scientific Reports,* 7**,** 40887.

LIU, W., VIVES-BAUZA, C., ACIN-PEREZ, R., YAMAMOTO, A., TAN, Y., LI, Y., MAGRANE, J., STAVARACHE, M. A., SHAFFER, S., CHANG, S., KAPLITT, M. G., HUANG, X. Y., BEAL, M. F., MANFREDI, G. & LI, C. 2009b. PINK1 defect causes mitochondrial dysfunction, proteasomal deficit and alpha-synuclein aggregation in cell culture models of Parkinson's disease. *PLoS One,* 4**,** e4597.

LIU, X., SULLIVAN, K. A., MADL, J. E., LEGARE, M. & TJALKENS, R. B. 2006. Manganese-induced neurotoxicity: the role of astroglial-derived nitric oxide in striatal interneuron degeneration. *Toxicol Sci,* 91**,** 521-31.

LIU, Y., BYRNE, P., WANG, H., KOLTICK, D., ZHENG, W. & NIE, L. H. 2014. A compact DD neutron generator-based NAA system to quantify manganese (Mn) in bone in vivo. *Physiol Meas,* 35**,** 1899-911.

LIUZZI, J. P., LICHTEN, L. A., RIVERA, S., BLANCHARD, R. K., AYDEMIR, T. B., KNUTSON, M. D., GANZ, T. & COUSINS, R. J. 2005. Interleukin-6 regulates the zinc transporter Zip14 in liver and contributes to the hypozincemia of the acute-phase response. *Proc Natl Acad Sci U S A,* 102**,** 6843-8.

LOEB, V., YAKUNIN, E., SAADA, A. & SHARON, R. 2010. The transgenic overexpression of alpha-synuclein and not its related pathology associates with complex I inhibition. *J Biol Chem,* 285**,** 7334-43.

LOPES DA FONSECA, T. & OUTEIRO, T. F. 2014. ATP13A2 and Alpha-synuclein: a Metal Taste in Autophagy. *Exp Neurobiol,* 23**,** 314-23.

LOPES DA FONSECA, T., PINHO, R. & OUTEIRO, T. F. 2016. A familial ATP13A2 mutation enhances alpha-synuclein aggregation and promotes cell death. *Hum Mol Genet,* 25**,** 2959-2971.

LOVITT, B., VANDERPORTEN, E. C., SHENG, Z., ZHU, H., DRUMMOND, J. & LIU, Y. 2010. Differential effects of divalent manganese and magnesium on the kinase activity of leucine-rich repeat kinase 2 (LRRK2). *Biochemistry,* 49**,** 3092-100.

LUCCHINI, R., ALBINI, E., PLACIDI, D., GASPAROTTI, R., PIGOZZI, M. G., MONTANI, G. & ALESSIO, L. 2000. Brain magnetic resonance imaging and manganese exposure. *Neurotoxicology,* 21**,** 769-75.

LUCCHINI, R. G., MARTIN, C. J. & DONEY, B. C. 2009. From manganism to manganese-induced parkinsonism: a conceptual model based on the evolution of exposure. *Neuromolecular Med,* 11**,** 311-21.

LUDTMANN, M. H., ANGELOVA, P. R., NINKINA, N. N., GANDHI, S., BUCHMAN, V. L. & ABRAMOV, A. Y. 2016. Monomeric Alpha-Synuclein Exerts a Physiological Role on Brain ATP Synthase. *J Neurosci,* 36**,** 10510-10521.

LUK, K. C., KEHM, V., CARROLL, J., ZHANG, B., O'BRIEN, P., TROJANOWSKI, J. Q. & LEE, V. M. 2012a. Pathological alpha-synuclein transmission initiates Parkinson-like neurodegeneration in nontransgenic mice. *Science,* 338**,** 949-53.

LUK, K. C., KEHM, V. M., ZHANG, B., O'BRIEN, P., TROJANOWSKI, J. Q. & LEE, V. M. 2012b. Intracerebral inoculation of pathological alpha-synuclein initiates a rapidly progressive neurodegenerative alpha-synucleinopathy in mice. *J Exp Med,* 209**,** 975-86.

LUK, K. C., SONG, C., O'BRIEN, P., STIEBER, A., BRANCH, J. R., BRUNDEN, K. R., TROJANOWSKI, J. Q. & LEE, V. M. 2009. Exogenous alpha-synuclein fibrils seed the formation of Lewy body-like intracellular inclusions in cultured cells. *Proc Natl Acad Sci U S A,* 106**,** 20051-6.

LUTZ, A. K., EXNER, N., FETT, M. E., SCHLEHE, J. S., KLOOS, K., LÄMMERMANN, K., BRUNNER, B., KURZ-DREXLER, A., VOGEL, F., REICHERT, A. S., BOUMAN, L., VOGT-WEISENHORN, D., WURST, W., TATZELT, J., HAASS, C. & WINKLHOFER, K. F. 2009. Loss of parkin or PINK1 function increases Drp1-dependent mitochondrial fragmentation. *J Biol Chem,* 284**,** 22938-51.

MA, Z., WANG, C., LIU, C., YAN, D. Y., DENG, Y., LIU, W., YANG, T. Y., XU, Z. F. & XU, B. 2017. The role S-nitrosylation in manganese-induced autophagy dysregulation in SH-SY5Y cells. *Environ Toxicol,* 32**,** 2428-2439.

MACDONALD, R. L. & OLSEN, R. W. 1994. GABAA Receptor Channels. *Annual Review of Neuroscience,* 17**,** 569-602.

MACLEOD, D., DOWMAN, J., HAMMOND, R., LEETE, T., INOUE, K. & ABELIOVICH, A. 2006. The familial Parkinsonism gene LRRK2 regulates neurite process morphology. *Neuron,* 52**,** 587-93.

MADEJCZYK, M. S. & BALLATORI, N. 2012. The iron transporter ferroportin can also function as a manganese exporter. *Biochim Biophys Acta,* 1818**,** 651-7.

MADER, B. J., PIVTORAIKO, V. N., FLIPPO, H. M., KLOCKE, B. J., ROTH, K. A., MANGIERI, L. R. & SHACKA, J. J. 2012. Rotenone inhibits autophagic flux prior to inducing cell death. *ACS Chem Neurosci,* 3**,** 1063-72.

MALECKI, E. A. 2001. Manganese toxicity is associated with mitochondrial dysfunction and DNA fragmentation in rat primary striatal neurons. *Brain Res Bull,* 55**,** 225-8.

MANCZAK, M., KANDIMALLA, R., FRY, D., SESAKI, H. & REDDY, P. H. 2016. Protective effects of reduced dynamin-related protein 1 against amyloid beta-induced

mitochondrial dysfunction and synaptic damage in Alzheimer's disease. *Hum Mol Genet,* 25**,** 5148-5166.

MANCZAK, M., KANDIMALLA, R., YIN, X. & REDDY, P. H. 2018. Mitochondrial division inhibitor 1 reduces dynamin-related protein 1 and mitochondrial fission activity. *Human Molecular Genetics,* 28**,** 177-199.

MANCZAK, M., SESAKI, H., KAGEYAMA, Y. & REDDY, P. H. 2012. Dynamin-related protein 1 heterozygote knockout mice do not have synaptic and mitochondrial deficiencies. *Biochim Biophys Acta,* 1822**,** 862-74.

MANNING-BOG, A. B., MCCORMACK, A. L., LI, J., UVERSKY, V. N., FINK, A. L. & DI MONTE, D. A. 2002a. The Herbicide Paraquat Causes Up-regulation and Aggregation of a-Synuclein in Mice. *The Journal of Biological Chemistry,* 277**,** 1641-1644.

MANNING-BOG, A. B., MCCORMACK, A. L., LI, J., UVERSKY, V. N., FINK, A. L. & DI MONTE, D. A. 2002b. The herbicide paraquat causes up-regulation and aggregation of alpha-synuclein in mice: paraquat and alpha-synuclein. *J Biol Chem,* 277**,** 1641-4.

MARSDEN, C. D. 1983. Neuromelanin and Parkinson's disease. *J Neural Transm Suppl,* 19**,** 121-41.

MARTIN, L. J., PAN, Y., PRICE, A. C., STERLING, W., COPELAND, N. G., JENKINS, N. A., PRICE, D. L. & LEE, M. K. 2006. Parkinson's disease alpha-synuclein transgenic mice develop neuronal mitochondrial degeneration and cell death. *J Neurosci,* 26**,** 41-50.

MARTINEZ-FINLEY, E. J., GAVIN, C. E., ASCHNER, M. & GUNTER, T. E. 2013. Manganese neurotoxicity and the role of reactive oxygen species. *Free Radic Biol Med,* 62**,** 65-75.

MARTINEZ-HERNANDEZ, A., BELL, K. & NORENBERG, M. 1977. Glutamine synthetase: glial localization in brain. 195**,** 1356-1358.

MARTINEZ-VICENTE, M., TALLOCZY, Z., KAUSHIK, S., MASSEY, A. C., MAZZULLI, J., MOSHAROV, E. V., HODARA, R., FREDENBURG, R., WU, D.-C., FOLLENZI, A., DAUER, W., PRZEDBORSKI, S., ISCHIROPOULOS, H., LANSBURY, P. T., SULZER, D. & CUERVO, A. M. 2008. Dopamine-modified alpha-synuclein blocks chaperone-mediated autophagy. *The Journal of clinical investigation,* 118**,** 777-788.

MARTINI-STOICA, H., XU, Y., BALLABIO, A. & ZHENG, H. 2016. The Autophagy-Lysosomal Pathway in Neurodegeneration: A TFEB Perspective. *Trends Neurosci,* 39**,** 221-234.

MATSUDA, N., SATO, S., SHIBA, K., OKATSU, K., SAISHO, K., GAUTIER, C. A., SOU, Y. S., SAIKI, S., KAWAJIRI, S., SATO, F., KIMURA, M., KOMATSU, M., HATTORI, N. & TANAKA, K. 2010. PINK1 stabilized by mitochondrial depolarization recruits Parkin to damaged mitochondria and activates latent Parkin for mitophagy. *J Cell Biol,* 189**,** 211-21.

MATSUMINE, H., SAITO, M., SHIMODA-MATSUBAYASHI, S., TANAKA, H., ISHIKAWA, A., NAKAGAWA-HATTORI, Y., YOKOCHI, M., KOBAYASHI, T., IGARASHI, S., TAKANO, H., SANPEI, K., KOIKE, R., MORI, H., KONDO, T., MIZUTANI, Y., SCHÄFFER, A. A., YAMAMURA, Y., NAKAMURA, S., KUZUHARA, S., TSUJI, S. & MIZUNO, Y. 1997. Localization of a gene for an autosomal recessive form of juvenile Parkinsonism to chromosome 6q25.2-27. *Am J Hum Genet,* 60**,** 588-96.

MATSUNAGA, K., MORITA, E., SAITOH, T., AKIRA, S., KTISTAKIS, N. T., IZUMI, T., NODA, T. & YOSHIMORI, T. 2010. Autophagy requires endoplasmic reticulum targeting of the PI3-kinase complex via Atg14L. 190**,** 511-521.

MATSUNAGA, K., SAITOH, T., TABATA, K., OMORI, H., SATOH, T., KUROTORI, N., MAEJIMA, I., SHIRAHAMA-NODA, K., ICHIMURA, T., ISOBE, T., AKIRA, S.,

NODA, T. & YOSHIMORI, T. 2009. Two Beclin 1-binding proteins, Atg14L and Rubicon, reciprocally regulate autophagy at different stages. *Nature Cell Biology,* 11**,** 385.

MAZZULLI, J. R., XU, Y. H., SUN, Y., KNIGHT, A. L., MCLEAN, P. J., CALDWELL, G. A., SIDRANSKY, E., GRABOWSKI, G. A. & KRAINC, D. 2011. Gaucher disease glucocerebrosidase and α-synuclein form a bidirectional pathogenic loop in synucleinopathies. *Cell,* 146**,** 37-52.

MAZZULLI, J. R., ZUNKE, F., ISACSON, O., STUDER, L. & KRAINC, D. 2016. alpha-Synuclein-induced lysosomal dysfunction occurs through disruptions in protein trafficking in human midbrain synucleinopathy models. *Proc Natl Acad Sci U S A,* 113**,** 1931-6.

MCCORMACK, A. L. & DI MONTE, D. A. 2003. Effects of L-dopa and other animo acids against paraquat-induced nigrostriatal degeneration. *Journal of Neurochemistry,* 85**,** 82-86.

MCCORMACK, A. L., THIRUCHELVAM, M., MANNING-BOG, A. B., THIFFAULT, C., LANGSTON, J. W., CORY-SLECHTA, D. A. & DI MONTE, D. A. 2002. Environmental risk factors and Parkinson's disease: selective degeneration of nigral dopaminergic neurons caused by the herbicide paraquat. *Neurobiol Dis,* 10**,** 119-27.

MCGEER, P. L., ITAGAKI, S., BOYES, B. E. & MCGEER, E. G. 1988. Reactive microglia are positive for HLA-DR in the substantia nigra of Parkinson's and Alzheimer's disease brains. *Neurology,* 38**,** 1285-91.

MCLEAN, J. R., SMITH, G. A., ROCHA, E. M., HAYES, M. A., BEAGAN, J. A., HALLETT, P. J. & ISACSON, O. 2014. Widespread neuron-specific transgene expression in brain and spinal cord following synapsin promoter-driven AAV9 neonatal intracerebroventricular injection. *Neurosci Lett,* 576**,** 73-8.

MEISSNER, C., LORENZ, H., WEIHOFEN, A., SELKOE, D. J. & LEMBERG, M. K. 2011. The mitochondrial intramembrane protease PARL cleaves human Pink1 to regulate Pink1 trafficking. *J Neurochem,* 117**,** 856-67.

MENG, H., YAMASHITA, C., SHIBA-FUKUSHIMA, K., INOSHITA, T., FUNAYAMA, M., SATO, S., HATTA, T., NATSUME, T., UMITSU, M., TAKAGI, J., IMAI, Y. & HATTORI, N. 2017. Loss of Parkinson's disease-associated protein CHCHD2 affects mitochondrial crista structure and destabilizes cytochrome c. *Nat Commun,* 8**,** 15500.

MEUER, K., SUPPANZ, I. E., LINGOR, P., PLANCHAMP, V., GÖRICKE, B., FICHTNER, L., BRAUS, G. H., DIETZ, G. P. H., JAKOBS, S., BÄHR, M. & WEISHAUPT, J. H. 2007. Cyclin-dependent kinase 5 is an upstream regulator of mitochondrial fission during neuronal apoptosis. *Cell Death & Differentiation,* 14**,** 651-661.

MILATOVIC, D., YIN, Z., GUPTA, R. C., SIDORYK, M., ALBRECHT, J., ASCHNER, J. L. & ASCHNER, M. 2007. Manganese induces oxidative impairment in cultured rat astrocytes. *Toxicol Sci,* 98**,** 198-205.

MILLER, K., OCHUDLO, S., OPALA, G., SMOLICHA, W. & SIUDA, J. 2003. [Parkinsonism in chronic occupational metallic mercury intoxication]. *Neurol Neurochir Pol,* 37 Suppl 5**,** 31-8.

MIRAGLIA, F., RICCI, A., ROTA, L. & COLLA, E. 2018. Subcellular localization of alpha-synuclein aggregates and their interaction with membranes. 13**,** 1136-1144.

MISKO, A., JIANG, S., WEGORZEWSKA, I., MILBRANDT, J. & BALOH, R. H. 2010. Mitofusin 2 Is Necessary for Transport of Axonal Mitochondria and Interacts with the Miro/Milton Complex. *The Journal of Neuroscience,* 30**,** 4232.

MIZUSHIMA, N., YOSHIMORI, T. & LEVINE, B. 2010. Methods in mammalian autophagy research. *Cell,* 140**,** 313-26.

MIZUSHIMA, N., YOSHIMORI, T. & OHSUMI, Y. 2011. The role of Atg proteins in autophagosome formation. *Annu Rev Cell Dev Biol,* 27**,** 107-32.

MO, R. K., WANG, J., HUANG, J. Y., WEN, Q. L. & HUANG, J. F. 2016. *Influence of manganese exposure via intracerebral injection on behavioristics and substantia nigra dopaminergic neurons in rats*.

MOGI, M., HARADA, M., KONDO, T., NARABAYASHI, H., RIEDERER, P. & NAGATSU, T. 1995. Transforming growth factor-β1 levels are elevated in the striatum and in ventricular cerebrospinal fluid in Parkinson's disease. *Neuroscience Letters,* 193**,** 129-132.

MOGI, M., HARADA, M., NARABAYASHI, H., INAGAKI, H., MINAMI, M. & NAGATSU, T. 1996. Interleukin (IL)-1β, IL-2, IL-4, IL-6 and transforming growth factor-α levels are elevated in ventricular cerebrospinal fluid in juvenile parkinsonism and Parkinson's disease. *Neuroscience Letters,* 211**,** 13-16.

MOGI, M., HARADA, M., RIEDERER, P., NARABAYASHI, H., FUJITA, K. & NAGATSU, T. 1994. Tumor necrosis factor-α (TNF-α) increases both in the brain and in the cerebrospinal fluid from parkinsonian patients. *Neuroscience Letters,* 165**,** 208-210.

MOON, H. E. & PAEK, S. H. 2015. Mitochondrial Dysfunction in Parkinson's Disease. *Experimental neurobiology,* 24**,** 103-116.

MOORS, T. E., HOOZEMANS, J. J. M., INGRASSIA, A., BECCARI, T., PARNETTI, L., CHARTIER-HARLIN, M.-C. & VAN DE BERG, W. D. J. J. M. N. 2017. Therapeutic potential of autophagy-enhancing agents in Parkinson's disease. 12**,** 11.

MORAIS, V. A., HADDAD, D., CRAESSAERTS, K., DE BOCK, P. J., SWERTS, J., VILAIN, S., AERTS, L., OVERBERGH, L., GRÜNEWALD, A., SEIBLER, P., KLEIN, C., GEVAERT, K., VERSTREKEN, P. & DE STROOPER, B. 2014. PINK1 loss-of-function mutations affect mitochondrial complex I activity via NdufA10 ubiquinone uncoupling. *Science,* 344**,** 203-7.

MORAIS, V. A., VERSTREKEN, P., ROETHIG, A., SMET, J., SNELLINX, A., VANBRABANT, M., HADDAD, D., FREZZA, C., MANDEMAKERS, W., VOGT-WEISENHORN, D., VAN COSTER, R., WURST, W., SCORRANO, L. & DE STROOPER, B. 2009. Parkinson's disease mutations in PINK1 result in decreased Complex I activity and deficient synaptic function. *EMBO Mol Med,* 1**,** 99-111.

MORENO, J. A., STREIFEL, K. M., SULLIVAN, K. A., LEGARE, M. E. & TJALKENS, R. B. 2009. Developmental exposure to manganese increases adult susceptibility to inflammatory activation of glia and neuronal protein nitration. *Toxicol Sci,* 112**,** 405-15.

MORENO, J. A., SULLIVAN, K. A., CARBONE, D. L., HANNEMAN, W. H. & TJALKENS, R. B. 2008. Manganese potentiates nuclear factor-kappaB-dependent expression of nitric oxide synthase 2 in astrocytes by activating soluble guanylate cyclase and extracellular responsive kinase signaling pathways. *J Neurosci Res,* 86**,** 2028-38.

MOUNT, M. P., LIRA, A., GRIMES, D., SMITH, P. D., FAUCHER, S., SLACK, R., ANISMAN, H., HAYLEY, S. & PARK, D. S. 2007. Involvement of interferon-gamma in microglial-mediated loss of dopaminergic neurons. *J Neurosci,* 27**,** 3328-37.

MUKHOPADHYAY, S. & LINSTEDT, A. D. 2011. Identification of a gain-of-function mutation in a Golgi P-type ATPase that enhances Mn2+ efflux and protects against toxicity. *Proc Natl Acad Sci U S A,* 108**,** 858-63.

MULLIN, S. & SCHAPIRA, A. 2013. α-Synuclein and mitochondrial dysfunction in Parkinson's disease. *Molecular neurobiology,* 47**,** 587-597.

MURPHY, K. E., GYSBERS, A. M., ABBOTT, S. K., TAYEBI, N., KIM, W. S., SIDRANSKY, E., COOPER, A., GARNER, B. & HALLIDAY, G. M. 2014. Reduced

glucocerebrosidase is associated with increased α-synuclein in sporadic Parkinson's disease. *Brain,* 137**,** 834-48.

NAKAMURA, K., NEMANI, V., AZARBAL, F., SKIBINSKI, G., LEVY, J., EGAMI, K., MUNISHKINA, L., ZHANG, J., GARDNER, B., WAKABAYASHI, J., SESAKI, H., CHENG, Y., FINKBEINER, S., NUSSBAUM, R., MASLIAH, E. & EDWARDS, R. 2011. Direct membrane association drives mitochondrial fission by the Parkinson disease-associated protein alpha-synuclein. *Journal of Biological Chemistry,* 286**,** 20701-20726.

NAKAMURA, K., NEMANI, V. M., WALLENDER, E. K., KAEHLCKE, K., OTT, M. & EDWARDS, R. H. 2008. Optical reporters for the conformation of alpha-synuclein reveal a specific interaction with mitochondria. *J Neurosci,* 28**,** 12305-17.

NAKAMURA, S. & YOSHIMORI, T. 2017. New insights into autophagosome-lysosome fusion. *J Cell Sci,* 130**,** 1209-1216.

NALLS, M. A., BLAUWENDRAAT, C., VALLERGA, C. L., HEILBRON, K., BANDRES-CIGA, S., CHANG, D., TAN, M., KIA, D. A., NOYCE, A. J., XUE, A., BRAS, J., YOUNG, E., VON COELLN, R., SIMÓN-SÁNCHEZ, J., SCHULTE, C., SHARMA, M., KROHN, L., PIHLSTROM, L., SIITONEN, A., IWAKI, H., LEONARD, H., FAGHRI, F., RAPHAEL GIBBS, J., HERNANDEZ, D. G., SCHOLZ, S. W., BOTIA, J. A., MARTINEZ, M., CORVOL, J.-C., LESAGE, S., JANKOVIC, J., SHULMAN, L. M., SUTHERLAND, M., TIENARI, P., MAJAMAA, K., TOFT, M., ANDREASSEN, O. A., BANGALE, T., BRICE, A., YANG, J., GAN-OR, Z., GASSER, T., HEUTINK, P., SHULMAN, J. M., WOOD, N., HINDS, D. A., HARDY, J. A., MORRIS, H. R., GRATTEN, J., VISSCHER, P. M., GRAHAM, R. R. & SINGLETON, A. B. 2019. Expanding Parkinson’s disease genetics: novel risk loci, genomic context, causal insights and heritable risk. 388165.

NALLS, M. A., PANKRATZ, N., LILL, C. M., DO, C. B., HERNANDEZ, D. G., SAAD, M., DESTEFANO, A. L., KARA, E., BRAS, J., SHARMA, M., SCHULTE, C., KELLER, M. F., AREPALLI, S., LETSON, C., EDSALL, C., STEFANSSON, H., LIU, X., PLINER, H., LEE, J. H., CHENG, R., IKRAM, M. A., IOANNIDIS, J. P., HADJIGEORGIOU, G. M., BIS, J. C., MARTINEZ, M., PERLMUTTER, J. S., GOATE, A., MARDER, K., FISKE, B., SUTHERLAND, M., XIROMERISIOU, G., MYERS, R. H., CLARK, L. N., STEFANSSON, K., HARDY, J. A., HEUTINK, P., CHEN, H., WOOD, N. W., HOULDEN, H., PAYAMI, H., BRICE, A., SCOTT, W. K., GASSER, T., BERTRAM, L., ERIKSSON, N., FOROUD, T., SINGLETON, A. B., , I. P. S. D. G. C., , P. S. S. G. P. S. R. T. O. G. I., 23ANDME, GENEPD, , N. R. C., , H. I. O. H. G., INVESTIGATOR, A. J. D., , C. F. H. A. A. R. I. G. E., , N. A. B. E. C., , U. K. B. E. C., CONSORTIUM, G. P. S. D. & GROUP, A. G. A. 2014. Large-scale meta-analysis of genome-wide association data identifies six new risk loci for Parkinson's disease. *Nat Genet,* 46**,** 989-93.

NAM, J. & KIM, K. 2008. Abnormal motor function and the expression of striatal dopamine D2 receptors in manganese-treated mice. *Biol Pharm Bull,* 31**,** 1894-7.

NANDI, D., TAHILIANI, P., KUMAR, A. & CHANDU, D. 2006. The ubiquitin-proteasome system. *J Biosci,* 31**,** 137-55.

NARENDRA, D., TANAKA, A., SUEN, D. & YOULE, R. 2008. Parkin is recruited selectively to impaired mitochondria and promotes their autophagy. *Journal of Cell Biology,* 183**,** 795-803.

NARHI, L., WOOD, S. J., STEAVENSON, S., JIANG, Y., WU, G. M., ANAFI, D., KAUFMAN, S. A., MARTIN, F., SITNEY, K., DENIS, P., LOUIS, J. C., WYPYCH, J., BIERE, A. L. & CITRON, M. 1999. Both familial Parkinson's disease mutations accelerate alpha-synuclein aggregation. *J Biol Chem,* 274**,** 9843-6.

NASCA, A., NARDECCHIA, F., COMMONE, A., SEMERARO, M., LEGATI, A., GARAVAGLIA, B., GHEZZI, D. & LEUZZI, V. 2018. Clinical and Biochemical Features in a Patient With Mitochondrial Fission Factor Gene Alteration. *Frontiers in genetics*, 9**,** 625-625.

NAUDET, N., ANTIER, E., GAILLARD, D., MORIGNAT, E., LAKHDAR, L., BARON, T. & BENCSIK, A. 2017. Oral Exposure to Paraquat Triggers Earlier Expression of Phosphorylated α-Synuclein in the Enteric Nervous System of A53T Mutant Human α-Synuclein Transgenic Mice. *Journal of neuropathology and experimental neurology*, 76**,** 1046-1057.

NICKLAS, W. J., VYAS, I. & HEIKKILA, R. E. 1985. Inhibition of NADH-linked oxidation in brain mitochondria by 1-methyl-4-phenyl-pyridine, a metabolite of the neurotoxin, 1-methyl-4-phenyl-1,2,5,6-tetrahydropyridine. *Life Sci*, 36**,** 2503-8.

NIKOLETOPOULOU, V., MARKAKI, M., PALIKARAS, K. & TAVERNARAKIS, N. 2013. Crosstalk between apoptosis, necrosis and autophagy. *Biochimica et Biophysica Acta (BBA) - Molecular Cell Research*, 1833**,** 3448-3459.

NISCHWITZ, V., BERTHELE, A. & MICHALKE, B. 2008. Speciation analysis of selected metals and determination of their total contents in paired serum and cerebrospinal fluid samples: An approach to investigate the permeability of the human blood-cerebrospinal fluid-barrier. *Anal Chim Acta*, 627**,** 258-69.

NIXON, R. A. 2013. The role of autophagy in neurodegenerative disease. *Nat Med*, 19**,** 983-97.

NORRIS, E. H., URYU, K., LEIGHT, S., GIASSON, B. I., TROJANOWSKI, J. Q. & LEE, V. M. 2007. Pesticide exposure exacerbates alpha-synucleinopathy in an A53T transgenic mouse model. *Am J Pathol*, 170**,** 658-66.

NUMADATE, A., MITA, Y., MATSUMOTO, Y., FUJII, S. & HASHIMOTO, Y. 2014. Development of 2-thioxoquinazoline-4-one derivatives as dual and selective inhibitors of dynamin-related protein 1 (Drp1) and puromycin-sensitive aminopeptidase (PSA). *Chem Pharm Bull (Tokyo)*, 62**,** 979-88.

O'DONNELL, K. C., LULLA, A., STAHL, M. C., WHEAT, N. D., BRONSTEIN, J. M. & SAGASTI, A. 2014. Axon degeneration and PGC-1alpha-mediated protection in a zebrafish model of alpha-synuclein toxicity. *Dis Model Mech*, 7**,** 571-82.

O'NEAL, S. & ZHENG, W. 2015. *Manganese Toxicity Upon Overexposure: A Decade in Review*.

O'NEAL, S. L., LEE, J.-W., ZHENG, W. & CANNON, J. R. 2014. Subacute manganese exposure in rats is a neurochemical model of early manganese toxicity. *Neurotoxicology*, 44**,** 303-313.

OGUNRIN, O., KOMOLAFE, M., SANYA, E., OSUBOR, C., AJOSE, O., A AKANDE, A. & MOSAKU, K. 2013. *Trace Metals in Patients with Parkinson's Disease: A Multi-Center Case-Control Study of Nigerian Patients*.

OKAMOTO, K., PERLMAN, P. S. & BUTOW, R. A. 2001. Targeting of green fluorescent protein to mitochondria. *Methods Cell Biol*, 65**,** 277-83.

OKAMOTO, Y., OSHIMA, R., INAGAKI, K., AITA, S., NISIOKA, H., KONDO, Y., ISHIZUKA, H., TAKADA, J. & NISHIDA, M. 1997. The presence of a manganese-rich particle in lysosome of rat pancreas due to excess manganese treatment. *Biochem Mol Biol Int*, 41**,** 389-94.

OKATSU, K., UNO, M., KOYANO, F., GO, E., KIMURA, M., OKA, T., TANAKA, K. & MATSUDA, N. 2013. A dimeric PINK1-containing complex on depolarized mitochondria stimulates Parkin recruitment. *J Biol Chem*, 288**,** 36372-84.

OLANOW, C. W., GOOD, P. F., SHINOTOH, H., HEWITT, K. A., VINGERHOETS, F., SNOW, B. J., BEAL, M. F., CALNE, D. B. & PERL, D. P. 1996. Manganese

intoxication in the rhesus monkey: a clinical, imaging, pathologic, and biochemical study. *Neurology,* 46**,** 492-8.
OLANOW, C. W., PERL, D. P., DEMARTINO, G. N. & MCNAUGHT, K. S. 2004. Lewy-body formation is an aggresome-related process: a hypothesis. *Lancet Neurol,* 3**,** 496-503.
OLSEN, M. L., HIGASHIMORI, H., CAMPBELL, S. L., HABLITZ, J. J. & SONTHEIMER, H. 2006. Functional expression of Kir4.1 channels in spinal cord astrocytes. *Glia,* 53**,** 516-28.
ORDONEZ-LIBRADO, J. L., ANAYA-MARTINEZ, V., GUTIERREZ-VALDEZ, A. L., COLIN-BARENQUE, L., MONTIEL-FLORES, E. & AVILA-COSTA, M. R. 2010. Manganese inhalation as a Parkinson disease model. *Parkinsons Dis,* 2011**,** 612989.
OSELLAME, L. D., RAHIM, A. A., HARGREAVES, I. P., GEGG, M. E., RICHARD-LONDT, A., BRANDNER, S., WADDINGTON, S. N., SCHAPIRA, A. H. & DUCHEN, M. R. 2013. Mitochondria and quality control defects in a mouse model of Gaucher disease--links to Parkinson's disease. *Cell Metab,* 17**,** 941-53.
PALACINO, J. J., SAGI, D., GOLDBERG, M. S., KRAUSS, S., MOTZ, C., WACKER, M., KLOSE, J. & SHEN, J. 2004. Mitochondrial dysfunction and oxidative damage in parkin-deficient mice. *J Biol Chem,* 279**,** 18614-22.
PALMIERI, M., IMPEY, S., KANG, H., DI RONZA, A., PELZ, C., SARDIELLO, M. & BALLABIO, A. 2011. Characterization of the CLEAR network reveals an integrated control of cellular clearance pathways. *Human Molecular Genetics,* 20**,** 3852-3866.
PAN-MONTOJO, F., SCHWARZ, M., WINKLER, C., ARNHOLD, M., O'SULLIVAN, G. A., PAL, A., SAID, J., MARSICO, G., VERBAVATZ, J. M., RODRIGO-ANGULO, M., GILLE, G., FUNK, R. H. & REICHMANN, H. 2012. Environmental toxins trigger PD-like progression via increased alpha-synuclein release from enteric neurons in mice. *Sci Rep,* 2**,** 898.
PANKIV, S., CLAUSEN, T. H., LAMARK, T., BRECH, A., BRUUN, J. A., OUTZEN, H., OVERVATN, A., BJORKOY, G. & JOHANSEN, T. 2007. p62/SQSTM1 binds directly to Atg8/LC3 to facilitate degradation of ubiquitinated protein aggregates by autophagy. *J Biol Chem,* 282**,** 24131-45.
PAPAVASILIOU, P., MILLER, S. & COTZIAS, G. 1966. Role of liver in regulating distribution and excretion of manganese. 211**,** 211-216.
PARIHAR, M. S., PARIHAR, A., FUJITA, M., HASHIMOTO, M. & GHAFOURIFAR, P. 2008. Mitochondrial association of alpha-synuclein causes oxidative stress. *Cell Mol Life Sci,* 65**,** 1272-84.
PARK, J.-S., DAVIS, R. L. & SUE, C. M. 2018. Mitochondrial Dysfunction in Parkinson's Disease: New Mechanistic Insights and Therapeutic Perspectives. *Current neurology and neuroscience reports,* 18**,** 21-21.
PARK, J., LEE, D. G., KIM, B., PARK, S. J., KIM, J. H., LEE, S. R., CHANG, K. T., LEE, H. S. & LEE, D. S. 2015a. Iron overload triggers mitochondrial fragmentation via calcineurin-sensitive signals in HT-22 hippocampal neuron cells. *Toxicology,* 337**,** 39-46.
PARK, J. D., CHUNG, Y. H., KIM, C. Y., HA, C. S., YANG, S. O., KHANG, H. S., YU, I. K., CHEONG, H. K., LEE, J. S., SONG, C. W., KWON, I. H., HAN, J. H., SUNG, J. H., HEO, J. D., CHOI, B. S., IM, R., JEONG, J. & YU, I. J. 2007. Comparison of high MRI T1 signals with manganese concentration in brains of cynomolgus monkeys after 8 months of stainless steel welding-fume exposure. *Inhal Toxicol,* 19**,** 965-71.
PARK, J. H., HOGREBE, M., GRUNEBERG, M., DUCHESNE, I., VON DER HEIDEN, A. L., REUNERT, J., SCHLINGMANN, K. P., BOYCOTT, K. M., BEAULIEU, C. L., MHANNI, A. A., INNES, A. M., HORTNAGEL, K., BISKUP, S., GLEIXNER, E. M.,

KURLEMANN, G., FIEDLER, B., OMRAN, H., RUTSCH, F., WADA, Y., TSIAKAS, K., SANTER, R., NEBERT, D. W., RUST, S. & MARQUARDT, T. 2015b. SLC39A8 Deficiency: A Disorder of Manganese Transport and Glycosylation. *Am J Hum Genet,* 97**,** 894-903.

PARKINSON, J. 2002. An essay on the shaking palsy. 1817. *J Neuropsychiatry Clin Neurosci,* 14**,** 223-36; discussion 222.

PENEDER, T. M., SCHOLZE, P., BERGER, M. L., REITHER, H., HEINZE, G., BERTL, J., BAUER, J., RICHFIELD, E. K., HORNYKIEWICZ, O. & PIFL, C. 2011. Chronic exposure to manganese decreases striatal dopamine turnover in human alpha-synuclein transgenic mice. *Neuroscience,* 180**,** 280-92.

PERES, T. V., EYNG, H., LOPES, S. C., COLLE, D., GONCALVES, F. M., VENSKE, D. K., LOPES, M. W., BEN, J., BORNHORST, J., SCHWERDTLE, T., ASCHNER, M., FARINA, M., PREDIGER, R. D. & LEAL, R. B. 2015. Developmental exposure to manganese induces lasting motor and cognitive impairment in rats. *Neurotoxicology,* 50**,** 28-37.

PERES, T. V., PARMALEE, N. L., MARTINEZ-FINLEY, E. J. & ASCHNER, M. 2016a. Untangling the Manganese-alpha-Synuclein Web. *Front Neurosci,* 10**,** 364.

PERES, T. V., SCHETTINGER, M. R., CHEN, P., CARVALHO, F., AVILA, D. S., BOWMAN, A. B. & ASCHNER, M. 2016b. "Manganese-induced neurotoxicity: a review of its behavioral consequences and neuroprotective strategies". *BMC Pharmacol Toxicol,* 17**,** 57.

PEREZ, R. G., WAYMIRE, J. C., LIN, E., LIU, J. J., GUO, F. & ZIGMOND, M. J. 2002. A role for alpha-synuclein in the regulation of dopamine biosynthesis. *J Neurosci,* 22**,** 3090-9.

PERIQUET, M., CORTI, O., JACQUIER, S. & BRICE, A. 2005. Proteomic analysis of parkin knockout mice: alterations in energy metabolism, protein handling and synaptic function. *J Neurochem,* 95**,** 1259-76.

PERL, D. P. & OLANOW, C. W. 2007. The neuropathology of manganese-induced Parkinsonism. *J Neuropathol Exp Neurol,* 66**,** 675-82.

PHAM, A. H., CHU, Q. N., MENG, S. & CHAN, D. C. 2012. Loss of Mfn2 results in progressive, retrograde degeneration of dopaminergic neurons in the nigrostriatal circuit. *Human Molecular Genetics,* 21**,** 4817-4826.

PIAO, Y., KIM, H. G., OH, M. S. & PAK, Y. K. 2012. Overexpression of TFAM, NRF-1 and myr-AKT protects the MPP(+)-induced mitochondrial dysfunctions in neuronal cells. *Biochim Biophys Acta,* 1820**,** 577-85.

PICCOLI, C., RIPOLI, M., QUARATO, G., SCRIMA, R., D'APRILE, A., BOFFOLI, D., MARGAGLIONE, M., CRISCUOLO, C., DE MICHELE, G., SARDANELLI, A., PAPA, S. & CAPITANIO, N. 2008. Coexistence of mutations in PINK1 and mitochondrial DNA in early onset parkinsonism. *J Med Genet,* 45**,** 596-602.

PIERREL, F., COBINE, P. A. & WINGE, D. R. 2007. Metal Ion availability in mitochondria. *Biometals,* 20**,** 675-82.

PIFL, C., KHORCHIDE, M., KATTINGER, A., REITHER, H., HARDY, J. & HORNYKIEWICZ, O. 2004. alpha-Synuclein selectively increases manganese-induced viability loss in SK-N-MC neuroblastoma cells expressing the human dopamine transporter. *Neuroscience letters,* 354**,** 34-37.

PINAL, C. S. & TOBIN, A. J. 1998. Uniqueness and redundancy in GABA production. *Perspect Dev Neurobiol,* 5**,** 109-18.

PINNELL, J. & TIEU, K. 2017. Mitochondrial Dynamics in Neurodegenerative Diseases.

PISANI, V., STEFANI, A., PIERANTOZZI, M., NATOLI, S., STANZIONE, P., FRANCIOTTA, D. & PISANI, A. 2012. Increased blood-cerebrospinal fluid transfer of albumin in advanced Parkinson's disease. *J Neuroinflammation,* 9**,** 188.

PITTS, K. R., YOON, Y., KRUEGER, E. W. & MCNIVEN, M. A. 1999. The dynamin-like protein DLP1 is essential for normal distribution and morphology of the endoplasmic reticulum and mitochondria in mammalian cells. *Mol Biol Cell,* 10**,** 4403-17.

PLOWEY, E. D., CHERRA, S. J., LIU, Y. J. & CHU, C. T. 2008. Role of autophagy in G2019S-LRRK2-associated neurite shortening in differentiated SH-SY5Y cells. *J Neurochem,* 105**,** 1048-56.

POLYMEROPOULOS, M. H., LAVEDAN, C., LEROY, E., IDE, S. E., DEHEJIA, A., DUTRA, A., PIKE, B., ROOT, H., RUBENSTEIN, J., BOYER, R., STENROOS, E. S., CHANDRASEKHARAPPA, S., ATHANASSIADOU, A., PAPAPETROPOULOS, T., JOHNSON, W. G., LAZZARINI, A. M., DUVOISIN, R. C., DI IORIO, G., GOLBE, L. I. & NUSSBAUM, R. L. 1997. Mutation in the alpha-synuclein gene identified in families with Parkinson's disease. *Science,* 276**,** 2045-7.

POOLE, A. C., THOMAS, R. E., ANDREWS, L. A., MCBRIDE, H. M., WHITWORTH, A. J. & PALLANCK, L. J. 2008. The PINK1/Parkin pathway regulates mitochondrial morphology. *Proc Natl Acad Sci U S A,* 105**,** 1638-43.

PRICE, K. S., FARLEY, I. J. & HORNYKIEWICZ, O. 1978. Neurochemistry of Parkinson's disease: relation between striatal and limbic dopamine. *Adv Biochem Psychopharmacol,* 19**,** 293-300.

PROTS, I., GROSCH, J., BRAZDIS, R.-M., SIMMNACHER, K., VEBER, V., HAVLICEK, S., HANNAPPEL, C., KRACH, F., KRUMBIEGEL, M., SCHÜTZ, O., REIS, A., WRASIDLO, W., GALASKO, D. R., GROEMER, T. W., MASLIAH, E., SCHLÖTZER-SCHREHARDT, U., XIANG, W., WINKLER, J. & WINNER, B. 2018. α-Synuclein oligomers induce early axonal dysfunction in human iPSC-based models of synucleinopathies. 115**,** 7813-7818.

PROTS, I., VEBER, V., BREY, S., CAMPIONI, S., BUDER, K., RIEK, R., BOHM, K. J. & WINNER, B. 2013. alpha-Synuclein oligomers impair neuronal microtubule-kinesin interplay. *J Biol Chem,* 288**,** 21742-54.

PROUKAKIS, C., DUDZIK, C. G., BRIER, T., MACKAY, D. S., COOPER, J. M., MILLHAUSER, G. L., HOULDEN, H. & SCHAPIRA, A. H. 2013. A novel α-synuclein missense mutation in Parkinson disease. 80**,** 1062-1064.

PRYDE, K. R., SMITH, H. L., CHAU, K. Y. & SCHAPIRA, A. H. 2016. PINK1 disables the anti-fission machinery to segregate damaged mitochondria for mitophagy. *J Cell Biol,* 213**,** 163-71.

PRZEDBORSKI, S. 2017. The two-century journey of Parkinson disease research. *Nat Rev Neurosci,* 18**,** 251-259.

PUERTOLLANO, R., FERGUSON, S. M., BRUGAROLAS, J. & BALLABIO, A. 2018. The complex relationship between TFEB transcription factor phosphorylation and subcellular localization. *The EMBO Journal,* 37**,** e98804.

PURISAI, M. G., MCCORMACK, A. L., CUMINE, S., LI, J., ISLA, M. Z. & DI MONTE, D. A. 2007. Microglial activation as a priming event leading to paraquat-induced dopaminergic cell degeneration. *Neurobiol Dis,* 25**,** 392-400.

PURNELL, P. R. & FOX, H. S. 2013. Autophagy-mediated turnover of dynamin-related protein 1. *BMC Neurosci,* 14**,** 86.

QI, X., QVIT, N., SU, Y. C. & MOCHLY-ROSEN, D. 2013. A novel Drp1 inhibitor diminishes aberrant mitochondrial fission and neurotoxicity. *J Cell Sci,* 126**,** 789-802.

QUADRI, M., FEDERICO, A., ZHAO, T., BREEDVELD, G. J., BATTISTI, C., DELNOOZ, C., SEVERIJNEN, L. A., DI TORO MAMMARELLA, L., MIGNARRI, A., MONTI,

L., SANNA, A., LU, P., PUNZO, F., COSSU, G., WILLEMSEN, R., RASI, F., OOSTRA, B. A., VAN DE WARRENBURG, B. P. & BONIFATI, V. 2012. Mutations in SLC30A10 cause parkinsonism and dystonia with hypermanganesemia, polycythemia, and chronic liver disease. *Am J Hum Genet,* 90**,** 467-77.

RABANAL-RUIZ, Y. & KOROLCHUK, V. I. 2018. mTORC1 and Nutrient Homeostasis: The Central Role of the Lysosome. *Int J Mol Sci,* 19.

RACETTE, B. A., SEARLES NIELSEN, S., CRISWELL, S. R., SHEPPARD, L., SEIXAS, N., WARDEN, M. N. & CHECKOWAY, H. 2017. Dose-dependent progression of parkinsonism in manganese-exposed welders. *Neurology,* 88**,** 344.

RADOSHEVICH, L., MURROW, L., CHEN, N., FERNANDEZ, E., ROY, S., FUNG, C. & DEBNATH, J. 2010. ATG12 Conjugation to ATG3 Regulates Mitochondrial Homeostasis and Cell Death. *Cell,* 142**,** 590-600.

RAHIL-KHAZEN, R., BOLANN, B. J., MYKING, A. & ULVIK, R. J. 2002. Multi-element analysis of trace element levels in human autopsy tissues by using inductively coupled atomic emission spectrometry technique (ICP-AES). *J Trace Elem Med Biol,* 16**,** 15-25.

RAMBOLD, A. S., KOSTELECKY, B., ELIA, N. & LIPPINCOTT-SCHWARTZ, J. 2011. Tubular network formation protects mitochondria from autophagosomal degradation during nutrient starvation. 108**,** 10190-10195.

RAMBOLD, A. S. & PEARCE, E. L. 2018. Mitochondrial Dynamics at the Interface of Immune Cell Metabolism and Function. *Trends in Immunology,* 39**,** 6-18.

RAMIREZ, A., HEIMBACH, A., GRÜNDEMANN, J., STILLER, B., HAMPSHIRE, D., CID, L. P., GOEBEL, I., MUBAIDIN, A. F., WRIEKAT, A. L., ROEPER, J., AL-DIN, A., HILLMER, A. M., KARSAK, M., LISS, B., WOODS, C. G., BEHRENS, M. I. & KUBISCH, C. 2006. Hereditary parkinsonism with dementia is caused by mutations in ATP13A2, encoding a lysosomal type 5 P-type ATPase. *Nat Genet,* 38**,** 1184-91.

RAMONET, D., PODHAJSKA, A., STAFA, K., SONNAY, S., TRANCIKOVA, A., TSIKA, E., PLETNIKOVA, O., TRONCOSO, J. C., GLAUSER, L. & MOORE, D. J. 2011. PARK9-associated ATP13A2 localizes to intracellular acidic vesicles and regulates cation homeostasis and neuronal integrity. *Human Molecular Genetics,* 21**,** 1725-1743.

RAO, K. V. & NORENBERG, M. D. 2004. Manganese induces the mitochondrial permeability transition in cultured astrocytes. *J Biol Chem,* 279**,** 32333-8.

RAPPOLD, P. M., CUI, M., CHESSER, A. S., TIBBETT, J., GRIMA, J. C., DUAN, L., SEN, N., JAVITCH, J. A. & TIEU, K. 2011. Paraquat neurotoxicity is mediated by the dopamine transporter and organic cation transporter-3. *PNAS,* 108**,** 20766-20771.

RAPPOLD, P. M., CUI, M., GRIMA, J. C., FAN, R. Z., DE MESY-BENTLEY, K. L., CHEN, L., ZHUANG, X., BOWERS, W. J. & TIEU, K. 2014. Drp1 inhibition attenuates neurotoxicity and dopamine release deficits in vivo. *Nature Communications,* 5**,** 5244.

REANEY, S. H., BENCH, G. & SMITH, D. R. 2006. Brain accumulation and toxicity of Mn(II) and Mn(III) exposures. *Toxicol Sci,* 93**,** 114-24.

REANEY, S. H., KWIK-URIBE, C. L. & SMITH, D. R. 2002. Manganese oxidation state and its implications for toxicity. *Chem Res Toxicol,* 15**,** 1119-26.

RECASENS, A., DEHAY, B., BOVE, J., CARBALLO-CARBAJAL, I., DOVERO, S., PEREZ-VILLALBA, A., FERNAGUT, P. O., BLESA, J., PARENT, A., PERIER, C., FARINAS, I., OBESO, J. A., BEZARD, E. & VILA, M. 2014. Lewy body extracts from Parkinson disease brains trigger alpha-synuclein pathology and neurodegeneration in mice and monkeys. *Ann Neurol,* 75**,** 351-62.

REDDI, A. R., JENSEN, L. T., NARANUNTARAT, A., ROSENFELD, L., LEUNG, E., SHAH, R. & CULOTTA, V. C. 2009. The overlapping roles of manganese and Cu/Zn SOD in oxidative stress protection. *Free Radic Biol Med,* 46**,** 154-62.

REEVE, A., SIMCOX, E. & TURNBULL, D. 2014. Ageing and Parkinson's disease: why is advancing age the biggest risk factor? *Ageing Res Rev,* 14**,** 19-30.

REEVE, A. K., LUDTMANN, M. H., ANGELOVA, P. R., SIMCOX, E. M., HORROCKS, M. H., KLENERMAN, D., GANDHI, S., TURNBULL, D. M. & ABRAMOV, A. Y. 2015. Aggregated alpha-synuclein and complex I deficiency: exploration of their relationship in differentiated neurons. *Cell Death Dis,* 6**,** e1820.

RENTSCHLER, G., COVOLO, L., HADDAD, A. A., LUCCHINI, R. G., ZONI, S. & BROBERG, K. 2012. ATP13A2 (PARK9) polymorphisms influence the neurotoxic effects of manganese. *Neurotoxicology,* 33**,** 697-702.

RICHARDSON, J. R., QUAN, Y., SHERER, T. B., GREENAMYRE, J. T. & MILLER, G. W. 2005. Paraquat neurotoxicity is distinct from that of MPTP and rotenone. *Toxicol Sci,* 88**,** 193-201.

RIEKER, C., DEV, K. K., LEHNHOFF, K., BARBIERI, S., KSIAZEK, I., KAUFFMANN, S., DANNER, S., SCHELL, H., BODEN, C., RUEGG, M. A., KAHLE, P. J., VAN DER PUTTEN, H. & SHIMSHEK, D. R. 2011. Neuropathology in Mice Expressing Mouse Alpha-Synuclein. *PLOS ONE,* 6**,** e24834.

RILEY, L. G., COWLEY, M. J., GAYEVSKIY, V., ROSCIOLI, T., THORBURN, D. R., PRELOG, K., BAHLO, M., SUE, C. M., BALASUBRAMANIAM, S. & CHRISTODOULOU, J. 2017. A SLC39A8 variant causes manganese deficiency, and glycosylation and mitochondrial disorders. *J Inherit Metab Dis,* 40**,** 261-269.

RITE, I., MACHADO, A., CANO, J. & VENERO, J. L. 2007. Blood-brain barrier disruption induces in vivo degeneration of nigral dopaminergic neurons. *J Neurochem,* 101**,** 1567-82.

ROBERTS, R. F., WADE-MARTINS, R. & ALEGRE-ABARRATEGUI, J. 2015. Direct visualization of alpha-synuclein oligomers reveals previously undetected pathology in Parkinson's disease brain. *Brain,* 138**,** 1642-1657.

ROBISON, G., SULLIVAN, B., CANNON, J. R. & PUSHKAR, Y. 2015. Identification of dopaminergic neurons of the substantia nigra pars compacta as a target of manganese accumulation. *Metallomics,* 7**,** 748-55.

ROBISON, G., ZAKHAROVA, T., FU, S., JIANG, W., FULPER, R., BARREA, R., MARCUS, M. A., ZHENG, W. & PUSHKAR, Y. 2012. X-ray fluorescence imaging: a new tool for studying manganese neurotoxicity. *PloS one,* 7**,** e48899-e48899.

ROCHA, E. M., DE MIRANDA, B. & SANDERS, L. H. 2018. Alpha-synuclein: Pathology, mitochondrial dysfunction and neuroinflammation in Parkinson's disease. *Neurobiol Dis,* 109**,** 249-257.

ROCHA, E. M., SMITH, G. A., PARK, E., CAO, H., BROWN, E., HAYES, M. A., BEAGAN, J., MCLEAN, J. R., IZEN, S. C., PEREZ-TORRES, E., HALLETT, P. J. & ISACSON, O. 2015. Glucocerebrosidase gene therapy prevents alpha-synucleinopathy of midbrain dopamine neurons. *Neurobiol Dis,* 82**,** 495-503.

ROCK, K. L., GRAMM, C., ROTHSTEIN, L., CLARK, K., STEIN, R., DICK, L., HWANG, D. & GOLDBERG, A. L. 1994. Inhibitors of the proteasome block the degradation of most cell proteins and the generation of peptides presented on MHC class I molecules. *Cell,* 78**,** 761-71.

ROCKENSTEIN, E., NUBER, S., OVERK, C. R., UBHI, K., MANTE, M., PATRICK, C., ADAME, A., TREJO-MORALES, M., GEREZ, J., PICOTTI, P., JENSEN, P. H., CAMPIONI, S., RIEK, R., WINKLER, J., GAGE, F. H., WINNER, B. & MASLIAH, E. 2014. Accumulation of oligomer-prone alpha-synuclein exacerbates synaptic and neuronal degeneration in vivo. *Brain,* 137**,** 1496-513.

RODENBURG, R. J. 2016. Mitochondrial complex I-linked disease. *Biochimica et Biophysica Acta (BBA) - Bioenergetics,* 1857**,** 938-945.

RODIER, J. 1955. Manganese poisoning in Moroccan miners. *Br J Ind Med,* 12**,** 21-35.
ROSTOVTSEVA, T. K., GURNEV, P. A., PROTCHENKO, O., HOOGERHEIDE, D. P., YAP, T. L., PHILPOTT, C. C., LEE, J. C. & BEZRUKOV, S. M. 2015. alpha-Synuclein Shows High Affinity Interaction with Voltage-dependent Anion Channel, Suggesting Mechanisms of Mitochondrial Regulation and Toxicity in Parkinson Disease. *J Biol Chem,* 290**,** 18467-77.
ROTH, J. A. 2006. Homeostatic and toxic mechanisms regulating manganese uptake, retention, and elimination. *Biol Res,* 39**,** 45-57.
ROTH, J. A. 2014. Correlation between the biochemical pathways altered by mutated parkinson-related genes and chronic exposure to manganese. *Neurotoxicology,* 44**,** 314-25.
ROTH, J. A. & EICHHORN, M. 2013. Down-regulation of LRRK2 in control and DAT transfected HEK cells increases manganese-induced oxidative stress and cell toxicity. *Neurotoxicology,* 37**,** 100-7.
ROTH, J. A., SINGLETON, S., FENG, J., GARRICK, M. & PARADKAR, P. N. 2010. Parkin regulates metal transport via proteasomal degradation of the 1B isoforms of divalent metal transporter 1. *J Neurochem,* 113**,** 454-64.
ROTHSTEIN, J. D., DYKES-HOBERG, M., PARDO, C. A., BRISTOL, L. A., JIN, L., KUNCL, R. W., KANAI, Y., HEDIGER, M. A., WANG, Y., SCHIELKE, J. P. & WELTY, D. F. 1996. Knockout of glutamate transporters reveals a major role for astroglial transport in excitotoxicity and clearance of glutamate. *Neuron,* 16**,** 675-86.
RUIPÉREZ, V., DARIOS, F. & DAVLETOV, B. 2010. Alpha-synuclein, lipids and Parkinson's disease. *Progress in Lipid Research,* 49**,** 420-428.
RUSSELL, R. C., TIAN, Y., YUAN, H., PARK, H. W., CHANG, Y.-Y., KIM, J., KIM, H., NEUFELD, T. P., DILLIN, A. & GUAN, K.-L. 2013. ULK1 induces autophagy by phosphorylating Beclin-1 and activating VPS34 lipid kinase. *Nature cell biology,* 15**,** 741-750.
RYBICKI, B. A., JOHNSON, C. C., UMAN, J. & GORELL, J. M. 1993. Parkinson's disease mortality and the industrial use of heavy metals in Michigan. *Mov Disord,* 8**,** 87-92.
SADLER, P. J. 1982. Trace elements in human and animal nutrition: by E J Underwood, Academic Press, New York. Fourth Edition 1977. pp 545. £31.20. ISBN 0-12-709065-7. *Biochemical Education,* 10**,** 36-36.
SAIJO, K., WINNER, B., CARSON, C. T., COLLIER, J. G., BOYER, L., ROSENFELD, M. G., GAGE, F. H. & GLASS, C. K. 2009. A Nurr1/CoREST pathway in microglia and astrocytes protects dopaminergic neurons from inflammation-induced death. *Cell,* 137**,** 47-59.
SALVADOR, G. A., URANGA, R. M. & GIUSTO, N. M. 2010. Iron and mechanisms of neurotoxicity. *Int J Alzheimers Dis,* 2011**,** 720658.
SAMARANCH, L., LORENZO-BETANCOR, O., ARBELO, J. M., FERRER, I., LORENZO, E., IRIGOYEN, J., PASTOR, M. A., MARRERO, C., ISLA, C., HERRERA-HENRIQUEZ, J. & PASTOR, P. 2010. PINK1-linked parkinsonism is associated with Lewy body pathology. *Brain,* 133**,** 1128-42.
SÁNCHEZ-DANÉS, A., RICHAUD-PATIN, Y., CARBALLO-CARBAJAL, I., JIMÉNEZ-DELGADO, S., CAIG, C., MORA, S., DI GUGLIELMO, C., EZQUERRA, M., PATEL, B., GIRALT, A., CANALS, J. M., MEMO, M., ALBERCH, J., LÓPEZ-BARNEO, J., VILA, M., CUERVO, A. M., TOLOSA, E., CONSIGLIO, A. & RAYA, A. 2012. Disease-specific phenotypes in dopamine neurons from human iPS-based models of genetic and sporadic Parkinson's disease. *EMBO Molecular Medicine,* 4**,** 380-395.

SANDERS, L. H., PAUL, K. C., HOWLETT, E. H., LAWAL, H., BOPPANA, S., BRONSTEIN, J. M., RITZ, B. & GREENAMYRE, J. T. 2017. Editor's Highlight: Base Excision Repair Variants and Pesticide Exposure Increase Parkinson's Disease Risk. *Toxicol Sci,* 158**,** 188-198.

SARAFIAN, T. A., RYAN, C. M., SOUDA, P., MASLIAH, E., KAR, U. K., VINTERS, H. V., MATHERN, G. W., FAULL, K. F., WHITELEGGE, J. P. & WATSON, J. B. 2013. Impairment of mitochondria in adult mouse brain overexpressing predominantly full-length, N-terminally acetylated human alpha-synuclein. *PLoS One,* 8**,** e63557.

SARDI, S. P., CLARKE, J., KINNECOM, C., TAMSETT, T. J., LI, L., STANEK, L. M., PASSINI, M. A., GRABOWSKI, G. A., SCHLOSSMACHER, M. G., SIDMAN, R. L., CHENG, S. H. & SHIHABUDDIN, L. S. 2011. CNS expression of glucocerebrosidase corrects alpha-synuclein pathology and memory in a mouse model of Gaucher-related synucleinopathy. *Proc Natl Acad Sci U S A,* 108**,** 12101-6.

SARDIELLO, M., PALMIERI, M., DI RONZA, A., MEDINA, D. L., VALENZA, M., GENNARINO, V. A., DI MALTA, C., DONAUDY, F., EMBRIONE, V., POLISHCHUK, R. S., BANFI, S., PARENTI, G., CATTANEO, E. & BALLABIO, A. 2009. A gene network regulating lysosomal biogenesis and function. *Science,* 325**,** 473-7.

SARKAR, S., MALOVIC, E., HARISCHANDRA, D. S., NGWA, H. A., GHOSH, A., HOGAN, C., ROKAD, D., ZENITSKY, G., JIN, H., ANANTHARAM, V., KANTHASAMY, A. G. & KANTHASAMY, A. 2018. Manganese exposure induces neuroinflammation by impairing mitochondrial dynamics in astrocytes. *Neurotoxicology,* 64**,** 204-218.

SASAKI, S., SHIRATA, A., YAMANE, K. & IWATA, M. 2004. Parkin-positive autosomal recessive juvenile Parkinsonism with alpha-synuclein-positive inclusions. *Neurology,* 63**,** 678-82.

SATAKE, W., NAKABAYASHI, Y., MIZUTA, I., HIROTA, Y., ITO, C., KUBO, M., KAWAGUCHI, T., TSUNODA, T., WATANABE, M., TAKEDA, A., TOMIYAMA, H., NAKASHIMA, K., HASEGAWA, K., OBATA, F., YOSHIKAWA, T., KAWAKAMI, H., SAKODA, S., YAMAMOTO, M., HATTORI, N., MURATA, M., NAKAMURA, Y. & TODA, T. 2009. Genome-wide association study identifies common variants at four loci as genetic risk factors for Parkinson's disease. *Nature Genetics,* 41**,** 1303.

SATO, S., UCHIHARA, T., FUKUDA, T., NODA, S., KONDO, H., SAIKI, S., KOMATSU, M., UCHIYAMA, Y., TANAKA, K. & HATTORI, N. 2018. Loss of autophagy in dopaminergic neurons causes Lewy pathology and motor dysfunction in aged mice. *Scientific Reports,* 8**,** 2813.

SCHAPIRA, A. H. 2009. Etiology and pathogenesis of Parkinson disease. *Neurol Clin,* 27**,** 583-603, v.

SCHAPIRA, A. H., COOPER, J. M., DEXTER, D., JENNER, P., CLARK, J. B. & MARSDEN, C. D. 1989. Mitochondrial complex I deficiency in Parkinson's disease. *Lancet,* 1**,** 1269.

SCHERZ-SHOUVAL, R., SHVETS, E., FASS, E., SHORER, H., GIL, L. & ELAZAR, Z. 2007. Reactive oxygen species are essential for autophagy and specifically regulate the activity of Atg4. 26**,** 1749-1760.

SCHNEIDER, J. S., DECAMP, E., CLARK, K., BOUQUIO, C., SYVERSEN, T. & GUILARTE, T. R. 2009. Effects of chronic manganese exposure on working memory in non-human primates. *Brain research,* 1258**,** 86-95.

SCHNEIDER, J. S., DECAMP, E., KOSER, A. J., FRITZ, S., GONCZI, H., SYVERSEN, T. & GUILARTE, T. R. 2006. Effects of chronic manganese exposure on cognitive and motor functioning in non-human primates. *Brain research,* 1118**,** 222-231.

SCHNEIDER, J. S., WILLIAMS, C., AULT, M. & GUILARTE, T. R. 2015. Effects of chronic manganese exposure on attention and working memory in non-human primates. *Neurotoxicology,* 48**,** 217-22.

SCHULER, F. & CASIDA, J. E. 2001. Functional coupling of PSST and ND1 subunits in NADH:ubiquinone oxidoreductase established by photoaffinity labelling. *Biochimica et Biophysica Acta,* 1506**,** 79-87.

SCOTT, I. & YOULE, R. J. 2010. Mitochondrial fission and fusion. *Essays in biochemistry,* 47**,** 85-98.

SEO, Y. A., LI, Y. & WESSLING-RESNICK, M. 2013. Iron depletion increases manganese uptake and potentiates apoptosis through ER stress. *Neurotoxicology,* 38**,** 67-73.

SEO, Y. A. & WESSLING-RESNICK, M. 2015. Ferroportin deficiency impairs manganese metabolism in flatiron mice. *Faseb j,* 29**,** 2726-33.

SETH, P. K. & CHANDRA, S. V. 1984. Neurotransmitters and neurotransmitter receptors in developing and adult rats during manganese poisoning. *Neurotoxicology,* 5**,** 67-76.

SETTEMBRE, C., DI MALTA, C., POLITO, V. A., GARCIA ARENCIBIA, M., VETRINI, F., ERDIN, S., ERDIN, S. U., HUYNH, T., MEDINA, D., COLELLA, P., SARDIELLO, M., RUBINSZTEIN, D. C. & BALLABIO, A. 2011. TFEB links autophagy to lysosomal biogenesis. *Science,* 332**,** 1429-33.

SETTEMBRE, C., ZONCU, R., MEDINA, D. L., VETRINI, F., ERDIN, S., ERDIN, S., HUYNH, T., FERRON, M., KARSENTY, G., VELLARD, M. C., FACCHINETTI, V., SABATINI, D. M. & BALLABIO, A. 2012. A lysosome-to-nucleus signalling mechanism senses and regulates the lysosome via mTOR and TFEB. *The EMBO Journal,* 31**,** 1095-1108.

SHAHMORADIAN, S. H., LEWIS, A. J., GENOUD, C., HENCH, J., MOORS, T. E., NAVARRO, P. P., CASTAÑO-DÍEZ, D., SCHWEIGHAUSER, G., GRAFF-MEYER, A., GOLDIE, K. N., SÜTTERLIN, R., HUISMAN, E., INGRASSIA, A., GIER, Y. D., ROZEMULLER, A. J. M., WANG, J., PAEPE, A. D., ERNY, J., STAEMPFLI, A., HOERNSCHEMEYER, J., GROßERÜSCHKAMP, F., NIEDIEKER, D., EL-MASHTOLY, S. F., QUADRI, M., VAN IJCKEN, W. F. J., BONIFATI, V., GERWERT, K., BOHRMANN, B., FRANK, S., BRITSCHGI, M., STAHLBERG, H., VAN DE BERG, W. D. J. & LAUER, M. E. 2019. Lewy pathology in Parkinson's disease consists of crowded organelles and lipid membranes. *Nature Neuroscience,* 22**,** 1099-1109.

SHERER, T. B., BETARBET, R., TESTA, C. M., SEO, B. B., RICHARDSON, J. R., KIM, J. H., MILLER, G. W., YAGI, T., MATSUNO-YAGI, A. & GREENAMYRE, J. T. 2003. Mechanism of toxicity in rotenone models of Parkinson's disease. *J Neurosci,* 23**,** 10756-64.

SHIBA-FUKUSHIMA, K., IMAI, Y., YOSHIDA, S., ISHIHAMA, Y., KANAO, T., SATO, S. & HATTORI, N. 2012. PINK1-mediated phosphorylation of the Parkin ubiquitin-like domain primes mitochondrial translocation of Parkin and regulates mitophagy. *Scientific Reports,* 2**,** 1002.

SHIMIZU, K., OHTAKI, K., MATSUBARA, K., AOYAMA, K., UEZONO, T., SAITO, O., SUNO, M., OGAWA, K., HAYASE, N., KIMURA, K. & SHIONO, H. 2001. Carrier-mediated processes in blood-brain barrier penetration and neural uptake of paraquat. *Brain Research,* 906**,** 135-142.

SHIMURA, H., HATTORI, N., KUBO, S., MIZUNO, Y., ASAKAWA, S., MINOSHIMA, S., SHIMIZU, N., IWAI, K., CHIBA, T., TANAKA, K. & SUZUKI, T. 2000. Familial

Parkinson disease gene product, parkin, is a ubiquitin-protein ligase. *Nat Genet,* 25**,** 302-5.

SHIN, J. H., KO, H. S., KANG, H., LEE, Y., LEE, Y. I., PLETINKOVA, O., TROCONSO, J. C., DAWSON, V. L. & DAWSON, T. M. 2011. PARIS (ZNF746) repression of PGC-1α contributes to neurodegeneration in Parkinson's disease. *Cell,* 144**,** 689-702.

SIDDIQUI, A., CHINTA, S. J., MALLAJOSYULA, J. K., RAJAGOPOLAN, S., HANSON, I., RANE, A., MELOV, S. & ANDERSEN, J. K. 2012. Selective binding of nuclear alpha-synuclein to the PGC1alpha promoter under conditions of oxidative stress may contribute to losses in mitochondrial function: implications for Parkinson's disease. *Free Radic Biol Med,* 53**,** 993-1003.

SIDORYK-WEGRZYNOWICZ, M., LEE, E., ALBRECHT, J. & ASCHNER, M. 2009. Manganese disrupts astrocyte glutamine transporter expression and function. *J Neurochem,* 110**,** 822-30.

SIDRANSKY, E. & LOPEZ, G. 2012. The link between the GBA gene and parkinsonism. *Lancet Neurol,* 11**,** 986-98.

SIKK, K., TABA, P., HALDRE, S., BERGQUIST, J., NYHOLM, D., ASKMARK, H., DANFORS, T., SORENSEN, J., THURFJELL, L., RAININKO, R., ERIKSSON, R., FLINK, R., FARNSTRAND, C. & AQUILONIUS, S. M. 2010. Clinical, neuroimaging and neurophysiological features in addicts with manganese-ephedrone exposure. *Acta Neurol Scand,* 121**,** 237-43.

SIMÓN-SÁNCHEZ, J., SCHULTE, C., BRAS, J. M., SHARMA, M., GIBBS, J. R., BERG, D., PAISAN-RUIZ, C., LICHTNER, P., SCHOLZ, S. W., HERNANDEZ, D. G., KRÜGER, R., FEDEROFF, M., KLEIN, C., GOATE, A., PERLMUTTER, J., BONIN, M., NALLS, M. A., ILLIG, T., GIEGER, C., HOULDEN, H., STEFFENS, M., OKUN, M. S., RACETTE, B. A., COOKSON, M. R., FOOTE, K. D., FERNANDEZ, H. H., TRAYNOR, B. J., SCHREIBER, S., AREPALLI, S., ZONOZI, R., GWINN, K., VAN DER BRUG, M., LOPEZ, G., CHANOCK, S. J., SCHATZKIN, A., PARK, Y., HOLLENBECK, A., GAO, J., HUANG, X., WOOD, N. W., LORENZ, D., DEUSCHL, G., CHEN, H., RIESS, O., HARDY, J. A., SINGLETON, A. B. & GASSER, T. 2009. Genome-wide association study reveals genetic risk underlying Parkinson's disease. *Nature Genetics,* 41**,** 1308.

SINGLETON, A. B., FARRER, M., JOHNSON, J., SINGLETON, A., HAGUE, S., KACHERGUS, J., HULIHAN, M., PEURALINNA, T., DUTRA, A., NUSSBAUM, R., LINCOLN, S., CRAWLEY, A., HANSON, M., MARAGANORE, D., ADLER, C., COOKSON, M. R., MUENTER, M., BAPTISTA, M., MILLER, D., BLANCATO, J., HARDY, J. & GWINN-HARDY, K. 2003. alpha-Synuclein locus triplication causes Parkinson's disease. *Science,* 302**,** 841.

SMIRNOVA, E., GRIPARIC, L., SHURLAND, D. L. & VAN DER BLIEK, A. M. 2001. Dynamin-related protein Drp1 is required for mitochondrial division in mammalian cells. *Molecular biology of the cell,* 12**,** 2245-2256.

SMIRNOVA, E., SHURLAND, D. L., RYAZANTSEV, S. N. & VAN DER BLIEK, A. M. 1998. A human dynamin-related protein controls the distribution of mitochondria. *J Cell Biol,* 143**,** 351-8.

SMITH, G. & GALLO, G. 2017. To mdivi-1 or not to mdivi-1: Is that the question? *Dev Neurobiol,* 77**,** 1260-1268.

SMITH, W. W., MARGOLIS, R. L., LI, X., TRONCOSO, J. C., LEE, M. K., DAWSON, V. L., DAWSON, T. M., IWATSUBO, T. & ROSS, C. A. 2005. α-Synuclein Phosphorylation Enhances Eosinophilic Cytoplasmic Inclusion Formation in SH-SY5Y Cells. 25**,** 5544-5552.

SNEAD, D. & ELIEZER, D. 2014. Alpha-synuclein function and dysfunction on cellular membranes. *Experimental neurobiology,* 23**,** 292-313.

SOLOWAY, S. 1976. Naturally occuring insecticides. *Environmental Health Perspectives,* 14**,** 109-117.

SON, J. H., SHIM, J. H., KIM, K.-H., HA, J.-Y. & HAN, J. Y. 2012. Neuronal autophagy and neurodegenerative diseases. *Experimental &Amp; Molecular Medicine,* 44**,** 89.

SPENCER, B., POTKAR, R., TREJO, M., ROCKENSTEIN, E., PATRICK, C., GINDI, R., ADAME, A., WYSS-CORAY, T. & MASLIAH, E. 2009. Beclin 1 gene transfer activates autophagy and ameliorates the neurodegenerative pathology in alpha-synuclein models of Parkinson's and Lewy body diseases. *J Neurosci,* 29**,** 13578-88.

SPILLANTINI, M. G., CROWTHER, R. A., JAKES, R., HASEGAWA, M. & GOEDERT, M. 1998. alpha-Synuclein in filamentous inclusions of Lewy bodies from Parkinson's disease and dementia with lewy bodies. *Proc Natl Acad Sci U S A,* 95**,** 6469-73.

SPILLANTINI, M. G., SCHMIDT, M. L., LEE, V. M., TROJANOWSKI, J. Q., JAKES, R. & GOEDERT, M. 1997. Alpha-synuclein in Lewy bodies. *Nature,* 388**,** 839-40.

SPRINGER, W. & KAHLE, P. J. 2011. Regulation of PINK1-Parkin-mediated mitophagy. *Autophagy,* 7**,** 266-78.

SRIRAM, K., LIN, G. X., JEFFERSON, A. M., ROBERTS, J. R., WIRTH, O., HAYASHI, Y., KRAJNAK, K. M., SOUKUP, J. M., GHIO, A. J., REYNOLDS, S. H., CASTRANOVA, V., MUNSON, A. E. & ANTONINI, J. M. 2010. Mitochondrial dysfunction and loss of Parkinson's disease-linked proteins contribute to neurotoxicity of manganese-containing welding fumes. *FASEB J,* 24**,** 4989-5002.

STANWOOD, G. D., LEITCH, D. B., SAVCHENKO, V., WU, J., FITSANAKIS, V. A., ANDERSON, D. J., STANKOWSKI, J. N., ASCHNER, M. & MCLAUGHLIN, B. 2009. Manganese exposure is cytotoxic and alters dopaminergic and GABAergic neurons within the basal ganglia. *J Neurochem,* 110**,** 378-89.

STEFANIS, L., LARSEN, K. E., RIDEOUT, H. J., SULZER, D. & GREENE, L. A. 2001. Expression of A53T mutant but not wild-type alpha-synuclein in PC12 cells induces alterations of the ubiquitin-dependent degradation system, loss of dopamine release, and autophagic cell death. *J Neurosci,* 21**,** 9549-60.

STENMARK, H. 2009. Rab GTPases as coordinators of vesicle traffic. *Nat Rev Mol Cell Biol,* 10**,** 513-25.

STEPHENSON, A. P., SCHNEIDER, J. A., NELSON, B. C., ATHA, D. H., JAIN, A., SOLIMAN, K. F., ASCHNER, M., MAZZIO, E. & RENEE REAMS, R. 2013. Manganese-induced oxidative DNA damage in neuronal SH-SY5Y cells: attenuation of thymine base lesions by glutathione and N-acetylcysteine. *Toxicol Lett,* 218**,** 299-307.

STERKY, F. H., LEE, S., WIBOM, R., OLSON, L. & LARSSON, N. G. 2011. Impaired mitochondrial transport and Parkin-independent degeneration of respiratory chain-deficient dopamine neurons in vivo. *Proc Natl Acad Sci U S A,* 108**,** 12937-42.

STEVENS, D. A., LEE, Y., KANG, H. C., LEE, B. D., LEE, Y. I., BOWER, A., JIANG, H., KANG, S. U., ANDRABI, S. A., DAWSON, V. L., SHIN, J. H. & DAWSON, T. M. 2015. Parkin loss leads to PARIS-dependent declines in mitochondrial mass and respiration. *Proc Natl Acad Sci U S A,* 112**,** 11696-701.

STICHEL, C. C., ZHU, X. R., BADER, V., LINNARTZ, B., SCHMIDT, S. & LUBBERT, H. 2007. Mono- and double-mutant mouse models of Parkinson's disease display severe mitochondrial damage. *Hum Mol Genet,* 16**,** 2377-93.

STOBART, J. & ANDERSON, C. 2013. Multifunctional role of astrocytes as gatekeepers of neuronal energy supply. 7.

STRAZIELLE, N. & GHERSI-EGEA, J. F. 2000. Choroid plexus in the central nervous system: biology and physiopathology. *J Neuropathol Exp Neurol,* 59**,** 561-74.

STRUVE, M. F., MCMANUS, B. E., WONG, B. A. & DORMAN, D. C. 2007. Basal ganglia neurotransmitter concentrations in rhesus monkeys following subchronic manganese sulfate inhalation. *Am J Ind Med,* 50**,** 772-8.

SU, Y. C. & QI, X. 2013. Inhibition of excessive mitochondrial fission reduced aberrant autophagy and neuronal damage caused by LRRK2 G2019S mutation. *Hum Mol Genet,* 22**,** 4545-61.

SUBRAMANIAM, S. R., VERGNES, L., FRANICH, N. R., REUE, K. & CHESSELET, M. F. 2014. Region specific mitochondrial impairment in mice with widespread overexpression of alpha-synuclein. *Neurobiol Dis,* 70**,** 204-13.

SUGENO, N., TAKEDA, A., HASEGAWA, T., KOBAYASHI, M., KIKUCHI, A., MORI, F., WAKABAYASHI, K. & ITOYAMA, Y. 2008. Serine 129 phosphorylation of alpha-synuclein induces unfolded protein response-mediated cell death. *J Biol Chem,* 283**,** 23179-88.

SUN, Q., ZHANG, J., FAN, W., WONG, K. N., DING, X., CHEN, S. & ZHONG, Q. 2011. The RUN domain of rubicon is important for hVps34 binding, lipid kinase inhibition, and autophagy suppression. *J Biol Chem,* 286**,** 185-91.

SUZUKI, H., WADA, O., INOUE, K., TOSAKA, H. & ONO, T. 1983. Role of brain lysosomes in the development of manganese toxicity in mice. *Toxicol Appl Pharmacol,* 71**,** 422-9.

SWANT, J., GOODWIN, J. S., NORTH, A., ALI, A. A., GAMBLE-GEORGE, J., CHIRWA, S. & KHOSHBOUEI, H. 2011. alpha-Synuclein stimulates a dopamine transporter-dependent chloride current and modulates the activity of the transporter. *J Biol Chem,* 286**,** 43933-43.

TABATA, K., MATSUNAGA, K., SAKANE, A., SASAKI, T., NODA, T. & YOSHIMORI, T. 2010. Rubicon and PLEKHM1 Negatively Regulate the Endocytic/Autophagic Pathway via a Novel Rab7-binding Domain. *Molecular Biology of the Cell,* 21**,** 4162-4172.

TAI, Y. K., CHEW, K. C., TAN, B. W., LIM, K. L. & SOONG, T. W. 2016. Iron mitigates DMT1-mediated manganese cytotoxicity via the ASK1-JNK signaling axis: Implications of iron supplementation for manganese toxicity. *Sci Rep,* 6**,** 21113.

TAKAMURA, A., KOMATSU, M., HARA, T., SAKAMOTO, A., KISHI, C., WAGURI, S., EISHI, Y., HINO, O., TANAKA, K. & MIZUSHIMA, N. 2011. Autophagy-deficient mice develop multiple liver tumors. *Genes Dev,* 25**,** 795-800.

TAKEDA, A., SOTOGAKU, N. & OKU, N. 2002. Manganese influences the levels of neurotransmitters in synapses in rat brain. *Neuroscience,* 114**,** 669-74.

TAN, J., ZHANG, T., JIANG, L., CHI, J., HU, D., PAN, Q., WANG, D. & ZHANG, Z. 2011. Regulation of intracellular manganese homeostasis by Kufor-Rakeb syndrome-associated ATP13A2 protein. *J Biol Chem,* 286**,** 29654-62.

TANG, Y. & LE, W. 2016. Differential Roles of M1 and M2 Microglia in Neurodegenerative Diseases. *Mol Neurobiol,* 53**,** 1181-94.

TANIK, S. A., SCHULTHEISS, C. E., VOLPICELLI-DALEY, L. A., BRUNDEN, K. R. & LEE, V. M. 2013. Lewy body-like alpha-synuclein aggregates resist degradation and impair macroautophagy. *J Biol Chem,* 288**,** 15194-210.

TANNER, C., KAMEL, F., ROSS, G., HOPPIN, J., GOLDMAN, S., KORELL, M., MARRAS, C., BHUDHIKANOK, G., KASTEN, M., CHADE, A., COMYNS, K., RICHARDS, M., MENG, C., PRIESTLEY, B., FERNANDEZ, H., CAMBI, F., UMBACH, D., BLAIR, A., SANDLER, D. & LANGSTON, J. 2011. Rotenone, paraquat, and Parkinson's disease. *Environmental Health Perspectives,* 119**,** 866-872.

TANNER, C. M., CHEN, B., WANG, W. Z., PENG, M. L., LIU, Z. L., LIANG, X. L., KAO, L. C., GILLEY, D. W. & SCHOENBERG, B. S. 1987. Environmental factors in the etiology of Parkinson's disease. *Can J Neurol Sci,* 14**,** 419-23.

TAPIAS, V., HU, X., LUK, K. C., SANDERS, L. H., LEE, V. M. & GREENAMYRE, J. T. 2017. Synthetic alpha-synuclein fibrils cause mitochondrial impairment and selective dopamine neurodegeneration in part via iNOS-mediated nitric oxide production. *Cell Mol Life Sci,* 74**,** 2851-2874.

TAYLOR, K. M., MORGAN, H. E., JOHNSON, A. & NICHOLSON, R. I. 2005. Structure–function analysis of a novel member of the LIV-1 subfamily of zinc transporters, ZIP14. *FEBS Letters,* 579**,** 427-432.

TAYLOR, K. S. M., COOK, J. A. & COUNSELL, C. E. 2007. Heterogeneity in male to female risk for Parkinson's disease. 78**,** 905-906.

THAYANIDHI, N., HELM, J. R., NYCZ, D. C., BENTLEY, M., LIANG, Y. & HAY, J. C. 2010. Alpha-synuclein delays endoplasmic reticulum (ER)-to-Golgi transport in mammalian cells by antagonizing ER/Golgi SNAREs. *Mol Biol Cell,* 21**,** 1850-63.

THEILLET, F. X., BINOLFI, A., BEKEI, B., MARTORANA, A., ROSE, H. M., STUIVER, M., VERZINI, S., LORENZ, D., VAN ROSSUM, M., GOLDFARB, D. & SELENKO, P. 2016. Structural disorder of monomeric alpha-synuclein persists in mammalian cells. *Nature,* 530**,** 45-50.

THIRUCHELVAM, M., BROCKEL, B., RICHFIELD, E., BAGGS, R. & CORY-SLECHTA, D. 2000. Potentiated and preferential effects of combined paraquat and maneb on nigrostriatal dopamine systems: environmental risk factors for Parkinson's disease? *Brain Research,* 873**,** 225-234.

THOMAS, H. E., ZHANG, Y., STEFELY, J. A., VEIGA, S. R., THOMAS, G., KOZMA, S. C. & MERCER, C. A. 2018. Mitochondrial Complex I Activity Is Required for Maximal Autophagy. *Cell Rep,* 24**,** 2404-2417.e8.

TIAN, Y., LI, Z., HU, W., REN, H., TIAN, E., ZHAO, Y., LU, Q., HUANG, X., YANG, P., LI, X., WANG, X., KOVACS, A. L., YU, L. & ZHANG, H. 2010. C. elegans screen identifies autophagy genes specific to multicellular organisms. *Cell,* 141**,** 1042-55.

TIEU, K. 2011. A guide to neurotoxic animal models of Parkinson's disease. *Cold Spring Harb Perspect Med,* 1**,** a009316.

TJALKENS, R. B., POPICHAK, K. A. & KIRKLEY, K. A. 2017. Inflammatory Activation of Microglia and Astrocytes in Manganese Neurotoxicity. *Advances in neurobiology,* 18**,** 159-181.

TJALKENS, R. B., ZORAN, M. J., MOHL, B. & BARHOUMI, R. 2006. Manganese suppresses ATP-dependent intercellular calcium waves in astrocyte networks through alteration of mitochondrial and endoplasmic reticulum calcium dynamics. *Brain Research,* 1113**,** 210-219.

TRAN, T. T., CHOWANADISAI, W., CRINELLA, F. M., CHICZ-DEMET, A. & LONNERDAL, B. 2002. Effect of high dietary manganese intake of neonatal rats on tissue mineral accumulation, striatal dopamine levels, and neurodevelopmental status. *Neurotoxicology,* 23**,** 635-43.

TSIKA, E., GLAUSER, L., MOSER, R., FISER, A., DANIEL, G., SHEERIN, U. M., LEES, A., TRONCOSO, J. C., LEWIS, P. A., BANDOPADHYAY, R., SCHNEIDER, B. L. & MOORE, D. J. 2014. Parkinson's disease-linked mutations in VPS35 induce dopaminergic neurodegeneration. *Hum Mol Genet,* 23**,** 4621-38.

TSUJI, S., CHOUDARY, P. V., MARTIN, B. M., STUBBLEFIELD, B. K., MAYOR, J. A., BARRANGER, J. A. & GINNS, E. I. 1987. A mutation in the human glucocerebrosidase gene in neuronopathic Gaucher's disease. *N Engl J Med,* 316**,** 570-5.

TSUNEMI, T., ASHE, T. D., MORRISON, B. E., SORIANO, K. R., AU, J., ROQUE, R. A., LAZAROWSKI, E. R., DAMIAN, V. A., MASLIAH, E. & LA SPADA, A. R. 2012. PGC-1alpha rescues Huntington's disease proteotoxicity by preventing oxidative stress and promoting TFEB function. *Sci Transl Med,* 4**,** 142ra97.

TUSCHL, K., CLAYTON, P. T., GOSPE, S. M., GULAB, S., IBRAHIM, S., SINGHI, P., AULAKH, R., RIBEIRO, R. T., BARSOTTINI, O. G., ZAKI, M. S., DEL ROSARIO, M. L., DYACK, S., PRICE, V., RIDEOUT, A., GORDON, K., WEVERS, R. A., CHONG, W. K. & MILLS, P. B. 2012. Syndrome of hepatic cirrhosis, dystonia, polycythemia, and hypermanganesemia caused by mutations in SLC30A10, a manganese transporter in man. *Am J Hum Genet,* 90**,** 457-66.

TUSCHL, K., MEYER, E., VALDIVIA, L. E., ZHAO, N., DADSWELL, C., ABDUL-SADA, A., HUNG, C. Y., SIMPSON, M. A., CHONG, W. K., JACQUES, T. S., WOLTJER, R. L., EATON, S., GREGORY, A., SANFORD, L., KARA, E., HOULDEN, H., CUNO, S. M., PROKISCH, H., VALLETTA, L., TIRANTI, V., YOUNIS, R., MAHER, E. R., SPENCER, J., STRAATMAN-IWANOWSKA, A., GISSEN, P., SELIM, L. A., PINTOS-MORELL, G., COROLEU-LLETGET, W., MOHAMMAD, S. S., YOGANATHAN, S., DALE, R. C., THOMAS, M., RIHEL, J., BODAMER, O. A., ENNS, C. A., HAYFLICK, S. J., CLAYTON, P. T., MILLS, P. B., KURIAN, M. A. & WILSON, S. W. 2016. Mutations in SLC39A14 disrupt manganese homeostasis and cause childhood-onset parkinsonism-dystonia. *Nat Commun,* 7**,** 11601.

TUTTLE, M. D., COMELLAS, G., NIEUWKOOP, A. J., COVELL, D. J., BERTHOLD, D. A., KLOEPPER, K. D., COURTNEY, J. M., KIM, J. K., BARCLAY, A. M., KENDALL, A., WAN, W., STUBBS, G., SCHWIETERS, C. D., LEE, V. M., GEORGE, J. M. & RIENSTRA, C. M. 2016. Solid-state NMR structure of a pathogenic fibril of full-length human alpha-synuclein. *Nat Struct Mol Biol,* 23**,** 409-15.

TYSNES, O. B. & STORSTEIN, A. 2017. Epidemiology of Parkinson's disease. *J Neural Transm (Vienna),* 124**,** 901-905.

UHL, G. R., HEDREEN, J. C. & PRICE, D. L. 1985. Parkinson's disease: loss of neurons from the ventral tegmental area contralateral to therapeutic surgical lesions. *Neurology,* 35**,** 1215-8.

USENOVIC, M. & KRAINC, D. 2012. Lysosomal dysfunction in neurodegeneration: the role of ATP13A2/PARK9. *Autophagy,* 8**,** 987-8.

USENOVIC, M., TRESSE, E., MAZZULLI, J. R., TAYLOR, J. P. & KRAINC, D. 2012. Deficiency of ATP13A2 leads to lysosomal dysfunction, α-synuclein accumulation, and neurotoxicity. *J Neurosci,* 32**,** 4240-6.

UVERSKY, V. N., LI, J. & FINK, A. L. 2001. Metal-triggered structural transformations, aggregation, and fibrillation of human alpha-synuclein. A possible molecular NK between Parkinson's disease and heavy metal exposure. *J Biol Chem,* 276**,** 44284-96.

VALENTE, E. M., ABOU-SLEIMAN, P. M., CAPUTO, V., MUQIT, M. M., HARVEY, K., GISPERT, S., ALI, Z., DEL TURCO, D., BENTIVOGLIO, A. R., HEALY, D. G., ALBANESE, A., NUSSBAUM, R., GONZÁLEZ-MALDONADO, R., DELLER, T., SALVI, S., CORTELLI, P., GILKS, W. P., LATCHMAN, D. S., HARVEY, R. J., DALLAPICCOLA, B., AUBURGER, G. & WOOD, N. W. 2004. Hereditary early-onset Parkinson's disease caused by mutations in PINK1. *Science,* 304**,** 1158-60.

VALENTE, E. M., BENTIVOGLIO, A. R., DIXON, P. H., FERRARIS, A., IALONGO, T., FRONTALI, M., ALBANESE, A. & WOOD, N. W. 2001. Localization of a novel locus for autosomal recessive early-onset parkinsonism, PARK6, on human chromosome 1p35-p36. *Am J Hum Genet,* 68**,** 895-900.

VANSTONE, J. R., SMITH, A. M., MCBRIDE, S., NAAS, T., HOLCIK, M., ANTOUN, G., HARPER, M.-E., MICHAUD, J., SELL, E., CHAKRABORTY, P., TETREAULT, M.,

CARE4RARE, C., MAJEWSKI, J., BAIRD, S., BOYCOTT, K. M., DYMENT, D. A., MACKENZIE, A. & LINES, M. A. 2015. DNM1L-related mitochondrial fission defect presenting as refractory epilepsy. *European Journal Of Human Genetics,* 24**,** 1084.

VENKATESHAPPA, C., HARISH, G., MYTHRI, R. B., MAHADEVAN, A., SRINIVAS BHARATH, M. M. & SHANKAR, S. K. 2012. Increased Oxidative Damage and Decreased Antioxidant Function in Aging Human Substantia Nigra Compared to Striatum: Implications for Parkinson's Disease. *Neurochemical Research,* 37**,** 358-369.

VERINA, T., KIIHL, S. F., SCHNEIDER, J. S. & GUILARTE, T. R. 2011. Manganese exposure induces microglia activation and dystrophy in the substantia nigra of non-human primates. *Neurotoxicology,* 32**,** 215-226.

VERINA, T., SCHNEIDER, J. S. & GUILARTE, T. R. 2013. Manganese exposure induces alpha-synuclein aggregation in the frontal cortex of non-human primates. *Toxicol Lett,* 217**,** 177-83.

VICARIO, M., CIERI, D., BRINI, M. & CALÌ, T. 2018. The Close Encounter Between Alpha-Synuclein and Mitochondria. 12.

VILAR, M., CHOU, H. T., LUHRS, T., MAJI, S. K., RIEK-LOHER, D., VEREL, R., MANNING, G., STAHLBERG, H. & RIEK, R. 2008. The fold of alpha-synuclein fibrils. *Proc Natl Acad Sci U S A,* 105**,** 8637-42.

VOGIATZI, T., XILOURI, M., VEKRELLIS, K. & STEFANIS, L. 2008. Wild type alpha-synuclein is degraded by chaperone-mediated autophagy and macroautophagy in neuronal cells. *J Biol Chem,* 283**,** 23542-56.

VOLPICELLI-DALEY, L. A., GAMBLE, K. L., SCHULTHEISS, C. E., RIDDLE, D. M., WEST, A. B. & LEE, V. M. Y. 2014. Formation of α-synuclein Lewy neurite-like aggregates in axons impedes the transport of distinct endosomes. *Molecular biology of the cell,* 25**,** 4010-4023.

VOLPICELLI-DALEY, L. A., LUK, K. C., PATEL, T. P., TANIK, S. A., RIDDLE, D. M., STIEBER, A., MEANEY, D. F., TROJANOWSKI, J. Q. & LEE, V. M. Y. 2011. Exogenous α-synuclein fibrils induce Lewy body pathology leading to synaptic dysfunction and neuron death. *Neuron,* 72**,** 57-71.

VON BERNHARDI, R., EUGENIN-VON BERNHARDI, L. & EUGENIN, J. 2015. Microglial cell dysregulation in brain aging and neurodegeneration. *Front Aging Neurosci,* 7**,** 124.

WAKABAYASHI, J., ZHANG, Z., WAKABAYASHI, N., TAMURA, Y., FUKAYA, M., KENSLER, T. W., IIJIMA, M. & SESAKI, H. 2009. The dynamin-related GTPase Drp1 is required for embryonic and brain development in mice. *J Cell Biol,* 186**,** 805-16.

WAKABAYASHI, K., TANJI, K., MORI, F. & TAKAHASHI, H. 2007. The Lewy body in Parkinson's disease: molecules implicated in the formation and degradation of alpha-synuclein aggregates. *Neuropathology,* 27**,** 494-506.

WAKAMATSU, M., ISHII, A., UKAI, Y., SAKAGAMI, J., IWATA, S., ONO, M., MATSUMOTO, K., NAKAMURA, A., TADA, N., KOBAYASHI, K., IWATSUBO, T. & YOSHIMOTO, M. 2007. Accumulation of phosphorylated α-synuclein in dopaminergic neurons of transgenic mice that express human α-synuclein. 85**,** 1819-1825.

WANG, A., COSTELLO, S., COCKBURN, M., ZHANG, X., BRONSTEIN, J. & RITZ, B. 2011a. Parkinson's disease risk from ambient exposure to pesticides. *Eur J Epidemiol,* 26**,** 547-55.

WANG, D., ZHANG, J., JIANG, W., CAO, Z., ZHAO, F., CAI, T., ASCHNER, M. & LUO, W. 2017. The role of NLRP3-CASP1 in inflammasome-mediated neuroinflammation

and autophagy dysfunction in manganese-induced, hippocampal-dependent impairment of learning and memory ability. *Autophagy,* 13**,** 914-927.

WANG, W., PEROVIC, I., CHITTULURU, J., KAGANOVICH, A., NGUYEN, L. T., LIAO, J., AUCLAIR, J. R., JOHNSON, D., LANDERU, A., SIMORELLIS, A. K., JU, S., COOKSON, M. R., ASTURIAS, F. J., AGAR, J. N., WEBB, B. N., KANG, C., RINGE, D., PETSKO, G. A., POCHAPSKY, T. C. & HOANG, Q. Q. 2011b. A soluble alpha-synuclein construct forms a dynamic tetramer. *Proc Natl Acad Sci U S A,* 108**,** 17797-802.

WANG, Y., LIU, J., CHEN, M., DU, T., DUAN, C., GAO, G. & YANG, H. 2016a. The novel mechanism of rotenone-induced alpha-synuclein phosphorylation via reduced protein phosphatase 2A activity. *Int J Biochem Cell Biol,* 75**,** 34-44.

WANG, Z., MIAO, G., XUE, X., GUO, X., YUAN, C., WANG, Z., ZHANG, G., CHEN, Y., FENG, D., HU, J. & ZHANG, H. 2016b. The Vici Syndrome Protein EPG5 Is a Rab7 Effector that Determines the Fusion Specificity of Autophagosomes with Late Endosomes/Lysosomes. *Molecular Cell,* 63**,** 781-795.

WASSERMAN, G. A., LIU, X., PARVEZ, F., AHSAN, H., LEVY, D., FACTOR-LITVAK, P., KLINE, J., VAN GEEN, A., SLAVKOVICH, V., LOIACONO, N. J., CHENG, Z., ZHENG, Y. & GRAZIANO, J. H. 2006. Water manganese exposure and children's intellectual function in Araihazar, Bangladesh. *Environ Health Perspect,* 114**,** 124-9.

WATERHAM, H. R., KOSTER, J., VAN ROERMUND, C. W., MOOYER, P. A., WANDERS, R. J. & LEONARD, J. V. 2007. A lethal defect of mitochondrial and peroxisomal fission. *N Engl J Med,* 356**,** 1736-41.

WEBB, J. L., RAVIKUMAR, B., ATKINS, J., SKEPPER, J. N. & RUBINSZTEIN, D. C. 2003. Alpha-Synuclein is degraded by both autophagy and the proteasome. *J Biol Chem,* 278**,** 25009-13.

WEDLER, F. C., DENMAN, R. B. & ROBY, W. G. 1982. Glutamine synthetase from ovine brain is a manganese(II) enzyme. *Biochemistry,* 21**,** 6389-96.

WEINREB, P. H., ZHEN, W., POON, A. W., CONWAY, K. A. & LANSBURY, P. T. 1996. NACP, A Protein Implicated in Alzheimer's Disease and Learning, Is Natively Unfolded. *Biochemistry,* 35**,** 13709-13715.

WERSINGER, C., RUSNAK, M. & SIDHU, A. 2006. Modulation of the trafficking of the human serotonin transporter by human alpha-synuclein. *Eur J Neurosci,* 24**,** 55-64.

WEST, A. B., COWELL, R. M., DAHER, J. P., MOEHLE, M. S., HINKLE, K. M., MELROSE, H. L., STANDAERT, D. G. & VOLPICELLI-DALEY, L. A. 2014. Differential LRRK2 expression in the cortex, striatum, and substantia nigra in transgenic and nontransgenic rodents. *J Comp Neurol,* 522**,** 2465-80.

WESTBROEK, W., GUSTAFSON, A. M. & SIDRANSKY, E. 2011. Exploring the link between glucocerebrosidase mutations and parkinsonism. *Trends in molecular medicine,* 17**,** 485-493.

WHITEHOUSE, P. J., HEDREEN, J. C., WHITE, C. L., 3RD & PRICE, D. L. 1983. Basal forebrain neurons in the dementia of Parkinson disease. *Ann Neurol,* 13**,** 243-8.

WILLIS, A. W., EVANOFF, B. A., LIAN, M., GALARZA, A., WEGRZYN, A., SCHOOTMAN, M. & RACETTE, B. A. 2010. Metal emissions and urban incident Parkinson disease: a community health study of Medicare beneficiaries by using geographic information systems. *Am J Epidemiol,* 172**,** 1357-63.

WINKEL, R., KUHN, W. & PRZUNTEK, H. 1995. Chronic intoxication with lead- and sulfur compounds may produce Parkinson's disease. *J Neural Transm Suppl,* 46**,** 183-7.

WINNER, B., JAPPELLI, R., MAJI, S. K., DESPLATS, P. A., BOYER, L., AIGNER, S., HETZER, C., LOHER, T., VILAR, M., CAMPIONI, S., TZITZILONIS, C., SORAGNI, A., JESSBERGER, S., MIRA, H., CONSIGLIO, A., PHAM, E.,

MASLIAH, E., GAGE, F. H. & RIEK, R. 2011. In vivo demonstration that α-synuclein oligomers are toxic. 108**,** 4194-4199.
WONG, Y. C., YSSELSTEIN, D. & KRAINC, D. 2018. Mitochondria–lysosome contacts regulate mitochondrial fission via RAB7 GTP hydrolysis. *Nature,* 554**,** 382.
WU, F., XU, H. D., GUAN, J. J., HOU, Y. S., GU, J. H., ZHEN, X. C. & QIN, Z. H. 2015. Rotenone impairs autophagic flux and lysosomal functions in Parkinson's disease. *Neuroscience,* 284**,** 900-11.
WU, X. F., BLOCK, M. L., ZHANG, W., QIN, L., WILSON, B., ZHANG, W. Q., VERONESI, B. & HONG, J. S. 2005. The role of microglia in paraquat-induced dopaminergic neurotoxicity. *Antioxid Redox Signal,* 7**,** 654-61.
XIE, N., WANG, C., LIAN, Y., ZHANG, H., WU, C. & ZHANG, Q. 2013. A selective inhibitor of Drp1, mdivi-1, protects against cell death of hippocampal neurons in pilocarpine-induced seizures in rats. *Neurosci Lett,* 545**,** 64-8.
XILOURI, M., BREKK, O. R., POLISSIDIS, A., CHRYSANTHOU-PITEROU, M., KLOUKINA, I. & STEFANIS, L. 2016. Impairment of chaperone-mediated autophagy induces dopaminergic neurodegeneration in rats. *Autophagy,* 12**,** 2230-2247.
XILOURI, M., BREKK, O. R. & STEFANIS, L. 2013. alpha-Synuclein and protein degradation systems: a reciprocal relationship. *Mol Neurobiol,* 47**,** 537-51.
XILOURI, M., VOGIATZI, T., VEKRELLIS, K., PARK, D. & STEFANIS, L. 2009. Abberant alpha-synuclein confers toxicity to neurons in part through inhibition of chaperone-mediated autophagy. *PloS one,* 4**,** e5515-e5515.
XIN, Y., GAO, H., WANG, J., QIANG, Y., IMAM, M. U., LI, Y., WANG, J., ZHANG, R., ZHANG, H., YU, Y., WANG, H., LUO, H., SHI, C., XU, Y., HOJYO, S., FUKADA, T., MIN, J. & WANG, F. 2017. Manganese transporter Slc39a14 deficiency revealed its key role in maintaining manganese homeostasis in mice. *Cell discovery,* 3**,** 17025-17025.
XIONG, N., JIA, M., CHEN, C., XIONG, J., ZHANG, Z., HUANG, J., HOU, L., YANG, H., CAO, X., LIANG, Z., SUN, S., LIN, Z. & WANG, T. 2011. Potential autophagy enhancers attenuate rotenone-induced toxicity in SH-SY5Y. *Neuroscience,* 199**,** 292-302.
XUE, R., MENG, Q., LU, D., LIU, X., WANG, Y. & HAO, J. 2018. Mitofusin2 Induces Cell Autophagy of Pancreatic Cancer through Inhibiting the PI3K/Akt/mTOR Signaling Pathway. *Oxidative Medicine and Cellular Longevity,* 2018**,** 1-8.
YAMADA, M., OHNO, S., OKAYASU, I., OKEDA, R., HATAKEYAMA, S., WATANABE, H., USHIO, K. & TSUKAGOSHI, H. 1986. Chronic manganese poisoning: a neuropathological study with determination of manganese distribution in the brain. *Acta Neuropathol,* 70**,** 273-8.
YAMANO, K. & YOULE, R. J. 2013. PINK1 is degraded through the N-end rule pathway. *Autophagy,* 9**,** 1758-69.
YASUDA, T., FUKUDA-TANI, M., NIHIRA, T., WADA, K., HATTORI, N., MIZUNO, Y. & MOCHIZUKI, H. 2007. Correlation between levels of pigment epithelium-derived factor and vascular endothelial growth factor in the striatum of patients with Parkinson's disease. *Exp Neurol,* 206**,** 308-17.
YIN, Z., ASCHNER, J. L., DOS SANTOS, A. P. & ASCHNER, M. 2008. Mitochondrial-dependent manganese neurotoxicity in rat primary astrocyte cultures. *Brain research,* 1203**,** 1-11.
YIN, Z., JIANG, H., LEE, E. S., NI, M., ERIKSON, K. M., MILATOVIC, D., BOWMAN, A. B. & ASCHNER, M. 2010. Ferroportin is a manganese-responsive protein that decreases manganese cytotoxicity and accumulation. *J Neurochem,* 112**,** 1190-8.

YOKEL, R. A. 2009. Manganese Flux Across the Blood–Brain Barrier. *NeuroMolecular Medicine,* 11**,** 297-310.

YOON, H., KIM, D.-S., LEE, G.-H., KIM, K.-W., KIM, H.-R. & CHAE, H.-J. 2011. Apoptosis Induced by Manganese on Neuronal SK-N-MC Cell Line: Endoplasmic Reticulum (ER) Stress and Mitochondria Dysfunction. *Environmental health and toxicology,* 26**,** e2011017-e2011017.

YOON, Y., PITTS, K. R. & MCNIVEN, M. A. 2001. Mammalian dynamin-like protein DLP1 tubulates membranes. *Mol Biol Cell,* 12**,** 2894-905.

YOULE, R. J. & VAN DER BLIEK, A. M. 2012. Mitochondrial fission, fusion, and stress. *Science,* 337**,** 1062-5.

YU, S., ZUO, X., LI, Y., ZHANG, C., ZHOU, M., ZHANG, Y. A., UEDA, K. & CHAN, P. 2004. Inhibition of tyrosine hydroxylase expression in alpha-synuclein-transfected dopaminergic neuronal cells. *Neurosci Lett,* 367**,** 34-9.

YU, W. H., DORADO, B., FIGUEROA, H. Y., WANG, L., PLANEL, E., COOKSON, M. R., CLARK, L. N. & DUFF, K. E. 2009. Metabolic activity determines efficacy of macroautophagic clearance of pathological oligomeric alpha-synuclein. *Am J Pathol,* 175**,** 736-47.

YUAN, Y. H., YAN, W. F., SUN, J. D., HUANG, J. Y., MU, Z. & CHEN, N. H. 2015. The molecular mechanism of rotenone-induced alpha-synuclein aggregation: emphasizing the role of the calcium/GSK3beta pathway. *Toxicol Lett,* 233**,** 163-71.

YUE, Z. 2007. Regulation of neuronal autophagy in axon: implication of autophagy in axonal function and dysfunction/degeneration. *Autophagy,* 3**,** 139-41.

ZALTIERI, M., GRIGOLETTO, J., LONGHENA, F., NAVARRIA, L., FAVERO, G., CASTREZZATI, S., COLIVICCHI, M. A., DELLA CORTE, L., REZZANI, R., PIZZI, M., BENFENATI, F., SPILLANTINI, M. G., MISSALE, C., SPANO, P. & BELLUCCI, A. 2015. alpha-synuclein and synapsin III cooperatively regulate synaptic function in dopamine neurons. *J Cell Sci,* 128**,** 2231-43.

ZARRANZ, J. J., ALEGRE, J., GOMEZ-ESTEBAN, J. C., LEZCANO, E., ROS, R., AMPUERO, I., VIDAL, L., HOENICKA, J., RODRIGUEZ, O., ATARES, B., LLORENS, V., GOMEZ TORTOSA, E., DEL SER, T., MUNOZ, D. G. & DE YEBENES, J. G. 2004. The new mutation, E46K, of alpha-synuclein causes Parkinson and Lewy body dementia. *Ann Neurol,* 55**,** 164-73.

ZHANG, J., CAO, R., CAI, T., ASCHNER, M., ZHAO, F., YAO, T., CHEN, Y., CAO, Z., LUO, W. & CHEN, J. 2013. The role of autophagy dysregulation in manganese-induced dopaminergic neurodegeneration. *Neurotox Res,* 24**,** 478-90.

ZHANG, J., FITSANAKIS, V. A., GU, G., JING, D., AO, M., AMARNATH, V. & MONTINE, T. J. 2003a. Manganese ethylene-bis-dithiocarbamate and selective dopaminergic neurodegeneration in rat: a link through mitochondrial dysfunction. *J Neurochem,* 84**,** 336-46.

ZHANG, S., FU, J. & ZHOU, Z. 2004. In vitro effect of manganese chloride exposure on reactive oxygen species generation and respiratory chain complexes activities of mitochondria isolated from rat brain. *Toxicol In Vitro,* 18**,** 71-7.

ZHANG, S., ZHOU, Z. & FU, J. 2003b. Effect of manganese chloride exposure on liver and brain mitochondria function in rats. *Environ Res,* 93**,** 149-57.

ZHANG, X., ZHOU, J. Y., CHIN, M. H., SCHEPMOES, A. A., PETYUK, V. A., WEITZ, K. K., PETRITIS, B. O., MONROE, M. E., CAMP, D. G., WOOD, S. A., MELEGA, W. P., BIGELOW, D. J., SMITH, D. J., QIAN, W. J. & SMITH, R. D. 2010. Region-specific protein abundance changes in the brain of MPTP-induced Parkinson's disease mouse model. *J Proteome Res,* 9**,** 1496-509.

ZHANG, Z., YAN, J., BOWMAN, A. B., BRYAN, M. R., SINGH, R. & ASCHNER, M. 2019. Dysregulation of TFEB contributes to manganese-induced autophagic failure and mitochondrial dysfunction in astrocytes. *Autophagy***,** 1-18.

ZHAO, F., CAI, T., LIU, M., ZHENG, G., LUO, W. & CHEN, J. 2009. Manganese induces dopaminergic neurodegeneration via microglial activation in a rat model of manganism. *Toxicol Sci,* 107**,** 156-64.

ZHEN, Y. & STENMARK, H. 2015. Cellular functions of Rab GTPases at a glance. *Journal of Cell Science,* 128**,** 3171.

ZHONG, Y., WANG, Q. J., LI, X., YAN, Y., BACKER, J. M., CHAIT, B. T., HEINTZ, N. & YUE, Z. 2009. Distinct regulation of autophagic activity by Atg14L and Rubicon associated with Beclin 1–phosphatidylinositol-3-kinase complex. *Nature Cell Biology,* 11**,** 468.

ZHOU, C., HUANG, Y., SHAO, Y., MAY, J., PROU, D., PERIER, C., DAUER, W., SCHON, E. A. & PRZEDBORSKI, S. 2008. The kinase domain of mitochondrial PINK1 faces the cytoplasm. *Proc Natl Acad Sci U S A,* 105**,** 12022-7.

ZHOU, C., ZHONG, W., ZHOU, J., SHENG, F., FANG, Z., WEI, Y., CHEN, Y., DENG, X., XIA, B. & LIN, J. 2012. Monitoring autophagic flux by an improved tandem fluorescent-tagged LC3 (mTagRFP-mWasabi-LC3) reveals that high-dose rapamycin impairs autophagic flux in cancer cells. *Autophagy,* 8**,** 1215-26.

ZHOU, Q., FU, X., WANG, X., WU, Q., LU, Y., SHI, J., KLAUNIG, J. E. & ZHOU, S. 2018. Autophagy plays a protective role in Mn-induced toxicity in PC12 cells. *Toxicology,* 394**,** 45-53.

ZHOU, Q., ZHANG, H., WU, Q., SHI, J. & ZHOU, S. 2017. Pharmacological manipulations of autophagy modulate paraquat-induced cytotoxicity in PC12 cells. *International journal of biochemistry and molecular biology,* 8**,** 13-22.

ZHU, J.-H., HORBINSKI, C., GUO, F., WATKINS, S., UCHIYAMA, Y. & CHU, C. T. 2007. Regulation of Autophagy by Extracellular Signal-Regulated Protein Kinases During 1-Methyl-4-Phenylpyridinium-Induced Cell Death. *The American Journal of Pathology,* 170**,** 75-86.

ZHU, M., QIN, Z. J., HU, D., MUNISHKINA, L. A. & FINK, A. L. 2006. Alpha-synuclein can function as an antioxidant preventing oxidation of unsaturated lipid in vesicles. *Biochemistry,* 45**,** 8135-42.

ZHU, P. P., PATTERSON, A., STADLER, J., SEEBURG, D. P., SHENG, M. & BLACKSTONE, C. 2004. Intra- and intermolecular domain interactions of the C-terminal GTPase effector domain of the multimeric dynamin-like GTPase Drp1. *J Biol Chem,* 279**,** 35967-74.

ZUCHNER, S., MERSIYANOVA, I. V., MUGLIA, M., BISSAR-TADMOURI, N., ROCHELLE, J., DADALI, E. L., ZAPPIA, M., NELIS, E., PATITUCCI, A., SENDEREK, J., PARMAN, Y., EVGRAFOV, O., JONGHE, P. D., TAKAHASHI, Y., TSUJI, S., PERICAK-VANCE, M. A., QUATTRONE, A., BATTALOGLU, E., POLYAKOV, A. V., TIMMERMAN, V., SCHRODER, J. M. & VANCE, J. M. 2004. Mutations in the mitochondrial GTPase mitofusin 2 cause Charcot-Marie-Tooth neuropathy type 2A. *Nat Genet,* 36**,** 449-51.